DEVELOPMENT AND VALIDATION OF A STRESS-BASED PROCEDURE FOR THE DESIGN OF MILITARY FLEXIBLE PAVEMENTS

BY

CARLOS RUBEN GONZALEZ

DISSERTATION

Submitted in partial fulfillment of the requirements
for the degree of Doctor of Philosophy in Civil Engineering
in the Graduate College of the
University of Illinois at Urbana-Champaign, 2015

Urbana, Illinois

Doctoral Committee:

Professor Erol Tutumluer, Chair
Professor Marshall R. Thompson
Professor Imad Al-Qadi
Professor Jeffery R. Roesler
Dr. Gary L. Anderton, US Army Corps of Engineers

ABSTRACT

This research study focuses on the development, validation and implementation of a new stress-based design procedure for military flexible airfield pavements. This proposed new procedure is based on the U.S. Army Corps of Engineers California Bearing Ratio (CBR) design methodology. The CBR design methodology has its roots on a very simple, but still reasonable theoretical approach, where the pavement is modeled by a single layer system described by the Boussinesq half-space stress model.

The objective to develop a new stress-based design procedure was fostered by the results of an extensive literature review on the early work done during the development of the original CBR procedure. This literature review revealed that the CBR procedure was fundamentally derived from sound theoretical basis and was actually developed as a stress-based methodology that followed a soil stress model proposed by O. K. Fröhlich in 1934. It was found that Fröhlich's stress equations for vertical stress, which make use of a stress concentration factor to improve predictions of stresses within a soil mass, can be used to derive the current form of the fundamental equation in which the CBR procedure is based on.

The discovery that the original CBR procedure pointed to a stress-based design approach led to the further investigation of the mathematical basis of the original CBR equation. This research focused its effort in the re-formulation of the basic CBR equation, corroborating its validity and developing a complete system for the design of flexible pavements using a stress-based approach.

The development and validation of the proposed stress-based design procedure was conducted with the following objectives. The first objective was to review and consolidate all historical information on the origins of the classical CBR equation and to reformulate its mathematical derivation into a stress-based approach. The second objective was to introduce a new stress-based criterion, called the CBR-Beta procedure, for design of flexible pavements. The third objective consisted of performing experiments to help validate the stress distribution within pavement structures subjected to various aircraft loadings. A full-scale experiment was developed to construct twelve flexible pavement test sections so that the proposed CBR-Beta

procedure could be implemented and studied in the field. The fourth objective was to further validate the proposed stress-based CBR design procedure utilizing the results of field traffic experiments, laboratory testing and modeling. Finally, the fifth objective was to consolidate all the results from full-scale traffic testing, validation of stress distribution within a pavement structure and modeling into a cohesive and complete stress-based design procedure.

The results of this study have demonstrated that the new re-formulation of the CBR procedure can be applied to the structural thickness designs of flexible pavements where subgrade shear failure is to be prevented. The new form of the CBR-Beta criterion was found to be of mechanistic nature and was validated by traffic tests. The new CBR-Beta design procedure compared favorably against the existing CBR and layered elastic procedures. The CBR-Beta procedure improved on the existing CBR procedure by: (i) making the performance criteria more visible in terms of vertical stress versus passes to failure, (ii) directly considering multi-wheel gear assemblies without resorting to gear equivalencies, and (iii) eliminating the need for thickness correction factors. All these new aspects of the CBR-Beta procedure were incorporated into a complete system and recommended for implementation as the standard for the design and evaluation of military airfield pavements.

To my father Ruben and my mother Carmen

ACKNOWLEDGEMENTS

I want to first express my gratitude to my graduate committee members for all their time and effort during the completion and revision of the research. Their comments and recommendations improved the quality of this research. I would like to thank my chairman, Professor Erol Tutumluer, for taking me under his wing and providing me with invaluable advice. I want to thank Professor Marshall Thompson, from whom the idea for this research study emanated.

I want to specially thank Dr. Walter R. Barker, with whom I spent countless hours sieving through mountains of data, reviewing and analyzing results and making sense of everything. His knowledge in the subject matter and practical ability to solve problems greatly helped me steer this research in the right direction.

Special thanks go to the good people at the U.S. Air Force Civil Engineering Center and the U.S. Army Transportation Systems Center for providing funding and allowing me to take the time to complete this work. Mr. George VanSteenburg, Mrs. Mary Adolf, Dr. Ray Rollings, Dr. Craig Rutland and Mr. Jim Greene all provided valuable comments during the design phase of this research and helped me keep the scope of work to a manageable size.

I also want to thank the pavement test section construction crew from the Airfields and Pavements Branch, Mr. Quint Mason, Mr. Tommy Carr and Mr. Tony Brogdon for providing assistance during the construction, testing and data collection phase. Without their help, willingness and interest in this research nothing would have come to fruition.

Finally, I would like to thank my wife Mary, my daughters Jennifer and Ingrid and my son Carlos for encouraging me to complete this work.

TABLE OF CONTENTS

CHAPTER 1 - INTRODUCTION

1.1 Introduction

The California Bearing Ratio (CBR) procedure has been the principal method used for the design of flexible pavements for both military roads and airfields since its development in the 1940's. Even though the use of more advanced analytical and numerical models such as the layered elastic and finite element method solutions became accepted for pavement design, the CBR design procedure still remains very valuable and is continued to be used by the military for the structural design and evaluation of permanent and expedient flexible pavements. Although originally thought to be a completely empirical procedure, an extensive literature review and analyses of its original mathematical formulation revealed the CBR procedure actually has its roots in a stress-based foundation model. This fact guided this research towards the main goal of proposing and possibly adopting a stress-based mechanistic-empirical design approach. Because of these early findings, three main objectives were devised for this research: (1) revise the original formulation of the CBR design procedure, (2) propose a stress-based design approach and (3) corroborate its validity for implementation and replacement of the current CBR design procedure. This chapter gives a short background on the origins of the CBR design procedure and summarizes the approach taken to fulfill these main objectives. A detailed description of the CBR procedure and mathematical foundation will be provided in subsequence chapters.

1.2 Background

CBR stands for California Bearing Ratio and its value represents the relative resistance to shear and penetration of a soil mass as compared to a standard material. A CBR test was originally developed by the California Department of Transportation before World War II and has been adopted after several modifications by the U.S. Department of Defense. The CBR of a soil mass has been standardized and is obtained from either laboratory tests following the ASTM D1883-05 standard conducted on samples obtained from representative soil samples of the area where the pavement will be constructed or, from in-situ field CBR tests following the ASTM D4429-09a standard. The CBR test was developed to measure the bearing capacity of subgrades

used for roadways and airfields. The CBR of a soil mass or pavement layer is expressed as a number on a scale from 0 to 100. A CBR equal to 100 represents the value assigned to a standard crushed limestone material.

The CBR design procedure was originally developed in the 1940's for the design of flexible pavements to support the then newly developed heavy aircraft bombers. The original airfield design curves were an extrapolation of the empirically-developed California pavement design curves for highway pavements. These original airfield design curves, which employed Boussinesq's theory of stress distribution in a homogenous half-space, were later modified using the results of extensive full-scale field testing. In 1955, the U. S. Army Corps of Engineers (USACE) proposed a procedure to determine pavement thickness based on the CBR value of subgrade layer.

Originally, the design of flexible pavements was done for what was then considered capacity operations and the original formulation of the CBR procedure only allowed for the consideration of single-wheel loads. With the development of newer heavy multi-wheel aircraft, such as the C-5A and B-747, a thickness adjustment factor (α-factor) was introduced within the CBR procedure to account for the effects of traffic operations other than capacity and to accommodate multi-wheel tire groups.

The CBR design procedure has also gained worldwide importance since this procedure is utilized to determine the Aircraft Classification Number (ACN). The 1983 edition of the International Civil Aviation Organization (ICAO) Aerodrome Design Manual (Doc 9157-AN/901), which is currently in use, prescribed the USACE CBR procedure as the basis for computing the ACN for civilian aircraft. The ACN is a number of great significance to the aircraft industry, because it is instrumental in determining which aircraft the airports are able to accept for operations.

Criticisms of the CBR design procedure were brought up in 2004 by the Information and Technology Platform for Transport, Infrastructure and Public Space (CROW). CROW is a nonprofit organization based in the Netherlands that conducts research in the areas of traffic, transport, and infrastructure and focuses on transfer of knowledge from research and standardization. The 2004 CROW report D04-09 "The PCN Runway Strength Rating and Load Control System" contained the following statement:

"It is now widely recognized that the U.S. Army Corps of Engineers' CBR method cannot adequately compute or predict pavement damage caused by new large aircraft."

In particular, the CBR procedure has come under scrutiny in consideration of pavement design and ACN evaluation for multi-wheel aircraft. A critical element at the center of this discussion is the use of the α-factor in the ICAO procedure for computing the ACN. The α-factor was deemed to be inadequate in representing multi-wheel aircraft scenarios (Barker 1994, 1994a; Airport Technology Research and Development Branch, 2004).

1.3 Research Idea

The current implementation of the CBR procedure for the design of flexible pavements is based on a mathematical equation expressing the required total thickness above a subgrade layer as a function of a single wheel load, size of contact area, design passes, and the subgrade CBR. This equation is represented by Equation 1.1 where ***t*** is the required thickness in inches (1 inch=25.2mm) above a subgrade with subgrade strength indicated by CBR, ***P*** is a single-wheel load in pounds (1 pound=4.45 N) applied on the surface, ***A*** is the tire contact area in squared inches (1 in^2=645 mm^2), and $\boldsymbol{\alpha}$ is a factor correcting for load repetitions. This equation was derived to limit the subgrade shear failure due to aircraft loadings by adding a combined thickness of asphalt and unbound granular materials above the subgrade layer.

$$t = \alpha \sqrt{\frac{P}{8.1CBR} - \frac{A}{\pi}} \tag{1.1}$$

The value of $\boldsymbol{\alpha}$ is defined in Equation 1.2. The value ***C***, which is known as coverages, represents the number of effective repetitions and accounts for the natural wander distribution of traffic that occurs in real pavements. A detained explanation of coverages will be given later on in this document.

$$\alpha = 0.15 + 0.23 \log_{10} C \tag{1.2}$$

The CBR design procedure, in its existing form, was lacking the ability to expand as new pavement materials, ground vehicles and aircraft were introduced. Therefore, it became evident that the current formulation of the CBR procedure had to be changed and improved to accommodate these new requirements. An initial in-depth review of the CBR equation was undertaken following a formulation similar to the one initially presented by Ullidtz (1998). Equation 1.1 can also be expressed in the form of Equation 1.3, where ***r*** is the radius of a circular loaded area and ***p*** is the applied tire pressure.

$$\left(\frac{r}{t}\right)^2 = \frac{1}{\alpha^2\left(\frac{p\pi}{8.1CBR}-1\right)} \tag{1.3}$$

The vertical stress, σ_z in a half-space semi-infinite solid has been defined by Boussinesq, and is expressed by Equation 1.4.

$$\sigma_z = p\left(1-\left[1+\left(\frac{r}{t}\right)^2\right]^{-\frac{3}{2}}\right) \tag{1.4}$$

When the CBR equation described by Equation 1.3 is substituted into Equation 1.4, the vertical stress is derived from the CBR equation and Boussinesq stress model becomes Equation 1.5.

$$\sigma_z = p\left(1-\left[1+\frac{1}{\alpha^2\left(\frac{p\pi}{8.1CBR}-1\right)}\right]^{-\frac{3}{2}}\right) \tag{1.5}$$

In Equation 1.5, σ_z may now be considered to represent a limiting vertical stress value derived from the CBR equation. When this limiting vertical stress value is plotted against the subgrade CBR for tire contact pressures of 100-psi (690 kPa), 200-psi (1380 kPa), and 300-psi (2070 kPa) and 5000 coverages, the resulting curves are shown in Figure 1.1. It can be observed, that the curves for the varying tire pressures are nearly linear and independent of tire contact pressure for subgrade CBR values below 12.

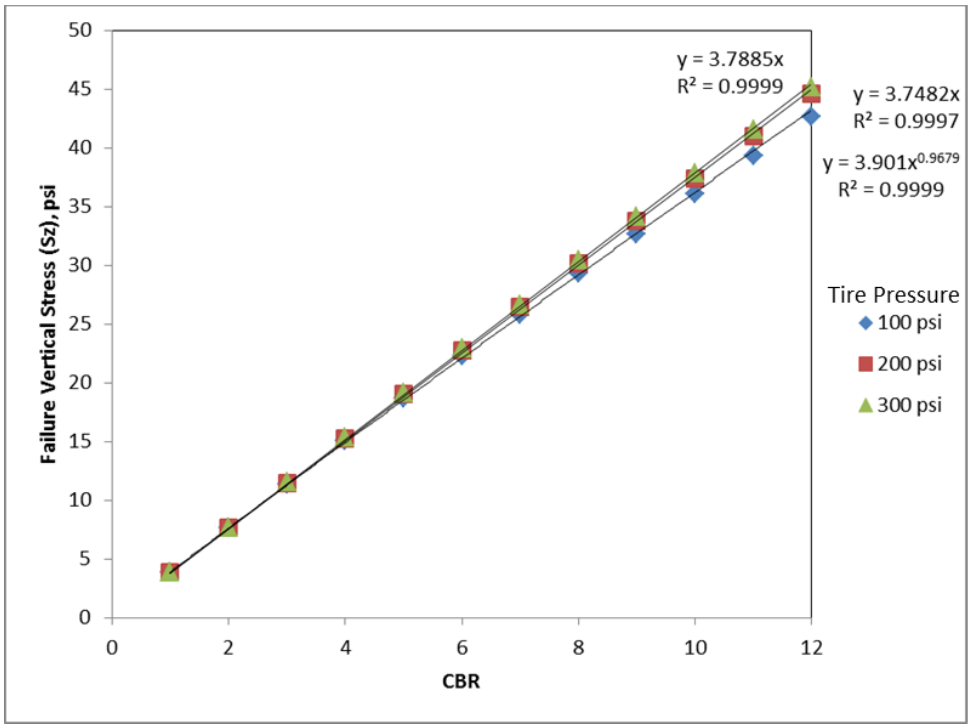

Figure 1.1 Relationship between CBR and vertical stress for CBR equation at varying tire contact pressures (1 psi = 6.9 kPa)

If the contact pressure is constant, for example at 100 psi (690 kPa), and the coverages levels are allowed to change, Equation 1.5 results can be shown as plotted in Figure 1.2. For the tire pressure and coverage levels used in this analysis, the vertical stress is not independent of the coverage levels. However, the coverage level curves are nearly linear and therefore their slopes, represented by the ratio σ_z /CBR, are only a function of the coverage levels.

Since the CBR is an index of the subgrade strength, the ratio σ_z /CBR, may now be considered to represent a limiting stress ratio. When the ratio σ_z /CBR is plotted against the coverage levels used in this analysis, the solid curve shown in Figure 1.3 may further be considered a transfer function based on vertical stress and CBR. Using this analytical approach, performance data from existing full-scale pavement experiments have also been plotted in Figure 1.3. It can be observed that the performance data line up very closely with the derived transfer function associated with the CBR equation. However, one important fact is that a specific stress distribution within a pavement structure was imposed by the use of the Boussinesq stress model.

The stress distribution from which the original CBR equation was derived was not known at the time of its development.

The analysis just described is a combination of a theoretical one-layer solution for vertical stress and the empirical derivation of flexible pavement thickness design curves from in-service and field tests. This implies that the methodology just derived inherits the same limitations of the current CBR equation. The ability to handle multiple layers still requires the utilization of equivalency factors. It is also assumed that all pavement layers are constructed according to the prescribed standards and that these upper layers will not suffer excessive shear deformation during traffic.

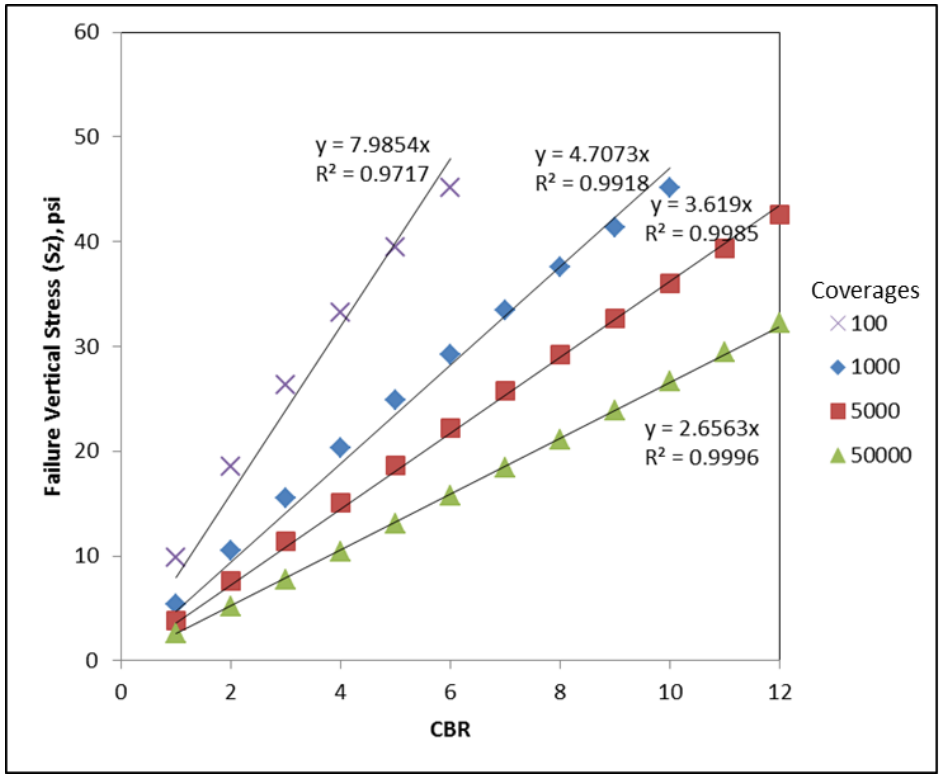

Figure 1.2 Relationship between CBR and vertical stress for CBR equation at varying coverage levels (1 psi = 6.9 kPa)

The results of the initial literature review and analysis pointed to the stress-based nature of the CBR design procedure and encouraged the author to further investigate the possibility of extending and improving the current implementation of the CBR design procedure. Since many

government agencies, especially the Army, Air Force and Navy, have a large investment in the CBR design technology, retaining some form of the CBR equation was deemed appropriate.

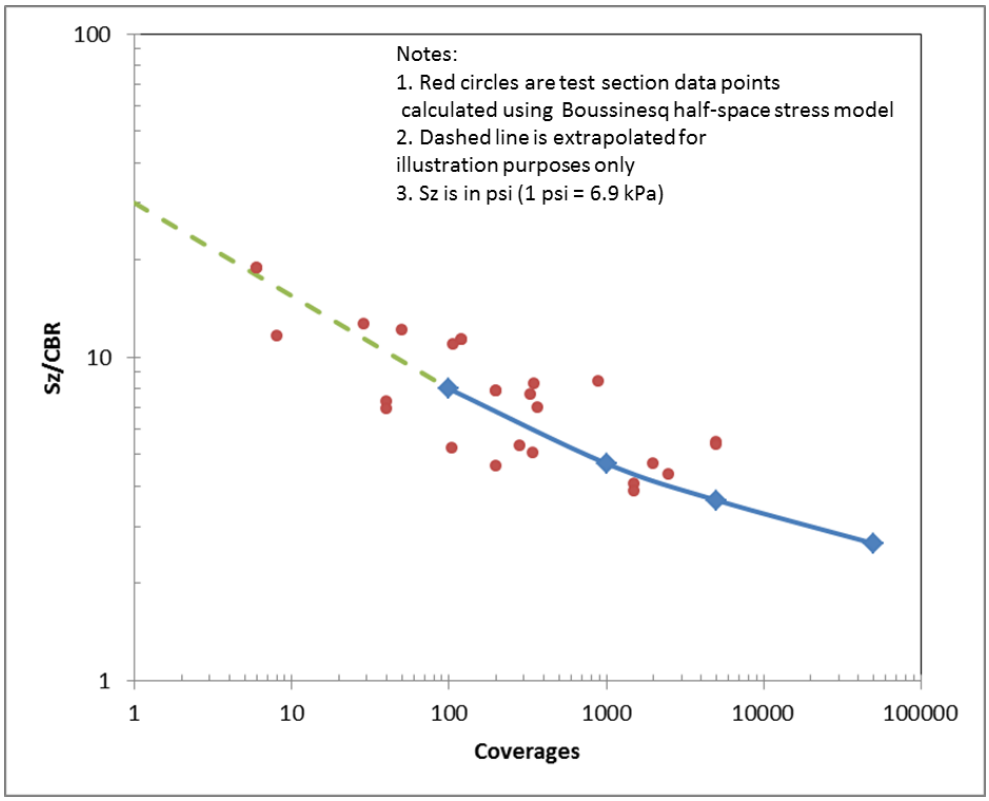

Figure 1.3 Stress-based transfer function derived of CBR equation and plotted against actual experimental

1.4 Objectives and Scope

A consequence of introducing any new methodology is that the proposed procedure has to be thoroughly reviewed, tested and validated. This research effort attempted to develop and validate a new stress-based design procedure using as its foundation the existing CBR design procedure. To accomplish this main objective, the following individual objectives or tasks were performed:

(a) Re-examine existing full-scale performance data and tailor performance data to proposed formulation;

(b) Express the CBR procedure in terms of the new stress-based CBR criteria;

(c) Validate stress distributions in constructed and trafficked flexible pavements;

(d) Validate the proposed stress-based CBR criteria; and

(e) Develop numerical models and software to incorporate solutions into a complete system for the design and evaluation of flexible pavement structures.

An experimental and analytical research effort was devised by constructing a full-scale flexible pavement test section at the U.S. Army Engineering Research and Development Center (ERDC) in Vicksburg, Mississippi. Flexible pavement test sections were constructed with different total pavement thicknesses, three different subgrade strengths, and three types of loading. All experimental test sections were instrumented with earth pressure cells and deflection gauges to measure pavement responses under loading. Traffic was applied with the ERDC Heavy Vehicle Simulator (Aircraft HVS-A), which has the capacity of applying gear loads up to about 110,000 lb (490 kN). Loads were applied to the test pavements with single F-15, single C-17 and dual C-17 aircraft tires. Stress distributions resulting from applied loads were examined and compared to predicted responses by the Fröhlich stress theory, layered elastic model and a non-linear finite element model. Multiple analyses were performed to assess the adequacy of the selected pavement response stress model to predict measured stresses. Results of these analyses helped validate the proposed stress-based CBR performance criteria.

1.5 Dissertation Outline

This dissertation is organized into nine chapters describing the origins of the CBR procedure, literature review, field testing and analyses performed to fulfill the objectives put forward. Detailed field and raw data used for the analyses and validation of the proposed stress-based CBR procedure are included in Appendices A through F. The following list of chapters provides a brief description of the content of each chapter.

- Chapter 1 presents a brief introduction along with the need, main objectives and scope of this dissertation.
- Chapter 2 presents detailed descriptions on the origins and history during the development of CBR design procedure as applied to military airfields.
- Chapter 3 contains descriptions of the pavement stress response models and theories of stress distribution used for the analyses of the test pavement sections constructed.

- Chapter 4 presents the mathematical derivation of the CBR equation expressed in terms of vertical stresses. Equations are presented relating the applied loading to corresponding pavement stress responses and their initial correlations to the proposed pavement field performance data.
- Chapter 5 presents the design, construction, and testing of full-scale pavement test sections with the purpose of collecting pavement response data to validate the proposed CBR-Beta procedure for the design of flexible pavements. A description of supplemental laboratory tests to characterize the pavement materials used in the test sections is summarized together with detailed information on instrumentation, traffic and loading patterns.
- Chapter 6 presents analyses of the relevant laboratory tests, test section data, traffic tests and modelling effort conducted in this research effort. Comparisons of predicted and measured stresses are presented for the different pavement models used in this research study. The performance of all test pavements is analyzed in terms of traffic cycles to failure and presented in terms of the CBR-Beta criteria.
- Chapter 7 presents a refinement of the initially proposed CBR-Beta criteria after a field case study proposed modifications at low levels of traffic. This chapter also summarizes the procedure used for the implementation framework of the proposed stress-based CBR procedure and its extendibility to modern cumulative damage concepts.
- Chapter 8 lists a number of conclusions derived from this research along with recommendations for future research.

CHAPTER 2 - ORIGINS OF THE CBR DESIGN PROCEDURE

2.1 Historical Perspective

The very beginning of the Army's involvement with the CBR procedure for the design of flexible airport pavement is well documented by Lenore Fine and Jesse A. Remington (Fine and Remington 1972). The Army's work on the CBR procedure began on 6 May 1941 when the newly assembled XB 19 aircraft was rolled out from the Douglas Hangar at Clover Field, Santa Monica, California and broke through the hangar apron pavement to a depth of about one foot (30.48 mm). After the aircraft was towed, with considerable difficulty, to one of the airport's asphalt runways, the aircraft caused noticeable damage as it taxied over the pavement surface. Not until June 27, 1941, when a recently laid concrete pavement was ready for use, did the XB 19 takeoff on its maiden flight to March Field, California. Colonel Kelton of the Los Angeles District reported to General Schley (Chief of Engineers) about the landing at March Field:

"No marking or imprint was evident at the point of landing, but as the ship lost speed, a faint depression and hairline cracks appeared, increasing in severity as the speed was further reduced. At the point where the ship turned to cross the oil-earth landing mat onto the apron, the depressions were at one inch in depth and the cracks quite large."

Colonel Kelton recognized the magnitude of the pavement problem, since he pointed out that the plane was lightly loaded and conditions were ideal—the weather was dry and the ground water table was low. He warned that worse damage was likely to occur, and after heavy rains, "extreme damage" could result from landings by a fully loaded XB 19 aircraft.

As a result of the experience with the XB 19, the Chief of the Air Corps, General Brett, insisted that runways should be of the heaviest construction, and in June 1941, he demanded that all new military airstrips should be constructed of Portland cement concrete with beam strength characteristics. General Brett's runway specifications were: adequate bearing capacity under very heavy loads, high skid resistance, and good visibility for night landings and easy

maintenance. General Plank of the Army Engineers considered General Brett's standards to be wholly unacceptable. General Plank stated, "*They wanted to introduce artificial concepts into engineering such as 'no runway will be built except out of concrete with Portland cement"*. But there are other ways to build runways, and we, the Engineers, would not go for that kind of thing." In an appeal to the construction agency, G 4, on 25 July 1941, Plank asked that engineering decisions be left to the Engineers. Stating that asphalt pavements could be designed to carry even the heaviest planes, he insisted that the surface textures could be altered to increase frictional resistance and the surface colors lightened to enhance visibility. He contended, high-type asphalt runways could be maintained almost as cheaply as concrete. Deciding in favor of the G 4, General Reybold handed down the ruling: airmen would state their functional requirements and Engineers would take it from there.

When General Schley retired as Chief of Engineers on 1 October 1941, a broadly conceived investigative effort was underway. Formulated by the Engineering Section, Office, Chief of Engineers (OCE), under William H. McAlpine, this effort had a five-fold mission:

- Insure adequately designed airports
- Eliminate wide variation in designs
- Limit the use of unproven theories
- Maintain competition between materials
- Lay the basis for further development of pavement criteria through behavioral studies

The overall objective was to write a new chapter in civil engineering and a sizable team of investigators was assigned to this mission. Two of the Corps' foremost technologists, hydraulic engineer Gail A. Hathaway and soils engineer Thomas A. Middlebrooks, (who was later to become a noted leader in the development of pavement design technology) were assigned to assist in Washington, DC. The research staff of the Waterways Experiment Station (WES) in Vicksburg, MS, was assigned responsibility for undertaking a series of special studies and district offices throughout the country began conducting tests and experiments. Because the civil organization could not provide all the needed skills, McAlpine brought in specialists from outside the Corps; among these recruits were James L. Land, a mainstay of the Alabama State

Highway Department since 1910, and Walter C. Ricketts, a chemical engineer who had worked for the Asphalt Institute. A number of prominent consultants also joined in the endeavor.

Because of General Brett's strong preference for concrete, the engineers gave close attention to rigid pavements. In 1926, H. H. Westergaard, Dean of Graduate Engineering at Harvard University, had published a theory for determining stresses produced by rolling loads. Dean Westergaard was concerned more with the validity of his analysis than with its application. Explaining his attitude, he told one engineer, "I have developed a theory, and it is mathematically sound, but whether it fits the facts of nature is up to you to prove." In fact, for validation purposes, McAlpine's primary goal was to verify Westergaard's theory by experiment. McAlpine's investigative plan called for large-scale tests at Wright Field, Ohio and control tests at Langley Field, Virginia. Even before the field experiment was fully underway, a family of rigid pavement design curves was developed using Westergaard's equations. Then, as data became available from the tests at Wright and Langley, the curves were adjusted. Design curves for wheel loads up to 60,000 lb (267 kN) were soon in use throughout the Corps. Only after further tests with different sets of variables would the curves find a place in the military Engineering Manual.

Concurrent with tests on rigid pavements, tests were being conducted on flexible pavements. There was little agreement among highway engineers as to how flexible pavements ought to be designed. Various design methods were implemented, all of them were empirical and none of them proven for wheel loads beyond 12,000 lb (53 kN). Because the problem was primarily related to soils, McAlpine turned it over to his soils experts, Thomas A. Middlebrooks and George E. Bertram. Both were solidly grounded in the theory of soil mechanics. Middlebrooks had done graduate work in the new science under Dr. Karl von Terzaghi at MIT and Bertram under Dr. Arthur Casagrande at Harvard. Their early efforts were exploratory. After a cursory look at the methods of state roads departments, their first surmise was that load bearing tests might be the answer.

Middlebrooks and Bertram began their effort with a study of load bearing test characteristics and execution. The two researchers examined plate load tests by trying plates of

different sizes, different rates of loading, and different ways of interpreting results. In addition to the plate loading tests, Middlebrooks and Bertram studied pavement failures at Tri-Cities Airport near Bristol, Tennessee. In a paper presented to the Highway Research Board in December 1941, Middlebrooks and Bertram reported two important discoveries. Their first discovery was that the allowable deflection for asphalt bomber strips would be far smaller than for asphalt roads. Their experiment showed that this deflection was 0.2 inch (5 mm) in contrast to the Asphalt Institute recommended value of 0.5 inch (13 mm). The second discovery was that load bearing tests produced unsatisfactory outcomes.

When Lieutenant Colonel James H. Stratton reported for duty in December 1941 as head of the Engineering Branch, he found only fragmentary data on airport design. Deeply concerned, Stratton gave close attention to the investigative effort. Immersing himself in the details of flexible pavement research, he quickly learned where matters stood. Kemp, project engineer at OCE, gave him a rundown on the Langley Field endeavor: experimental sections, designed with the help of the Asphalt Institute, were nearing completion; tests would soon commence. However, Kemp was pessimistic about the outcome, for he questioned the institute's claim that thick bituminous surfaces provided measurable beam strength. In briefing their new chief, Middlebrooks and Bertram pointed to a possible solution. Their study of state highway practices had led them to conclude that the California method, strongly backed by Land, Alabama State Highway Department representative called as consultant for the project, held considerable promise. Middlebrooks was in correspondence with Thomas E. Stanton, Materials and Research Engineer of the California Division of Highways, and Bertram had been to Sacramento to confer with the originator of the method (the California method for design of flexible pavements), O. James Porter, and Stanton's assistant.

The Langley tests were decisive. In February 1942, the Virginia airbase was bustling with activity. Each agency had its own representative on the field. Robert F. Jackson was there from the Louisville District to direct the experiments. Frederick C. Field was there as an observer for the Asphalt Institute, and Bertram was there from Washington as Stratton's representative. A scraper was filled with dirt to apply loads of 13,000 lb (58 kN) on the front tires and 20,000 lb (89 kN) on the rear tires. After 25 passes, 6 of the 14 test sections had begun

to rut; after 50 passes, 10 of the sections had failed, and the rest had developed a definite wave. Designed supposedly for wheel loads of 60,000 lb (267 kN), the Langley pavements rapidly deteriorated under loads of 20,000 lb (89 kN). On reading Bertram's report of the experiment, Stratton decided to stop theorizing and to send for O. James Porter at once.

As a junior engineer for the California Division of Highways in the late 1920's, Porter had investigated pavement failures throughout the state. Most of the trouble stemmed from porous, loosely compacted soil, which took up moisture, became plastic and remolded as wheels rolled over the pavement. Porter thought of the untouched lodes of disintegrated granite in the mountains of California and the large deposits of gravel in the river valleys. Compacted fills of these materials topped by thin wearing courses seemed to him the common-sense prescription for inexpensive and durable roads. He devised a simple procedure, the California Bearing Ratio (CBR) test, for measuring the shear resistance of base and subbase materials. Experience proved that his test could be relied upon. He also helped to originate a superior method of compaction control, the modified density test associated with the name of Ralph R. Proctor. Porter was able to develop curves showing the relationship between bearing ratios and pavement thicknesses for wheel loads up to 12,000 lb (53 kN) and to correlate these curves with field performance. During a trip to Washington, Porter decided to offer Stratton a compaction method, CBR test, and curves for heavy wheel loads derived from traffic tests.

Porter was deep in conversation with Middlebrooks and Bertram and found their ideas were far apart. Stratton sent for Dr. Arthur Casagrande, a world renowned figure in the field of soil mechanics and foundation engineering. After lengthy talks with Middlebrooks and Porter, Casagrande suggested a procedure. Extrapolating Porter's curves was the first order of business. Working separately and using different methods, they plotted tentative curves for wheel loads up to 70,000 lb (312 kN). After comparing notes, they found that their results were close. They then began planning a series of tests for checking their extrapolations.

The test program was labeled "crash." Early in March 1942, Stratton issued rush orders to five division engineers. Four were to investigate pre-war commercial runways, which had been down long enough for the subsoil moisture to equalize. Colonel Bragdon in the South

Atlantic Division was to choose an airstrip built on sandy clay, a fairly good subsoil; Colonel Scott in the Southwestern Division, one of lean black clay, a rather poor foundation; Colonel Elliott in the Upper Mississippi Division, one on Fargo clay, a highly plastic material; and Colonel Besson in the Missouri River Division, one on a porous subgrade subject to frost action. Tournapulls with wheel loads of 12,500 lb to 50,000 lb (56 kN to 222 kN) would be towed over the pavements until failure occurred or 10,000 runs had been made. Each experiment would test one point on the extrapolated curves. Broader in scope and critically important was the task given Colonel Hannum in the South Pacific Division. At Stockton Air Base, near Sacramento, Porter would conduct a crucial test. Stockton's original runway, built by the city in 1936, had failed during the winter of 1940-1941 under the weight of light Army training aircraft. An abandoned taxiway nearby, constructed at the same time and along the same lines remained intact. The subgrade was adobe, the base course was six inches of compacted sandy loam, and the surface was a seal coat of emulsified asphalt. The plan was to test the taxiway and a special, Porter designed-section to be built on top of the taxiway.

In a short period of time, Stratton had telegrams reporting the progress of tests on commercial runways at Dothan, Alabama; Corpus Christi, Texas; Fargo, North Dakota; and Lewistown, Montana. In the meantime at Stockton, Porter and company set a blazing pace. On 10 March, Bertram arrived in Sacramento and gave the signal to begin. By the 13th, deflection gages were in place, and Porter was taking readings as a light aircraft taxied over the pavement. By the 20th, the surface had developed hairline cracks, and Porter had seen enough to know that the pavement was incapable of withstanding deflections of 0.1 inch (2.54 mm) or even 0.05 inch (1.27 mm). Construction of the test section started the following day. Built to Porter's specifications (a thoroughly compacted base course of sand and gravel, increasing gradually in thickness from 6 inches to 48 inches (152 mm to 1219 mm) and topped by 3 inches (76 mm) of asphalt concrete), the section was complete on the 24th. Tests proceeded rapidly, first with Tournapulls exerting wheel loads of 5,000 lb (223 kN), 10,000 lb (445 kN), 25,000 lb (111 kN) and 40,000 lb (178 kN) and then with a B-24 Liberator bomber. By early April, the experiment had shown that the extrapolated curves were fairly accurate and that allowable deflection was in hundredths rather than in tenths of an inch.

Early in April, Porter faced a skeptical group, the senior soils men of the engineer divisions who had come to Sacramento for a 5 day course in the California method. At the end of the course, one student, styling himself as the principal objector, declared, *"Engineering starts with theory, and the California method has no foundation whatever in theory."* In reply to his critics, Porter pointed out, *"We are not contending that this tentative design is accurate, but that it is the simplest and most practical method now available."* The news from Sacramento created quite a stir in professional circles. Reports of the meeting, passed by word of mouth, raised eyebrows and produced sharp critics. Professors, researchers and state highway officials were frankly dubious. Most foundations experts took a "wait and see" attitude. The Air Corps' Buildings and Grounds Division was "inclined to be skeptical," and the Navy's Bureau of Yards and Docks was openly opposed. Probably the most strenuous objections came from the Asphalt Institute. At several conferences with Middlebrooks and Bertram, Asphalt Institute representatives argued unsuccessfully for thicker asphalt pavements and thinner base courses than Porter prescribed. All those who challenged the Corps' approach received the assurance:

> *"It has never been the policy of the Engineer Department to standardize to the extent that research and development would be stifled, and we don't want to do that now."*

Research contracts with Harvard and MIT testified to the Corps' interest in developing a rationale, but to evolve a theory might take years. The CBR procedure was available and workable, and Stratton intended to use it. Tests at Stockton would continue, and a chapter on flexible pavement design, soon to appear in the Engineering Manual, would set the Corps' seal of approval on the California method.

2.2 Extrapolations of California Design Curves

With the acceptance of the California method for the design of flexible pavements for heavy bomber aircraft, the Corps was faced with the problem of extrapolating the highway design curves to design curves appropriate for airfield pavements. In 1942, the California procedure was based on two design curves: Curve A used for light and medium traffic and Curve B used for light traffic (Porter 1949). The curves as presented by Porter are shown in Figure 2.1.

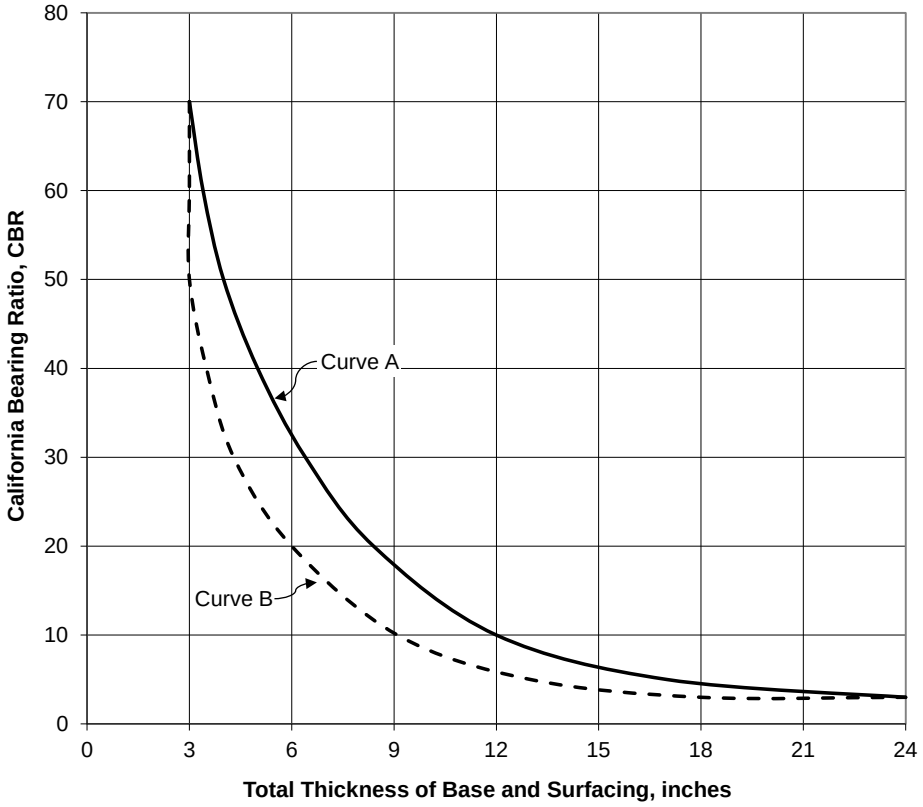

Figure 2.1 Total thickness of base and surfacing in relation to CBR values (after Porter, 1949, 1 inch=25.4 mm)

At the time of selection of the California method, the design curves A and B were not associated with a particular wheel load—only light and medium traffic. Although the highway curves were originally drawn for lighter wheel loads, it was known from service behavior of the pavements that 9,000-lb (40 kN) truck loads were supported without distress throughout the life of the pavement (Middlebrooks 1950). Using engineering logic based on differences between highway traffic and airfield traffic, it was decided that Curve A, would represent a 12,000-lb (53 kN) airplane wheel load, and Curve B would represent a 7,000-lb (31 kN) wheel load. The 7,000-lb (31 kN) wheel load was chosen as the load for Curve B, since this load was the approximate wheel loading of training planes and represented the lightest traffic requirement for airfields (Middlebrooks 1950). It was believed that Curve A was considered the most reliable; therefore, it was used as a basis for the extrapolation.

Selection of the methodology for extrapolating the curves was based on the results of static load tests and engineering logic. Static load tests had shown that the deformation under wheel load of an adequately designed flexible pavement is comprised of three factors: settlement of the subgrade, compaction of the base and the surface, and elastic deformation (Middlebrooks 1950). By engineering logic, shear deformation was eliminated because in a satisfactory pavement because the shearing stress does not exceed the shearing strength. Service behavior records of adequate pavements had indicated that it was necessary for elastic deformation to govern over an extensive period of use. Accordingly, the Office of Civil Engineering (OCE) decided to develop empirical curves by extrapolating the original data on the basis of the elastic theory (Middlebrooks 1950). It was further reasoned that since all bearing tests are essentially shear tests and since shear deformation must be eliminated in a satisfactory pavement, shear stresses should be used as the guide in making the extrapolation.

Based on a review of airplane tire data, a uniform tire pressure of 60 pounds per square inch (414 kPa) was determined to represent airplanes in use at the time of the analysis. Wheel loads of 25,000-lb (111 kN), 40,000-lb (178 kN), and 70,000-lb (1778 kN) were selected to cover the range of heavy aircraft loads. Contact areas, represented by a circular shape, were computed from wheel loads and tire pressures. Stress tables, published by Leo Jurgenson in 1934, permitted the computations of shear stress distribution with depth for the different wheel loads as shown in Figure 2.2 (Middlebrooks 1950).

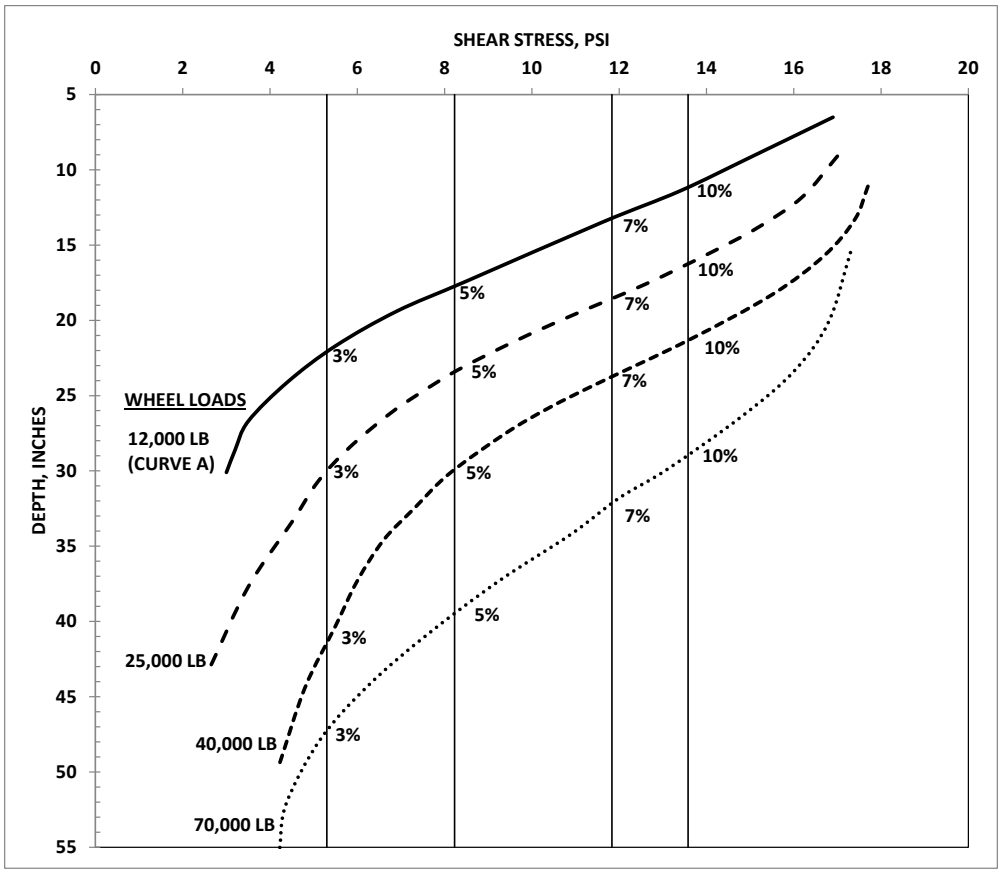

Figure 2.2 Extrapolation of highway pavement thicknesses (Middlebrooks 1950)
(1 lb=4.45 N, 1 inch=25.4 mm, 1 psi=6.9 kPa)

Using Curve A from Figure 2.1, the pavement thicknesses required to support heavy highway traffic for various values of CBR were determined. These thicknesses and the stress distribution curve for the 12,000-lb (53 kN) wheel load allowed the determination of the shear stress at the top of the subgrade for each CBR. The shear stress determined in this manner represented the allowable shear stress for the respective CBR using the allowable shear stresses and stress distribution curves for each of the tire loads. These were the preliminary design curves developed and presented at a meeting of consultants in Washington, DC, which included engineers from the OCE, Porter, and Professor Casagrande. The consultants had each made independent calculations to extrapolate the basic curves. Those of Porter were based on an allowable deformation, whereas those of Professor Casagrande were based on relationships between the relative sizes of the loaded areas. The three sets of computations were in substantial agreement. It was decided that the average thicknesses shown by the three extrapolations were

reasonable for the low CBR values; however, the majority of the members agreed that the less conservative values should be chosen for the higher CBR values (Middlebrooks 1950). The tentative design curves, shown in Figure 2.3, were developed from the three extrapolations and the best judgment of the OCE engineers and consultants.

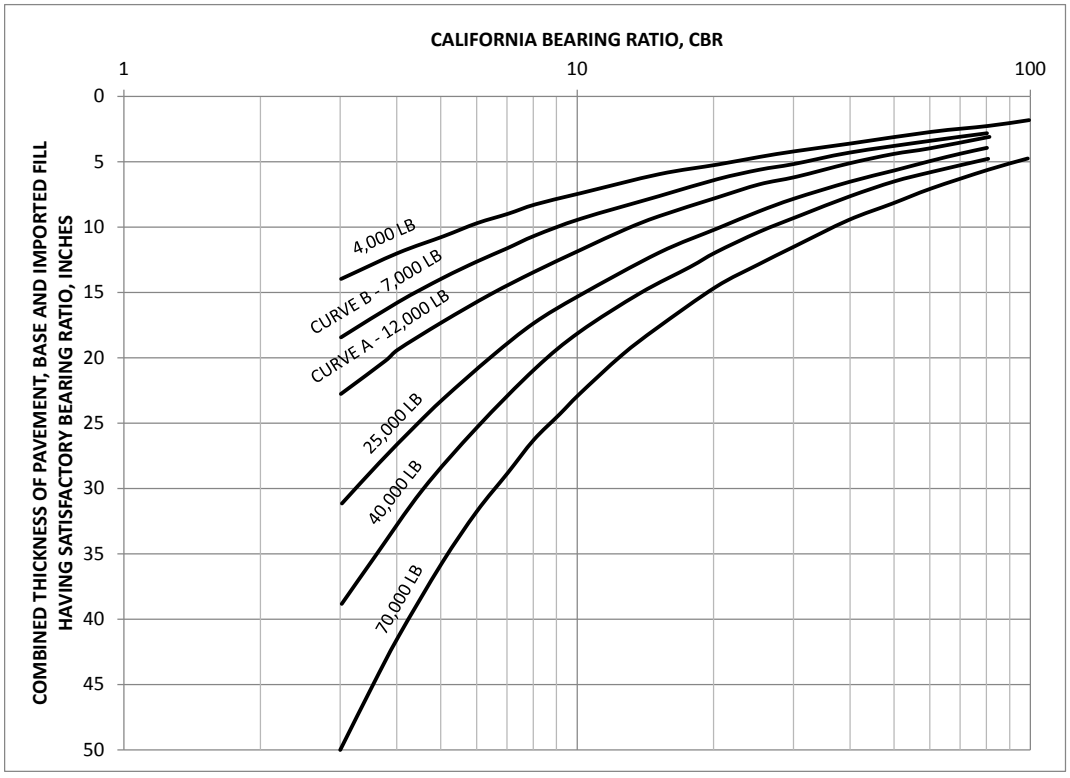

Figure 2.3 Tentative design curves for flexible pavements (after Porter 1949) (1 inch=25.4 mm, 1 lb=4.45 N)

Although the engineering logic applied in the extrapolation may be slightly flawed, in that shear deformation in a flexible pavement can never be completely eliminated but is only reduced to an acceptable amount for a given number of aircraft loadings; the logic does set the foundation for the CBR procedure for design of flexible pavements. This foundation can be stated as a methodology that provides sufficient thickness of pavement structure above each point in the pavement to reduce the shear deformation in the pavement to an acceptable amount.

2.3 Validation of Tentative Design Curves

Immediately after adopting the tentative CBR design curves for design of flexible pavements, efforts were undertaken to validate the curves. The first effort at validation, as reported by Fine (Fine and Remington 1972), was to conduct load tests at existing airfields, and to construct a special pavement test section for traffic testing at the Stockton Airbase. The initial results of the test verified the curves sufficiently to include the curves in the Corps' Engineering Manual. An important outgrowth of the research effort for verifying the California design procedure was the establishment, in 1943, of the Flexible Pavement Laboratory at WES.

Early in the investigation, W. J. Turnbull, Chief of the Soils Division at the WES, had been assigned the task of performing an analysis of the CBR test procedure. By spring of 1943, WES had emerged as the leading center of flexible pavement research. Because of the growing research need, Turnbull recruited foundation experts, Charles R. Foster and William H. Jervis, and experienced highway engineer, John F. Redus, Jr.; W. Keith Boyd, a pioneer in flexible pavement design, was hired to head the research effort. Boyd quickly increased the staff of the research group, and before long, the team reached 25 in number. Two notable additions to the staff were Bruce G. Marshall and Richard Ahlvin. During the latter part of 1943, a long-range research program had been launched, which included laboratory and field investigations of base course design, compaction methods, and moisture conditions under pavements of asphalt surfaces (Fine and Remington 1972). Of the eleven papers presented in the 1950 symposium on the Development of CBR Flexible Pavement Design Method for Airfields, six were written by personnel from the WES. In the symposium, the paper by Foster listed some 93 lines of data that were used for the development of design curves for single wheel loads. Even with the extensive testing and evaluation of flexible pavements, the tentative design curves remained virtually unchanged through 1949 (Middlebrooks 1950; Ahlvin 1991).

2.4 Development of California Bearing Ratio (CBR) Equation

In a letter dated 5 August 1949 from the WES to the OCE concerning studies pertaining to the CBR design curves, it was stated that:

"…the Flexible Pavement Laboratory has attempted to reduce the family of curves to a single formula. Such a step would give a better understanding of the functions of each of the variables and would aid in comparing the empirical data for failed and satisfactory pavements. The Flexible Pavement Laboratory has tried several schemes, but in most cases the deviation from the existing curves was excessive. The best scheme developed so far was presented as a discussion paper to the CBR Symposium by Mr. Fergus."

In the discussion, Fergus (ASCE, 1950) made the assumption that for a constant contact pressure, the ratio of the thickness to the radius of the loaded area is a constant. Fergus expressed the relationship by the equation:

$$\frac{z}{r} = a \quad or \quad z = ar = a\sqrt{\frac{P}{\pi p}} = \frac{a}{\sqrt{\pi p}}\sqrt{P} = K\sqrt{P} \tag{2.1}$$

where:

z = thickness of required pavement

a = arbitrary constant

r = radius of loaded area

P = total wheel load

p = contact pressure

K = constant when $\boldsymbol{a}$ and $\boldsymbol{p}$ are constants

From Equation 2.1 the value of K is seen to be:

$$K = \frac{z}{\sqrt{P}} \tag{2.2}$$

Using Equation (2.2) and pavement thicknesses, as determined from the design curves in the Engineering Manual and the Stockton Test section No. 2, Fergus was able to develop the data given in Table 2.1.

Table 2.1 Pavement Thickness[1] Required for a Given Wheel Load(from "Mathematical Expression of the CBR Relations, COE Technical Report No. 3-441, November 1956)

CBR	5,000 lb		15,000 lb		40,000 lb		70,000 lb		150,000 lb		200,000 lb		Average *K*
	t	*K*	*t*	*K*	*t*	*K*	*t*	*K*	*t*	*K*	*t*	*K*	
3	14.0	0.198	25.0	0.204	37.5	0.188	49.6	0.187	75.0	0.194	89.5	0.200	0.195
4	12.2	0.173	21.4	0.175	31.7	0.159	40.7	0.154	64.0	0.165	75.5	0.169	0.166
5	11.0	0.156	18.8	0.154	27.7	0.139	36.0	0.136	56.5	0.146	66.5	0.149	0.147
6	9.9	0.140	16.9	0.138	24.9	0.125	32.2	0.122	50.7	0.131	60.0	0.134	0.132
7	9.2	0.130	15.4	0.126	22.8	0.113	29.3	0.111	46.0	0.119	54.5	0.122	0.120
8	8.5	0.120	14.1	0.115	20.7	0.104	26.9	0.102	42.5	0.110	50.5	0.113	0.111
9	8.0	0.113	13.0	0.106	19.2	0.096	25.0	0.094	39.8	0.103	47.0	0.105	0.103
10	7.5	0.106	12.1	0.099	17.9	0.090	23.3	0.088	37.3	0.096	44.4	0.099	0.096
15	5.4	0.076	8.9	0.073	13.4	0.067	17.9	0.068	29.0	0.075	35.0	0.078	0.073
20	---	---	6.7	0.055	10.6	0.053	14.7	0.056	25.0	0.065	28.8	0.064	0.059
30	---	---	---	---	6.9	0.035	10.5	0.040	19.5	0.050	20.9	0.047	0.043
40	---	---	---	---	4.4	0.022	7.6	0.029	16.5	0.043	16.3	0.036	0.033
50	---	---	---	---	---	---	5.6	0.021	14.0	0.036	13.3	0.030	0.029
60	---	---	---	---	---	---	---	---	12.5	0.032	11.2	0.025	0.029
70	---	---	---	---	---	---	---	---	---	---	9.5	0.021	0.021
80	---	---	---	---	---	---	---	---	---	---	8.3	0.019	0.019
90	---	---	---	---	---	---	---	---	---	---	7.4	0.017	0.017
100	---	---	---	---	---	---	---	---	---	---	6.6	0.015	0.015

[1] Pavement thickness ***t,*** is in inches (1 inch=25.4 mm, 1 lb=4.45 N)

Fergus observed that for a given CBR the value of K could be considered, for all practical purposes, to be constant. Using the average value of K, Fergus developed design curves in Figure 2.4, which he compared with the design curves in the design manual (Figure 2.3) and with the tentative curves for loads from 5,000 to 200,000 lb (22 kN to 890 kN). He also used test data from pavement performance studies to validate the design curves. Figure 2.5 indicates that the

relationship between CBR and K tends to divide the data between failed and satisfactory pavements.

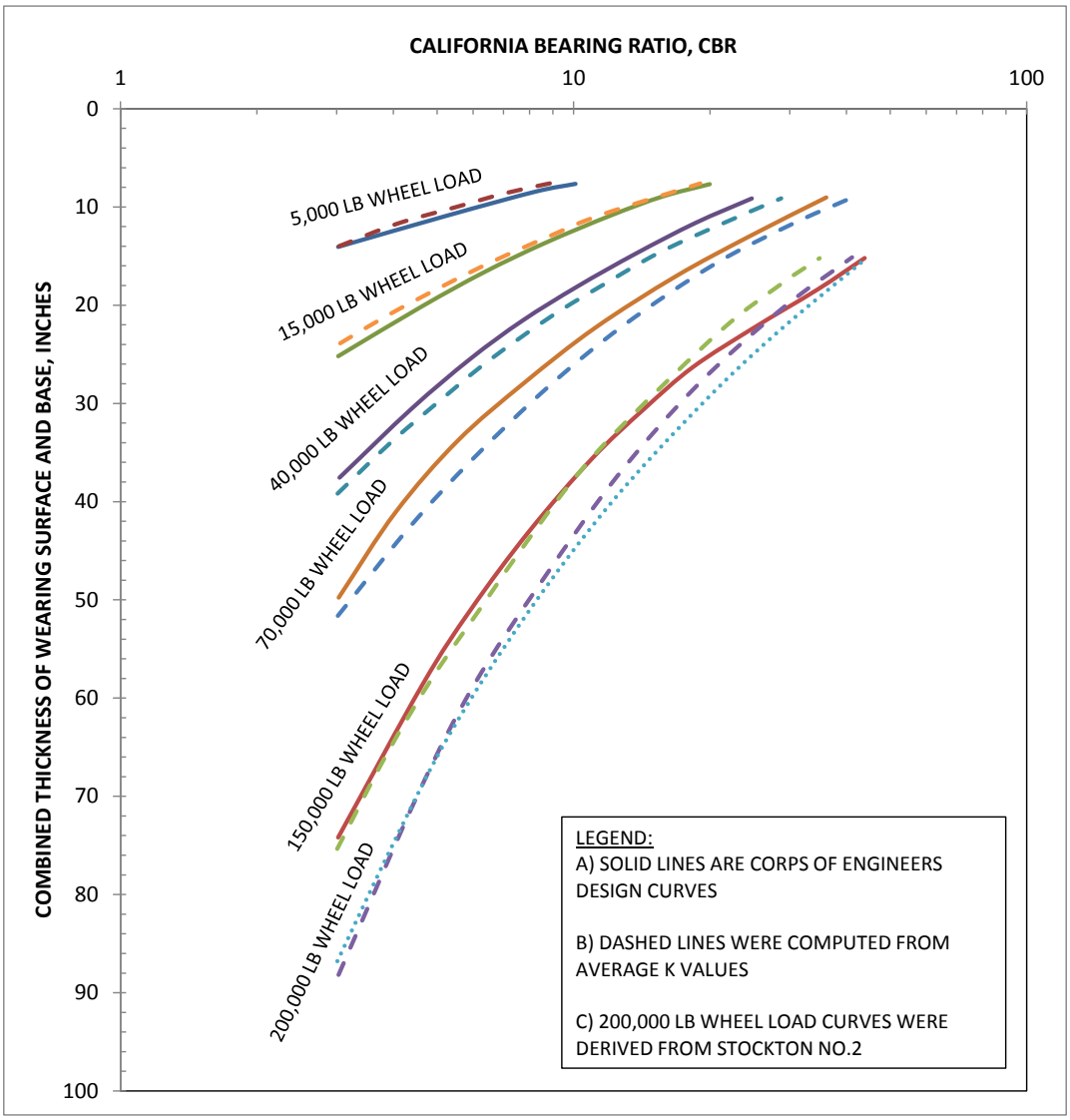

Figure 2.4 Comparison of existing design curves with curves from K-values (after Fergus 1949) (1 inch=25.4 mm)

Fergus noted in his analysis that no value of contact pressure had been assigned to the criteria, although it had been designated as a constant. By reviewing the data and assumptions in deriving the design curves, Fergus considered the curve presented in Figure 2.5 to be valid for contact pressures up to and including at least 100 psi (690 kPa).

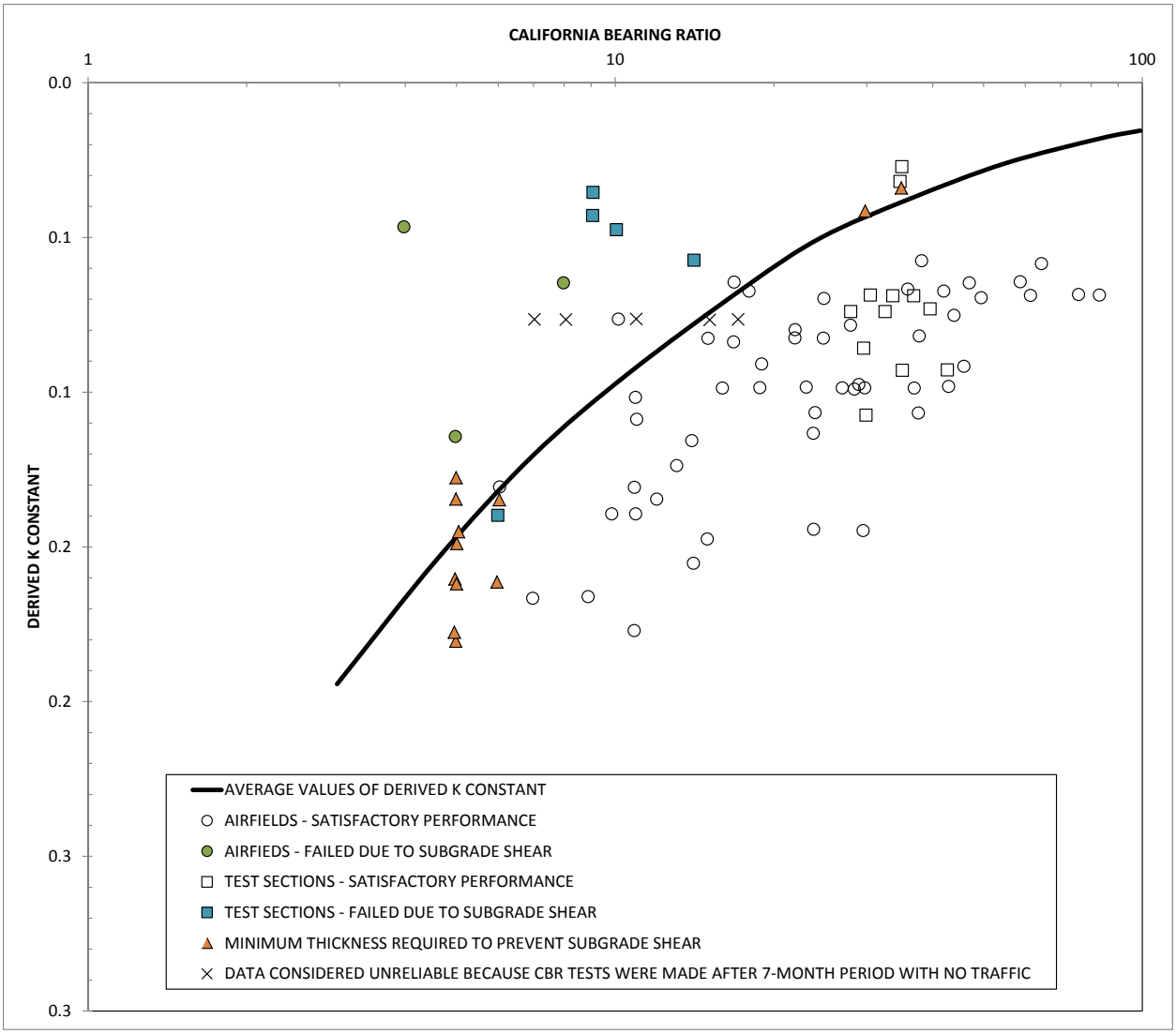

Figure 2.5 Correlation of design curve with airfield evaluation data (after Fergus 1949)

In a letter dated 5 August 1949, the WES presented a set of design curves that were proposed for the design of flexible pavements. Concerning the curves, the following explanations were given:

> *"These curves include the adjustments to give a constant K value for CBR values of 10 and less. It will be noted that the curves of 10 and less consist of parallel straight lines, which is to be expected since these can be expressed by the formula given previously. The curves for CBR values above 10 cannot be expressed in this manner, and straight line plots were not used. These curves are well validated up to a wheel load of about 50,000*

lb (222 kN), but the curves above 50,000 lb(222 kN) have been drawn to tie into the data from Stockton Test No. 2."

Thus, it is seen that the expression developed by Fergus was accepted as valid up to a CBR of approximately 10 percent. Another letter dated 5 December 1949, from the WES to the OCE addressed the issue of adjustment of single-wheel design curves to higher tire pressures. The adjustment from the low tire pressure to the higher tire pressure was made by increasing the required thickness of a base and pavement a sufficient amount so that the theoretical deflections produced by the tire with the higher pressure would equal the theoretical deflections produced by the tire with the lower pressure. The theoretical deflections were based on Boussinesq formula (Equation 2.3) applicable to a semi-infinite elastic solid with a Poisson's ratio of 0.5.

$$w = \frac{3P}{2E(r^2+z^2)^{\frac{1}{2}}} \tag{2.3}$$

where:

w = deflection under the center of the loaded area

E = modulus of elastic of semi-infinite solid and,

P, r, z = have been previously defined.

The same letter stated, if r and z represent the values for 100 psi (690 kPa) tire pressures and r_1 and z_1 are values for any given higher pressure, then from Equation 2.3 at equal deflections it follows that:

$$r^2 + z^2 = r_1^2 + z_1^2 \tag{2.4}$$

The WES report (WES 1956) described the efforts which resulted in the development of the classical CBR equation. The engineers engaged in the defining the direction and accomplishment of this work included Messrs. Turnbull, Foster, and Ahlvin. The report showed the relationship, given in Equation 2.5, linking pavement thickness, load and tire pressure.

$$\frac{t^2}{P} + \frac{1}{p\pi} = D \tag{2.5}$$

where

D = constant

t = thickness

P, p = have been previously defined.

From Equations 2.2 and 2.5, it was apparent that the relationship between D and K could be expressed by Equation 2.6.

$$D = K^2 + \frac{1}{p\pi} \tag{2.6}$$

Following the work of Fergus, values of K for 100 psi (690 kPa) and 200 psi (1380 kPa) design curves were determined. Given the values of K and Equation 2.6, the values of D could be computed for the different values of CBR. The product of D and CBR was found to be substantially constant for CBR values below about 10 to 12. Table 2.2 contains the data used to develop the constant to represent the product of D and CBR. According to the 1956 WES report, the average value of the product of D and CBR was 0.1236 and had the units of square inches per pound (mm^2 per N). Equation 2.7 shows the relationship between D and CBR.

$$D = \frac{0.1236}{CBR} \quad in \quad \frac{in^2}{lb}\left(145x\frac{mm^2}{N}\right) \tag{2.7}$$

Equation 2.7 can also be written as,

$$D = \frac{1}{8.1CBR} \quad in \quad \frac{in^2}{lb}\left(145x\frac{mm^2}{N}\right) \tag{2.8}$$

Table 2.2 Average values of Constant K as function of CBR for 100 psi (690 kPa) and 200 psi (1380 kPa) tire contact pressure

	Values of K		Values of K^2		Values of $D = K^2 + 1/(p\pi)$		Values of D x CBR	
CBR	100-psi	200-psi	100-psi	200-psi	100-psi	200-psi	100-psi	200-psi
3	0.195	0.199	0.0380	0.0396	0.0412	0.0412	0.124	0.124
4	0.166	0.171	0.0276	0.0292	0.0307	0.0308	0.123	0.123
5	0.147	0.152	0.0216	0.0231	0.0248	0.0247	0.124	0.123
6	0.132	0.138	0.0174	0.0190	0.0206	0.0206	0.124	0.124
7	0.120	0.126	0.0144	0.0159	0.0176	0.0175	0.123	0.122
8	0.111	0.118	0.0123	0.0139	0.0155	0.0155	0.124	0.124
9	0.103	0.110	0.0106	0.0121	0.0138	0.0137	0.124	0.123
10	0.096	0.104	0.0092	0.0108	0.0124	0.0124	0.124	0.124
12	0.085	0.093	0.0072	0.0087	0.0104	0.0102	0.125	0.123

Table 2.2 Average values of Constant K as function of CBR for 100 psi (690 kPa) and 200 psi (1380 kPa) tire contact pressure								
15	0.073	0.082	0.0053	0.0067	0.0085	0.0083	0.128	0.125
17	0.067	0.075	0.0045	0.0056	0.0077	0.0072	0.130	0.123
20	0.059	0.068	0.0035	0.0046	0.0067	0.0062	0.133	0.124

The value of D can be substituted into Equation 2.5 to yield Equation 2.9, which results in one forms of the CBR equation.

$$t = \sqrt{P\left[\frac{1}{8.1CBR} - \frac{1}{p\pi}\right]} \tag{2.9}$$

By using the relationship between tire pressure and contact area, Equation 2.9 can be reformed to give the CBR equation in the classical form of Equation 2.10.

$$t = \sqrt{\frac{P}{8.1CBR} - \frac{A}{\pi}} \tag{2.10}$$

2.5 Thickness Reduction Factor for Single-Wheel Loading

A letter dated 18 April 1949 from WES to the OCE (WES June 1951) indicated that the Air Force was considering establishing airfield categories which would be based on a very small amount of traffic. Because of the anticipated Air Force action, WES conducted a study to determine the reduction in design thickness that could be permitted for very light usage. The test data used in the study to make the recommendations for the thickness reduction are given in Table 2.3. Figure 2.6 shows the plot of percent of design thickness versus aircraft coverages for the data given in Table 2.3. Concerning the data, the following statement is made in the WES report:

> *"There is some spread to the data, but there is no doubt that a relationship exists between percentage of design thickness and the coverages required to produce failure."*

Table 2.3. Data used to develop thickness reduction (18 April 1949)
(1 inch=25.4 mm, 1 lb=4.45 N)

Site (1)	Id (2)	Wheel Load, lb (3)	Thickness, in. (4)	Coverages to Produce Failure (5)	CBR (6)	Design Thickness, in. (7)	Percent of Design $\frac{(4)}{(7)}\times 100$ (8)	Remarks (9)
Stockton No. 1		25,000	12	200	5	23.5	51	Coverage and failure data from plate 15, B-29 report; CBR values from Symposium in January 1949 Proceedings of A.S.C.E.
			14.5	300			62	
			18	500			77	
			22	1000			94	
			24.5	2000			104	
			25	3000			106	
		40,000	20	200	5	28.5	70	Coverage and failure data from plate 15, B-29 report; CBR values from Symposium in January 1949 Proceedings of A.S.C.E. using extrapolated curve on plate 15.
			26.5	500			93	
			31	1000			109	
			36	2000			125	
			38	3000			133	
Stockton No. 2	Item 1	200,000	39	150	6	60	65	Stockton Appendix E – page E-14
	2a		44	1700	9	48	92	Stockton Appendix E – page E-14
	2b		46.5	2000	10	45	103	Stockton Appendix E – page E-14
	5a		18	10	14	37	49	Stockton Appendix E – page E-22 CBR values are average of before and after (using values recommended by W.E.S.).
	5b		20.5	60	16	34	60	
	6		24.5	360	13	40	61	
	7		30	1500	13	40	75	
	8		34	1140	17	33	103	
	B		30	1300	8	50	78	
Barksdale	Item 5	20,000	10.5	250	5	21.5	48	Coverage and failure data from plate 15, B-29 report; CBR values from Symposium in January 1949 Proceedings of A.S.C.E.
			13	500			60	
			15.5	1000			73	
			17.5	3000			81	
			18	5000			84	
		50,000	17.5	200	5.5	29	61	Coverage and failure data from plate 15, B-29 report; CBR values from Symposium in
			20.5	500			71	
			24	1000			82	

Table 2.3. Data used to develop thickness reduction (18 April 1949) (1 inch=25.4 mm, 1 lb=4.45 N)

Site (1)	Id (2)	Wheel Load, lb (3)	Thickness, in. (4)	Coverages to Produce Failure (5)	CBR (6)	Design Thickness, in. (7)	Percent of Design $\frac{(4)}{(7)} \times 100$ (8)	Remarks (9)
			26	3000			90	January 1949 Proceedings of A.S.C.E. CBR is average of range of 5 to 6.
			26.5	5000			92	
W.E.S. Test Section	Item 1	37,000	9	400	10	17.5	52	Data from Symposium in January 1949 Proceedings of A.S.C.E.
	302	37,000	11	100	14	14	78	Data from Symposium in January 1949 Proceedings of A.S.C.E.
	4 (1A-2-1 lane b)	37,000	13	About 4 00	13	15	87	Data from asphalt stability report, coverages from diary.
	4 (1A-2-1 lane c)	37,000	16	Prior to 400	5	27	59	
	49 (2A-2-1 lane c)	37,000	16	About 350	4	31	52	
	60 (3A-2-3 lane c)	37,000	16	Prior to 260	2	45	36	
Minden, Nevada Airfield	NE-SW	25,000	18	385	5	23.5	77	Symposium in January 1949 Proceedings of A.S.C.E.
Bergstrom, Texas Airfield	NW-SE Pit 3	15,000	17	358	6	17	100	Symposium in January 1949 Proceedings of A.S.C.E.
Birmingham, Alabama Airfield	NE-SW	23,000	7	194	4	26	27	Symposium in January 1949 Proceedings of A.S.C.E.

In establishing the WES relationship, it was recognized that a conservative curve to incorporate all the data would be of no particular benefit; therefore, the criteria curve was placed through the data. The criteria recommended by WES are stated, “A solid bold curve is shown on

the plot which has been established arbitrarily at 33.33 percent at 10 (coverages); 50 percent at 100; 75 percent at 500; 90 percent at 1000; and 100 percent of thickness at 2000 coverages."

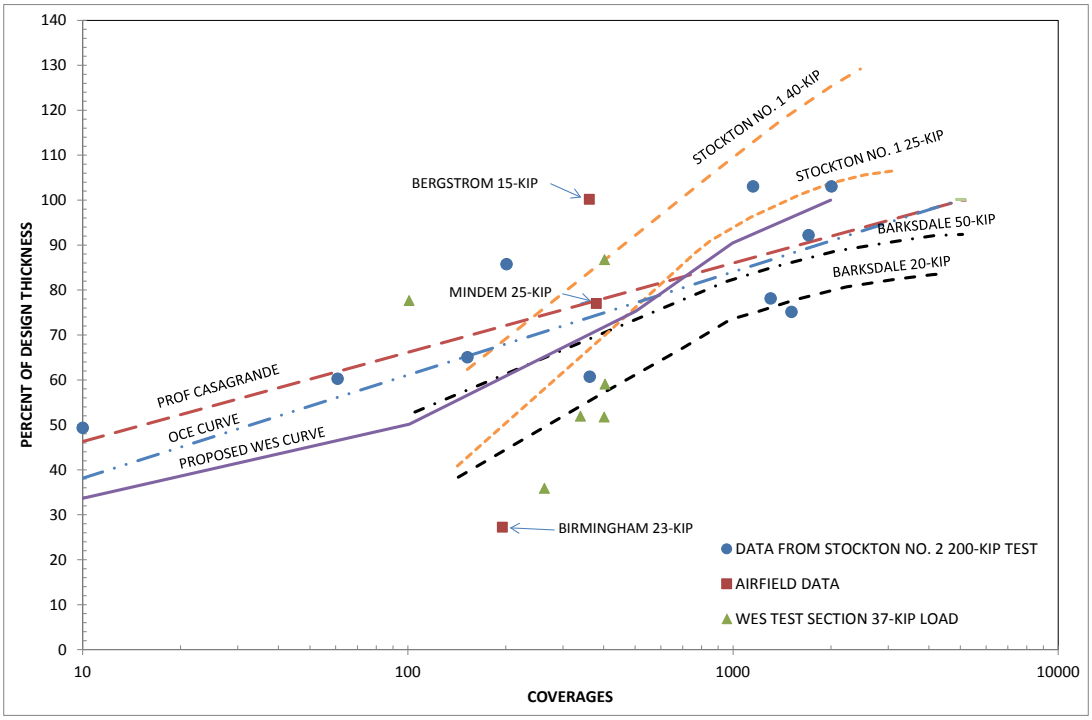

Figure 2.6 Suggested thickness reduction curves (18 April 1949) (1 kip=1000 lb=4.45 kN)

Figure 2.6 also shows the criteria labeled as Professor Casagrande's curve and the OCE curve. It is noted that the WES criteria established the 100 percent design thickness to be at 2,000 coverages, whereas Professor Casagrande's and the OCE criteria considered the design thickness to be at 5,000 coverages. It appears that the OCE criteria could be represented by the following equation:

$$\frac{\%t}{100} = 0.23\, log_{10}(C) + 0.15 \qquad (2.11)$$

where:

C = number of coverages

In this same letter, the WES presented assumptions and equations for computing coverages. Back in 1949, the assumptions for computing coverages were:

- Each runway is serviced by two taxiways, and a cycle composed of one landing and one take-off applies one pass to each taxiway and two passes to the runway
- Seventy-five percent of all operations on the runway are such that the tire tracks for each gear are uniformly distributed over a zone 25 feet (7.62 m) wide
- All operations at the airfield are on the same runway.

Based on the above assumptions, the equation developed for computing coverages for a taxiway was expressed mathematically as

$$C = \frac{0.75\, c\, n\, w}{(12.5)(12)} \tag{2.12}$$

where

C = number of coverages

c = number of cycles

n = number of wheels on each gear

w = width of the tire print in inches (1 inch=25.4mm).

For the runway, the equation to compute coverages was:

$$C = \frac{0.75(2c)nw}{(25)(12)} \tag{2.13}$$

It is noted that, based on Equations 2.12 and 2.13 for a given number of cycles of operations, the number of coverages for the runway and taxiway would be the same. Instruction Report Number 4 (WES 1959) provides the relationship (Figure 2.7) between percent design thickness and coverages. The relationship in Figure 2.7 corresponds to the OCE curve of Figure 2.6. In this case, a capacity operation was defined as 5,000 coverages, and the relationship was extended beyond capacity operations. Actually, at this time, six levels of traffic were defined: 25,000 coverages for very intense channelization, 5,000 coverages for capacity operation, 1,000 coverages for normal full operation, 200 coverages for minimum operation, 40 coverages for emergency operation, and 8 coverages for assault operation. To design for the different levels of traffic, the expression for the percent design thickness (Equation 2.11) was added to the classic CBR equation to give Equation 2.14.

$$t = (0.23\ \log_{10} C + 0.15)\sqrt{\frac{P}{8.1CBR} - \frac{A}{\pi}} \qquad (2.14)$$

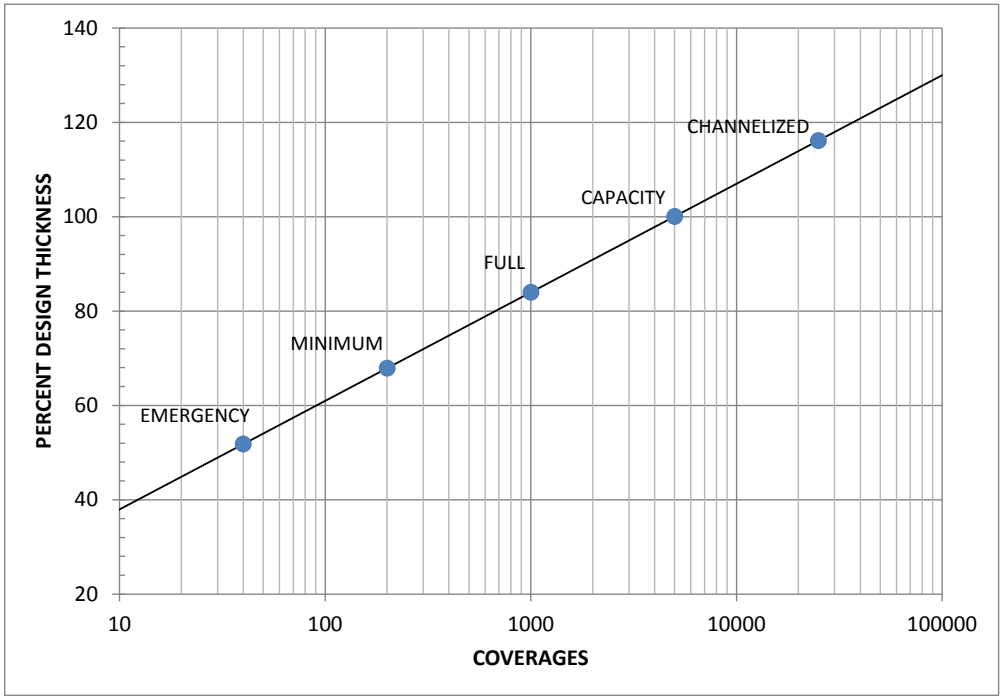

Figure 2.7 Relationship between coverage and percent design thickness (Instruction Report 4, 1959)

2.6 Definition of Coverages

An earlier section of Instruction Report Number 4 (WES 1959) introduces the term coverages as a means of quantifying traffic volume. In the literature review, the term coverages, was first encountered in the report on the Stockton No. 2 Test (Department of the Army 1948). A coverage was defined as one repetition of the test load applied to every point in a given traffic lane. In the Stockton No. 2 Test, the traffic was distributed laterally uniformly across the traffic lane. In Instruction Report No. 4, published in 1959, a coverage was defined as a sufficient number of passes of a wheel load in adjacent parallel wheel paths to completely cover a given lane within a pavement surface. This definition assumed uniform distribution of traffic across the traffic lane. Equations 2.12 and 2.13 for computing coverages were based on uniform distributed traffic across the traffic lane.

In the early 1970s, Brown and Thompson (1973) published a report describing the development of improved traffic distribution concepts. In the revised traffic distribution computations, the fundamental concept was that the traffic is normally distributed rather than uniformly distributed. For this assumption, Brown and Thompson gave the definition of coverage as the maximum number of tire prints, or partial tire prints, applied to the pavement surface at that point where maximum accumulation occurs. Volume I of the Multi-Wheel Heavy Gear Load (MWHGL) reports (WES November 1971) also presented the development of the methodology of computing coverages. One of the major considerations in the computation of coverages for pavement design was the distribution of traffic across the pavement width. Previously, the traffic distribution, referred to as aircraft wander (w_w), was defined as the width of pavement in which 75 percent of the aircraft traffic would operate. As stated above, one of the earlier assumptions was that the traffic within the wander width would be uniformly distributed. In the earlier work, the wander width was given as 25 feet (7.62 m) for runways and 12.5 (3.81 m) feet for taxiways. With the revised traffic distribution concepts, the definition of wander width was maintained as the width of pavement within which 75 percent of the traffic would operate, but the new concept assumed that the traffic within this width would be normally distributed.

Based on traffic studies reported by Vedros (Vedros 1960), Brown and Thompson (1973) assigned a wander width of 70 inches (1.78 m) for the traffic distribution on taxiways and 140 inches (3.56 m) for the traffic on runways. Concerning the wander width for military pavements, the MWHGL reports contained the following statement:

> *"It has been determined, on the basis of an analysis of a small amount of actual military aircraft traffic distribution, that wander widths of 40 and 80 in.(1.02 m and2.04 m) should be used in determining pass per coverage ratios for taxiways and runways, respectively. These values represent the best values obtainable from existing data and are subject to change if and when additional actual traffic distribution data are obtained."*

The MWHGL report provided no reference for the analysis of military aircraft distribution, and appeared to be in conflict with the Brown and Thompson's report. Both reports were published about the same time with the MWHGL referencing the Brown and Thompson

report as being in preparation. The conflict between the two reports was not resolved, but the current criteria for computing coverages are based on wander widths of 70 inches (1.78 m) and 140 inches (3.56 m) for taxiways and runways, respectively.

Based on methodology by Brown and Thompson, the equation for computing coverages (C_x) at a particular offset, x_o, from the centerline due to n_o operations of an aircraft having m number of tires is the following:

$$C_x = n_o \sum_{i=1}^{m} P_i \tag{2.15}$$

where

P_i = probability of tire i to traverse the point o.

The probability that tire i will traverse point o is computed from a normal distribution function by the following equation:

$$P_i = \int_{x_0-\frac{w}{2}}^{x_0+\frac{w}{2}} \left[\frac{1}{\sigma} e^{-\frac{1}{2}\left(\frac{x-x_i}{\sigma}\right)}\right] dx \tag{2.16}$$

where:

P_i = probability that tire i will traverse a point on the pavement located a distance x_o from the centerline of the pavement

x_o = distance from the pavement centerline to the point on the pavement for which the probability will apply

x_i = distance from the centerline of the aircraft to the centerline of tire ***i***

w = width of the tire contact area

σ = standard deviation of the aircraft traffic distribution, which is equal to one half the wander-width divided by 1.15 (currently the wander-width is 70 inches (1.78 m) for taxiways and 140 inches (3.56 m) for runways).

The current CBR-Alpha procedure uses Equations 2.15 and 2.16 for computing the pass-to-coverage ratio for an aircraft. Based on Equation 2.15, the definition for the pass-to-coverage ratio for an aircraft for a point on the pavement is the inverse of the sum of the probability of each tire to traverse a point on the pavement. The minimum value of the pass-to-coverage ratio

for the points across the pavement is the pass-to-ratio assigned to the aircraft. In the current procedure, the pass-to-coverage ratio is computed at 6-inch (152 mm) intervals across the pavement surface, and the minimum value is selected as pass-to-coverage ratio for the aircraft under analysis.

2.7 Equivalent Single-Wheel Load

The equivalent single-wheel load (ESWL) is the load on a single-wheel that would have the same detrimental effect on a pavement as a given load on a particular multi-wheel group. The single-wheel can be defined either as having the same contact area as an individual tire of the multi-wheel group or as having the same contact pressure as an individual tire of the multi-wheel group. The problem with the above definition is that the effect of traffic on a pavement is a very complex pavement parameter to compute; therefore, the term ESWL must be defined in terms of some other parameter. In the Stockton No. 2 Test, test sections were subjected to both single-wheel traffic and dual-tandem wheel traffic. Deflections and stresses were measured for both types of gear. Although comparisons were made between the deflections and stresses for the two types of gear, the study was not translated into ESWL, possibly for two reasons. First, the concept of ESWL had not been developed and second, no failures ever developed under the multi-wheel traffic, thus pavement performance could not be evaluated. One of the recommendations from the Stockton No. 2 Test report was:

> *"Before it can definitely be determined how much benefit can be expected from the use of multiple wheels, a traffic test section should be constructed and tested to failure with total thicknesses of pavement and base course designed for such multiple wheels. Such a test could not be performed on this project, because the thicknesses were greater than would be required for such a multiple wheel assembly."*

A letter to the OCE dated 27 April 1948 (WES 1951) from the Flexible Pavement Laboratory addressed a number of issues concerning flexible pavement design. The letter was in response to an earlier letter dated 18 March 1948 from the OCE, which reported difficulties discussed during a Board of Consultant's meeting of the pavement designer and the airplane designer. Two of the difficulties identified were the issues of multiple wheel assemblies and heavier aircraft, for which the WES letter contained the following statement:

"If the wheels of a multiple-wheel system are spaced far enough apart, the stresses from adjacent wheels will not overlap and the effect on the subgrade will be no more detrimental than for a load equal to that on the individual tire."

In this letter, the Flexible Pavements Laboratory states that they (the Flexible Pavements Laboratory) had furnished the OCE with procedures for resolving the single-wheel design curve into curves for various assemblies. Table 2.4 suggested tire spacing for various tire loads which insures no overlap of stress in subgrades with CBR values of 5 and more. In regard to the spacing in Table 2.4, the following statement is made:

"These spacings are much wider than those now in current use and may be considered entirely impracticable from the stand point of the airplane designer. If they were adopted, however, it would mean that flexible pavement designs could be based on the tire load and would be independent of the gross load of the airplane."

It is not clear as to the methodology used to determine the tire spacing in Table 2.4, but it is probably the procedures presented in the paper by Boyd and Foster in the ASCE Symposium (1950). This correspondence showed that there was, at this time, a keen awareness of the balance between airplane design considerations and pavement design considerations and that compromise between the two considerations would be beneficial.

Table 2.4 Center-to-center tire spacing for twin or tandem gear to insure no stress overlap on subgrades with a CBR of 5 or more (from a WES letter dated 27 April 1948)

Tire Load (lb)	Tire Spacing (inches)
5,000	30
10,000	43
20,000	58
30,000	70
37,500	76
40,000	79
50,000	87
Note: 1 inch=25.4 mm, 1 lb=4.45 N	

In the 1950 ASCE Symposium, Boyd and Foster presented a paper describing the method by which the B-29 design curves were developed and showed the extension that may be applied

to any given assembly. Figure 2.8 is the schematic diagram of the B-29 dual wheel assembly showing the concept of overlapping of stress for a thin and a thick flexible pavement. In Figure 2.8, S=37.5 inches (953 mm), d =20 inches (508 mm) and the tire width is 17.5 inches (444 mm).

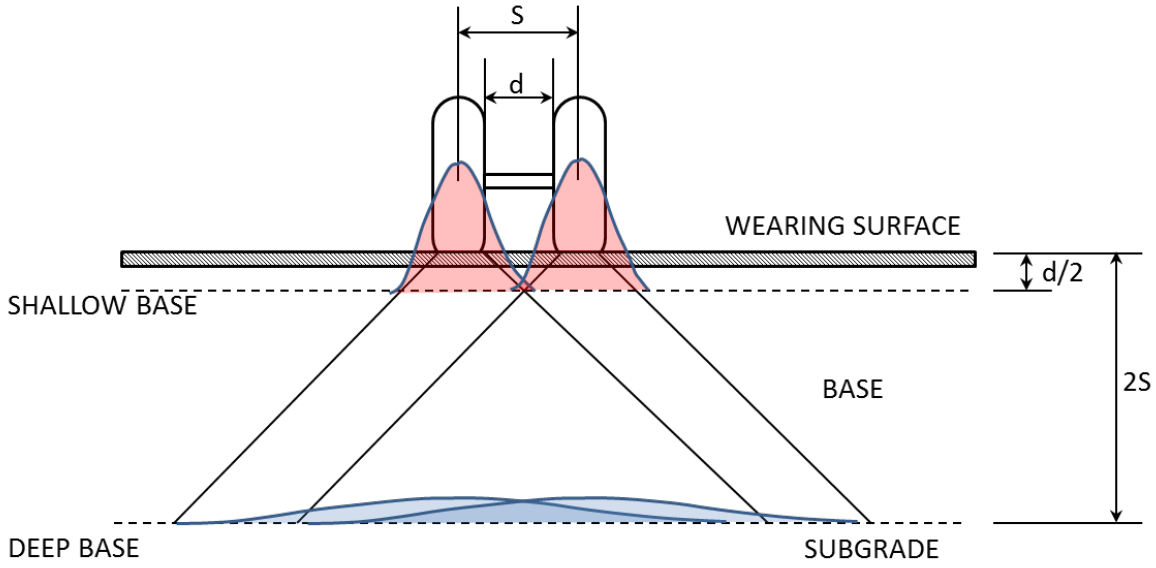

Figure 2.8 Schematic diagram of B-29 wheel assembly (Boyd and Foster 1950)

The concept presented by Boyd and Foster (1950) was that at some shallow base thickness, at the top of the subgrade, the two wheels of the dual assembly would act as practically independent 30,000-lb (133.5-kN) tires, with little or no overlapping of stresses. Likewise, for a very thick base, the stresses from the two wheels would overlap such that, for all practical purposes, the stresses at the top of the subgrade would be the same as for a single 60,000-lb (267-kN) load. Therefore, the pavement design thickness for the B-29 must range between the thickness for the 30,000-lb (133.5-kN) and 60,000-lb (267-kN) single wheel loads. With this reasoning, the approach for developing the design curves for the B-29 was reduced to:

- Finding the thickness at which each tire stresses the subgrade as an independent unit; and
- Finding the thickness at which the two tires stress the subgrade as one single unit.

The thickness at which each tire of the B-29 dual assembly acts as an independent unit, and the thickness at which two tires act as a single unit were determined by comparisons of

vertical stresses, shearing stresses and deflections. The vertical and shearing stresses were computed using Boussinesq's formulas assuming homogeneous material. The deflections were determined using a graphical method described in detail in the Boyd and Foster (1950) paper. For each parameter, Table 2.5 summarizes the values of maximum thicknesses at which each tire acted as an independent unit and the minimum thicknesses at which the assembly acts as a single unit.

Table 2.5 Thicknesses defining unit behavior

Reference Parameter at Top of Subgrade	Maximum Thickness at which Tires Act as Independent Units (in.)	Minimum Thickness for which Assembly Act as One Single Unit (in.)
Vertical stress	17	80
Shear stress	20	70
Deflection	10	75

Note: 1 in.=25.4 mm

Since the 10-in. (254 mm) thickness, as determined based on the subgrade deflection, was more conservative, deflection was chosen as the parameter on which to develop the design curves for the B-29. For thicknesses of 10 in. (254 mm) and less, the B-29 design would be based on a 30,000-lb (133.5-kN) single-wheel load and for thicknesses 75 in. (191 mm) and greater, the B-29 design would be based on a 60,000-lb (267-kN) single-wheel load. The thickness requirements between these two limits should vary in an orderly manner. From inspection of the dimensions of the B-29 gear (Figure 2.8), the maximum distance at which the tires would act independently was approximately equal to one-half of the clear distance (d) between the tires, and the minimum distance at which the assembly acts as a single unit was approximately twice the centerline spacing (s) of the tires. Based on this analysis, the design curves of any gear assembly was to be based on the ratios of *d/2* and *2S*.

As the CBR pavement design methodology developed, a number of facets of the Boyd and Foster paper were influential. These facets include:

- The concept of the design thickness for multiple-wheel assemblies being based on an equivalent single wheel

- The use of the deflection at the top of the subgrade being the basis for determining the single-wheel load to represent the multiple-wheel assemblies
- The fact that the more conservative approach (deflection) was chosen for determining the ESWL
- The establishment of the ratios, *d/2* and *2S*, for determining the depths for judging the behavior of multiple-wheel assemblies.

In a study reported in Technical Memorandum No. 3 349 (WES 1955), Turnbull, Foster, and Ahlvin re-evaluated the methods for resolving the existing single-wheel design criteria for flexible airfield pavements into criteria for multiple-wheel assemblies. The methods to be re-evaluated were developed within the studies of pavement design criteria for the B-29, which was reported by Boyd and Foster. The purpose of the study authorized in 1953 was to determine:

- Whether or not the present tentative method of resolving single-wheel criteria into criteria for multiple assemblies was adequate
- Means for obtaining better results if the present method was not adequate
- What additional verification, if any, was needed for the present method of resolution or for a suggested alternate method

Data from previous studies represented the basis for Turnbull's study. The referenced publications were:

- Report on Certain Requirements for Flexible Pavement Design for B-29 Planes (WES 1645)
- Accelerated Traffic Test at Stockton Airfield (Stockton Test No. 2) (Porter 1949)
- Design Curves for Very Heavy Multiple-wheel Assemblies (Boyd and Foster 1950)
- Investigation of Stress Distribution in a Homogeneous Clayey Silt Test Section (Report No.1) (WES 1951)
- The Stress Produced in a Semi-Infinite Solid by Pressure on Part of the Boundary (Love 1929)
- Investigation of Stress Distribution in a Homogeneous Sand Test Section (WES 1949)
- Multi-wheel Test Section with Lean-Clay Subgrade (HQDA 1952)

Turnbull's study also provided more insight into the development of the multiple-wheel criteria by Boyd and Foster that is referred to as the original analysis. The report stated that:

> *"The original analysis of deflection data considered that strain was an important criterion and that the critical strain is represented by the rate of change of deflection with offset along the deflection profile."*

It is also stated that, although the slope of deflection profiles was accepted as an important criterion, data were not adequate to develop such profiles, and it was assumed that the maximum deflection was representative of the critical slope. An additional simplification was that the maximum deflection for a dual assembly occurred beneath the center of one wheel. The report clarified that:

> *"With the additional data now available, deflection profiles can be developed and the magnitudes and positions of maximum deflections beneath multiple-wheel assemblies can be reasonably determined."*

Based on an analysis of the data from multiple-wheel traffic testing, it was concluded that design criteria in the present procedure provided designs that were slightly unconservative and thus considered to be inadequate. This inadequacy led to a determination that a better design procedure was needed. Because of the reasoning that the critical strain is related to deflection, the researchers favored the deflection as the parameter on which to base the computations of the equivalent single wheel load. The rationale given in the report was as follows:

> *"From this analysis, it appears that a single-wheel load, which yields the same maximum deflection as a multiple-wheel load, will produce equal or more severe strains in the subgrade or base than will the multiple-wheel load. The single load may, therefore, be considered equivalent to the multiple-wheel load for purposes of design, and this equivalent single-wheel load can be used to develop designs for multiple-wheel assemblies."*

Previously, in the development of the design curves, it was stated that the more conservative approach was selected. Now, in this study, it has been stated that the existing

procedure is unconservative. Regarding conservatism, this report makes the following statements:

> *"The slopes of some of the single-wheel deflection profiles in plates 6, 9, and 11 are appreciably greater than their dual-wheel counter parts. Therefore, for design purposes, it might be considered that assuming the single-wheel loads equivalent to their dual counterparts would introduce too much conservatism. As will be shown later, however, the proposed method gives design criteria only a little more conservative than that currently used, which has been shown to be slightly on the unconservative side."*

This logic and new methodology for computing deflections under single and multiple-wheel assemblies permitted the development of the procedure for computing the equivalent single wheel. The procedure involved equating the deflections between the single-wheel and the multiple-wheel assemblies. In equating these deflections, the contact area of the single wheel is taken to be constant and the same as that of one wheel of the multiple-wheel assembly. Determining the ESWL for a number of depths assured the definition of the relation between the ESWL and depth. This relationship could then be used with the established single-wheel design criteria to develop further criteria for multiple-wheel assemblies.

A review analysis was also conducted of ESWL based on the vertical and shear stresses at the top of the subgrade. As reported, the results of the analysis were the same as the initial analysis. With regard to the distribution of stress beneath loads, the following statement was made:

> *"Additional evidence has become available that shows the distribution of stresses beneath wheel loads or simulated wheel loads to be much as indicated by computations based on the Boussinesq theory of elasticity."*

The stress based methods were dismissed from further consideration because the original analysis concluded that the stress based methods for multiple-wheel assemblies were less conservative than the deflection-based method and the deflection procedure was already unconservative. Based on the analyses performed in Turnbull's report, the following conclusions were reported:

- *"The present tentative method of resolving single-wheel into multiple-wheel designs gives criteria slightly on the unconservative side."*
- *"Neither vertical stress nor maximum shear stress provides an adequate basis for relating the effects of single-wheel and multiple-wheel assemblies."*
- *"Strains, which are in effect the slopes of deflection versus offset curves, provide the best basis for arriving at single-wheel loads that are equivalent, for design purposes, to multiple-wheel loads."*
- *"These strains are adequately represented in relative magnitude by theoretical maximum deflections, and satisfactory design criteria for multiple-wheel assemblies can be developed from established single-wheel criteria on the basis of equal maximum deflections."*

On the basis of the recommendation in Turnbull's report, deflections were chosen as the basis of computing the ESWL for multiple-wheel assemblies. Replacing the single-wheel load term *P* in Equation 2.14, with the *ESWL,* transforms the CBR equation and makes able to handle multiple-wheel assemblies as is shown in Equation 2.17.

$$t = (0.23\ \log_{10} C + 0.15)\sqrt{\frac{ESWL}{8.1\ CBR} - \frac{A}{\pi}} \tag{2.17}$$

2.8 Development of Thickness Adjustment Factor

As discussed previously, in the 1950's the CBR equation was developed and extended to include a thickness reduction term as shown in Equations 2.14 and 2.17. With the proliferation of larger aircraft, both commercial and military, carrying heavy loads on multi-wheel gear, the FAA and U.S. Military joined to collaborate on a testing program to evaluate the effects of heavily loaded multi-wheel gear on airfield pavements. As a result of this collaboration, the U.S. Army Corps of Engineers (USACE) was tasked to construct pavement sections to represent full-scale pavements. Using simulated gear representing the C-5A and Boeing 747 aircraft, the pavements sections were tested to failure. Mr. Jim Sale and Mr. Richard Ahlvin headed the construction of a test load cart, full-scale test pavements, and the pavement testing to failure (Waterways Experiment Station 1971). The test program, referred to as the Multi-Wheel Heavy Gear Load (MWHGL) test, produced data which, at the time, were considered the only reliable

test data for heavily-loaded multi-wheel gear. Even today the data from the MWHGL test is a major source of design criteria for today's large aircraft.

The analysis of the data from the MWHGL test program led the reformulation of Equation 2.17 in terms of a load adjustment factor, α, which was a function of traffic volume and number of tires in the multi-wheel group. The introduction of the α-factor resulted in the present form of the classical form of the CBR design equation:

$$t = \alpha\sqrt{\frac{PESWL}{8.1CBR} - \frac{A}{\pi}} \tag{2.18}$$

Cooksey and Ladd (1971) defined in graphical form the value of α, and discussed the development of the thickness reduction curves. By studying Figures 1 and 2 contained in the Cooksey and Ladd report, it can be concluded that a large amount of uncertainty exists in the placement of the α-curves for the twin-tandem and 12-wheel tire groups. From the three curves shown in Figure 3 of the Cooksey and Ladd report, the complete set of α-curves were drawn as shown in Figure 2.9.

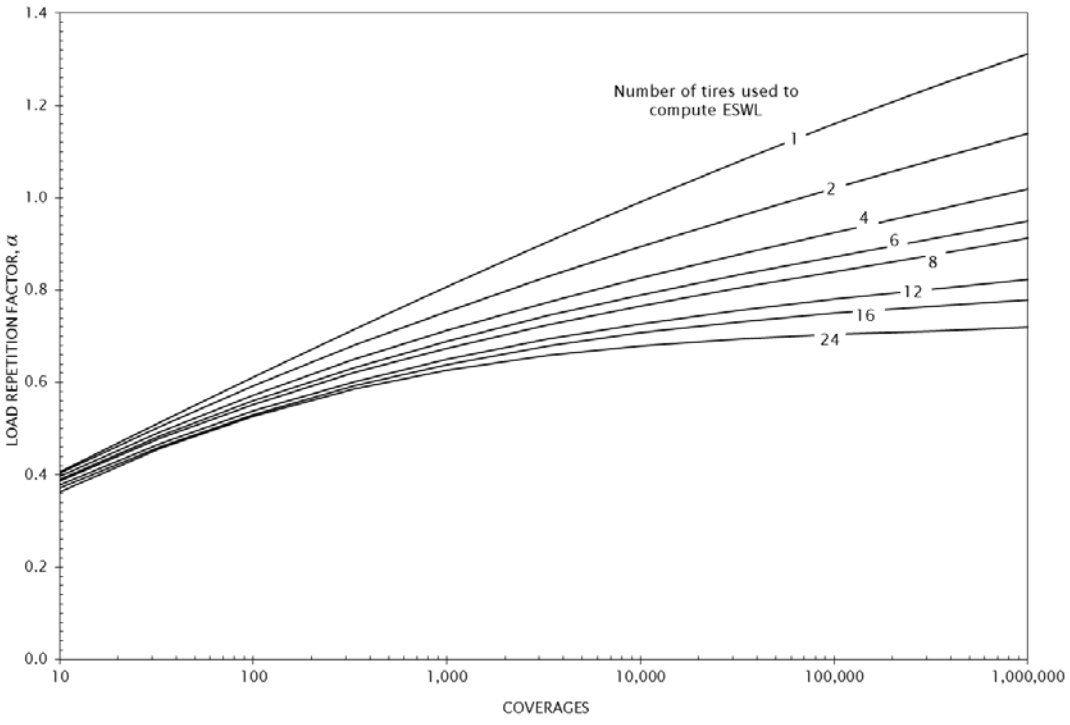

Figure 2.9 Alpha-Curves (α-curves) as defined by Cooksey and Ladd (1971)

Significant factors in the development of the α-curves are that the data were very limited, the 12-wheel α-curve was conservatively placed, the curves were extrapolated beyond the bounds of the data, extrapolation of the curves was by engineering judgment, and placement of the set of α-curves was based on the placement of the 12-wheel, 4-wheel, and single-wheel curves. In the 1970's, α-curves were inserted into the pavement design computer programs by digitizing the curves by hand and inserting the data into the design program as data statements. Later, the data for each curve were modeled with third order polynomials.

2.9 Summary

The study of the origins of the CBR design procedure, from its inception as a set of highway curves to its final form of the CBR equation, provides a unique historical perspective about the limitations and assumptions made during its development. Originally developed from completely empirical curves, the CBR highway design curves, which were only based on thickness and subgrade CBR, evolved to the realm of airfield flexible pavements by conducting comparative analyses of equal shear stresses at higher wheels loads. From there, a set of tentative airfield design curves were obtained for aircraft loading. These tentative curves were validated by the use of field performance data and observation of in-service airfield pavements.

The accepted CBR design curves were then consolidated into a single equation by applying linear elastic layer analyses based on Boussinesq single-layer half-space theory. This single equation, known from now on as the CBR equation, was also successfully verified against in-service pavements and test section traffic data. The introduction of heavier aircraft with multi-wheel gears required further adjustments to the basic CBR equation. Since the CBR equation is intended for a single-wheel gear, the equivalent single-wheel load concept was introduced to correct this deficiency.

Since the newly formulated equation only accounted for traffic defined only as capacity operations, it was also important to extend the basic equation to traffic operations other than the capacity operations definition. Because aircraft wander from side to side during ground operations, the term coverage was introduced to account for this variability and take advantage of the fact that each aircraft pass does not cause a stress application at the same lateral position on the pavement. Pavement thickness adjustment factors were introduced to either increase or

reduce the pavement thickness calculated from the standard CBR equation for aircraft passes other than 5000 coverages. These factors were called the alpha-factors and they were determined from results of full-scale experimental test sections.

The CBR equation, in its current form, has been adjusted as the need to account for traffic levels, aircraft loading, and landing gear type evolved. These adjustments have sometimes been implemented without a theoretical basis, adding an uncertainty as to the validity of these changes and the impact on its original formulation. Since the Boussinesq half-space stress model was used to derive the original CBR equation, a specific and unknown stress distribution based on the vertical stress directly under a single-wheel was forced by definition. The issue of stress distribution will be addressed in subsequence chapters and will form the basis for exploration of stress distribution models other than those originally proposed by Boussinesq.

CHAPTER 3 - STRESS DISTRIBUTION MODELS FOR PAVEMENT STRUCTURES

3.1 Introduction

This chapter covers the most commonly used theories of stress distribution within pavements structures induced by the application of wheel loads. These theories range from single-layer linear elastic half-space, to multi-layer linear systems and finite element non-linear pavement models. There are a variety pavement models proposed by researchers within the pavement community that account for several aspects of pavement response, including rutting in the asphalt and pavement layers, non-linearity of pavement materials and dynamic behavior under traffic. However, these methods usually are harder to implement in practice for the design and evaluation procedures of military pavements due to additional requirements in determining additional materials properties and parameters. For this reason, one of the goals of this research was to only consider and evaluate those pavement models that have practical potential and implementation in the field of operations. The systems chosen in this research were the Boussinesq single-layer pavement response, the Fröhlich soil stress model, the multi-layer linear elastic solution and an axisymmetric non-linear finite element model. These models, excluding the finite element model, have routinely been used to simulate pavement structures, derived design parameters and backcalculate pavement material properties.

3.2 Boussinesq Single-Layer Model

To be able to analyze, design or evaluate a pavement structure, it is necessary to assess the magnitude and the distribution of stresses due to surface loads imparted by ground vehicles or aircraft tires. The magnitude of these stresses is required to make sure that the pavement material strength is not exceeded and as consequence cause pavement failure. A well-known solution for determining the state of stress within a semi-infinite elastic solid, was put forward by Boussinesq (Jumikis, 1964). Boussinesq made the assumption that under the influence of gravity there was enough confinement pressure to prevent the particles of soil from sliding relative to each other, and thus approximate the behavior of an elastic solid. His theory is based on the

solution of the mathematical theory of elasticity of a homogeneous, isotropic and elastic semi-infinite solid and a Poisson's ratio of 0.5. Figure 3.1 depicts a diagram describing the solution for a concentrated vertical load. The stresses solved by the system are only due to the external concentrated load ***P*** since the elastic solid it is assumed to have no weight and is initially not stressed.

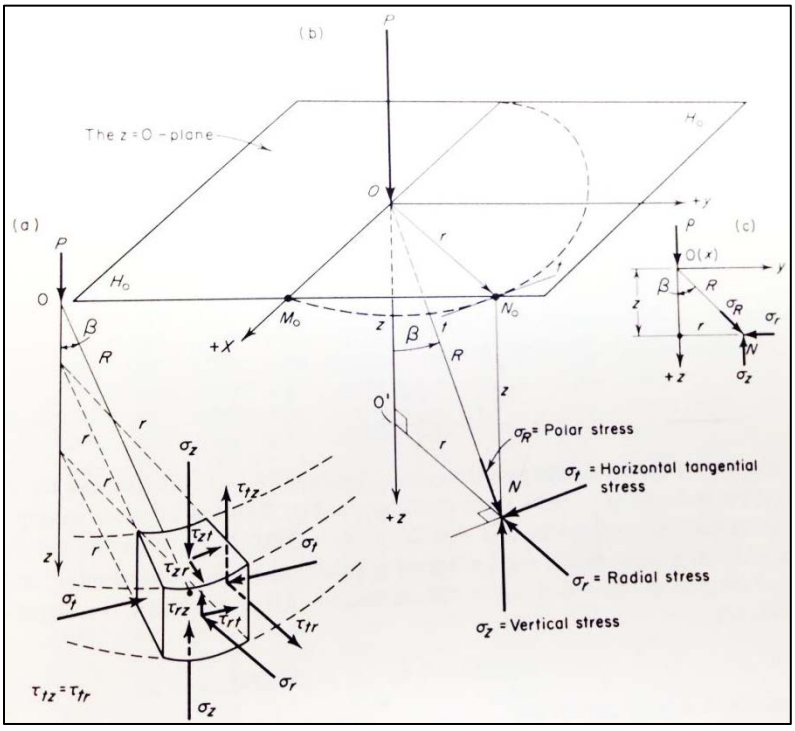

Figure 3.1 Boussinesq Solution (after Jumikis, 1964)

Jumikis presents the stress equations developed by Boussinesq in terms of polar coordinates and are presented in the equations that follow for radial, vertical and shear stresses, respectively.

$$\sigma_R = \frac{3P\cos\beta}{2\pi R^2} \tag{3.1}$$

$$\sigma_z = \sigma_R cos^2\beta \tag{3.2}$$

$$\tau_{rz} = \frac{\sigma_R \sin 2\beta}{2} \tag{3.3}$$

Of particular interest is the solution of Equation 3.2 for the vertical stresses at depths directly and along a line under the concentrated load. Jumikis presents the derived equation for this case as

$$\sigma_z = \frac{3}{2}\frac{P}{\pi z^2}\frac{1}{\left[1+\left(\frac{r}{z}\right)^2\right]^{\frac{5}{2}}} \tag{3.4}$$

Equation 3.4 has been extensively used, not only to determine vertical stresses within pavement structures, but in determining the vertical stresses applied to masses of soil due to building footings. Since the loads for aircraft and ground vehicles are applied to the surface through contact areas rather than point loads, Equations 3.4 was extended by subdividing the loaded area into infinitesimal parts and integrating over the loaded area. One solution important to the analysis of pavement structures is the solution of a circular uniformly loaded area for vertical stresses directly below the center of the circular area. Equation 3.5 shows the solution for vertical stress derived from Equation 3.4 for this latter case.

$$\sigma_z = \sigma_o\left[1 - \frac{z^2}{(r_0{}^2+z^2)^{\frac{3}{2}}}\right] \tag{3.5}$$

where, $\boldsymbol{r_o}$ is the radius of the circular loaded area and $\boldsymbol{\sigma_o}$ is the surface uniformly applied pressure.

3.3 Fröhlich Stress Model

The solution of Boussinesq equations was modified and generalized by O. K. Fröhlich (Fröhlich, 1934) to account for the increase of the modulus of a soil mass with depth. A parameter he called $\boldsymbol{n}$ was introduced that would reflect the ability of the soil mass to concentrate or distribute the stresses. This parameter was later called the stress concentration factor. Jumikis (1964) presented a derivation of Fröhlich equations for a point load with the assumptions that now the semi-infinite solid was no longer isotropic and therefore the stress distribution capabilities of the soil change with a stress concentration factor. The final equations describing Fröhlich's stress model are listed as follows.

Vertical Stress:

$$\sigma_z = \frac{nP}{2\pi z^2} cos^{n+2}\beta \quad (3.6)$$

Horizontal Stress:

$$\sigma_r = \frac{nP}{2\pi z^2} cos^{n}\beta sin^{2}\beta \quad (3.7)$$

Shear Stress:

$$\tau = \frac{nP}{2\pi z^2} cos^{n+1}\beta sin\beta \quad (3.8)$$

Like in the case of Boussinesq solution, Fröhlich's solution was also derived for a Poisson's ratio of 0.5. In Fröhlich's solution, a stress concentration factor ***n*** = 3 is only possible for an isotropic, elastic solid with a constant modulus of elasticity. If ***n*** = 3 is substituted in Equations 3.6 through 3.8, Fröhlich's equations reduce to those of Boussinesq. Therefore, Boussinesq equations can be thought of as a subset of the solution provided by Fröhlich.

As the stress concentration factor ***n*** increases, so is the stress concentration under the load. According to Fröhlich, values of ***n*** > 4 applied to small loading areas with large applied stresses that would cause the soil to quickly shear near the loading area. When ***n*** decreases, the soil has the tendency to spread the stresses over a larger area. Since one of the main tasks of a pavement structure is to distribute the loads over a wider area, pavement structures are expected to have stress concentration factors less than four (***n*** < 4). Figures 3.2 and 3.3 illustrate the effect of changing the stresses concentration factor, ***n*** from 2 to 4, on the resulting magnitude and distribution of the vertical stress under a C-17 single tire. The C-17 tire was assumed to have a circular loaded area and uniform pressure. As can be seen in these figures, the higher the stress concentration factor, the higher the computed stresses are at any depth and the more concentrated the stress profile becomes (Figure 3.3).

It should be pointed out that since Fröhlich stress model assumes a one-layer system, accordingly, pavement structures with multiple layers will also be treated as a one-layer system. The impact of the stress distribution on the asphalt, base, and subbase layers is all accounted for by Fröhlich's model through the use an appropriate ***n***-factor.

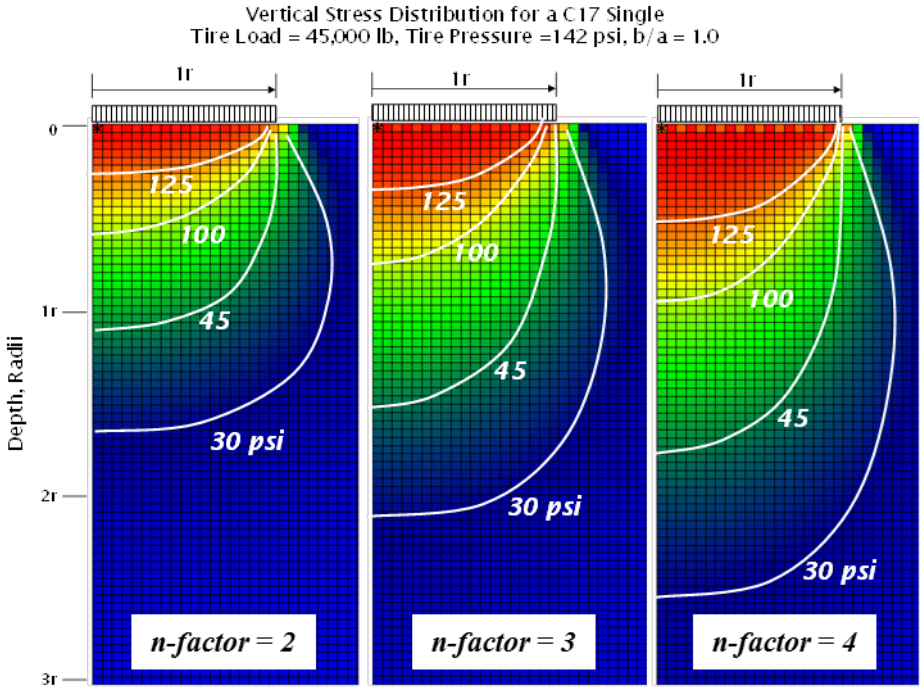

Figure 3.2 Effect of stress concentration factor on the vertical stresses for a C-17 Tire (1 psi=6.9 kPa)

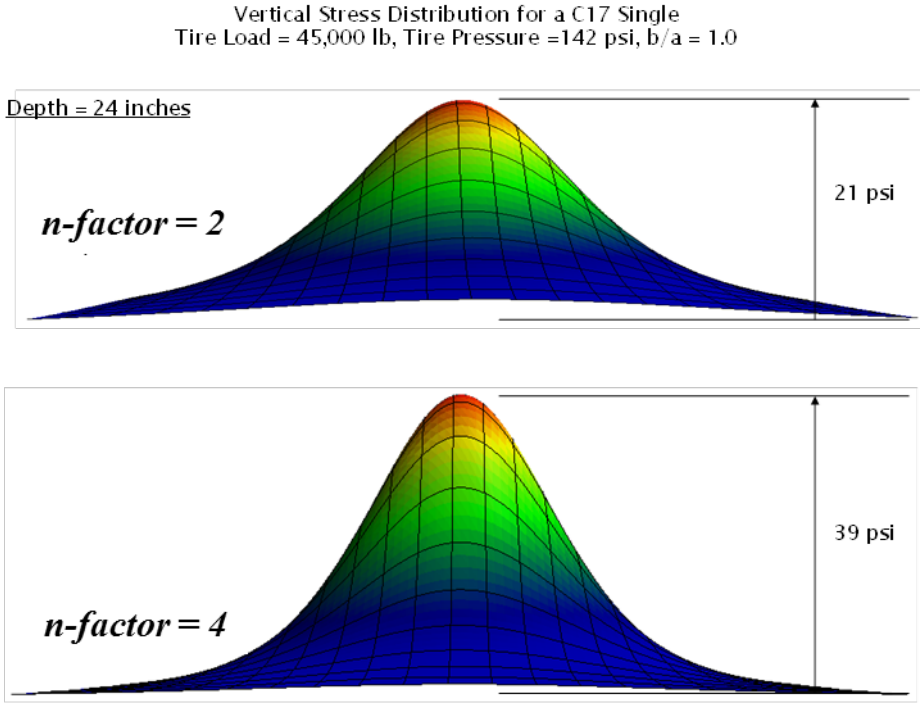

Figure 3.3 Effect of stress concentration factor on the distribution vertical stresses for a C-17 Tire. Depth of calculation was 24 inches. (1 inch=25.4 mm, 1 psi= 6.9 kPa)

3.4 Multi-layer Linear Elastic Model

The multi-layer linear elastic system is an improvement over the single-layer systems postulated by Boussinesq and Fröhlich. A layered pavement system is simulated by the systems depicted in Figure 3.4. In this system, all materials within the pavement structure are assumed to be linear, elastic, isotropic and homogeneous. All layers are infinite in the horizontal direction and have a finite thickness associated with each layer, with the exception of the last layer which is considered to have infinite thickness. All layers must also act as a composite system with no separation between layers and a set of boundary conditions must be satisfied. All layers are modeled by a modulus of elasticity, *E*, a Poisson's Ratio μ, and a thickness. Loads are applied at the surface through circular loaded areas with constant contact pressure and static loads.

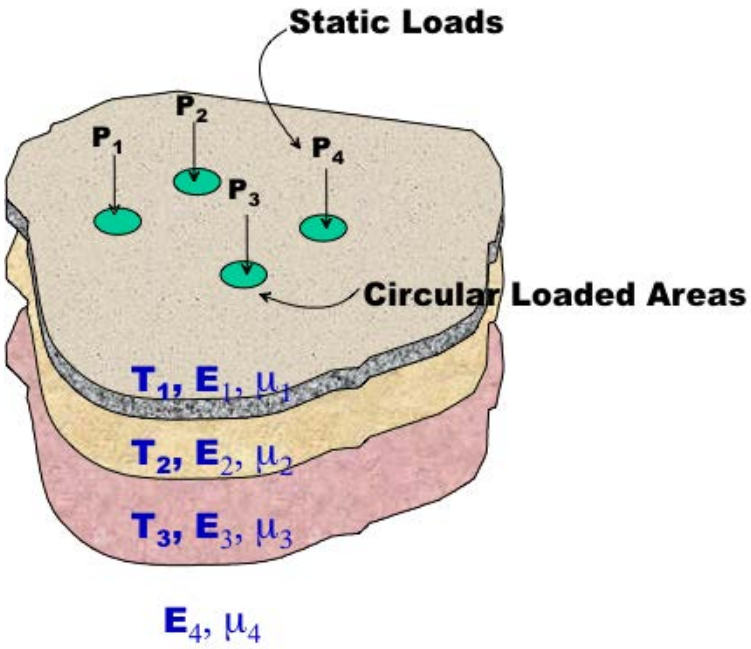

Figure 3.4 Multi-Layer Elastic Pavement System

A solution for this layered system was proposed by Burmister in 1942. He showed that a stress function Φ would satisfy both a set of boundary conditions and equations of equilibrium. The stress function Φ is shown as follows for a system of *N* number of layers.

$$\Phi_1 = J_0(mr)[(A_1 + B_1 z)e^{mz} + (C_1 + D_1 z)e^{-mz}]$$

$$\Phi_2 = J_0(mr)[(A_2 + B_2 z)e^{mz} + (C_2 + D_2 z)e^{-mz}]$$

…

$$\Phi_{N-1} = J_0(mr)[(A_{N-1} + B_{N-1}z)e^{mz} + (C_{N-1} + D_{N-1}z)e^{-mz}]$$

$$\Phi_N = J_0(mr)[(A_N + B_N z)e^{mz} + (C_N + D_N z)e^{-mz}] \quad (3.9)$$

Where,

- $J_o(mr)$ *i*s a Bessel function of the first kind of zero order
- *m* is a continuous function of integration
- *r* and *z* are the coordinates from the center of circular loaded area
- *1, 2, … N-1, N* are the pavement layer number starting from the surface
- A_i, B_i, C_i, D_i are constants of integration which depend on the boundary and interface conditions

This system of equations is solved for a set of boundary conditions as follows:

- All stresses and deflections must be equal to zero at infinite depth, *z*
- At the surface, the vertical stress is equal to zero, except under the load where the vertical stress is equal to the applied surface pressure
- All vertical stresses above and below an interface at a specific offset must be equal
- At all interfaces, except the top surface, the following values above and below an interface and at an specific offset must be equal
    - vertical deflections
    - horizontal deformations
    - shear stress for “rough” interfaces or zero for “smooth” interfaces
- The deflections in the vertical and horizontal directions must be zero at their respective infinite distance.

The application of this system of layers has the advantage of simulating the layers as they are laid out in real pavement. Layers with different material properties can be directly modeled by assigning appropriate values of modulus of elasticity. In addition, multiple loading can be easily handled by assuming superposition of stresses. However, joints and cracks that might exist in the pavement cannot be modeled. One important aspect of this pavement model is that the stress

distribution within the pavement structure will dependent on the values assigned to each individual layer. Stiffer layers near the surface will tend to spread the load out more than less stiff layers.

Multiple computer programs have been developed throughout the years for the solution of these systems, including BISAR, CHEVRON, ELSIM5, ILLIPAVE, LEAF, WESLEA and JULEA, which can effectively be used for determining stresses within a pavement structure. In this research, the layered elastic computer code selected for analysis is based on the source code currently implemented in the U.S. Army Corps of Engineer, Pavement-Transportation Computer Aided Structural Engineering (PCASE) software.

3.5 Axisymmetric Non-Linear Finite Element Model

There exists considerable amount of research that has been done in the area of pavements that implement some form of finite element modeling. One of the main objectives of this research was to select an existing finite element model that is better suited to the simulation of tire loads acting on layered flexible pavement structures. The selected finite element model should be able to give reasonable answers at a minimal cost in terms of execution time, entry and reduction of data and adaptability to pavement problems.

For the reasons just mentioned, the author decided to use an axisymmetric, non-linear finite element method (FEM) developed from a two-dimensional implementation done by Hinton and Owen (1989). Hinton and Owens implementation is based on a displacement method were the unknown nodal deformations resulting from applied forces are calculated. Their finite element method is well documented in their publication and its formulation follows a modern mathematically standard with the use of 8-node isoparametric finite elements.

Hinton and Owens implementation of a two-dimensional finite element solution was modified to handle two-dimension plane stress and plane strain solutions as well as axisymmetric solutions of multi-layer pavement systems. This author have had previous experience modeling geogrid systems within pavements with this finite element model, however, additional validation was performed during this research from the results of test section data to be discussed during the analysis sections of this document.

Hinton and Owen's finite element code was extended from a linear elastic material solution to a non-linear material solution by the use of a hyperbolic soil model proposed by Kulhawy, Duncan and Bolton (1969) and Duncan and Chang (1970),. Kulhawy et al.(1969) proposed that the non-linear behavior of soil materials could be represented by the use of a stress-strain curve similar to that shown in Figure 3.5, and by a hyperbola of the form expressed by Equation 3.10.

$$\sigma_1 - \sigma_3 = \frac{\varepsilon_1}{a+\varepsilon_1} = \frac{1}{\frac{a}{\varepsilon_1}+b} \tag{3.10}$$

As the strain ε_1 in Equation 3.10 increases, an asymptotic or ultimate value of $(\sigma_1-\sigma_3)_{ult}$ is reached. The initial modulus $\boldsymbol{E_t}$ can be determined by taking the derivative of Equation 3.10 with respect to ε_1 resulting in Equation 3.11.

$$E_t = \frac{a}{(a+b\varepsilon_1)^2} \tag{3.11}$$

As ε_1 approaches a value of zero, E_t then becomes the ratio $1/a$. The values of E_t and $(\sigma_1-\sigma_3)_{ult}$ can be determined from laboratory stress-strain data if the hyperbola in Equation 3.10 is transformed as follows.

$$\frac{\varepsilon_1}{(\sigma_1-\sigma_3)} = a + b\varepsilon_1 \tag{3.12}$$

If the stress-strain curve is known, Equation 3.12 allows the determination of E_t and $(\sigma_1-\sigma_3)_{ult}$ by plotting the data as shown in Figure 3.6, passing a best-fit line through the data points and determining the slope b and intercept a. Since it is entirely possible that the soil non-linear behavior will not exactly follow the assumed hyperbolic model, Duncan and Chang (1970) defined what they called a failure ratio R_f as shown in Equation 3.13.

$$R_f = \frac{(\sigma_1-\sigma_3)_f}{(\sigma_1-\sigma_3)_{ult}} \tag{3.13}$$

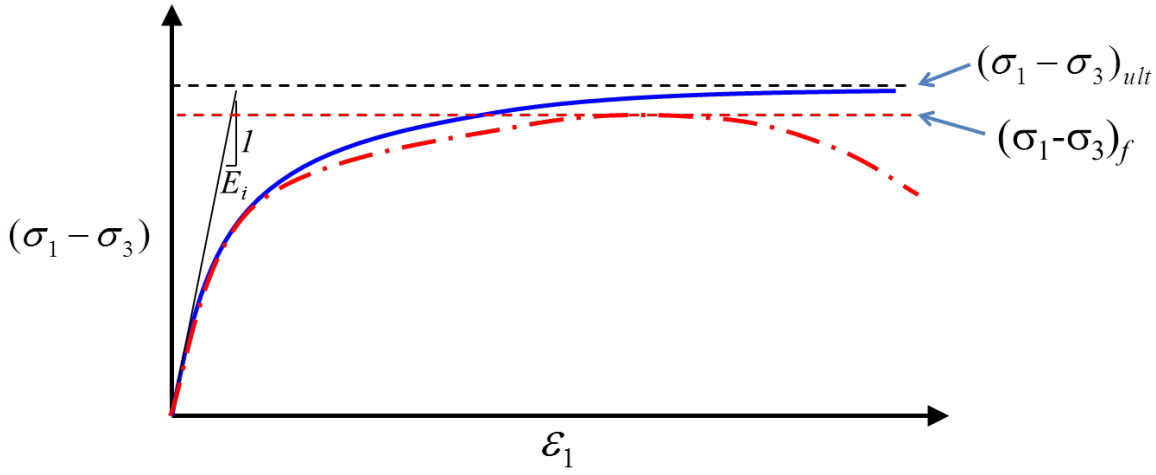

Figure 3.5 Hyperbolic Non-linear Soil Model

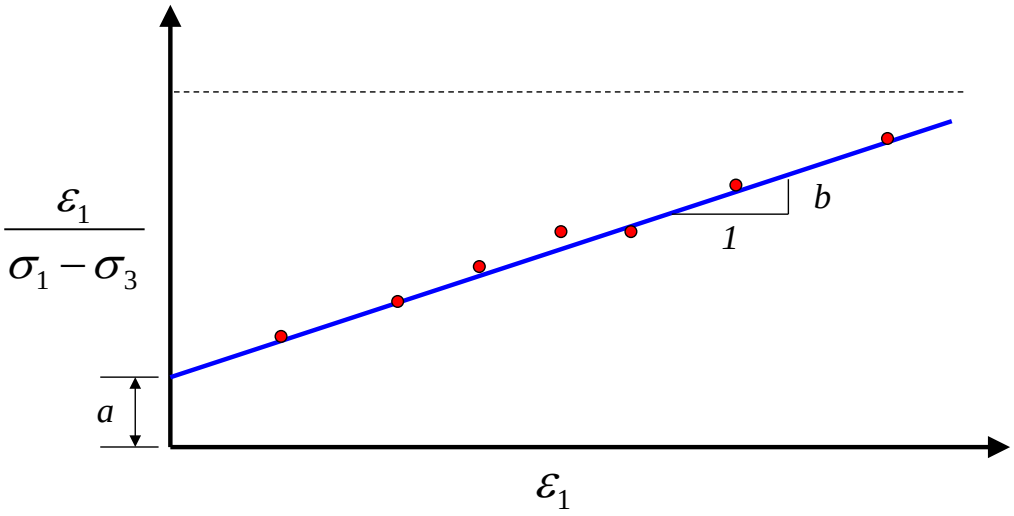

Figure 3.6 Transformed Hyperbolic Non-linear Soil Model

In Equation 3.13, $(\sigma_1$-$\sigma_3)_f$ represents the compressive strength of the soil at failure. The failure ratio is a measure of how close the laboratory stress-strain curve can be approximately by the hyperbola and typically ranges from 0.5 to 1.0 for most soils.

Kulhawy et al. (1969) proceeded to propose that the initial tangent modulus was a function of the confining pressure as illustrated in Figure 3.7 and defined by Equation 3.14.

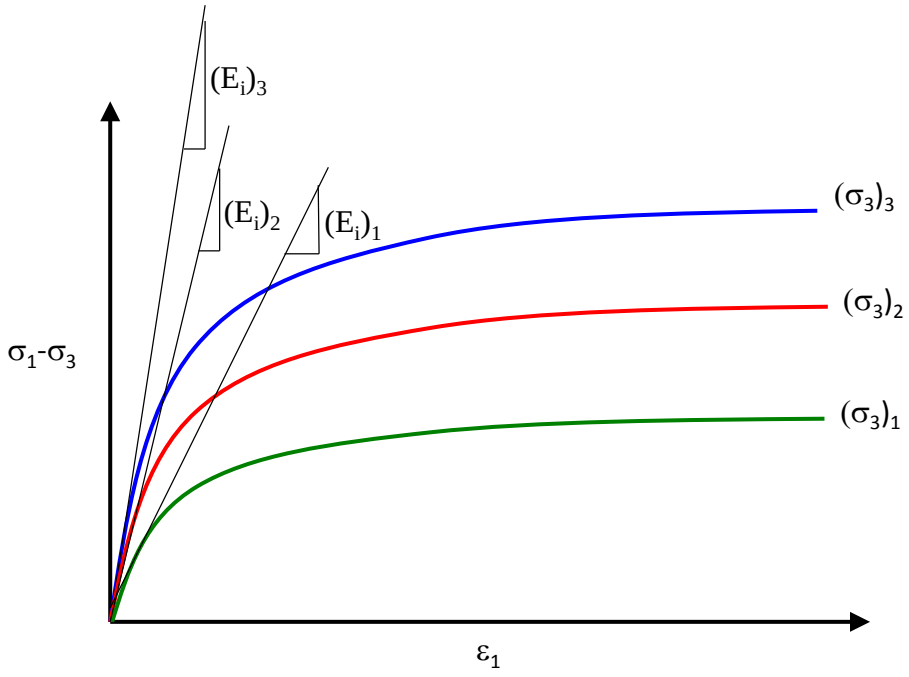

Figure 3.7 Dependency of initial modulus of elasticity E_i with confining pressure σ_3

$$E_i = Kp_a\left(\frac{\sigma_3}{p_a}\right)^n \tag{3.14}$$

where E_i is the initial tangent modulus, σ_3 is the minor principal stress, p_a is a reference stress usually set as the atmospheric pressure, K is a modulus number and n is an exponent determining the rate of variation between E_i and σ_3. Equations 3.13 and 3.14 are combined with the Mohr-Coulomb shear failure criterion defined mathematically by Equation 3.15 to determine the change in tangent modulus of elasticity at any point of the stress-strain curve.

$$(\sigma_1 - \sigma_3)_f = \frac{2\,c\,cos\phi + 2\,\sigma_3\,sin\phi}{1 - sin\phi} \tag{3.15}$$

Finally, the equation defining the tangent modulus is shown by Equation 3.16.

$$E_t = \left[1 - \frac{R_f(1-sin\phi)(\sigma_1-\sigma_3)}{2\,c\,cos\phi + 2\,\sigma_3\,sin\phi}\right] Kp_a\left(\frac{\sigma_3}{p_a}\right)^n \tag{3.16}$$

The non-linear axisymmetric finite element model implemented here uses a stress analysis where the total load is applied at equally small incremental loads to follow the stress-strain curve defined by the hyperbolic model and Equation 3.16 as shown in Figure 3.8.

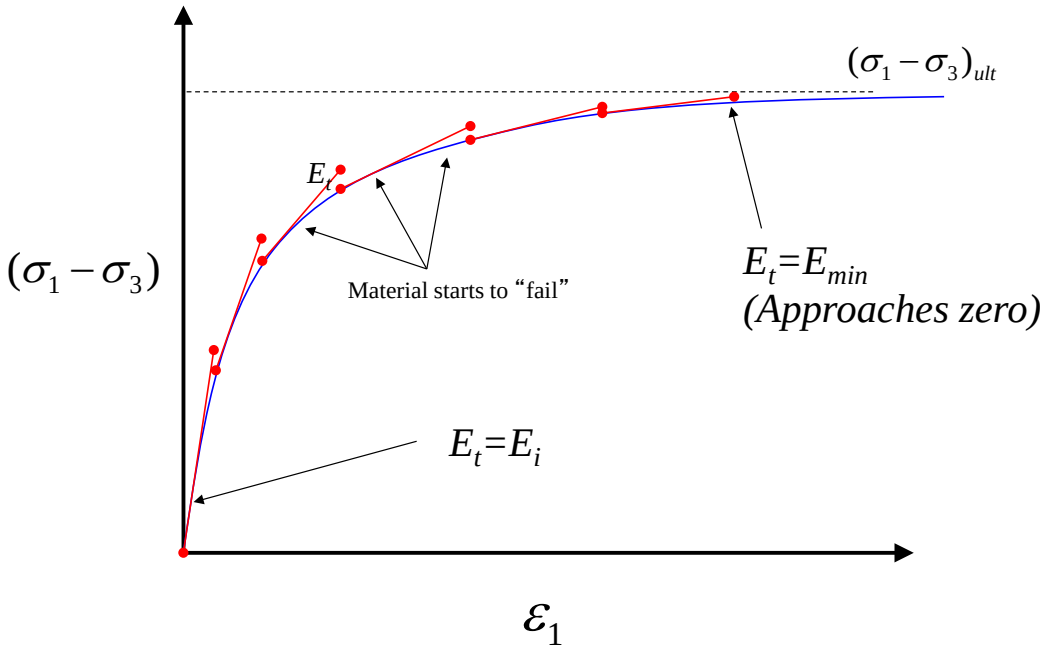

Figure 3.8 Incremental load solution

An additional feature added by the author to the basic Hinton and Owen model, was to maintain of a constant bulk modulus throughout the incremental analysis as shown in Figure 3.9. In essence, a constant bulk modulus prevents any volumetric change thus forcing the soil to fail in shear and avoid in this manner numerical problems when the modulus of elasticity tends to decrease near zero. This feature was implemented by using Equation 3.17 for a bulk modulus with an initial Poisson's ratio and then re-computing the Poisson's ratio (Equation 3.18) with this initial bulk modulus for the remaining of the load increments.

$$\overline{B_i} = \frac{E_t}{3(1-2\,v_i)} \tag{3.17}$$

$$v = \frac{1}{2}\left(1 - \frac{E_t}{3\overline{B_i}}\right) \tag{3.18}$$

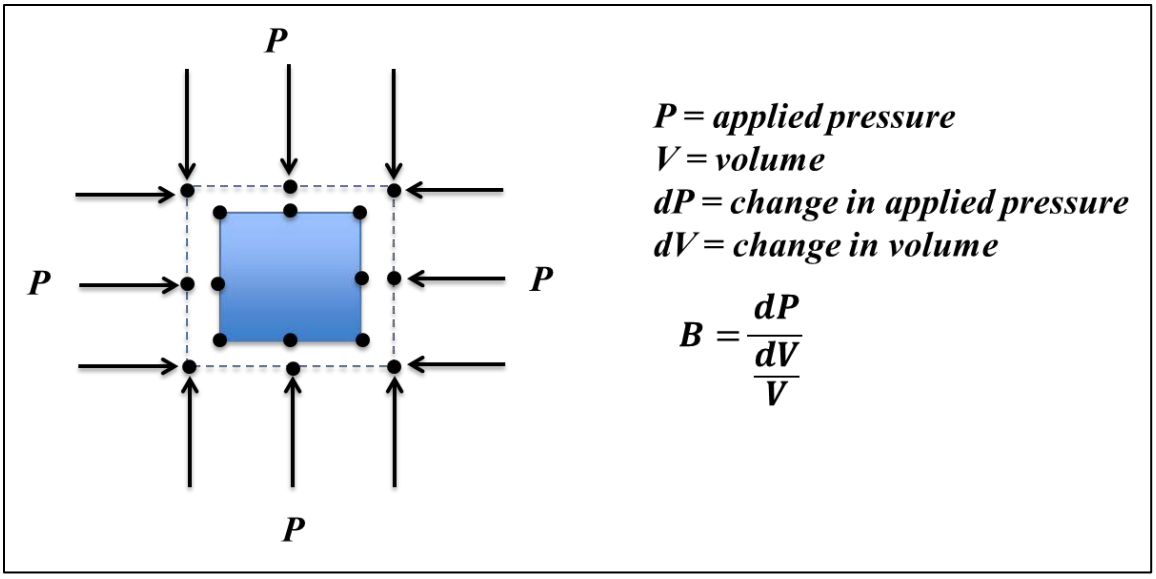

Figure 3.9 Constant bulk modulus assumption implemented in axisymmetric finite element method

As an illustration of this concept, let's assume the values for initial modulus of elasticity $E_{initial}$, initial Poisson's ratio $\nu_{initial}$, R_f, n, and deviator stress σ_1-σ_3, as shown in Figure 3.10. With these values, the tangential modulus (E_t) assigned to a finite element at any load step can be calculated using Equation 3.16. The Poisson's ratio is recomputed as given by Equation 3.18 and plotted against the tangential modulus of elasticity. The shear modulus, expressed by Equation 3.19, can also be plotted against the tangential modulus of elasticity.

$$G = \frac{E_t}{2(1+\nu)} \tag{3.19}$$

It can be observed from Figure 3.10 that as the tangential modulus of elasticity decreases from its initial value of 12,000 psi (82.8 MPa), the Poisson's ratio increases from its initial value of 0.3 to a value that approaches 0.5. At the same time, the shear modulus decreases from its initial value of approximately 4,600 psi (31.7 MPa) to a value near zero when the Poisson's ratio approaches a value of 0.5. This implies that by keeping the initial bulk modulus of a finite element constant, that finite element will be forced to undergo shear deformation instead of collapsing. Likewise, if the state of stress is changed such that the confinement is increased (such as in granular materials near the loaded area) the resulting effect would be of greater resistance to shear. Therefore, the concept of the constant bulk modulus has the potential to effectively handle

the collapse of finite elements in a simulation and the tendency of granular materials to resist shear forces when they are confined.

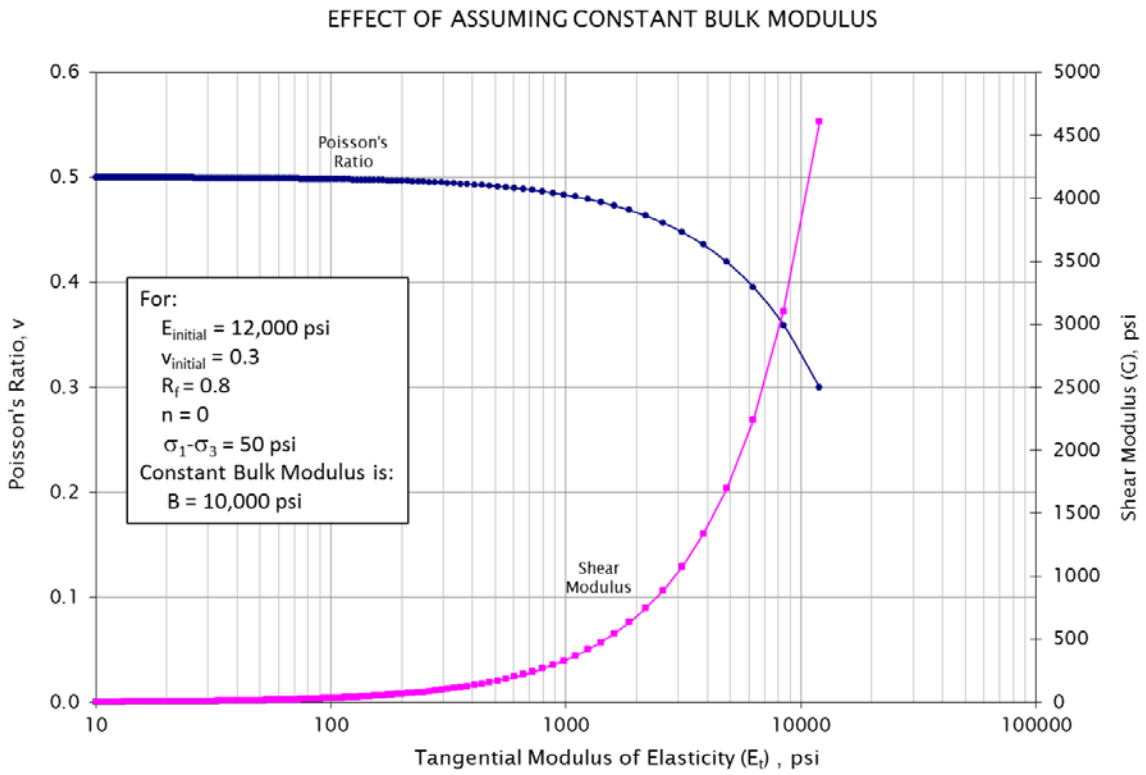

Figure 3.10 For constant bulk modulus, the interrelationships of Poisson's ratio, Elastic Modulus and Shear Modulus using the Duncan and Chang Model (1 psi = 6.9 kPa)

3.6 Summary

The prediction of stresses within a pavement structure greatly depends on the type of model used and the ability of the model to duplicate the actual behavior of the material under loading. Materials that exhibit non-linear behavior under load will give unsatisfactory stress predictions if linear material models are used. The selection of a response parameter to assess the bearing capacity of a pavement structure is also a critical issue, since it will influence that complexity of the model to be selected and the ability of the user to define accurate parameters that would define that model.

Increasing the complexity of a pavement model not always improves the prediction of stresses within a pavement structure. However, more advanced model are necessary to supplement material testing, since not all possible cases of loading conditions and material strengths can be tested. In such cases, the application of more advanced models will supplement and fill gaps, such as insufficient data points, as well as helping analyzed the accuracy and reliability of data collected in the laboratory and in the field.

In this research study, the single-layer Fröhlich stress model, the layered linear elastic model and an ax-symmetric hyperbolic non-linear material model were selected to model actual experimental pavement sections. Their state of stress predictions will be compared to each other and against stresses measured from within the pavement sections constructed for this research study.

In particular, the application of Fröhlich's stress model will be discussed in the next chapter to help derive the CBR equation from the point of view of vertical stresses. This derivation will show the stress-based nature of the CBR equation and will help define and formalize the proposed stress-based design procedure.

CHAPTER 4 - REFORMULATION OF THE CBR EQUATION

4.1 Introduction

When the U.S. Army Corps of Engineers selected the California method, they were accepting empirically developed thickness design curves. In extending the curves from highway loads to aircraft loads, the Corps employed Boussinesq's theory of stress distribution in a homogenous half-space. Even with the use of theoretical analyses to extend the curves to higher loads, the design curves were considered empirical, since they were originally based on empirical curves. Without realizing it, the developers of the CBR equation formulated an equation that represented a specific stress distribution. Recognizing that the CBR equation represents a specific stress distribution supports the argument that the CBR design method fits the definition of a mechanistic-empirical design procedure. That is, the procedure was derived from a model for computing stress and criteria that is based on the ratio of the computed stress with the measured soil strength. The ratio of computed stress to soil strength was related to pavement performance by traffic test data, therefore the design procedure may be defined as mechanistic-empirical procedure.

In extending the design criteria from single-wheel to multiple-wheel assemblies, pavement researchers considered vertical and shear stresses and deflection as the basis for computing an equivalent single-wheel load (ESWL) for a multiple-wheel assemble. The analysis performed while developing the ESWL methodology indicated the procedures based on stress to be un-conservative. On the other hand, the procedure based on deflection was deemed more conservative and provided a better fit for the performance data available at that time. Until this research effort was conducted, the reason why the stress-based CBR procedure would not provide a methodology of handling multiple wheel loads was not clear. This research helped reformulate the CBR equation to directly consider multiple-wheel assemblies and represent a more complete stress-based mechanistic-empirical procedure.

With the reformulation of the CBR equation, the mechanistic nature of the CBR pavement design procedure is readily apparent. The following sections explain how the CBR equation was

redeveloped to show its stress-based origin. The equation is also reformulated to consider traffic volume and multiple-wheel loads in a more direct manner.

4.2 Re-development of the CBR Equation

Stress distribution in a homogeneous half-space can be described by the use of a stress concentration factor. The stress concentration factor was introduced by Professor Otto Karl Fröhlich (Jumikis 1964; Jumikis 1969; Ullidtz 1998) to explain the fact that early measurements of stresses showed that the theory of elasticity was not totally satisfactory. As defined in the Lockbourne No. 2 report, the concentration factor (*n*) is an empirical exponent introduced into the Boussinesq equation to make computed stresses agree more closely with measured stresses. About Fröhlich's concentration factor, Jumikis states:

> *"Thus, by modifying Boussinesq's isotropic, semi-infinite medium of constant elasticity to an anisotropic, semi-infinite medium, Fröhlich made the subject of the complex stress distribution problem more comprehensible and far-reaching than in Boussinesq's problem."*

The equation for the vertical stress due to a point load, *P*, is of great importance in the redevelopment and reformulation of the CBR equation. The general form of the equation as given by Ullidtz (1998) is:

$$\sigma_t = \frac{nP}{2\pi z^2} cos^{n+2}\theta \qquad (4.1)$$

where

P = applied point load at the surface

σ_t = vertical stress at an arbitrary point

R = distance from the point load to the location of σ_t

θ = angle between the vertical line and the line connecting load application point and an arbitrary point in the soil where to calculate the stress

n = Fröhlich's stress concentration factor.

Using Equation 4.1, the stress at any arbitrary location in a semi-infinite medium due to a loaded area can be determined by integrating over the loaded area. When the concentration factor *n* is equal to 3, Equation 4.1 is the same as the Boussinesq equations for stress. For a vertical stress at depth *t* along the centerline of a uniformly distributed circular load, Equation 4.1 reduces to:

$$\sigma_t = \sigma_o \left[1 - \frac{1}{\left(\sqrt{1 + \left(\frac{r}{t} \right)^2} \right)^n} \right] \tag{4.2}$$

where

r = radius of the load area

t = depth to the location of the computed stress

n = stress concentration factor

σ_o = applied stress over the loaded area.

For a stress concentration factor *n* equal to 3, Equation 4.2 is identical to the Boussinesq equation for the vertical stress under a uniformly loaded circular area. When the concentration factor is equal to 2, Equation 4.2 reduces to Equation 4.3.

$$\sigma_t = \sigma_0 \left[1 - \frac{1}{1 + \left(\frac{r}{t} \right)^2} \right] \tag{4.3}$$

Equation 4.3 can also be rewritten in the form of Equation 4.4.

$$\sigma_t = \sigma_0 \left[\frac{1}{1 + \left(\frac{t}{r} \right)^2} \right] \tag{4.4}$$

The original airfield design curves based on shear stress were an extrapolation of the California pavement design curves for highway pavements (American Society of Civil Engineers

1950; Ahlvin 1991). The extrapolated curves were modified and verified by extensive full-scale field testing. The first airfield design curves were represented by the following design equation.

$$t = K\sqrt{P} \tag{4.5}$$

where

P = wheel load in pounds

t = thickness in inches

K = a constant that was a function of subgrade CBR and tire contact pressure.

The values of K for the original design curves are given in Table 4.1. If it is assumed that the load P is applied as a uniform pressure p over a circular area with a radius r, then Equation 4.5 can be rewritten as:

$$t = K\sqrt{p\pi r^2} \tag{4.6}$$

Equation 4.6 can also be expressed as:

$$\left(\frac{t}{r}\right)^2 = K^2 p\pi \tag{4.7}$$

Equation 4.7 can now be substituted into Equation 4.4 to obtain Equation 4.8.

$$\sigma_t = \sigma_o\left[\frac{1}{1+K^2 p\pi)}\right] \tag{4.8}$$

Since both, σ_o and p, are the applied surface pressure over a circular area of radius r, Equation 4.8 can be written in the following form.

$$\sigma_t = \left[\frac{1}{\pi\left(K^2 + \frac{1}{p\pi}\right)}\right] \tag{4.9}$$

When both sides of Equation 4.9 are divided by the CBR, Equation 4.9 can be rewritten as:

$$\frac{\sigma_t \pi}{CBR} = \frac{1}{\left[K^2 + \frac{1}{p\pi}\right] CBR} \tag{4.10}$$

A common criterion for design of structures is to limit the ratio of the applied stress to allowable strength. Applying this concept to flexible pavements, one criterion is to limit the ratio of stress to the strength occurring at the top of the subgrade. In Equation 4.10, σ_t represents the applied stress at the top of the subgrade, and the CBR represents the strength of the subgrade. Thus, in a properly designed flexible pavement, the left side of the equation should be a constant since all the pavements were to be designed for the same life. The stress σ_t then becomes the design stress σ_{design} for specific subgrade strength. Continuing with the assumption that the left side of Equation 4.10 is constant, the right side of Equation 4.10 must also be a constant as well as the denominator of the right side of the equation. As shown in Table 2.1, the value of the denominator can be evaluated for given values of *K*. It was found that the average value of the denominator of the right side of Equation 4.8 was approximately 0.1236, which resulted in the right side of the equation being a constant with value of 8.1 in units of pounds per square inch (56 kPa). Such value represents the design criterion for capacity operations. Referring the constant for capacity operation as β_1, the design criteria for the design curves developed in the 1940's is represented by Equation 4.11.

$$\frac{\sigma_{design} \pi}{CBR} = \beta_1 = 8.1 \text{ in psi (56 kPa)} \tag{4.11}$$

Equation 4.9 can now be rewritten as Equation 4.12.

$$\beta_1 = \frac{1}{CBR\left[K^2 + \frac{1}{\pi p}\right]} \tag{4.12}$$

Using Equation 4.12, the value of k is found to be:

$$K = \sqrt{\frac{1}{\beta_1 CBR} - \frac{1}{\pi p}} \tag{4.13}$$

Substituting the value of *K* as given in Equation 4.13 into Equation 4.5, the following equation for pavement thickness is obtained.

$$t = \sqrt{\frac{1}{\beta_1 CBR} - \frac{1}{\pi p}}\sqrt{P} \tag{4.14}$$

Considering the relationship between *P* and *p*, Equation 4.14 can be rewritten as:

$$t = \sqrt{\frac{p}{\beta_1 CBR} - \frac{1}{\pi}}\sqrt{A} \tag{4.15}$$

Since β_1 is equal to *8.1*, Equation 4.15 can now be rewritten to yield one of the classic forms of the CBR equation as follows:

$$\frac{t}{\sqrt{A}} = \sqrt{\frac{p}{8.1\,CBR} - \frac{1}{\pi}} \tag{4.16}$$

The previous reasoning showed that Turnbull, Foster, and Ahlvin's CBR design equation was obtained by considering the stress distribution as defined by Fröhlich's concentration factor. The earlier development of the CBR equation was based on the imposed requirement that the deflection at a depth *t* for constant ratios of $\frac{t}{r}$ would be a constant. Such requirement is also met when the stress distribution as described by Fröhlich has a stress concentration factor equal to 2. The classic form of the CBR equation described by Equation 4.16 can also be rearranged to explicitly show the ratio of thickness to the radius of the loaded area as shown in Equation 4.17.

$$\frac{t}{r} = \sqrt{\frac{\pi\, p}{8.1\,CBR} - 1} \tag{4.17}$$

where

p = pressure applied to loaded area

r = radius of the loaded area

t = thickness of pavement structure.

4.3 Criteria for Single-Wheel Gears

As has been discussed, a thickness adjustment factor was introduced into the classic CBR equation to adjust the pavement thickness to account for the requirement of different volumes of traffic. As originally developed, the CBR equation was to define the thickness requirement for a traffic volume for capacity operation of an airfield pavement of 5,000 coverages. The first thickness adjustment factor for traffic volume other than capacity operations was defined by the expression:

$$factor = 0.23\log(C) + 0.15 \tag{4.18}$$

When Equation 4.18 is applied, Equation 4.17 becomes:

$$\frac{t}{r} = (0.23\log(C) + 0.15)\sqrt{\frac{\pi p}{8.1\ CBR} - 1} \tag{4.19}$$

At 5,000 coverages, the value of Equation 4.18 is approximately 1.0. Later, Equation 4.18 was dropped, and a thickness adjustment factor, α, was substituted for Equation 4.18. The thickness adjustment factor, α, was developed to account for both traffic volume and number of tires in the tire group of the design aircraft. Thus, α became a function of both traffic volume in terms of coverages and number of tires in the tire group, and the general form of the CBR became as shown in Equation 4.20.

$$\frac{t}{r} = \alpha\sqrt{\frac{\pi p}{8.1\ CBR} - 1} \tag{4.20}$$

In Equation 4.20, the value *8.1* inside the radical is a constant related back to the origin of the CBR equation with the α-factor inserted to consider traffic volume. The criteria defined by Equation 4.20 will be known in this research study as the CBR-Alpha criteria. In Equation 4.20, α is applied outside of the radical and is a multiplier of both terms under the radical. However, as has been shown, the stress criterion is contained only in the first term under the radical. By applying the thickness adjustment factor outside the radical it caused the stress criterion to be modified. The amount of modification to the criterion is a function of the relative magnitude between the first and the second terms under the radical. If the *8.1* constant is replaced with β which is a function of the traffic volume, then α in Equation 4.20 can be dropped, and the CBR equation, in terms of β, becomes:

$$\frac{t}{r} = \sqrt{\frac{\pi p}{\beta\ CBR} - 1} \tag{4.21}$$

For a single tire, α is a function only of the traffic volume. Designating α_1 as the value of α for a single tire and substituting α_1 into Equation 4.20 for the thickness adjustment factor, the following equation is obtained

$$\frac{t}{r} = \alpha_1 \sqrt{\frac{\pi p}{8.1\ CBR} - 1} \tag{4.22}$$

In Equation 4.21, β is also a function of traffic volume. Therefore, for identical values of *t/r*, the right side of Equation 4.21 can be set equal to the right side of Equation 4.22 to obtain Equation 4.23.

$$\sqrt{\frac{\pi p}{\beta CBR} - 1} = \alpha_1 \sqrt{\frac{\pi p}{8.1 CBR} - 1} \tag{4.23}$$

Equation 4.23 is then solved for β to obtain the following relationship between α_1 and β.

$$\beta = \frac{\pi p}{CBR\left[\frac{\pi p \alpha_1^2}{8.1 CBR} - \alpha_1^2 + 1\right]} \tag{4.24}$$

Equation 4.24 shows that when α_1 is equal to 1, the value of β is a constant, which is *8.1*, and when α_1 is zero, which means no pavement thickness is required, the value of β/π is equal to *p/CBR*. Referring back to Equation 4.11, β/π is also equal to σ_{design}/CBR. Therefore, when $p = \sigma_{design}$, no pavement is required. For any other value of α_1, the value of β will be a function of the *p/CBR* ratio. Since α_1 is related to single-wheel traffic volume and β is related to α_1 by Equation 4.24, β can be related to single-wheel traffic volume directly by Equation 4.24. Figure 4.1 provides an example of the relationship between β and traffic in terms of coverages.

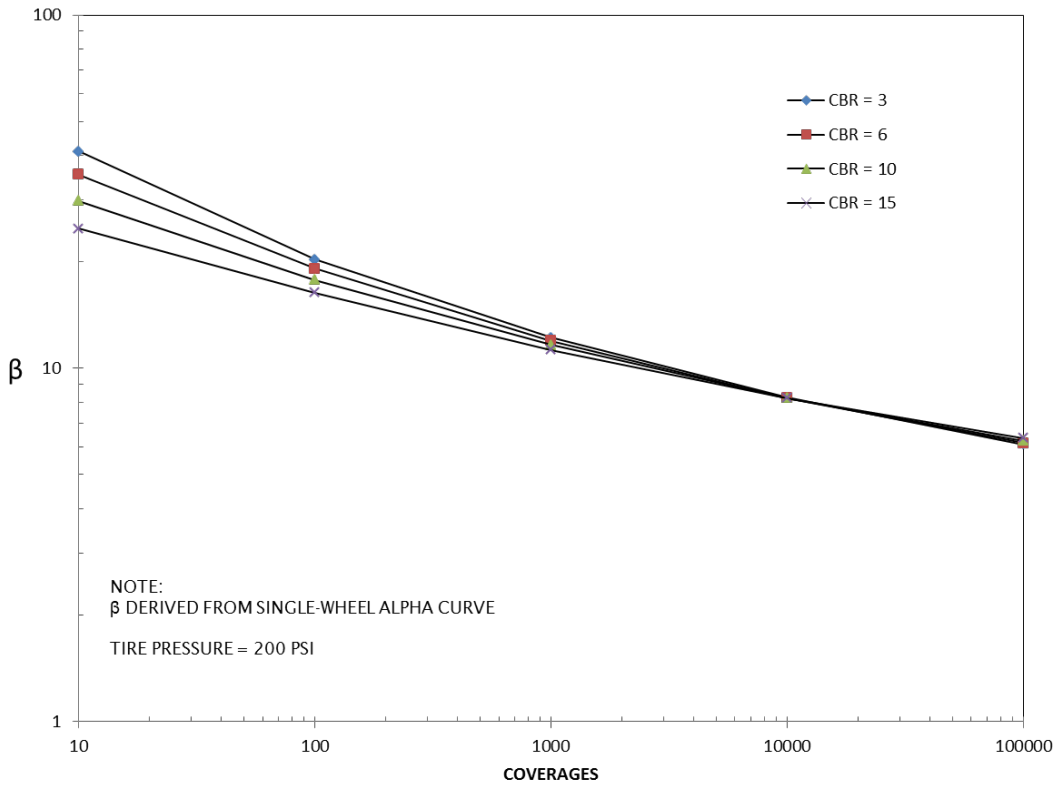

Figure 4.1 Relationship between Beta and coverage as developed from single-wheel criteria (1 psi=6.9 Kpa)

In developing the relationship of Figure 4.1, p was assumed to be constant at a value of 200 psi (1380 kPa). For a level of traffic of approximately 10,000 coverages, β is a constant equal to *8.1* over the range of CBR values used. This represents the level of traffic for which α_1 is equal to 1. For levels of traffic lower than 10,000 coverages, β decreases with increasing CBR, and at traffic levels above 10,000 coverages, the reverse is true. The mathematical explanation for the difference between α and β is that α is applied outside the radical and, therefore, a multiplier of both terms under the radical, whereas, β is applied to only one term under the radical.

The analytical development presented suggests that the proper criterion is a stress criterion as represented by β. The data shown in Figure 4.1 were used to develop an equation for stress criterion based on β. The form of the equation was chosen to be:

$$\log \beta = \frac{a + c \log Coverages}{1 + b \log Coverages} \qquad (4.25)$$

The values of the constants a, b, and c were determined by assuming three points of fit for the relationship. The values of β chosen for the fit were 79.4, 8.1, and 5 for traffic levels of 1, 10,000, and 1,000,000 coverages, respectively. The computed values for the constants a, b, and c, were 1.8998, 0.2276 and 0.0411, respectively. Replacing such values in Equation 4.25 yields the performance criteria in terms of β for single-wheel assemblies.

$$\log \beta = \frac{1.8998 + 0.0411 \log Coverages}{1 + 0.2276 \log Coverages} \tag{4.26}$$

In Figure 4.1, it is seen that the relationship given by Equation 4.25 follows very close to the relationship representing a CBR value of 6. With the relationship between β and traffic volume defined in Equation 4.26, Equation 4.21 can be used to compute pavement thicknesses for any level of traffic. Figure 4.2 provides a comparison between thicknesses computed using the β criteria and the thicknesses computed using the α_1 criteria.

For thicknesses determined in this manner, the ratio of σ_{design}/CBR will be a constant for a given level of traffic. For a traffic level of 10,000 coverages, the thicknesses computed by both procedures are identical. For a CBR value of 6, the thicknesses computed by both procedures are in very close agreement for the entire range of traffic levels. The thicknesses as determined by both procedures are in very close agreement for all values of CBR for traffic levels above 10,000 coverages. The only areas of significant difference between the two procedures are for CBR values of 3 and 15 and low levels of traffic. Figure 4.3 provides another comparison of α and β criteria for the single wheel loading.

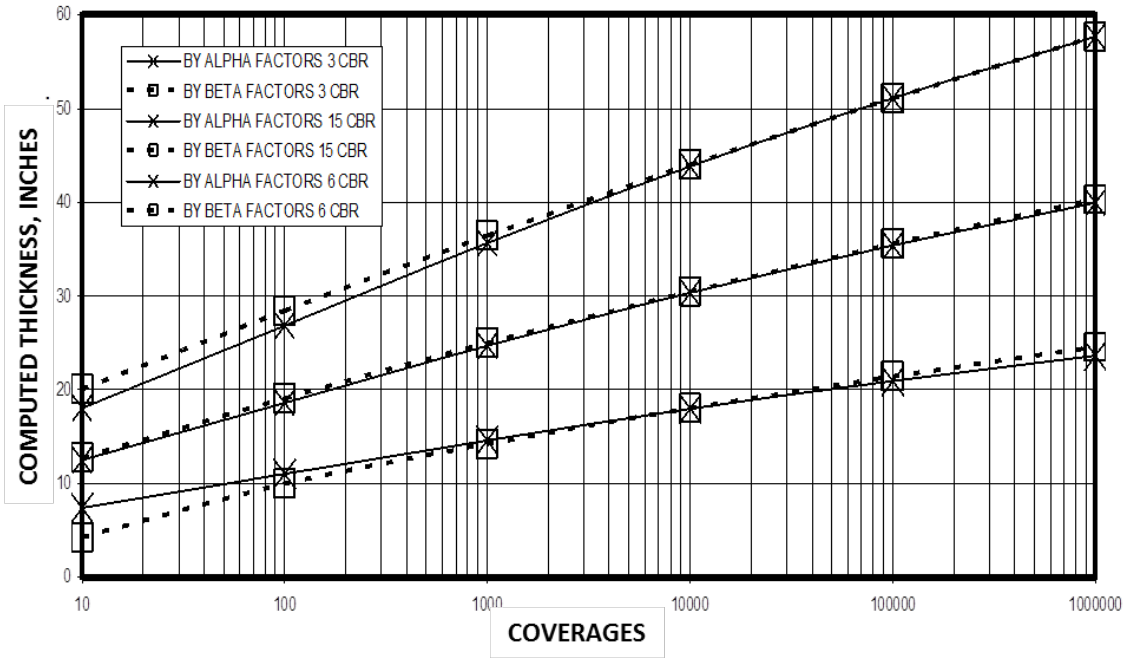

Figure 4.2 Comparison of α-criteria with β-criteria for single wheel

(1 inch=25.4 mm)

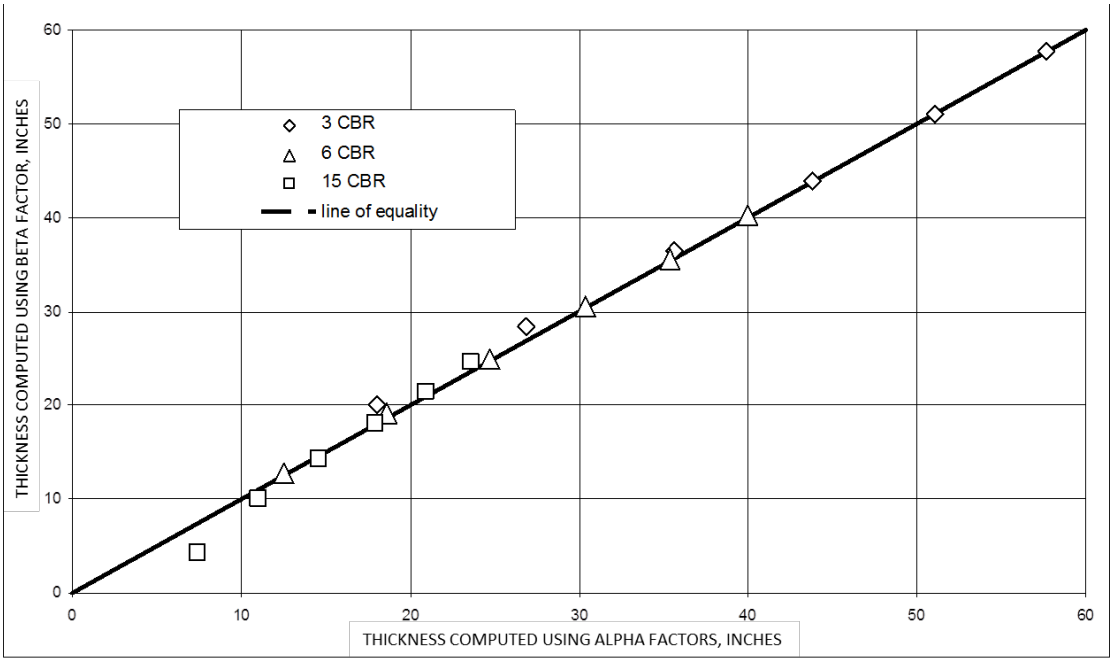

Figure 4.3 Comparison of thicknesses based on α-criteria and β-criteria

(1 inch=25.4 mm)

From the above analysis, it is apparent that for a single-wheel loading, the formulation of the CBR equation in terms of β is essentially the same as that of the original formulation in terms of α_1. One important aspect of the new formulation is that the mechanistic nature of the CBR design methodology and the stress criteria are now apparent.

4.4 Criteria for Multi-Wheel Gears

Although the new formulation of the CBR equation is considered more robust than the original formulation when considering single-wheel assemblies, the real benefit of the new formulation is in handling multi-wheel loading. There are two means of providing design criteria for multi-wheel tire groups. The first is through the use of equivalent single-wheel loads in a manner that is used in the current implementation of the CBR design procedure. The principle of the equivalent single-wheel for handling multi-wheel assemblies is to determine a single-wheel load that would have the same effect on pavement performance as does the tire group assembly. Since the newly formulated CBR equation is really based on the vertical stress at the top of the subgrade, that vertical stress would be the response parameter on which to base the equivalent single-wheel load (ESWL). Here, the ESWL is defined as that load applied on a single wheel that would produce the same maximum deflection or stress as does the multi-wheel assembly. When considering the conversion of the method of ESWL computation from deflection to vertical stress, the 1955 work done by Turnbull, Foster, and Ahlvin was reviewed. Foster (et.al.) considered shear and vertical stresses along with deflection as a basis for computing the ESWL. Their analysis concluded that the stress-based ESWL procedures were un-conservative, but that the deflection based ESWL procedure could be used for developing design criteria for multi-wheel assemblies. The fact that in the earlier studies, the stress-based ESWL procedure was considered to be un-conservative certainly provided reasons to be cautious in developing criteria based on vertical stress. Later, studies conducted in the analysis of the MWHGL test section data indicated the deflection based ESWL resulted to be overly conservative, and required the introduction of the thickness correction factor into the classical CBR equation.

4.5 Review of Current Equivalent Single-Wheel Load Approach (ESWL)

In the current CBR equation, where the alpha factor is applied outside the radical of equation 4.20 (CBR-Alpha), the ESWL at a specified depth is defined as the load on a single tire that would produce the same elastic deflection at the specified depth in an elastic half-space having a constant elastic modulus and a Poisson's ratio equal to 0.5, as would the tire group. The elastic deflection at the specified depth is computed for both the tire group and for a single tire having the same contact area as an individual tire of the tire group. Since the contact area of the ESWL tire remains constant and the load is varied by changing the contact pressure, the ESWL is determined by the following equation:

$$ESWL = \frac{\delta_{mwl}}{\delta_{swl}} SWL \tag{4.27}$$

where:

SWL = load on the single wheel used to compute the single wheel deflection
δ_{mwl} = elastic deflection due to the multi-wheel loading
δ_{swl} = elastic deflection due to the single-wheel loading.

When Cooksey and Ladd (1971) analyzed the performance data from the multiple-heavy gear load tests (MGHWL) test section, they concluded that the deflection-based ESWL was over-predicting the true ESWL and that the over- prediction was a function of the number of tires. The solution chosen by Cooksey and Ladd was to develop thickness adjustment factors to account for both repetitions and over-predictions of the ESWL. The thickness adjustment factor was referred to as the alpha factor (α factor). Thus, when Equation 4.20 is used as the multi-wheel design criteria, the α-factor of Equation 4.20 is the product of the repetition alpha, (α_r), and the load correction alpha, (α_l). Since α_r for a multi-wheel tire group should ideally be identical to the repetition alpha as is used for a single wheel loading, then the following relationship for α_l should hold:

$$\alpha_l = \frac{\alpha}{\alpha_1} \tag{4.28}$$

where

α = total thickness correction factor needed for a multi-wheel tire group

α_1 = thickness correction factor needed for a single tire.

Equation 4.28 can be used, along with the data in the alpha curves proposed by Cooskey and Ladd (1971), to compute the load related alpha factor for various tire groups. At 10,000 coverages, α_1 has a value of approximately 1.0. Therefore, at 10,000 coverages, the load-related alpha will equal the total alpha correction factor. Applying a thickness adjustment can be approximated by an adjustment to the ESWL. Since the α-factor thickness adjustment is applied outside the radical in Equation 4.20, the adjustment to the ESWL needed to approximate the α-adjustment is the square of the α-factor. At 10,000 coverages, the following approximate relationship holds

$$t = \alpha\sqrt{\frac{ESWL}{8.1CBR} - \frac{A}{\pi}} = \sqrt{\frac{\alpha_1^2 ESWL}{8.1CBR} - \frac{\alpha_1^2 A}{\pi}} \approx \sqrt{\frac{\zeta ESWL}{8.1CBR} - \frac{A}{\pi}} \tag{4.29}$$

In Equation 4.29, ζ is a correction to account for over- or under-estimating the ESWL and is equal to the α-factor squared. In Equation 4.29, the first term under the radical is typically an order of magnitude larger than the second term, therefore it can be assumed that the ζ factor actually only corrects for the ESWL. Based on the α-curves in current use, the values of α at 10,000 coverages for the 2-tire, 4-tire, and 6-tire assemblies are approximately 0.89, 0.82, and 0.78, respectively. Therefore at 10,000 coverages, the adjustments needed for the ESWL to approximate the thickness adjustments for the 2-tire, 4-tire, and 6-tire assemblies are 0.79, 0.67, and 0.61, respectively. The study by Barker and Gonzalez (2006) showed that more appropriate values of the 10,000-coverage thickness reduction factors α for the 4-tire and 6-tire assemblies are 0.78 and 0.72, respectively. These data produce adjustment factors ζ for the ESWL for the 4-tire and 6-tire assemblies of 0.61 and 0.52, respectively. The above analysis implied the following:

- The ESWL based on deflection over-estimates the “true” ESWL
- The ESWL over-estimation is a function of the number of tires.
- At 10,000 coverages, the ratios of the “true” ESWL to the deflection-based ESWL are in the order of 0.79, 0.61, and 0.52 for 2-wheel, 4-wheel, and 6-wheel assemblies, respectively

4.6 Comparison of Stress-Based ESWL with Deflection-Based ESWL

With the assumption that the stress-based ESWL computed with *n=2* represents the "true" ESWL, the criteria developed for the single-wheel assemblies would also be applicable to multi-wheel assemblies. To prove the assumption, pavement thicknesses were computed for 10,000 coverages of single, twin, twin-tandem, and triple-tandem aircraft. These thicknesses were computed for a range of CBR values using the current α-factor design criteria and the single-wheel *β*-criteria. Figures 4.4, 4.5, 4.6 and 4.7, show thickness comparisons for the F-15, Boeing 737, Boeing 747, and Boeing 777 aircraft.

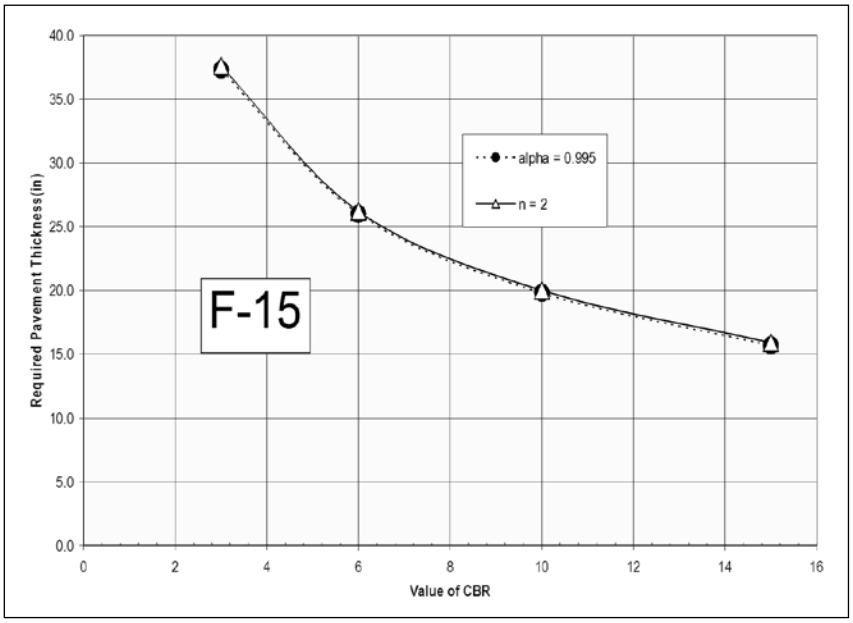

Figure 4.4 Comparison of thicknesses between α and β criteria for the F-15 Aircraft (1 inch=25.4 mm)

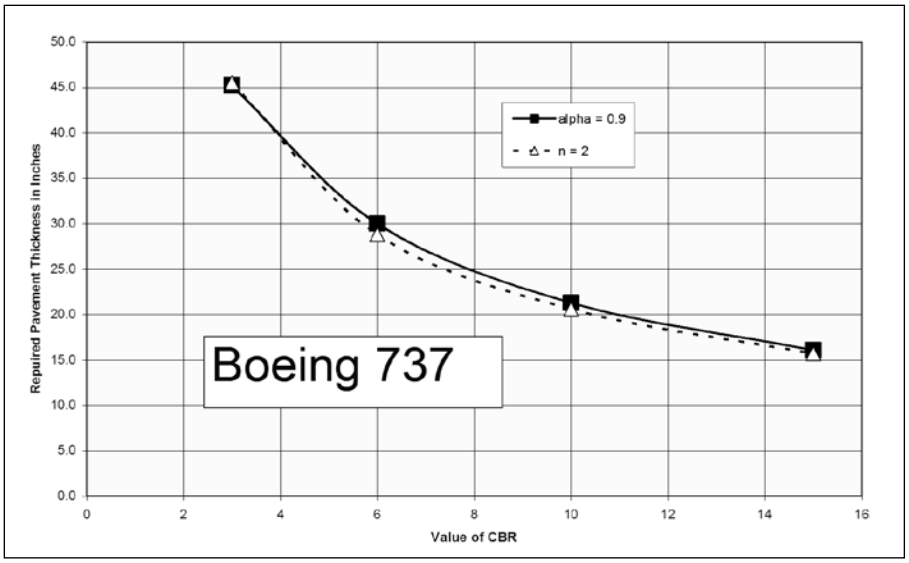

Figure 4.5 Comparison of thicknesses between α and β criteria for the Boeing 737 (1 inch=25.4 mm)

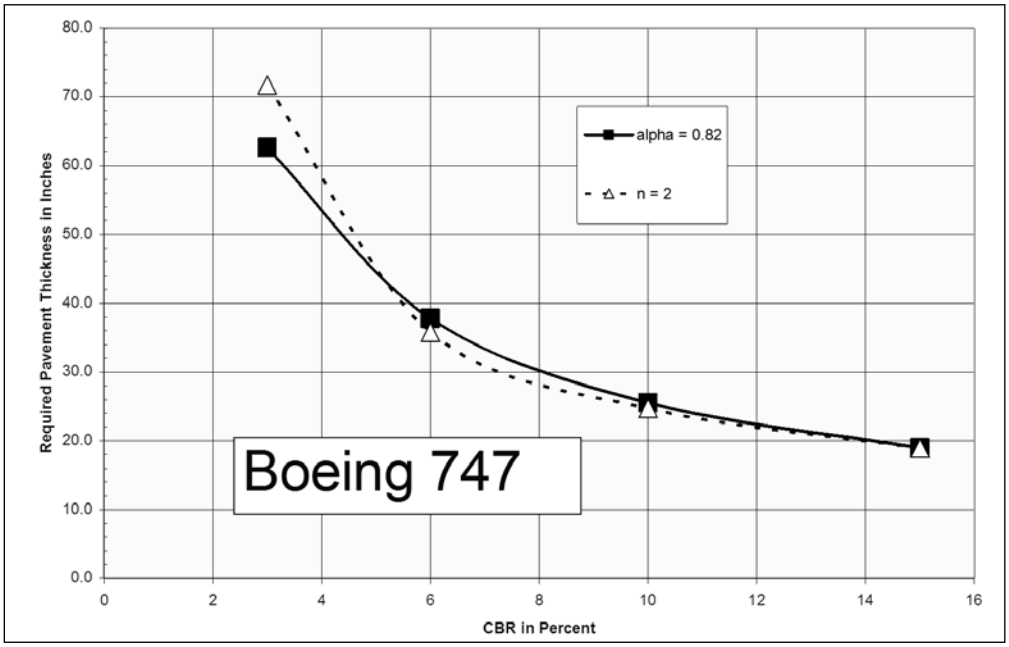

Figure 4.6 Comparison of thicknesses between α and β criteria for the Boeing 747 (1 inch=25.4 mm)

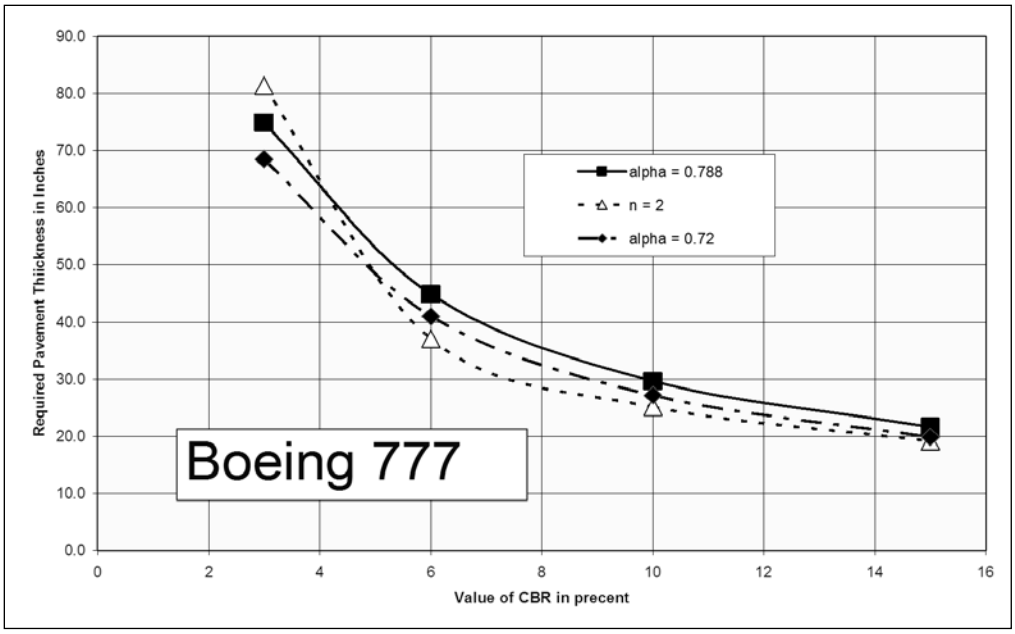

Figure 4.7 Comparison of thicknesses between α and β criteria for the Boeing 777 (1 inch=25.4 mm)

For the single-wheel assembly, the thicknesses computed with both criteria are essentially identical. This was expected since the β-criteria were mathematically derived from the α-factor criteria, which at 10,000 coverages are essentially identical. For multi-wheel assemblies, the differences of thicknesses between the two criteria are a function of the number of tires and the CBR values. Figure 4.5 shows that for the twin-tire assembly the computed thickness is greater than for the single-wheel assembly, although the difference is small.

The above thicknesses were computed based on β criteria developed from the single-wheel α-factor curve. A more direct approach for developing the multi-wheel β criteria consists of backcalculating β from the test section data and developing the relationship between β and test section performance represented by the number of coverages to failure. Test data tabulated in the Barker and Gonzalez report (Barker and Gonzalez 1994) and test section data collected by the FAA (Hayhoe 2004) allowed formulating the relationship between β and number of coverages to for a stress concentration factor of equal to two. Such a relationship is presented in Equation 4.30 and Figure 4.8 shows the curve function along with the criteria for single wheels.

$$\log(\beta) = \frac{1.7782 + 0.2397 \log(Coverages)}{1 + 0.5031 \log(Coverages)} \tag{4.30}$$

The data in Figure 4.8 indicates that the single-wheel criteria, as developed from the single-wheel α-factor curve, does not provide a good fit of the test section data and that a better fit can be obtained using Equation 4.26. Fitting the data as previously discussed, results in the criteria as given by Equation 4.30.

In addition, Figure 4.8 shows that the curve drawn for the multi-wheel fits the data from the test sections studied. Therefore, a single criteria curve could be used for both single-wheel and all multi-wheel assemblies and that the use of the α-factor can be eliminated from the design criteria.

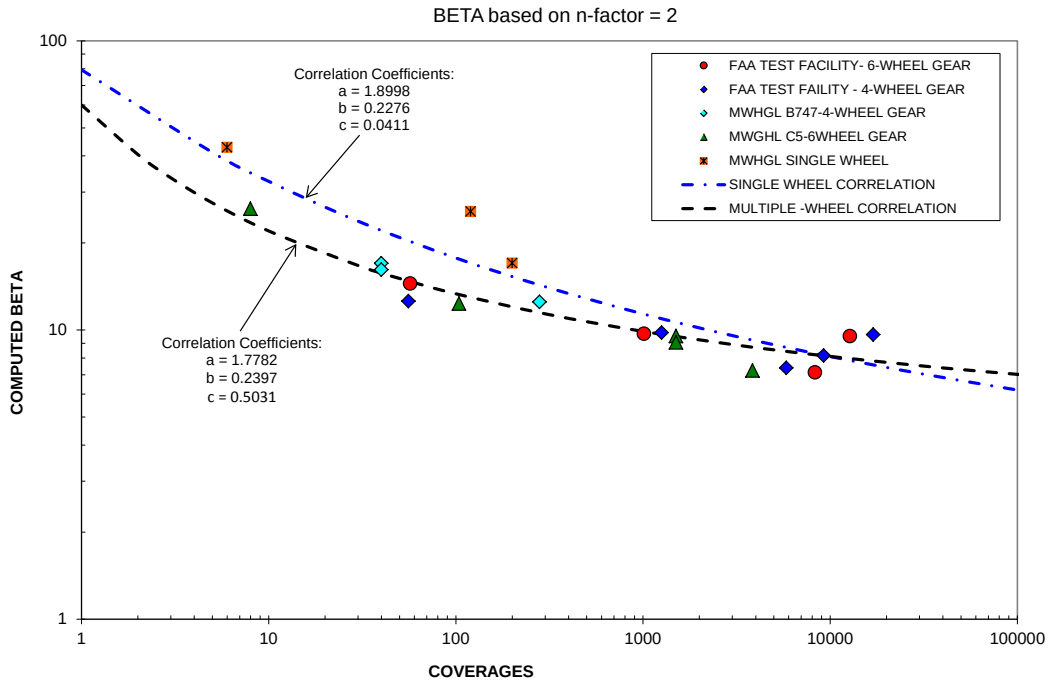

Figure 4.8 Comparison of *n*=2 criteria with α criteria

4.7 CBR-Beta Criteria for Multi-Wheel Aircraft

Figure 4.9 provides a comparison of the multi-wheel test data for concentration factors values equal to 2 and 3. The figure shows that there is minimal offset between the two data sets and no discernable difference in the scatter of the data. From this comparison it can be inferred that the design criteria could be developed assuming a concentration factor of either 2 or 3. In developing the criteria for different values of the concentration factor, the stress-based CBR

equation was reformulated in a form for which the stress concentration factor was also an independent variable. This way, variations in the stress distribution can be evaluated when developing the design criteria.

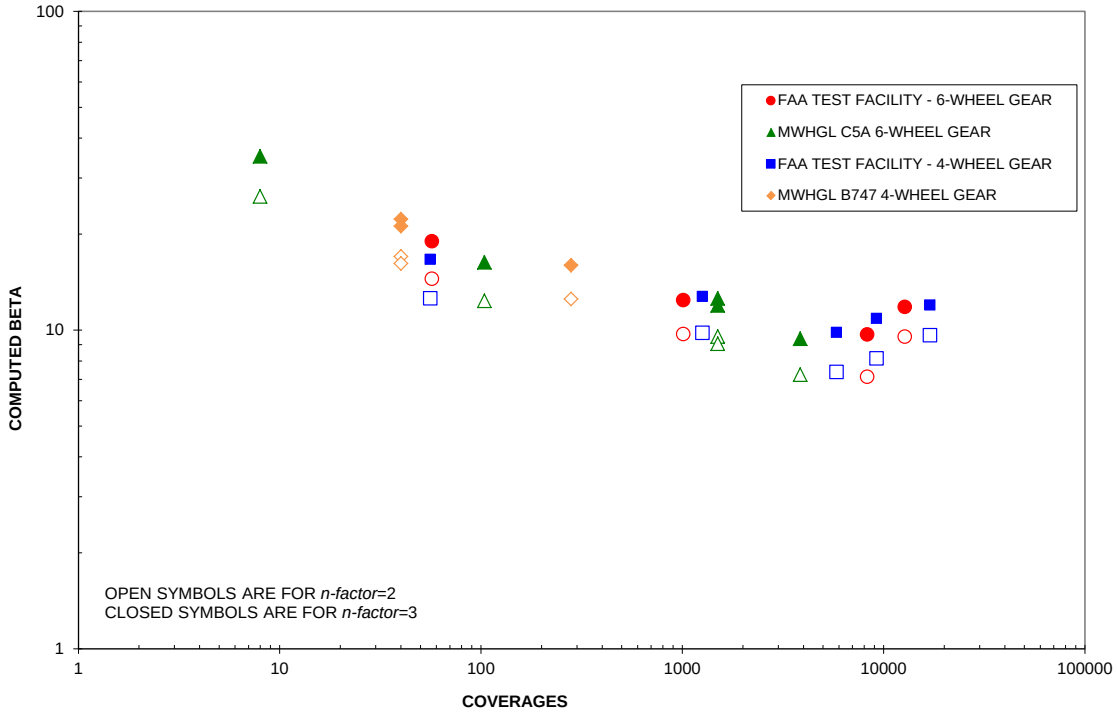

Figure 4.9 Comparison of test data for n=2 and n=3

The general form for the stress-based CBR equation for any stress concentration factor *n*, and a circular loaded area with radius *r*, has been derived and is shown in Equation 4.31.

$$\frac{t}{r} = \frac{1}{\sqrt{\left(\frac{1}{1-\frac{\beta CBR}{\pi p}}\right)^{\frac{2}{n}} - 1}} \tag{4.31}$$

The computation of the β values for the test data are based on the assumption that the tire loads are applied over uniformly loaded circular areas. For single-wheel loads, Equation 4.2 computes the vertical stress for given values of *n*, whereas Equation 4.1 can be integrate over the loaded areas and used for multi-wheel loads. With the ability to compute β based on any arbitrary stress concentration factor and with the indication that criteria could be developed for different values

for the stress concentration factor, the main objective now consists of selecting the most appropriate stress concentration factor. The analysis of measured stresses due to applied loads and computed stresses suggests that the best correlation is obtained for a stress concentration factor between 2 and 3.

4.8 Development of Correlation Between n-factor and CBR

According to Fröhlich, the magnitude of the stress concentration factor depends upon the nature of the soil and the size of the loaded area (Jumikis 1969). A stress concentration factor of 3 is applicable for an isotropic body with a constant modulus of elasticity. For sands, according to Fröhlich, a concentration factor of 4 would be applicable. The Stockton No. 2 Test included four instrumented test pavement sections of which stresses were measured for different loading and time of the day. The subgrade of the four sections varied between the three subgrade groups. One section had subgrade with a CBR of 6 which belongs to the "weak" group; another section subgrade was in "medium strength" group with a CBR of 20. The last two sections had subgrade belonging to the "strong" subgrade group with CBR of 70 and 80, respectively. The asphalt thickness for all of the sections was 6 inches (152 mm).

The measured stress data were compared with theoretical stresses in plots of the vertical distribution of stress with depth. In the plots given in the Stockton No. 2 Test report, it is seen that a large portion of the scatter in the measured data can be explained by the difference in pavement temperature. For each of the items, the low temperature data indicate a Fröhlich theoretical concentration factor of less than 2 to be appropriate. The majority of the data falls between the theoretical curves corresponding to concentration factors of 2 and 4. The high temperature data for all items plotted between the theoretical curves of $n = 4$ and $n = 6$. The measured stresses from the sections characterized by a strong subgrade plotted more closely to the theoretical curve of $n = 6$ than the data from the other sections. It is readily apparent that the lower temperatures and, thus stiffer asphalt, resulted in greater stress distribution and, thus, lower apparent stress concentration factor. The analysis revealed also that stronger granular subgrades resulted in less stress distribution and thus higher stress concentration factors.

In the WES stress distribution study, Report No. 1, on the clayey-silt test section data, indicated that Boussinesq's theory underestimates measured stresses. The report included the statement:

> *"There is consistent trend for the measured stresses to be greater than theoretical values at points directly beneath the loaded area and to be equal to or less than theoretical values elsewhere."*

The sand test section report states that there was a marked trend for the measured vertical stresses to exceed computed stresses. These examples agree with the theoretical studies by Fröhlich that for soil systems where the modulus increases with depth the stress concentration is greater than for a homogenous soil section, thus the stress concentration is greater than 3. Likewise, the stiffer the upper layer is relative to the subgrade, the lower is the stress concentration. The decrease in stress concentration corresponds to a decrease of the concentration factor. The Stockton No. 2 Test suggests that for a weaker subgrade (CBR = 6), a stress concentration factor of 2 may apply, and for a medium strength subgrade (CBR = 20), a stress concentration factor of 3 may be more appropriate. Therefore, for stronger subgrades, a higher stress concentration would apply. For a subgrade with a CBR lower than 6, it is assumed that the stress concentration factor would be lower than 2. In light of this analysis, the immediate conclusion is the stress concentration factor should be expressed as a function of the subgrade CBR. Figure 4.10 shows one possible relationship between stress concentration factor and subgrade CBR that could be employed in developing the design criteria.

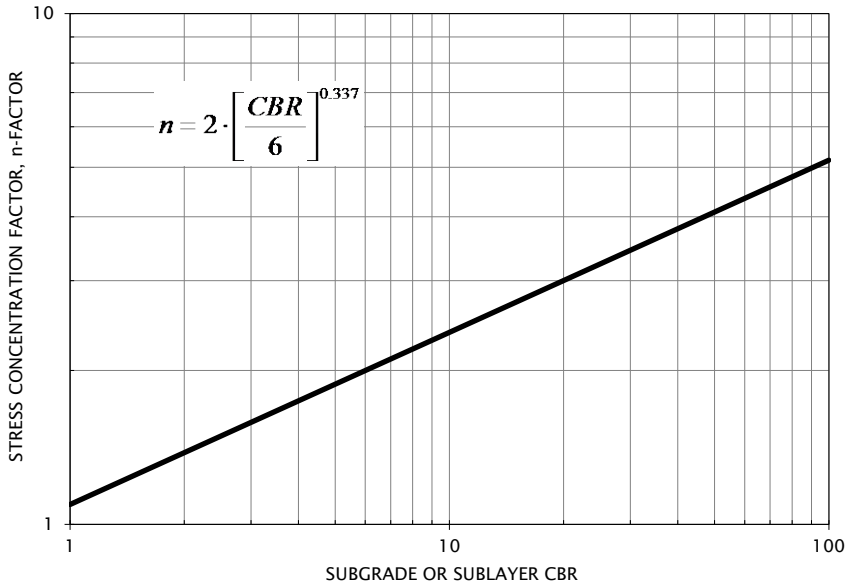

Figure 4.10 Relationship between stress concentration factor and CBR

The relationship between CBR and stress concentration factor was compared with the stress distributions obtained using layered elastic theory. Using the material characterization procedure given by Barker and Brabston (1975), the stress at the top of the subgrade was computed for different thicknesses of pavement over a range of subgrade CBR values. Figure 4.11 presents the stress distributions based on the layered elastic analysis along with the stress distributions computed with the stress concentration factor that best matches the layered-elastic computed stresses. The data in Figure 4.12 indicate that the stress distribution computed using layered elastic theory is a function of CBR. For a range of CBR values from 3 to 15, the *n*-factors that produce equivalent stress distributions range from 1.15 to 1.9.

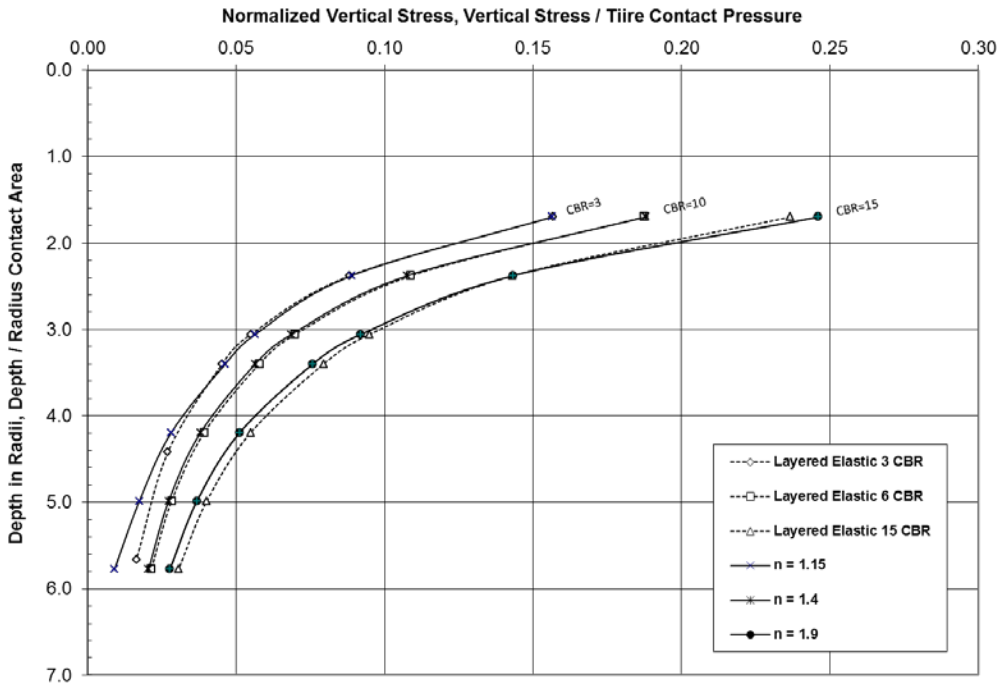

Figure 4.11 Comparison of stress distribution based on layered elastic theory with stress distribution based stress concentration factors

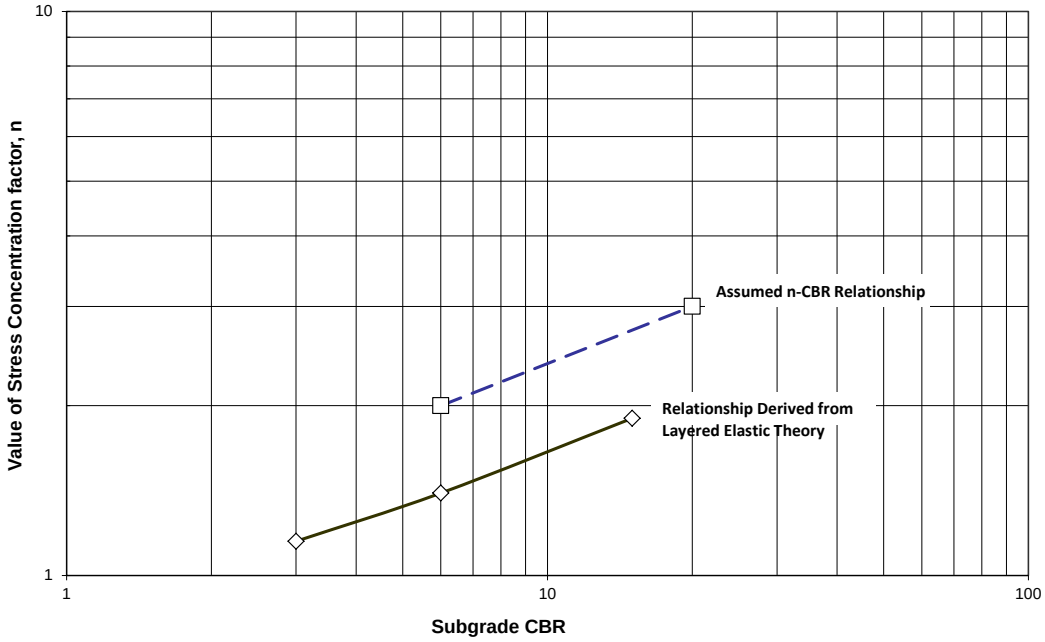

Figure 4.12 Comparison of relationship between stress distribution and CBR

As a check on the concept of the variable stress concentration factor, design thicknesses for the F-15, Boeing 747, and C-17 aircraft were computed based on *n*-factor being a function of CBR. The thicknesses were computed for a range of CBR values, for 10,000 coverages and were based on the β coverage relationship developed from the single-wheel α- factor curve. The design curves for the three aircraft are shown in Figures 4.13 through 4.15. From these figures, it is possible to note that the stress distribution, corresponding to a stress concentration factor equal to 2 and as a function of the CBR, results in less pavement thickness for CBR values lower than 6 and greater pavement thickness for CBR values greater than 6. The results obtained using the variable stress concentration factor for the single-wheel aircraft could have been predicted, but predicting the results for the multi-wheel aircraft is more difficult. This is because, as the CBR is decreased, the stress distribution is increased (stress concentration factor decreases). This would lower the vertical stress under the center of a tire but would increase the stress due to adjacent tires; therefore, the net change in the stress would be difficult to predict and will depend of gear geometry.

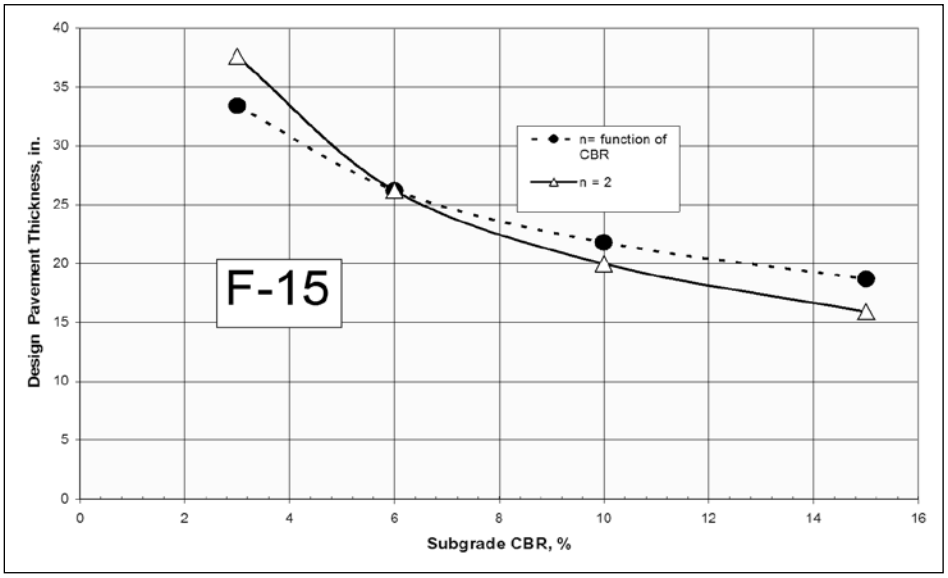

Figure 4.13 Design curves for F-15 using *n* as function of CBR
(1 inch=25.4 mm)

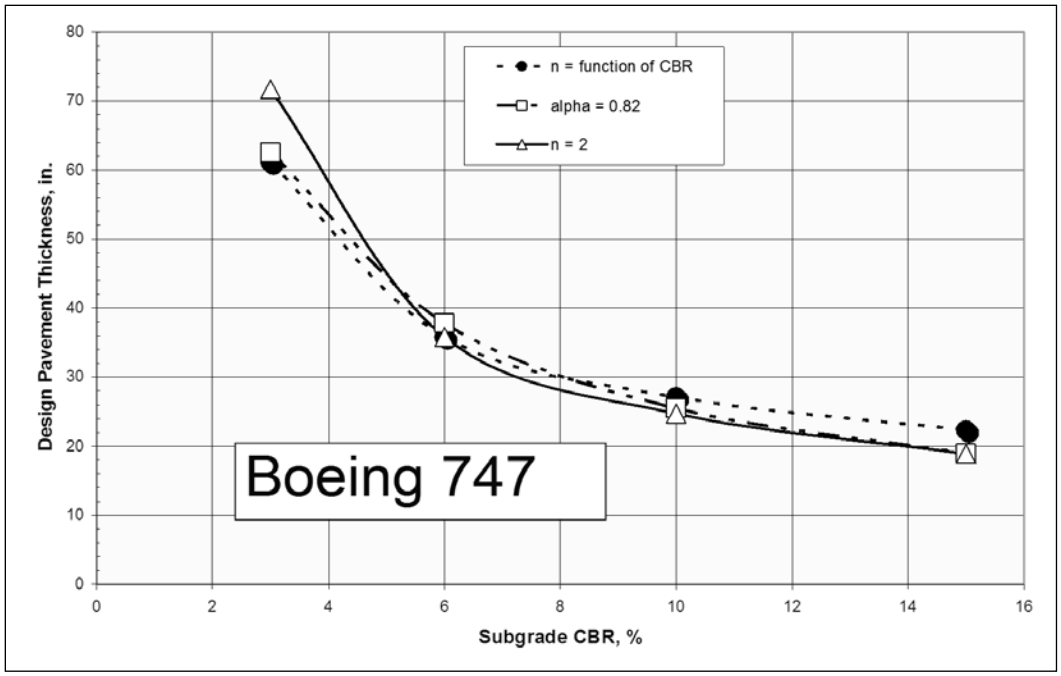

Figure 4.14 Design curves for Boeing 747 using *n* as function of CBR (1 inch=25.4 mm)

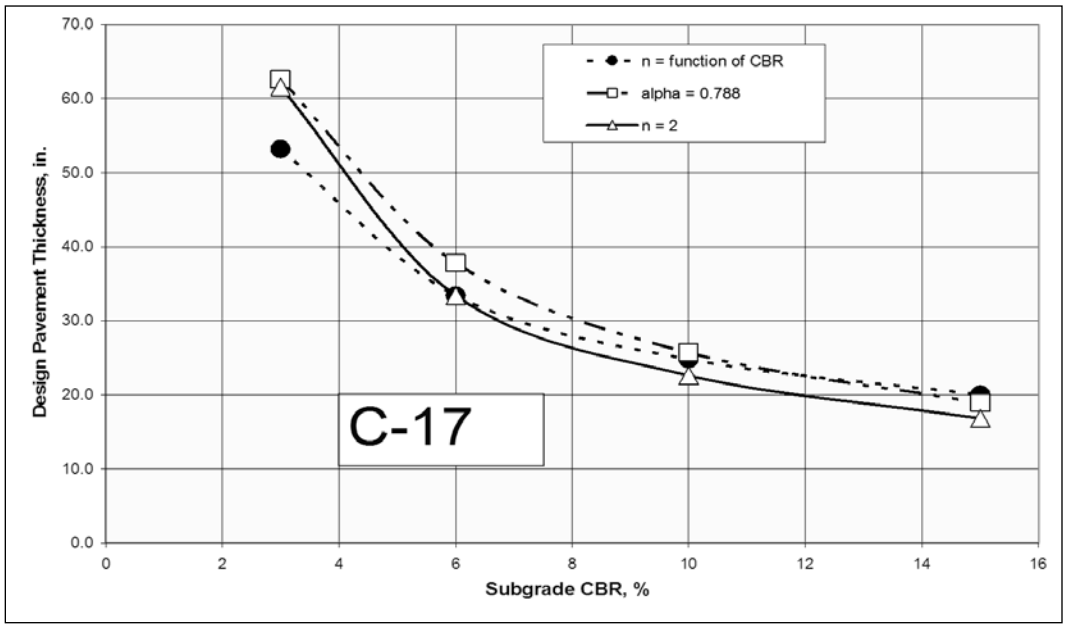

Figure 4.15 Design curves for C -17 using *n* as function (1 inch=25.4 mm)

As the analysis indicated, the design thickness for a Boeing 747 based on the variable stress concentration factor agrees fairly well with the thickness based on the α-factor. For fixed stress concentration factors, the design thickness corresponding to a CBR of 3 is greater than the thickness calculated with the variable stress concentration factor or the α-factor. The design

thickness for the C-17 based on the α-factor is greater than the design thickness based on the stress concentration factor, either fixed or variable. However, it should be recalled that a reanalysis of the test data indicated the α-factor for a 6-wheel gear should be reduced to 0.72, which would result in a better agreement with the thickness based on the variable stress concentration factor. An extensive review of the literature, theoretical stress analyses and engineering logic, have provided justification to recommend that the pavement design criteria should be based on the concentration factor being a function of the subgrade CBR.

4.9 Computing Coverages and Stress Repetitions

Early in the development of the CBR design procedure, the concept of coverages was used to quantify an effective traffic volume. A single coverage is applied to a point on the pavement surface is when that point is within the tire-print width as an aircraft tire traverses the point. With the development of the design criteria in terms of a subgrade stress parameter, it can be postulated that, instead of coverages, a more appropriate parameter to represent traffic volume is the number of stress repetitions at the top of the subgrade. To quantify traffic volume, the layered elastic design procedure, as implemented for the military, counted strain repetitions at the top of the subgrade according to the aircraft gear geometry. Since the design thickness for a flexible pavement is relatively insensitive to traffic volume, particularly at the higher volumes of traffic, the value of the refinement in quantifying traffic is questionable. Considering the stage of the development of the β design methodology, the additional complexity of determining stress repetitions was not warranted and therefore left as a recommendation for future research.

4.10 Comparison of Stress-based Criteria with Layered Elastic Strain Criteria

In 2005, representatives of some European countries advocated the use of pavement design criteria as given in the CROW report (CROW 2004). The procedure presented in the CROW report consisted of a layered elastic response model and vertical stain criteria identified as the “Shell criteria”. The subgrade strain criterion within the CROW procedure is represented by the following equation.

$$\log(N_s) = k_0 + k_1 \log(\varepsilon_z) \tag{4.32}$$

where:

N_s = number of allowable load applications

k_0, k_1 = material constants

ε_z = compressive strain on top of the subgrade

For calculations of the Pavement Classification Number (PCN) used in pavement evaluations, the CROW report recommended the Shell 85 percent relationship with values of 17.289 and 4.00 for k_0 and k_1, respectively. The report also included a Shell 50 percent relationship for which k_0 and k_1 were 17.789 and 4.00 respectively. Since the CROW criteria were recommended for application to North Atlantic Treaty Organization (NATO) for the evaluation and design of flexible pavements, it is interesting to compare these criteria with the β and the latest layered elastic criteria. The β criteria, for the stress concentration factor of 2, is given by the following equation

$$\log(\beta) = \frac{1.7782 + 0.2397 \log(Coverages)}{1 + 0.5031 \log(Coverages)} \qquad (4.30 \text{ bis})$$

In 1994, WES recommended to the FAA subgrade strain criteria as developed from layered elastic analysis of data from prototype full-scale test sections. The criteria were again recommended in 2005 after a re-analysis of the test data which included data from the new FAA pavement test facility. The criteria being recommended for the layered elastic procedure was

$$\log(\varepsilon_z) = \frac{2.1582 + 1.3723 \log(Coverages)}{1 + 0.4115 \log(Coverages)} \qquad (4.33)$$

where ε_z is the strain at the top of the subgrade.

Using the correlation, $E_{subgrade}$ = 1500 CBR in psi ($E_{subgrade}$ = 10350 CBR in kPa), the vertical strain criteria in Equation 4.33 can be converted to β criteria by the following relationship.

$$\beta \approx \pi \varepsilon_z 1500 \qquad (4.34)$$

Likewise, the β criteria can be converted to strain criteria by Equation 4.35.

$$\varepsilon_z \approx \frac{\beta}{\pi\, 1500} \qquad (4.35)$$

Figure 4.16 shows the vertical strain criteria, derived from the β criteria, compared with the strain criteria from the CROW report and the criteria recommended to FAA in 1994 and

2005. Also, Figure 4.16 contains data points from the FAA test facility. The difference between the CROW strain criteria and the WES layered elastic criteria is apparent, whereas the β criteria agrees in shape and form with the WES layered-elastic criteria.

The offset between the curves of the β criteria and the layered-elastic criteria was expected since the layered elastic model represents more load distribution than does the stress concentration factor model (with *n*-factor equal to 2). The second comparison is shown in Figure 4.17 and is obtained by converting the WES layered elastic strain criteria to β criteria. Again, it is seen that the two criteria appear to be identical except for the offset. This offset is the resulting differences in the stress distribution and has been discussed earlier in this document. The next comparison is made by converting the CROW strain criteria to β criteria as is shown in Figure 4.17. Again, there is a large difference in the results between the two criteria except for a narrow range from 10,000 coverages to 100,000 coverages.

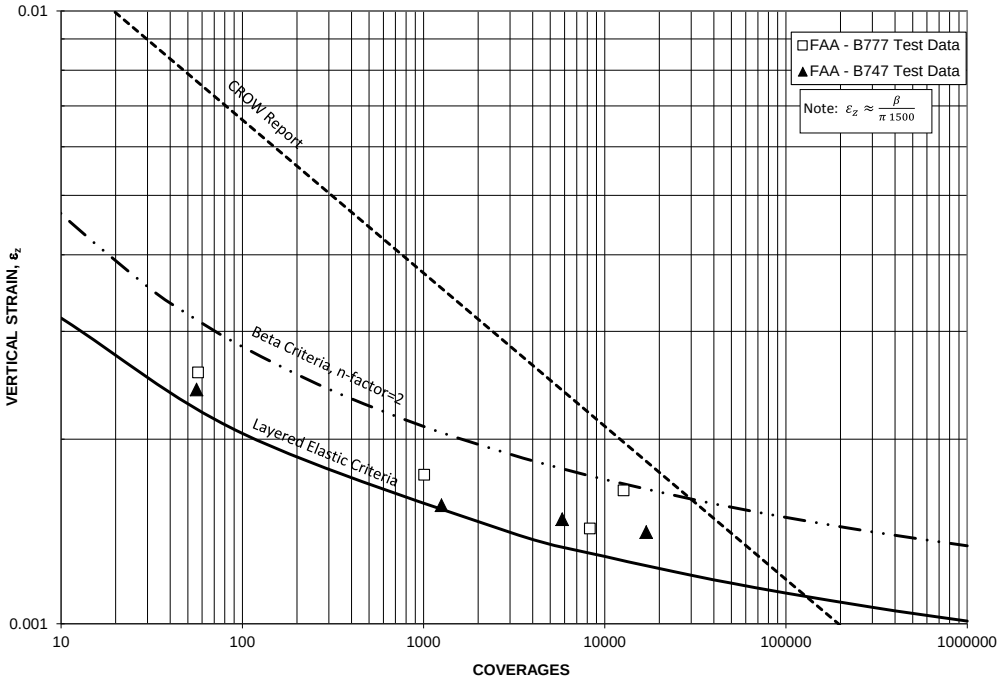

Figure 4.16 Comparison of strain criteria

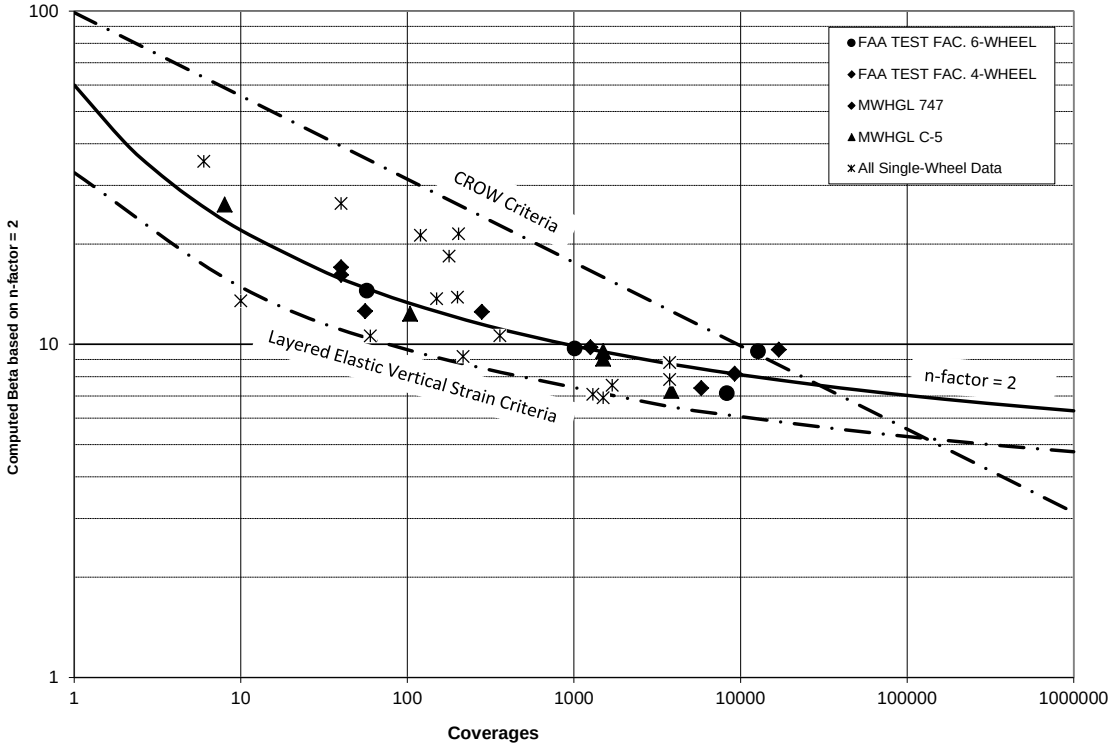

Figure 4.17 Comparison of Beta criteria with criteria from layered elastic criteria

The development of the CROW criteria is not well known, but it is obvious that the criterion does compare favorably with the WES layered elastic procedure. Another consideration is how traffic is counted. The WES criteria are related to traffic in terms of coverages, but the CROW criterion is in terms of strain repetitions. Since thickness is relatively insensitive to traffic volume, the method of defining traffic would not account for the difference in the criteria.

To conclude, the comparison of the β criteria with the strain criteria highlights the mechanistic nature of the CBR design procedure. For flexible pavement design, the good agreement of the β criteria with the WES layered-elastic strain criteria provides for a high degree of confidence in using the β criteria for pavement design supporting multi-wheel heavy aircraft and aircraft having single-wheel gear.

4.11 Summary

The re-development of the CBR equation directly from Fröhlich' stress model demonstrated that the original CBR equation has as its foundation on a mechanistic approach. It was demonstrated that the standard CBR equation emerges from a performance model dictated by a stress concentration *n*, with a value of = 2. This is a significant finding because it imposes on the CBR equation a stress distribution dictated by *n-factor* = 2. This means that the CBR design procedure of standard flexible pavement can be approximated by this distribution, which in turn hints at the use of a stress ratio approach as developed for the CBR-Beta criteria.

The derivation of the CBR equation in terms of vertical stress was performed for a single-wheel assembly. However, the use of the stress ratio approach in terms of the CBR-Beta, not only facilitates the expansion of this analysis from single-wheel to multi-wheel loadings, but also to any traffic level. In expanding the use of the CBR equation from single-wheel to multi-wheel gears, the need to use an ESWL adjustment is eliminated. In addition, it was shown that the correction currently applied to the ESWL by the load repetition factor (alpha factor) is in the order of 0.52 times the load on a six-wheel gear. With the CBR-Beta approach, any landing gear with any geometry can now be accommodated directly without resorting to ESWL schemes.

Comparative analyses between the CBR-Beta and the layered elastic method pointed to the proposition of a correlation between the subgrade CBR and the *n-factor* as implemented by Fröhlich's stress model. The stress distribution was calculated directly under a single-wheel of a standard layered pavement system for different CBR values and subsequently correlated to different *n-factors*. For a standard pavement structure, a theoretical relationship between the subgrade CBR and the *n-factor* was developed. The *n-factor* increases as the subgrade CBR increases in a linear fashion when plotted on a logarithm-logarithm scale.

The current WES layered-elastic vertical subgrade strain criteria were compared to β criteria by converting the vertical strain on the subgrade to a limiting stress value. The two criteria compared favorably when plotted against actual test section data. The curves have the same shape and only differ on the offset along the performance data points.

The results of the theoretical analyses performed here are encouraging, but required extensive validation from full-scale traffic experiments. The next few chapters will present the results of a validation process conducted for this research study.

CHAPTER 5 - VALIDATION OF PROPOSED CRITERIA

5.1 Introduction

This chapter presents the design, construction, and testing of full-scale pavement test sections with the purpose of collecting pavement response data to validate the proposed CBR-Beta procedure for the design of flexible pavements. A description of supplemental laboratory tests to characterize the pavements materials used in the test sections is provided. A description of instrumentation, traffic and loading patters is also included in this chapter.

5.2 Pavement Test Section Design

A pavement test section was constructed for the purpose of validating the CBR-Beta design procedure. The test section consisted of three traffic lanes; each lane was divided into four pavement items with different pavement structures. Figure 5.1 shows a profile view of the pavement test items dimensions and their strength characteristics.

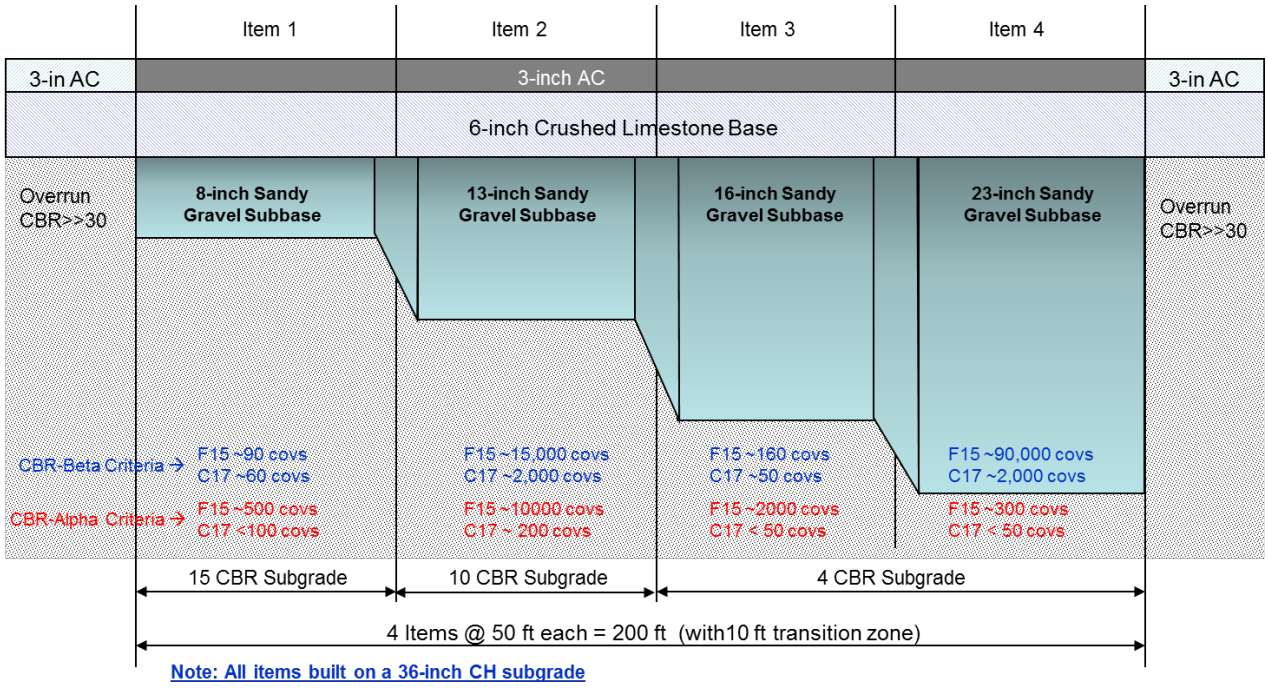

Figure 5.1 Pavement test section design details (1 inch=25.4 mm, 1 ft=0.3048 m)

The aircraft gear loads that were selected for traffic testing included the F-15 tire, the C-17 dual tire and the C-17 single tire. The tire pressures were of 325 psi (2241 kPa) for the F-15 tire and 142 psi (980 kPa) for the C-17 tires. These load conditions were selected to evaluate the pavements' structural behavior when subjected to aircraft loads typically included in the Air Force medium to modified-heavy design traffic patterns.

The test section thicknesses above the subgrade varied from 17 inches to 32 inches (432 mm to 813 mm). The asphalt concrete surface and the crushed-limestone base layer were built to a constant thickness of 3 inches (76 mm) and 6 inches (152 mm), respectively. The subbase thicknesses varied from 8 inches to 23 inches (203 mm to 584 mm). The reasons for maintaining constant asphalt surface and base layer thicknesses were twofold. First, these thicknesses maintained compatibility with the full-scale testing utilized for the multi-wheel heavy gear load (MWHGL) study in which the asphalt surface and the base layer had the thicknesses of 3 inches (76 mm) and 6 inches (152 mm), respectively, for each pavement section (Ledbetter et al. 1971). Second, since the purpose of the test section was to validate the CBR-Beta procedure, which is concerned primarily with the determination of the thickness of the subbase for given subgrade strengths, it was necessary to eliminate asphalt and base thicknesses as variables as much as possible. The subbase material was sandy gravel with a design CBR of 30%. The subgrade design CBR was 4% for the thicker sections and 10% and 15% for the remaining sections. The coverage levels shown in Figure 5.1, and therefore the section thicknesses, were initially chosen to fill the gaps (represented by ovals shown in Figure 5.2) in terms of failure points in the CBR-Beta tentative performance curve. Figure 5.1 shows the predicted coverages to failure computed with the CBR-Alpha and CBR-Beta procedures.

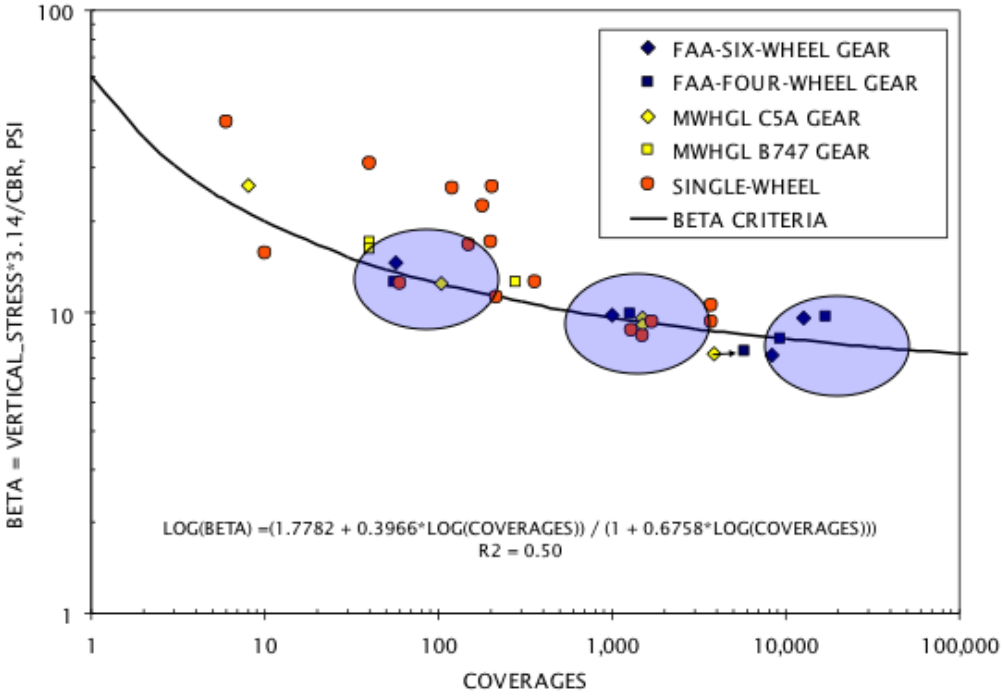

Figure 5.2 Beta-coverages curve and pavement failure data
(1 psi=6.9 kPa)

5.3 Test Section Location

The full-scale test section was located inside Hangar 4 of the Airfields and Pavements Branch testing facility at the U.S. Army Engineer Research and Development Center, Vicksburg, Mississippi. The facility was covered and protected from rainfall but was not temperature controlled. Figure 5.3 shows a view from the south end of the Hangar 4 looking to the north and an aerial view of Hangar 4 depicting the area covered by the test section. The test section was located in the eastern one-half and northern two-thirds of the covered structure. The in-situ soil was a lean clay (loess) deposit and the depth to the groundwater table was approximately 6 feet (1.83 m).

The test section was 200 feet (61 m) long and 40 feet (12.2 m) wide with paved areas at each end of the section. The test section was divided transversely into four longitudinal test items differentiated by the thickness of the subbase and strength of the subgrade. The test items

were 40 feet (12.2 m) long and were separated by a 10-foot (3.05 m) transition zone. The length of the test section was divided longitudinally into three traffic lanes.

Figure 5.3 Testing facility and test sections

5.4 Test Section and Pavement Structure Layout

Lanes 1 and 3 were used for single-wheel traffic, and Lane 2 was used for dual-wheel traffic. The traffic lane widths were 5 feet (1.52 m), 10 feet (3.05 m), and 5 feet (1.52 m) for the F-15 single-wheel gear at 325 psi (2242 kPa), C-17 dual-wheel gear at 142 psi (980 kPa) and C-17 single-wheel gear at 142 psi (980 kPa), respectively. A 5-ft (1.52 m) pavement zone at the end of each test item was considered as a transition zone between items and was not considered in the analysis. Figure 5.4 illustrates the as constructed cross-section layouts and transition zones between test items.

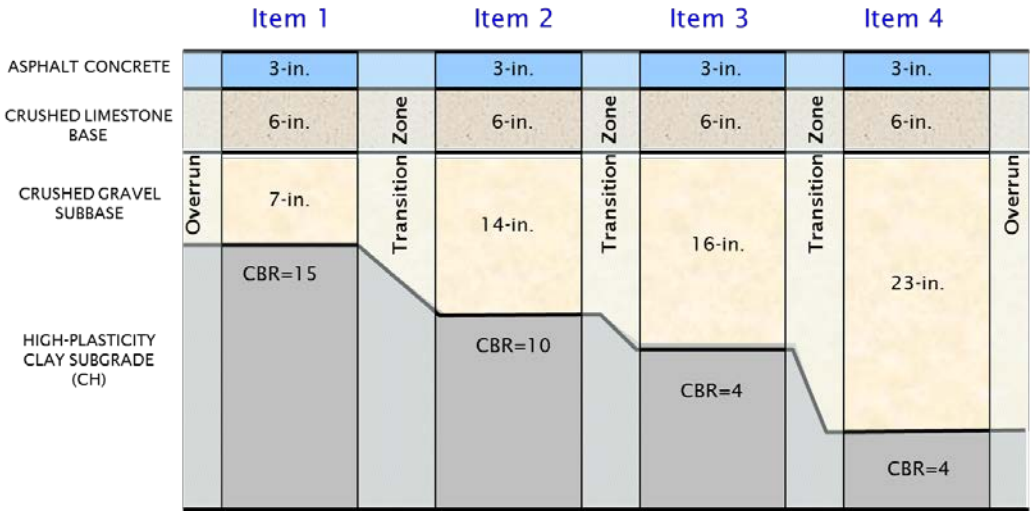

Figure 5.4 As-constructed pavement cross-section profiles

(1 inch=25.4 mm)

5.5 Description of Pavement Materials

A description of the pavement materials used as subgrade, subbase, base and asphalt concrete are provided in this section. A summary of field and laboratory tests for each of these materials is also provided.

5.5.1 Subgrade Material

All test items were constructed over a compacted high-plasticity clay (Vicksburg Buckshot Clay) material. The material was extracted from a borrow pit located about 10 miles (16 km) south of Vicksburg, Mississippi, in the flood-plain of the Mississippi River. The soil had a Liquid Limit (LL) of 79 and Plasticity Index (PI) of 51, and was classified as high-plasticity clay (CH). The soil's specific gravity was 2.74. The soil gradation curve is contained in Figure 5.5. The results from laboratory compaction, according to modified Proctor ASTM D1557, are summarized in Figure 5.6. The optimum moisture content was found to be 20% and the corresponding maximum dry density was 104 pcf (16.34 kN/m^3).

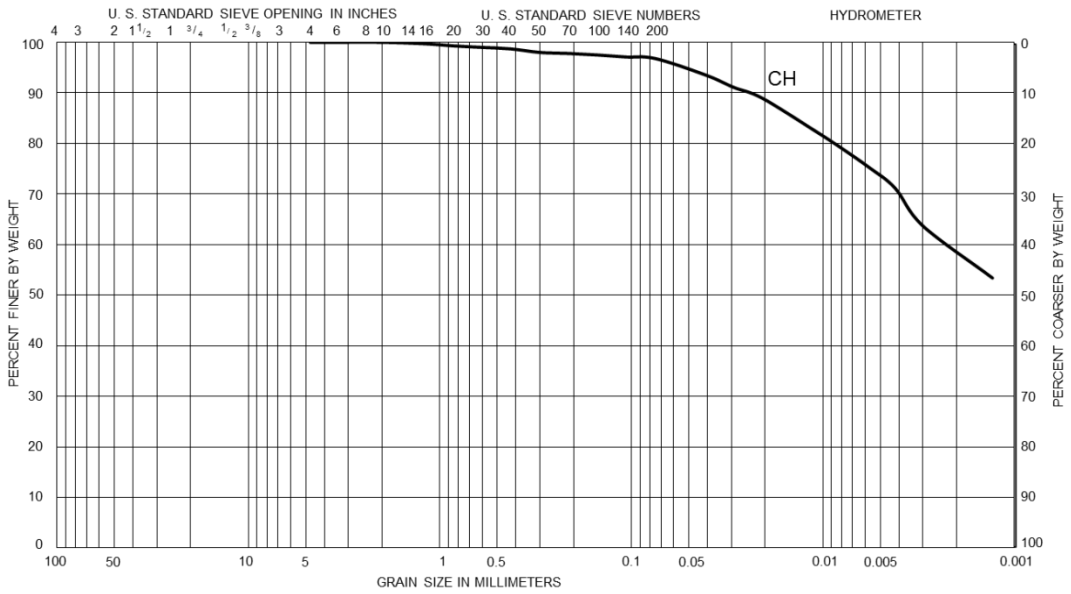

Figure 5.5 CH Subgrade grain size distribution

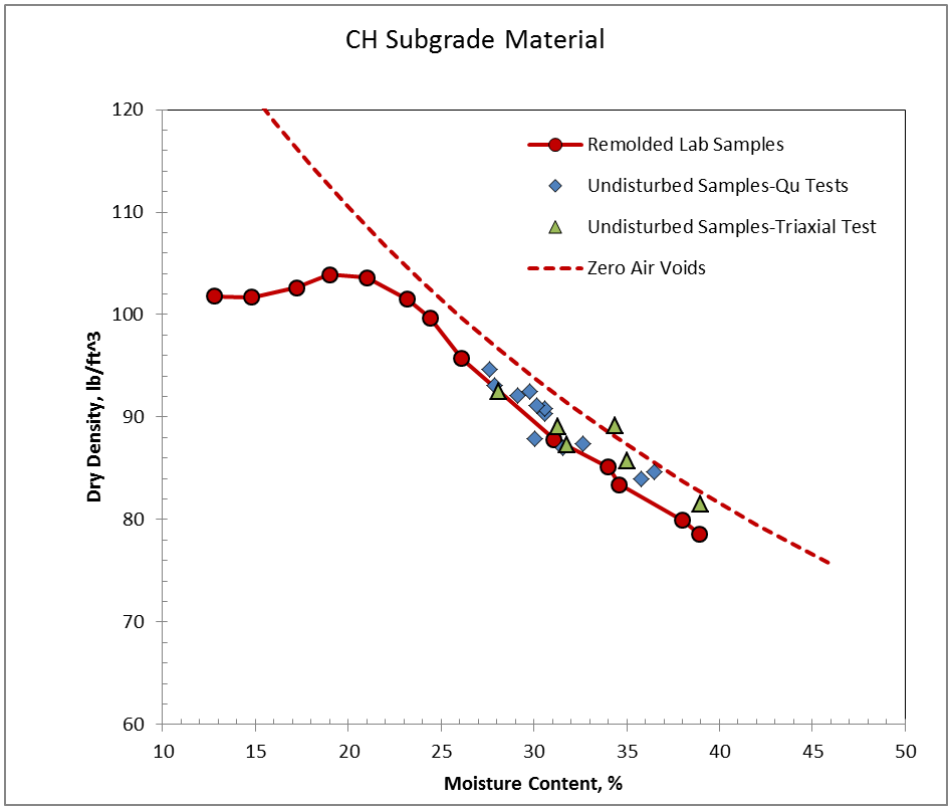

Figure 5.6 Subgrade (CH) moisture-density curve (1 pcf=0.157 kN/m^3)

The design subgrade CBR values selected for the test section construction were 4%, 10%, and 15%, respectively. The high plasticity clay moisture content required to achieve these CBR

values was determined from moisture content versus CBR relationship (Figure 5.7) developed at ERDC from historical field and laboratory test data. After placement of the subgrade material, undisturbed samples were obtained to conduct laboratory triaxial compression testing. The as-constructed moisture-density results of field-collected undisturbed samples are also presented in Figure 5.6. It is noted that, for the CBR values selected for construction, all points fall on the wet side of the optimum moisture content.

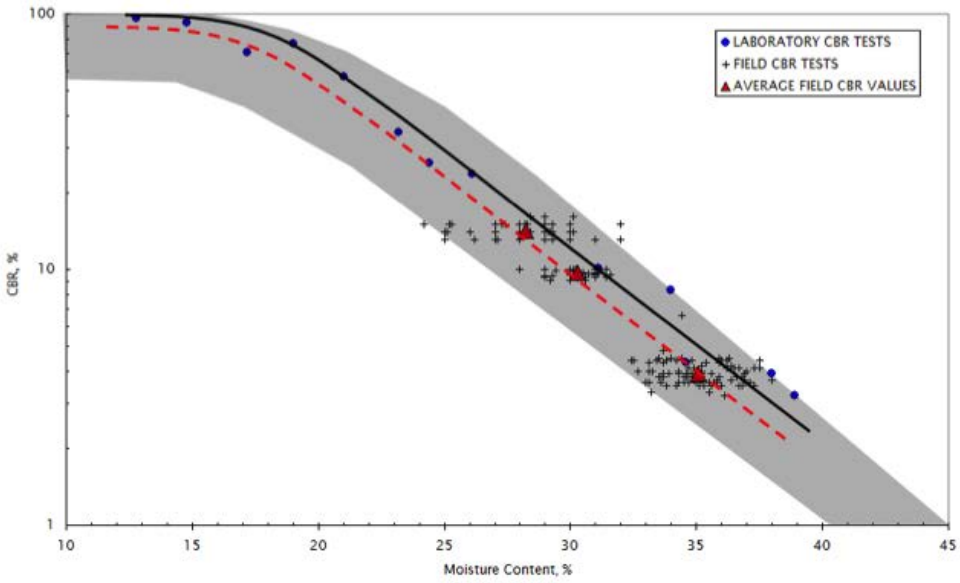

Figure 5.7 Subgrade CBR-moisture content curve and CBR field test results

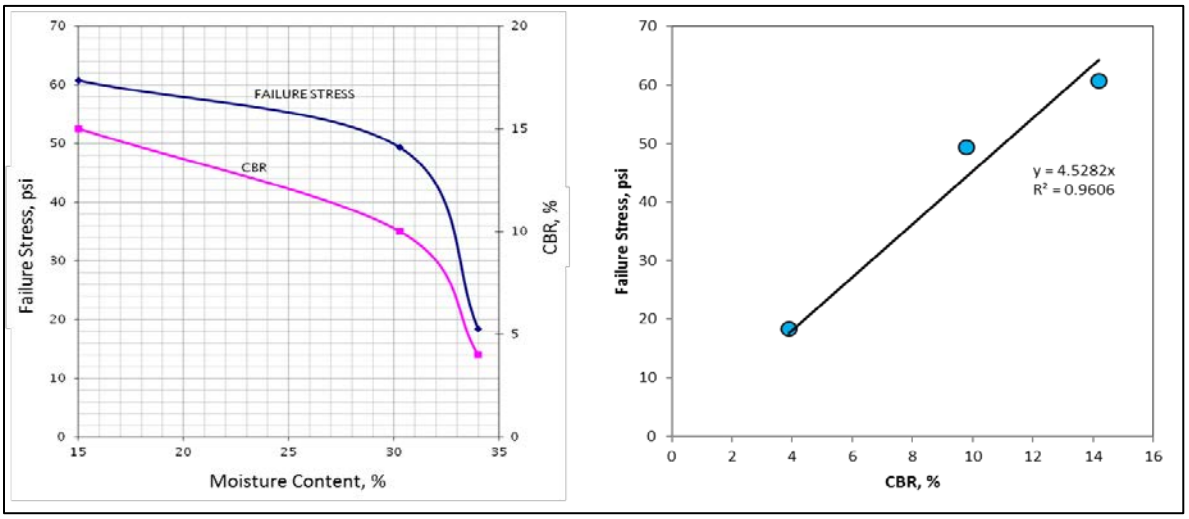

Figure 5.8 Relationships between subgrade material moisture content, CBR, and failure stress (1 psi=6.9 kPa)

The triaxial tests were drained and had a confining pressure of 15 psi (104 kPa). Laboratory CBR tests were also conducted according to the ASTM D1883-07e2 procedure. The data contained in Figure 5.8 shows the relationships between moisture content, CBR and failure stress. Figure 5.9 summarizes the deviator stress-strain data from the triaxial tests on the subgrade material characterized by CBR values of 4, 10, and 15 with respective moisture contents of 34%, 30%, and 27%. Figure 5.10 shows the resulting Mohr's circles from the triaxial test results conducted on the subgrade CH soil. Table 5.1 summarizes strength material properties for each target CBR value. The ultimate stress difference was computed using the hyperbolic soil model developed by Kondner (1963), represented in Equation 5.1. The failure stress difference was determined from laboratory test results from the test specimens. A detailed analysis of this data is provided in the analysis chapter and Appendix A.

$$(\sigma_1 - \sigma_3) = \frac{\varepsilon_1}{\frac{1}{E_i} + \frac{\varepsilon_1}{(\sigma_1 - \sigma_3)_{ult}}} \quad (5.1)$$

where:

$(\sigma_1\text{-}\sigma_3)$ = principal stress difference

$(\sigma_1\text{-}\sigma_3)_{ult}$ = asymptotic value of the stress difference at large axial strain

ε_1 = axial strain

E_i = initial tangent modulus

Table 5.1 Subgrade material characteristics

CBR	$(\sigma_1\text{-}\sigma_3)_{ult}$, *psi*	$(\sigma_1\text{-}\sigma_3)_f$, *psi*	*c, psi*	*φ, °*	*w, %*
4	21.2	18.4	9.2	0	34
10	55.1	49.3	25.7	0	30
15	68.9	60.7	30.4	0	27
Note: 1 psi=6.9 kPa					

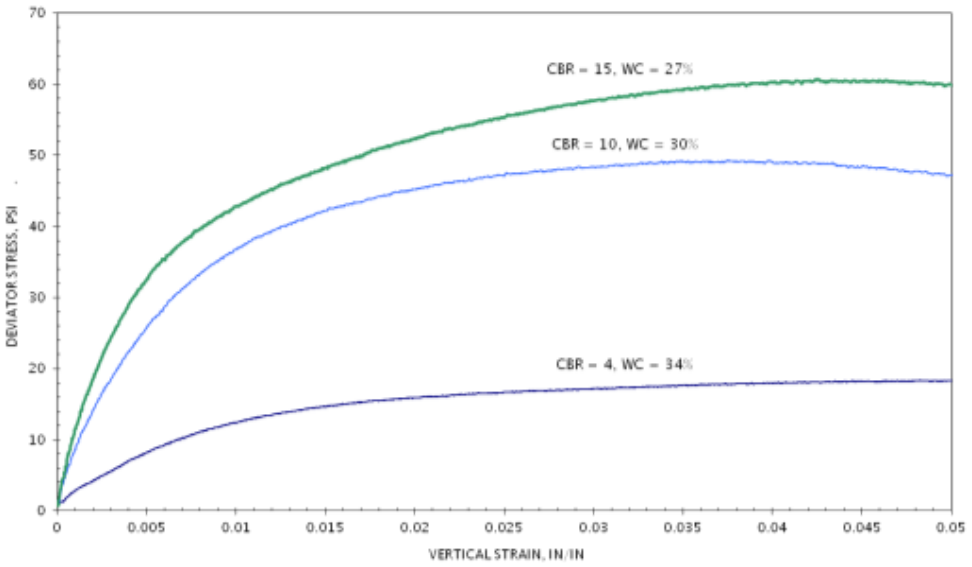

Figure 5.9 Stress-strain data from confined, drained triaxial compression tests on the subgrade soil (1 psi=6.9 kPa)

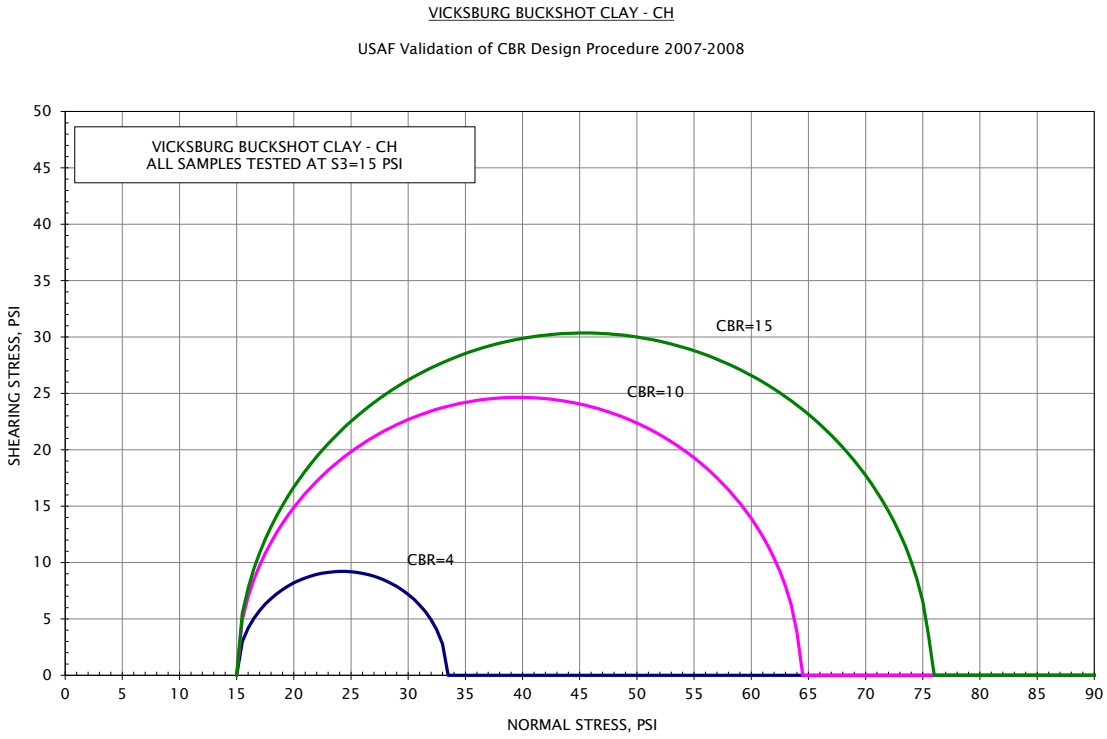

Figure 5.10 Subgrade material Mohr circles at different CBR values (1 psi=6.9 kPa)

5.5.2 Subbase Material

The subbase material consisted of a blended mixture of 67% by weight crushed aggregate and 33% by weight No. 10 crushed limestone. The aggregate material was obtained from a gravel pit near Crystal Springs about 40 miles southeast of Vicksburg, Mississippi. The aggregate material larger than 1 inch (25.4 mm) nominal diameter was crushed. The crushed limestone was obtained from a local supplier and originated from Kentucky. Figure 5.11 shows the grain-size distributions of the blended mix as well as the predicted distribution of the blend and the measured distribution of the final blend that was used for construction. The modified Proctor moisture-density compaction curve is shown in Figure 5.12. The optimum moisture content for the subbase material was 5.4% and the maximum dry density was 127 lb/ft^3 (19.94 kN/m^3).

Three triaxial compression tests were conducted with the blended material under drained conditions and at confining pressures of 5 psi (34.5 kPa), 15 psi (103.5 kPa) and 30 psi (207 kPa). The tests were conducted at a controlled strain deformation rate. The strain rate was set to 1% strain per minute. The tests ended at a total deformation of approximately 0.85 inches (22 mm). Figure 5.13 shows the Mohr's circles obtained from the triaxial test results at the confining pressures selected. The triaxial data indicated an angle of internal friction of 48 degrees and cohesion of 8 psi (55 kPa).

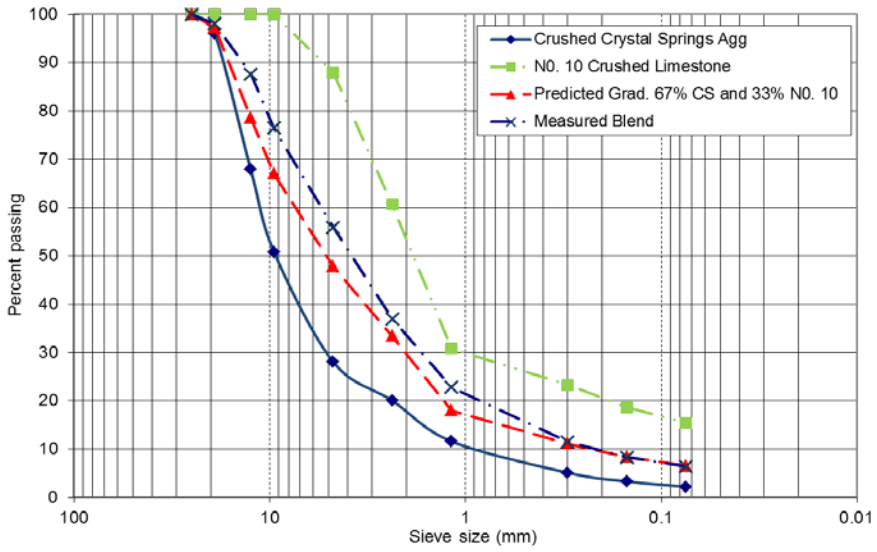

Figure 5.11 Subbase aggregate blend grain size distributions

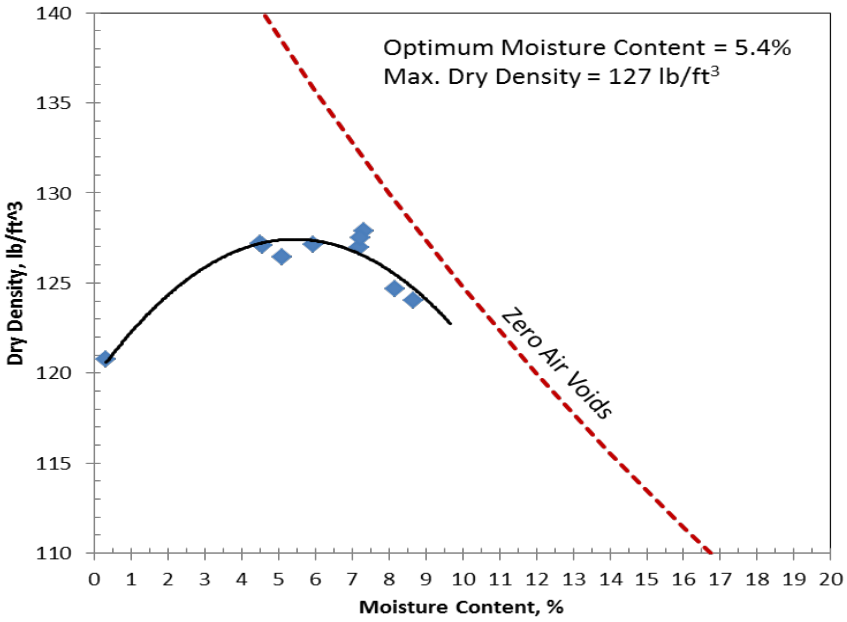

Figure 5.12 Modified Proctor moisture-density compaction curve for subbase material

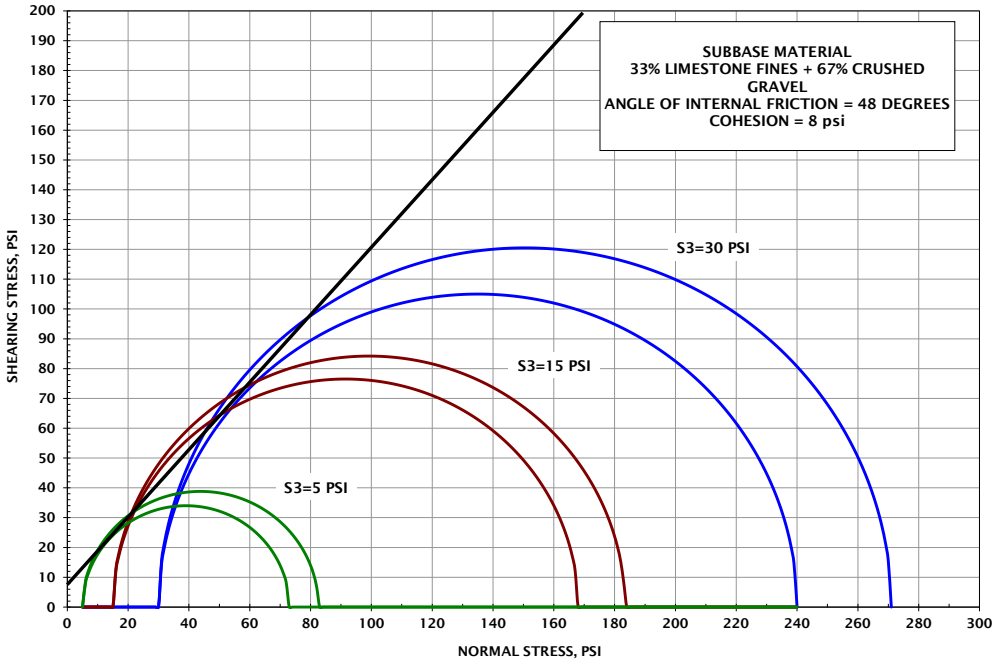

Figure 5.13 Mohr's circles of the subbase blend material (1 psi=6.9 kPa)

5.5.3 Base Material

The base course for all test items was a 6 inches-thick (152 mm) layer constructed of crushed limestone. Figure 5.14 shows the material's grain-size distribution. The material was classified as well-graded gravel (GW). The modified Proctor moisture-density compaction curve is shown in Figure 5.15. The optimum moisture content for the base material was 5.2% and the maximum dry density was 145 pcf (22.78 kN/m^3). Figure 5.16 shows the Mohr's circles obtained from the triaxial compression test results conducted at confining pressures of 5 psi (34.5 kPa), 15 psi (13.5 kPa), and 30 psi (207 kPa). The angle of internal friction was determined to be 50 degrees, and the cohesion was 7 psi (48.3 kPa).

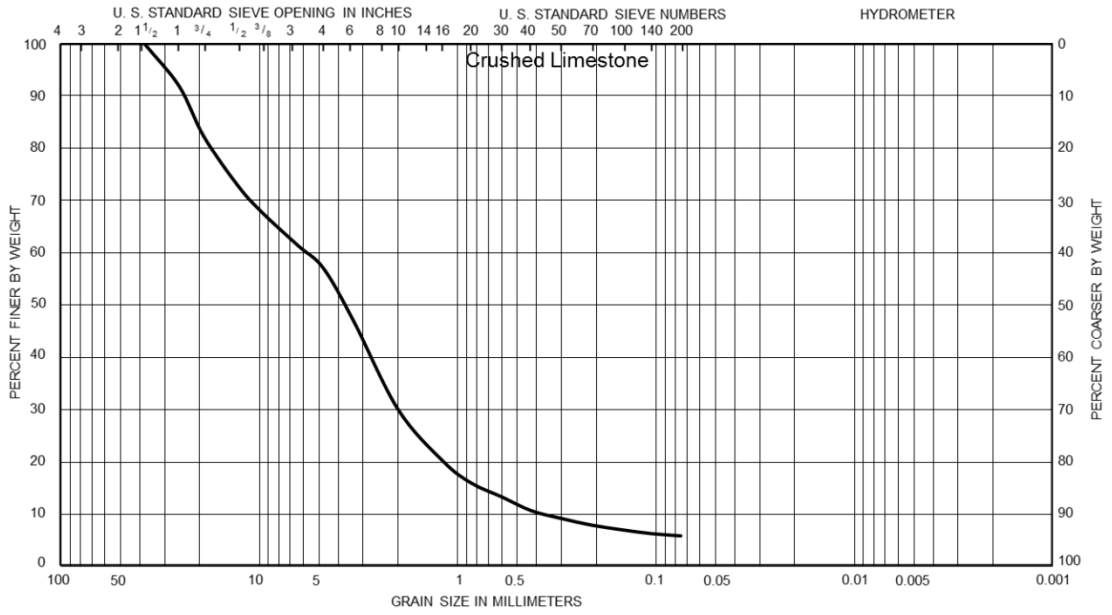

Figure 5.14 Base course material grain size distribution

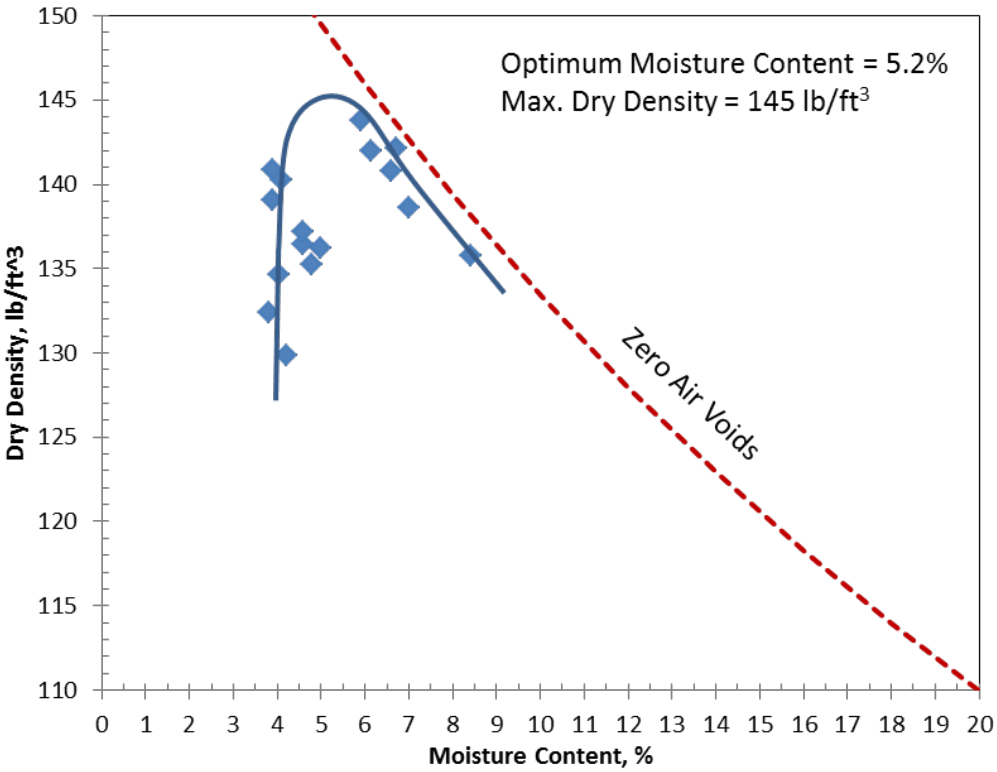

Figure 5.15 Modified Proctor moisture-density compaction curve for base material

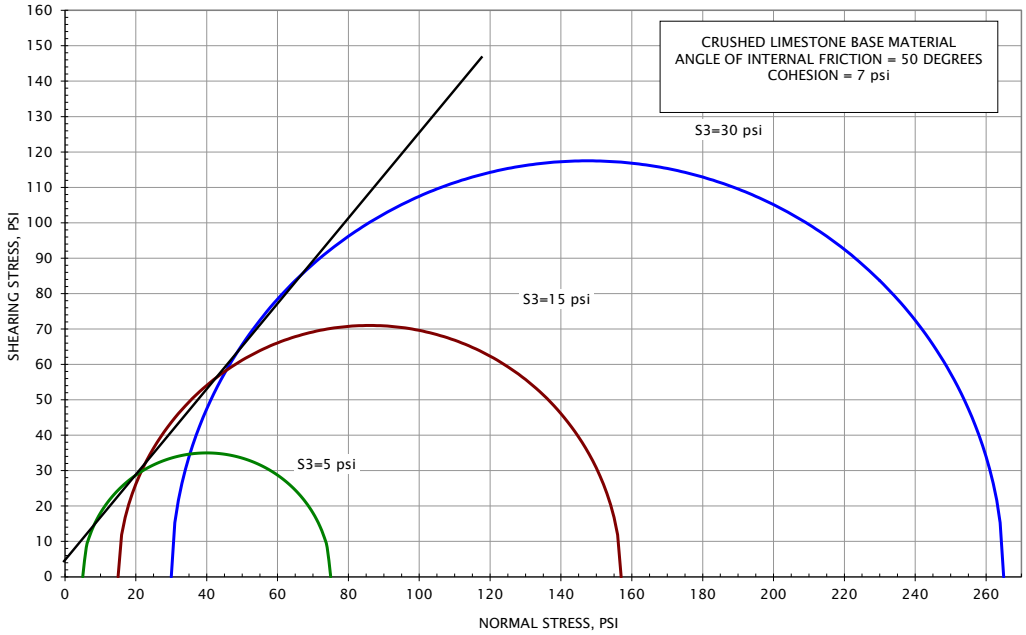

Figure 5.16 Base course material Mohr's circles (1 psi=6.9 kPa)

5.5.4 Asphalt Concrete

The asphalt concrete layer was 3 inches (76 mm) thick for each test item. The asphalt mixture was supplied by a local asphalt plant located in Vicksburg, Mississippi. The asphalt mixture and the layer construction were in compliance with the Unified Facility Guide Specification (UFGS) 32-12-15 standards for construction of airfield pavements and it was designed using the Marshall Design Criteria. Table 5.2 contains the 75-blow mix specification and the mixture characteristics used in the test sections. Table 5.3 contains the mixture's grain-size distribution. Figure 5.17 compares the mixture's grain size distribution with the gradation limits required by the UFGS 32-12-15. The mixture gradation was within the UFGS gradation 2 limits except for the material passing the 9.5 mm sieve that exceeded the upper specification limit of 4.8%. Nevertheless, such excess in percentage passing was within the acceptable tolerance as indicated in the UFGS 32-12-15, Table 10. The aggregate material classified as GW and had a specific gravity of 2.41. The nominal maximum aggregate size of the mixture was 9.5 mm. The asphalt content was 5.05%.

Table 5.2 Asphalt mixture characteristics

Test Property	75-Blow Mix Specification	Test Section Asphalt Mixture
Min. Stability, lb	2150	2108.00
Flow, 0.01 in,	8 - 16	11.00
Air Voids, %	3 - 5	2.75
Percent Voids in Mineral Aggregate (VMA), %	13 - 15	14.10
Dust Proportion	0.8 - 1.2	1.12
Asphalt Content, %	---	5.05
Density, lb/ft^3	---	146.30
Specific Gravity	---	2.41
PG Grade	PG 67-22	
1 lb=4.45 N, 1 inch=25.4 mm, 1 ft=3048 mm, 1 pcf =0.157 kN/m^3		

Table 5.3 Asphalt mixture grain-size distribution		
Grain Size		**Asphalt Concrete**
Sieve Size	**Metric, mm**	**% Finer**
1	25.4	100.0
0.75	19.0	100.0
0.5	12.5	97.2
0.375	9.5	93.8
4	4.75	65.6
8	2.36	46.9
16	1.18	36.2
30	0.6	29.5
50	0.3	16.1
100	0.15	9.7
200	0.075	5.3

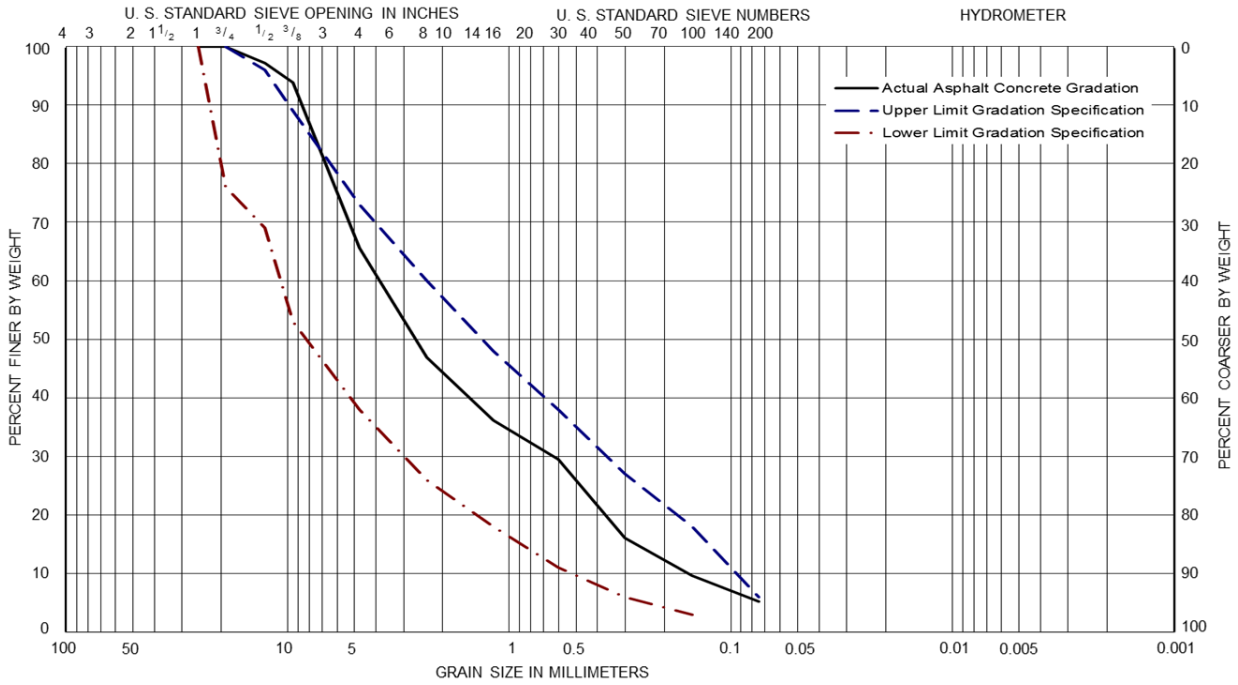

Figure 5.17 Grain size distribution of the asphalt mixture compared with UFGS specifications

5.6 Test Section Construction

The test section was constructed between October 2007 and May 2008. All construction work was performed by ERDC personnel, except for the placement of the hot-mix asphalt concrete surface. The asphalt concrete layer was placed by a local contractor.

5.6.1 Excavation of Test Sections

The excavated area was 40 feet (12.2 m) wide and 200 feet (61 m) long with ramps on each end to facilitate equipment entry. Because the area was constructed over an under-consolidated natural silt (CL, loess), French drains were placed along the entire length of the hangar at a depth of about 10 feet (3.05 m), with access wells for pumping water from the drains. The normal depth of the water table is less than 9 feet (2.74 m). Over the past half century, numerous test sections have been constructed in Hangar 4, requiring excavation up to 6 feet (1.83 m) deep. For this test section, the depth of the area to be excavated contained remnants of past test sections, which required excavation of about 5.5 feet (1.68 m) to ensure the removal of all the non-uniform materials. The excavated area was then backfilled with 2 feet (0.61 m) of CL to provide a stable, uniform foundation for the placement of the CH upper subgrade. A plastic moisture barrier was placed between the CL material and the processed CH subgrade material.

The CH material was placed and compacted in four lifts for the subgrade of Item 1. After placement of the CH material for Item 1, the CL fill was graded to the proper depth to allow placement of the CH subgrade for Item 2. The CH material was again placed and compacted in four lifts over a plastic moisture barrier. For Items 3 and 4, the CL layer was graded to the proper elevations to allow the placement of the CH material layer. A lift of CH material was first placed in Item 4, followed by subsequent lifts for both Items 3 and 4, which were placed at the same time to obtain a total layer thickness of 2 feet (0.61 m) of CH material. Figure 5.18 shows the construction final profile of the CL and CH layers that were built for this test section. Figure 5.19 shows the test section excavation.

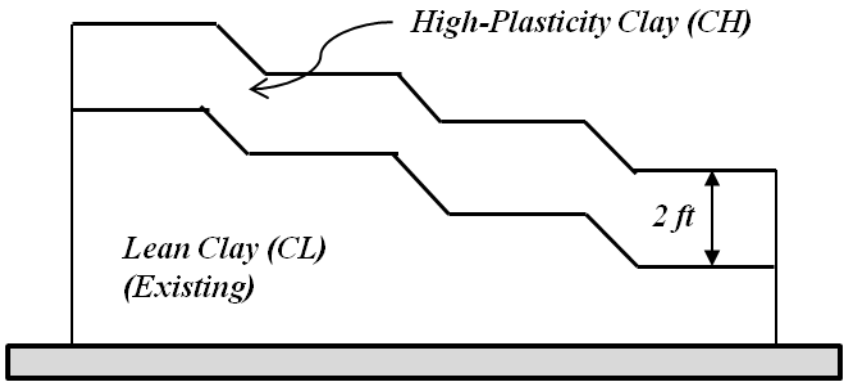

Figure 5.18 Test section CH subgrade profile construction scheme (1 ft=0.3048 m)

Figure 5.19 Excavation of test section

5.6.2 Construction of Subgrade Layer

After excavation and placement of the fill, the subgrade consisted of three distinct layers. The lower layer, at a depth greater than 5.5 feet (1.68 m), was the native material of wind-deposited silt. Attempts to compact this layer resulted in pumping water from the high-perched water table. The material was very weak at depths greater than 2 feet (0.61) below the excavated level. The CBR of the material at depths below 10 feet (3.05 m) was estimated to be less than 2.

The layer just above the natural loess silt was the compacted CL soil that served as a construction platform and provided a uniform foundation. The thickness of the CL layer was varied to accommodate the different profiles of the test items. The CL material was placed and compacted over the natural subgrade. In each item, the thickness of the layer was graded such that the surface of the subbase was at the same elevation for all items. The final subgrade layer consisted of 2 feet (0.61 m) of a heavy clay (Vicksburg Buckshot Clay) compacted at moisture contents of 27%, 30%, and 34% to achieve the design CBR values of 15% (Item 1), 10% (Item 2), and 4% (Items 3 and 4), respectively.

The subgrade material was processed at a facility next to Hangar 4 before its placement. Material processing consisted of spreading the clay in a uniform strip to a depth of approximately 12 inches (305 mm) and tilling the soil with a rotary mixer to break all material clumps and ensure uniformity. The subgrade design CBR for each test item was achieved by adding water or drying the CH material to the appropriate moisture content predicted from Figure 5.7.

The processed CH subgrade material was then hauled to the test section and spread at a sufficient thickness to produce a 6 inch-thick compacted lifts. The 2 feet-thick (0.61 m) subgrade was placed in 6 inch (152 mm) lifts and compacted with three passes of an Ingram Compaction LLC rubber-tire roller loaded at 70,000 lb (312 kN) with seven tires inflated at 100 psi (690 kPa). This was subsequently followed by two passes with a steel-wheel roller (DynaPac CA-25 Vibratory Compactor). After compaction, CBR tests were conducted in at least four locations per item, and moisture content samples were obtained. Table 5.4 contains the CBR test results for each lift and test section item.

Table 5.4 Field CBR test results on the subgrade layer during construction[1]

	1st Lift	2nd Lift	3rd Lift	4th Lift	Surface
Item 1	14.0	12.6	13.4	13.0	15.0
	13.7	14.1	14.9	16.1	16.2
	14.9	13.0	14.3	13.2	13.8
	14.9	14.5	14.8	15.0	14.0
	15.3	14.2	13.9	13.2	13.2
	14.5	14.3	13.6	14.5	13.8
	13.0	13.0	13.8	14.5	15.5
	13.4	14.6	13.6	14.1	13.9

Table 5.4 Field CBR test results on the subgrade layer during construction[1]					
	1st Lift	**2nd Lift**	**3rd Lift**	**4th Lift**	**Surface**
	13.0	14.9	13.6	13.2	15.4
	14.9	15.1	14.3	14.9	13.6
	12.6	15.3	13.8	15.2	15.9
	15.5	15.3		14.8	14.1
Average subgrade CBR					14.2
Standard Deviation					0.9
Item 2	10.4	9.9	10.1		9.8
	9.6	9.4	10.1		10.6
	9.5	9.3	9.1		10.4
	10.0	10.3	10.4		9.5
	9.9	10.4	9.5		9.8
	9.5	10.2	10.1		10.2
	9.3	10.2	10.1		9.3
	9.6	9.9	9.4		9.5
	9.6	10.2	9.3		9.6
	9.1	9.6	10.2		9.5
	9.6	9.8	10.3		9.5
	9.7	9.5	9.1		9.2
Average subgrade CBR					9.8
Standard Deviation					0.4
Items 3 and 4	4.2	4.4	4.0	3.8	3.8
	3.8	4.0	3.8	4.6	3.5
	3.9	4.5	3.7	3.9	3.6
	3.5	3.8	4.0	3.7	4.0
	3.7	4.5	3.7	3.5	3.8
	3.8	4.0	3.5	4.1	3.7
	3.5	4.4	3.5	4.0	3.2
	3.9	4.4	3.6	3.7	3.4
	3.8	3.9	4.4	3.6	3.3
	4.5	4.4	4.1	4.3	3.7
	3.8	3.9	4.4	4.0	3.8
	3.5	4.4	4.1	4.3	3.8
			3.4		3.1
			3.5		3.4
			3.5		3.5
					4.5
					3.8
					3.7
					3.7
					3.8
					3.7
					4.2

Table 5.4 Field CBR test results on the subgrade layer during construction[1]					
	1st Lift	**2nd Lift**	**3rd Lift**	**4th Lift**	**Surface**
					4.2
					4.3
					4.0
					4.2
					4.2
					3.9
					4.8
					3.3
					3.6
					4.3
					4.1
Average subgrade CBR					3.9
Standard Deviation					0.4
[1] Lifts were approximately 6 inches (152 mm) thick					

When the strength and moisture content of the material were not sufficiently close to the target values, the material was processed to adjust the moisture content by either adding water or allowing the material to air dry. After achieving the correct strength (in terms of CBR) of the lift, the lift surface was scarified by lightly tilling prior to placing the next lift; this process was repeated for each subsequent lift. During the construction process, the material was not allowed to lose moisture. During breaks in the construction process, the surface of the compacted layer was lightly sprinkled with water and covered with plastic sheeting. Each test item was overbuilt a few inches to allow for the final grading of the subgrade surface prior to placement of the subbase material. After the subgrade final grading, the subgrade was sampled with a 3 inch-diameter (76-mm diameter) Shelby tubes, and earth pressure cells (EPC) were installed. Installation of EPC and instrumentation will be discussed later in this chapter. Figures 5.20 through 5.23 show the subgrade material during the process of watering, mixing and placement.

Figure 5.20 Addition of water to the subgrade material

Figure 5.21 Subgrade material processing

Figure 5.22 Placement of subgrade material

Figure 5.23 Subgrade layer covered after compaction

5.6.3 Construction of Subbase Layer

The subbase material, a blended mix of 67% crushed aggregate (Figure 5.24, left) and 33% No. 10 crushed limestone (Figure 5.24, right) was placed in incremental lifts to total

between thicknesses of 7 to 23 inches (178 mm to 584 mm) to achieve the required design thicknesses above the respective subgrade. The subbase material was delivered by dump trucks and placed in 5 to 7 inch-thick (127 mm to 178 mm) lifts. Each lift was compacted by 22 passes of a vibratory steel-wheel roller. Target moisture content to achieve 100% modified Proctor compaction was 3.5%. During compaction, the subbase material was kept moist by sprinkling each lift with water prior to each pass of the vibratory roller. Figures 5.25 and 5.26 show stockpiled subbase material and subbase placement, respectively.

Figure 5.24 Subbase blended mix

Figure 5.25 Stockpile of blended subbase material

The dry density, wet density, and moisture content of the subbase material were monitored during compaction to determine at what pass level the material would achieve maximum density. A nuclear gage was used to obtain measurements of dry density and moisture content in accordance to ASTM D 6938-10. Maximum field density was achieved after approximately 16 to 18 passes of the self-propelled vibratory steel roller. The moisture content remained constant at about 3.5% during placement. Figure 5.27 shows dry density, wet density,

Figure 5.26 Placement of subbase layer

and moisture content values as a function of the number of passes of the vibratory roller. Table 5.5 contains the measured values of density (wet and dry) and moisture content in relation to the number of passes of the vibratory roller. CBR tests were conducted after placement and final compaction of the granular material. Table 5.6 contains the CBR test results for each test item.

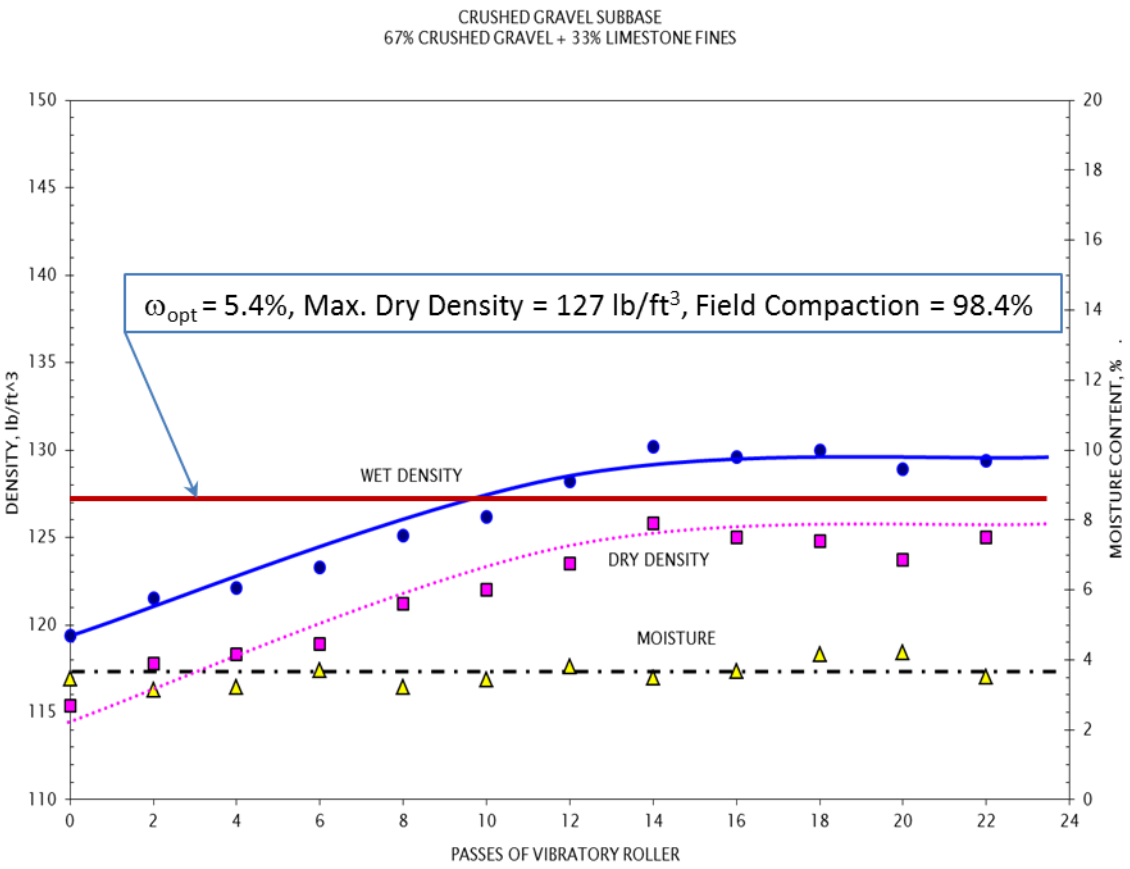

Figure 5.27 Subbase material field characteristics (1 lb/ft^3=16.02 kg/m^3)

Table 5.5 Subbase characteristics changing with passes of the vibratory roller

Passes	Wet Density, lb/ft^3	Dry Density, lb/ft^3	Moisture Content, %
0	119.40	115.40	3.47
2	121.50	117.80	3.14
4	122.10	118.30	3.21
6	123.30	118.90	3.70
8	125.10	121.20	3.22
10	126.20	122.00	3.44
12	128.20	123.50	3.81
14	130.20	125.80	3.50
16	129.60	125.00	3.68

Table 5.5 Subbase characteristics changing with passes of the vibratory roller			
Passes	Wet Density, lb/ft^3	Dry Density, lb/ft^3	Moisture Content, %
18	130.00	124.80	4.17
20	128.90	123.70	4.20
22 (final values)	129.40	125.00	3.52
Note: 1 lb/ft^3=0.157 kN/m^3			

Table 5.6 CBR test results for the subbase layer			
Item 1	Item 2	Item 3	Item 4
26.3	20.8	15.0	18.0
24.2	20.8	15.0	18.0
24.8	20.8	16.5	19.0
26.9	21.1	7.0	82.9
28.4	21.4	7.7	84.4
27.5	22.3	7.6	86.9
18.3	17.4	9.2	65.4
21.4	17.7	8.9	63.3
20.2	18.0	10.1	61.2
16.2	22.9	24.2	23.9
15.9	23.9	21.7	21.4
15.6	23.9	19.9	25.1
			30.6
			31.2
			30.3
			15.3
			15.6
			13.5
Average subgrade CBR (final values)			
22.1	20.9	13.6	39.2
Standard Deviation of CBR			
4.8	2.2	6.0	26.6

5.6.4 Construction of Base Layer

The base course was a 6 inch-thick (152-mm thick) layer of ASTM 568 crushed limestone. Figure 5.28 shows the placement process of base course material. The base lift was compacted by applying 16 passes of a self-propelled vibratory steel roller. Figure 5.29 shows

dry density, wet density and moisture content values as a function of the number of passes of the vibratory roller following the same procedure used for the subbase material. The base material achieved maximum density in about 10 passes of the vibratory roller. Moisture content remained constant at approximately 3% during placement. Table 5.7 contains the measured values of density (wet and dry) and moisture content relative to the number of passes of the vibratory roller. CBR tests were conducted after placement and final compaction of the granular material. Table 5.8 summarizes the CBR test results for each test item. Since the maximum field compaction achieved during the construction of the base was only about 92% of the maximum dry density (modified Proctor), the field CBR values shown in Table 5.8 were lower than anticipated for a crushed limestone base, which usually has CBR values between 80 and 100. The base was compacted on the dry side of the optimum moisture content, as depicted by Figure .5.15, where small changes in water content have large effects on the final field density.

Figure 5.28 Placement of Base layer

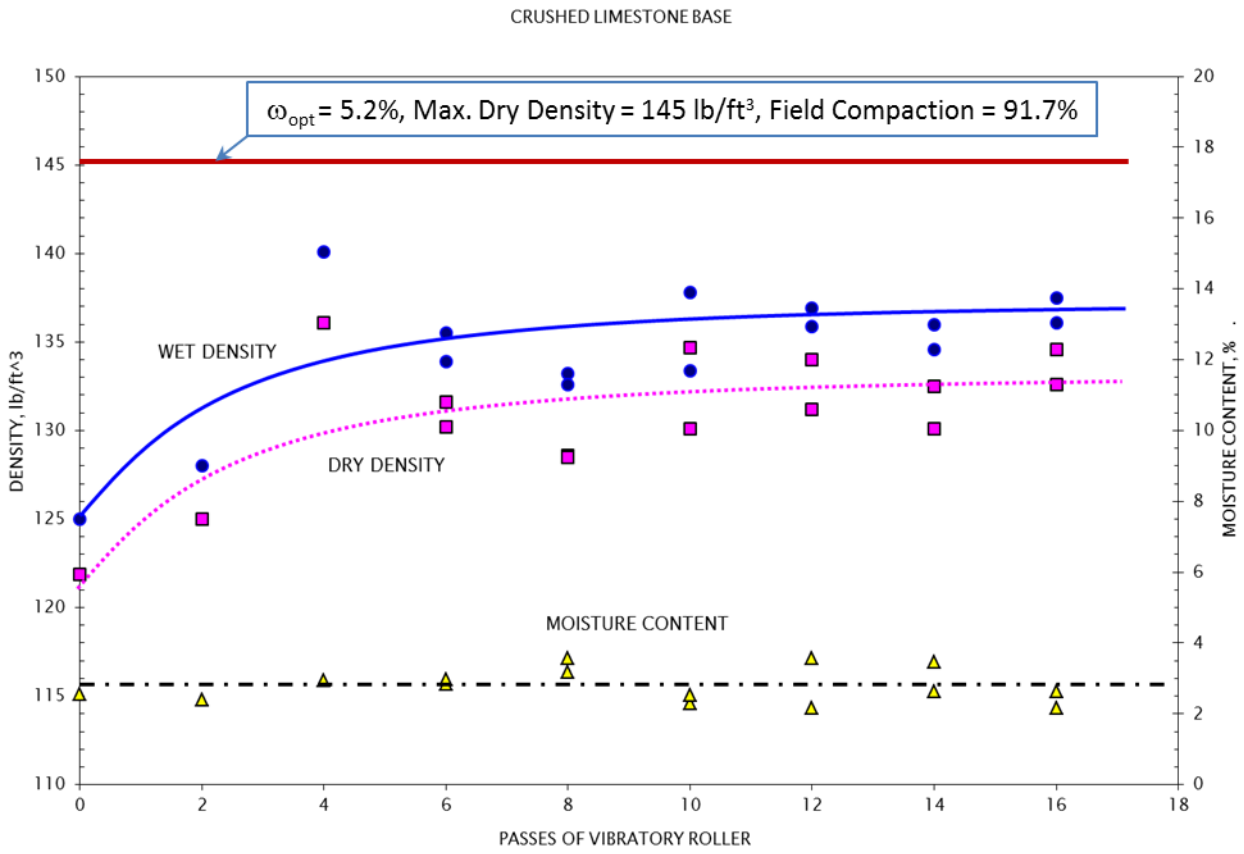

Figure 5.29 Base material field compaction characteristics (1 lb/ft^3=16.02 kg/m^3)

Table 5.7 Base characteristics changing with passes of the vibratory roller			
Passes	**Wet Density, lb/ft^3**	**Dry Density, lb/ft^3**	**Moisture Content, %**
0	125.00	121.90	2.54
2	128.00	125.00	2.40
4	140.10	136.10	2.94
6	133.90	130.20	2.84
6	135.50	131.60	2.96
8	133.20	128.60	3.58
8	132.60	128.50	3.19
10	137.80	134.70	2.30
10	133.40	130.10	2.54
12	135.90	131.20	3.58
12	136.90	134.00	2.16
14	134.60	130.10	3.46

Table 5.7 Base characteristics changing with passes of the vibratory roller			
Passes	**Wet Density, lb/ft^3**	**Dry Density, lb/ft^3**	**Moisture Content, %**
14	136.00	132.50	2.64
16	136.10	132.60	2.64
16 (final values)	137.50	134.60	2.15
Note: 1 lb/ft^3=0.157 kN/m^3			

Table 5.8 Field CBR test results for the base layer			
Item 1	**Item 2**	**Item 3**	**Item 4**
41.3	24.5	21.1	41.0
35.5	31.2	22.0	44.3
39.8	27.5	18.3	38.8
48.3	32.1		
Average Base Field CBR (final values)			
41.2	28.8	20.5	41.4
Standard Deviation of Field CBR values			
5.3	3.5	1.9	2.8

5.6.5 Construction of Asphalt Concrete Layer

The asphalt mixture was provided and placed by a local asphalt contractor. Paving operations started on January 14, 2008. The air and ground temperatures were 60°F (15.6^{o}C). The temperature of the asphalt mix at the plant was 300°F (149^{o}C). When the mix reached the site, the asphalt temperature was between 285°F and 295°F (140^{o}C to146^{o}C). After compaction, the asphalt mat had a temperature of 270°F (132^{o}C). The asphalt mixture was placed in a 4 inch-thick (102-mm) lift and compacted to a thickness of 3.25 inches (82.6 mm). The density of the compacted layer was between 135 lb/ft^3 and 141 lb/ft^3 (21.21 kN/m^3 and 22.15 kN/m^3). The asphalt layer was placed in the three paving lanes in a north-south direction. Lanes 1 and 2 were 13 feet (3.96 m) wide and Lane 3 was 14 feet (4.27 m) wide. All lanes were paved the full length of the test section or 200 feet (61 m). Figures 5.30, 5.31 and 5.32 show some of the paving operations. After placement, the asphalt layer was allowed to cure for one month before the application of any test traffic.

Figure 5.30 Paving operations, mat placement

Figure 5.31 Paving operations, break-down rolling

Figure 5.32 Paving operations, rubber-tire roller compaction

5.7 Field Testing and Sampling

Field CBR testing was conducted at multiple locations on each layer and in each test item. Table 5.9 summarizes the average CBR values that can be considered pre-traffic. This testing was accomplished prior to the placement of the asphalt layer.

Table 5.9. Pre-traffic average CBR values

Pavement Layer	Item 1	Item 2	Item 3	Item 4	Average for Traffic Lane
Base	41.2	28.8	20.5	41.4	33.0
Subbase	22.1	20.9	13.6	39.2	24.0
Subgrade	14.2 (15)	9.8 (10)	3.9 (4)	3.9 (4)	

Note: Values in parentheses represent target CBR values.

Table 5.10 Average Final Layer Thicknesses			
Pavement Layer	Target Thickness, in	As-Built Thickness,, in	Deviation in Elevation, in
Asphalt Concrete	3	3	0.48
Base	6	6	0.44
Subbase, Item1	6	7	0.45
Subbase, Item2	14	14	0.45
Subbase, Item3	16	16	0.45
Subbase, Item4	23	23	0.45
Subgrade	---	---	0.45
Note: 1 in.=25.4 mm			

Each layer was tested with Dynatest Falling Weight Deflectometer (FWD) Model 8082-011. A summary of falling weight data collected during testing is included in Appendix C. Elevation measurements were also obtained after completion of each pavement layer. Figure 5.33 shows a plan view of the profile points for the subgrade, subbase, base and surface layers, respectively. Figure 5.34 shows an elevation profile for each section item and the position within the layer of the earth pressure cells (EPC) and single-depth deflectometer (SDD) sensors. The horizontal lines within each item represent the average interface location between pavement layers. Table 5.10 summarizes layer thickness (target and as-built) and average deviation (in absolute value) from the reference elevation. EPC and SDD gauges were installed approximately 3 inches below the base, subbase and subgrade interfaces to avoid breakage of the sensors during construction and compaction procedures.

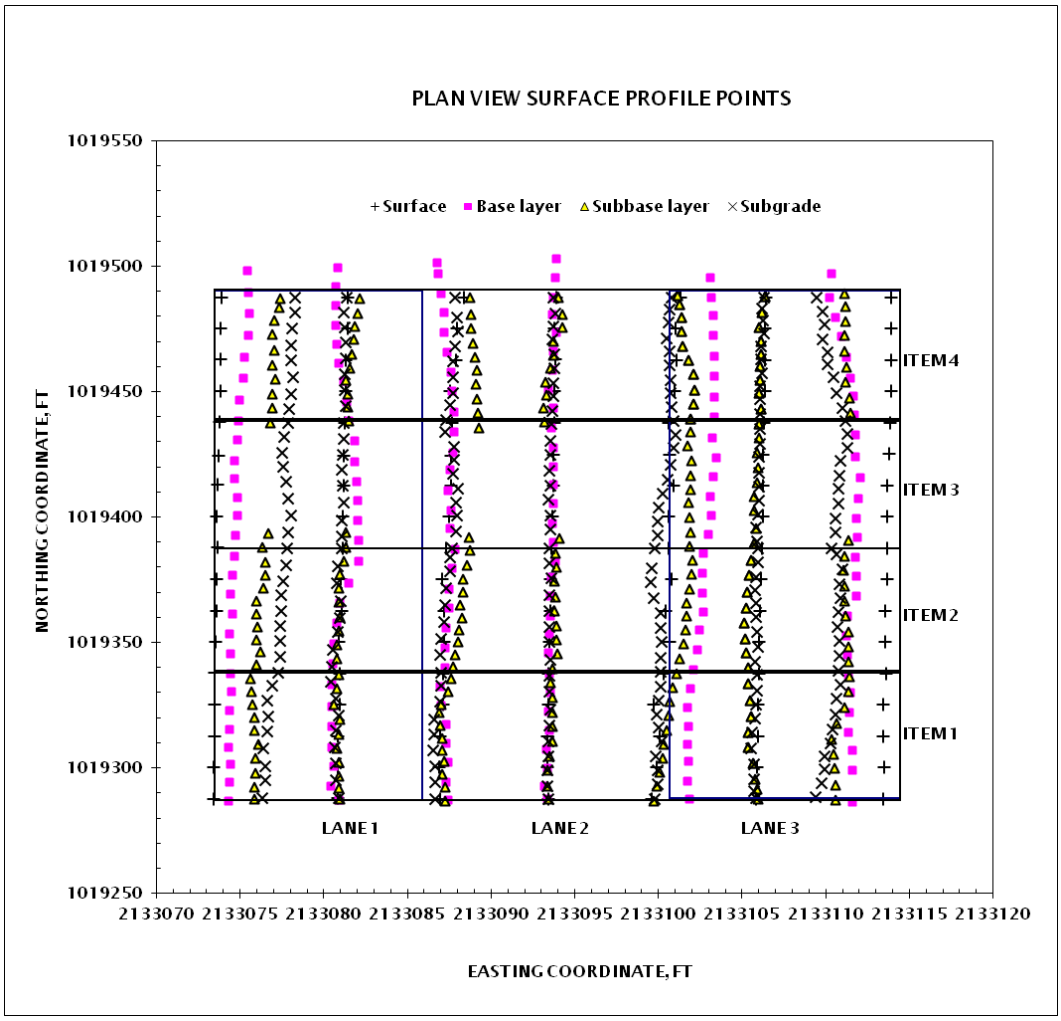

Figure 5.33 Plan view surface profile points for each layer (1 ft=0.3048 m)

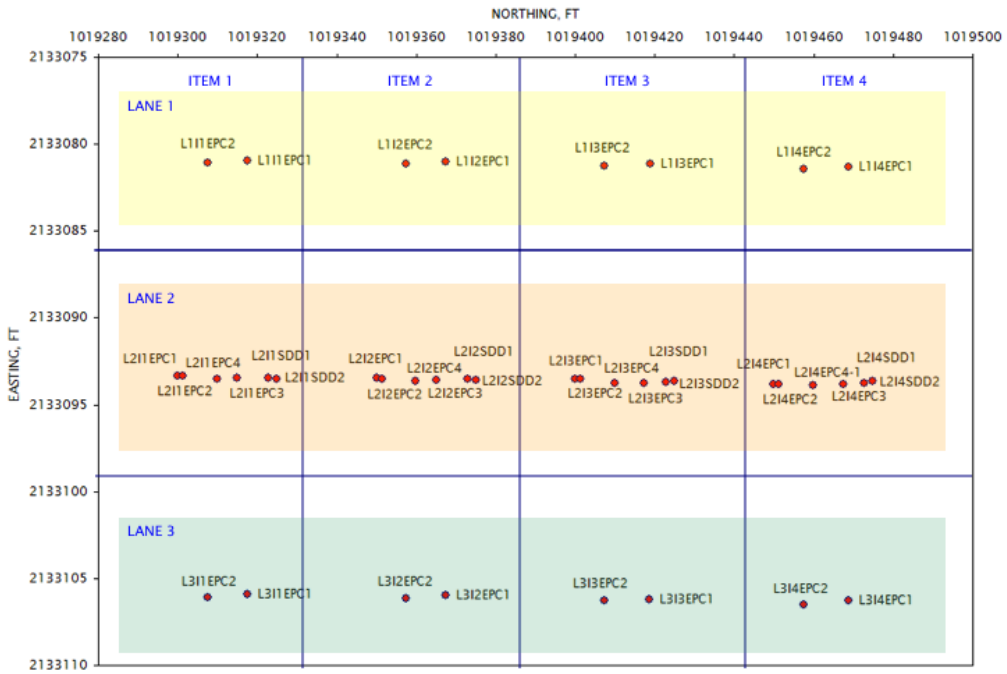

(a) Plan view

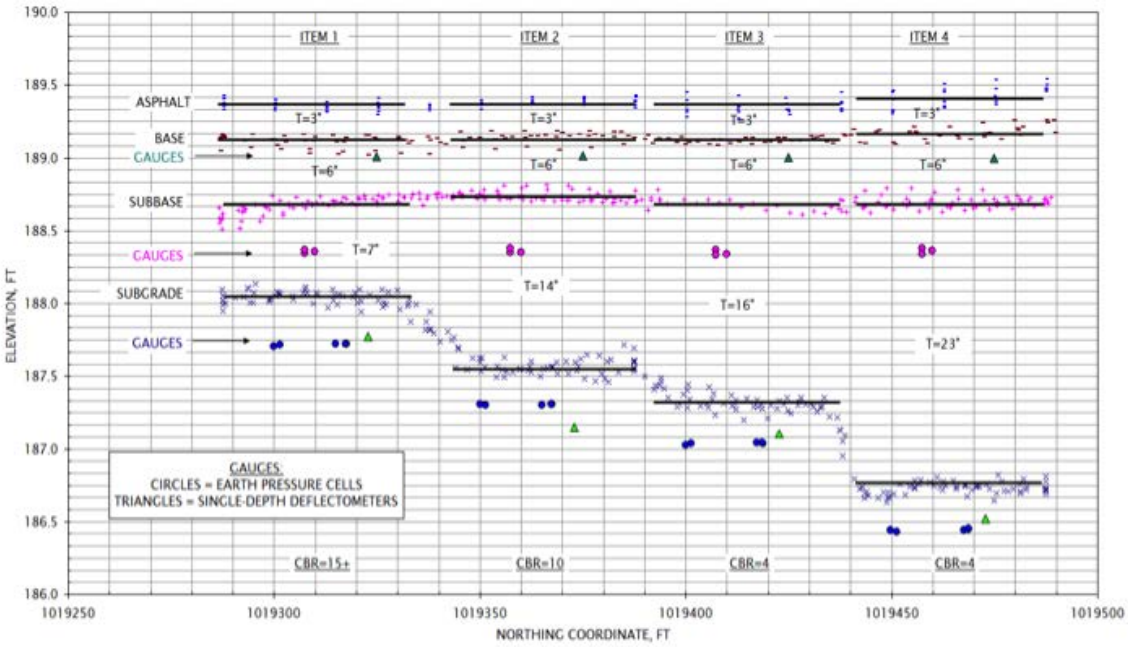

(b) Cross section view

Figure 5.34 Instrumentation layout (1 in.=25.4 mm, 1 ft=0.3048 m)

5.8 Instrumentation of Test Sections

Instrumentation was installed throughout the test section to monitor pavement performance under traffic. The instrumentation included temperature sensors, EPC, SDDs and surface strain gages. A discussion of on placement of all these gauges is presented in this section.

5.8.1 Temperature Sensors

Eight temperature sensors were installed in the test section at four different locations. The sensors are called *i-button*s and are manufactured by The Transtec Group, Inc., Austin, TX. They are self-contained, programmable small units capable of reading temperature for up to two years depending on the data collection frequency. At each location, one sensor was mounted at a depth of about 3 inches (76 mm), corresponding to the bottom of the asphalt layer, while another sensor was installed just below the asphalt surface. A mixture of asphalt and sand was used to initially place and protect the sensors within the asphalt layer. Two additional temperature sensors used to measure air temperature, were installed approximately 5 feet (1.52 m) above the pavement surface and located strategically on the north and south ends of the test section. Figure 5.35 shows a schematic of the locations and placement of the temperature sensors installed within the test section.

Since trafficking over each test lane and item was conducted during different periods throughout the year, a record of pavement surface temperatures was kept by the use of the temperature sensors embedded in the asphalt. Figure 5.36 shows the pavement temperature recordings during testing. Trafficking started with Lane 1 (C-17 single), followed by Lane 3 (F-15 Single) and finished with Lane 2 (C-17 dual). The vertical lines in Figure 5.36 mark the start and end dates of traffic on each test lane. The horizontal bars superimpose over the temperature log are the average temperatures occurring during the week of testing. Testing of each test item is identified in the figure by the capital letter I followed by a number (i.e. I1=Item 1, I2=Item 2, etc.).

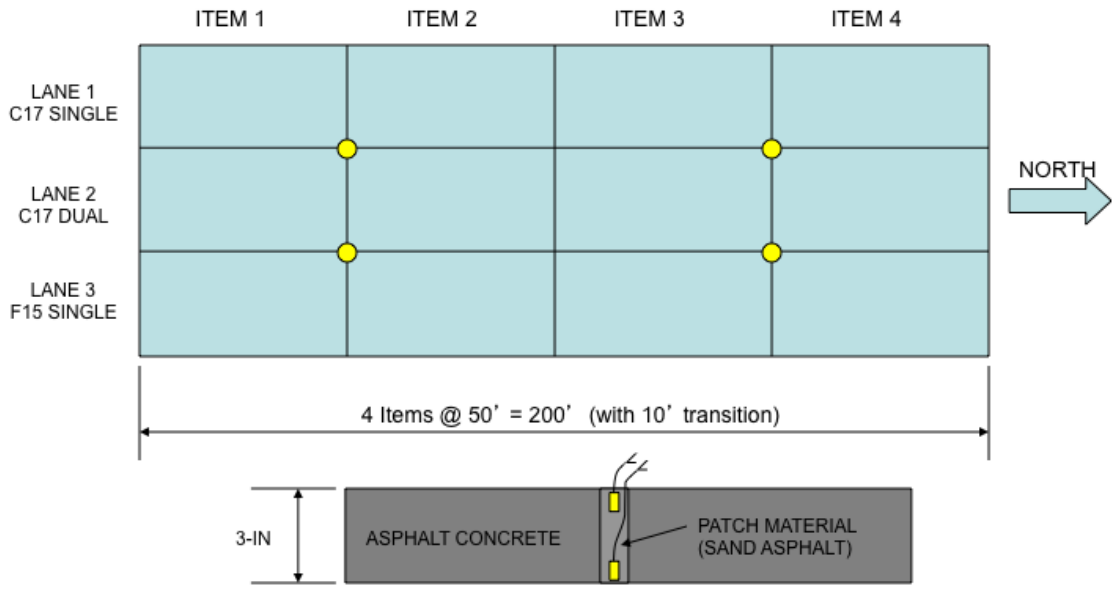

Figure 5.35 Temperature sensor locations (1 ft=0.3048 m)

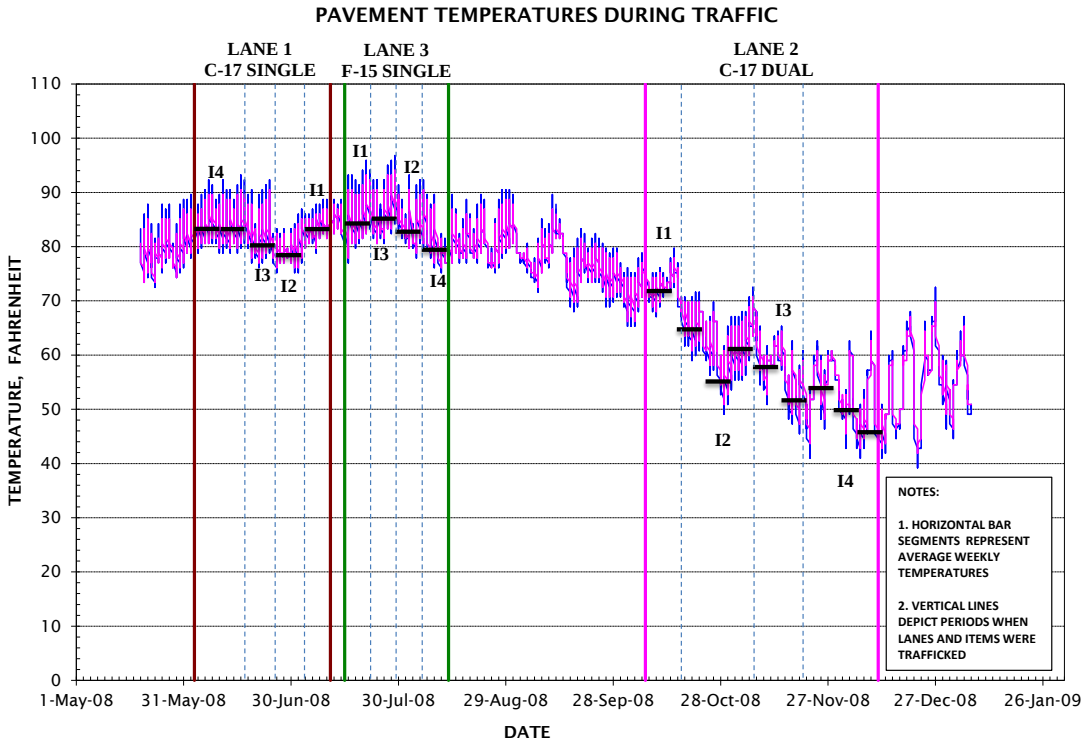

Figure 5.36 Pavement temperature recordings during traffic (^{o}C=5(^{o}F-32)/9)

5.8.2 Earth Pressure Cells

The EPC (Geokon model 3500) were manufactured by Geokon, Lebanon, NH. The model 3500 was circular with a diameter of 9 inches (229 mm). The EPC gauges consisted of two stainless steel plates welded together around the edge and leaving a narrow space within, which was filled with de-aired hydraulic oil. The space was hydraulically connected to a pressure transducer that converted the oil pressure to an electrical signal transmitted through a signal cable to the data logger. The pressure transducers had a voltage output range of 0V to 5V DC and were attached to the data cable with a sealed, water-resistant connection

Two EPC gauges were installed in each test item. In Item 1 of Lanes 1, 2 and 3, 200-psi (1380-kPa) capacity cells were embedded about 3 inches (76 mm) into the subbase and 100-psi (690-kPa) capacity cells were embedded about 3 inches (76 mm) into the subgrade. In Items 2, 3 and 4 of Lanes 1, 2 and 3, 200-psi (1380-kPa) capacity cells were placed about 3 inches (76 mm) into the subbase, and 60-psi (414 kPa) capacity cells were placed about 3 inches (76 mm) into the subgrade. In addition, all the items of Lane 2 were also instrumented with two additional EPC gauges to measure horizontal pressures. These EPC gauges were located on the center lane on the subgrade. Figure 5.37 shows the EPC locations for each lane and item. To assure continuous contact between the cell plates and the soil, the cells were backfilled with a thin layer of sand material.

5.8.3 Single-Depth Deflectometer

Single-depth deflectometers (SDD) were custom built for this full-scale testing. These sensors were designed to measured relative displacement of a layer and consisted of a linear variable differential transformer (LVDT) mounted on a spring. The sensors had a range of ±1 inch (±25 mm). Figure 5.38 shows an SDD after installation. Two SDD gauges were installed in each item of Lane 2 and located 3 inches (76 mm) below the asphalt layer and at the top of the subgrade and anchored at a depth of 10 feet (3.05 m) below the pavement surface (Figure 5.37). However, due to poor reliability of these SDD sensors, the data from this instrumentation was not considered in the study.

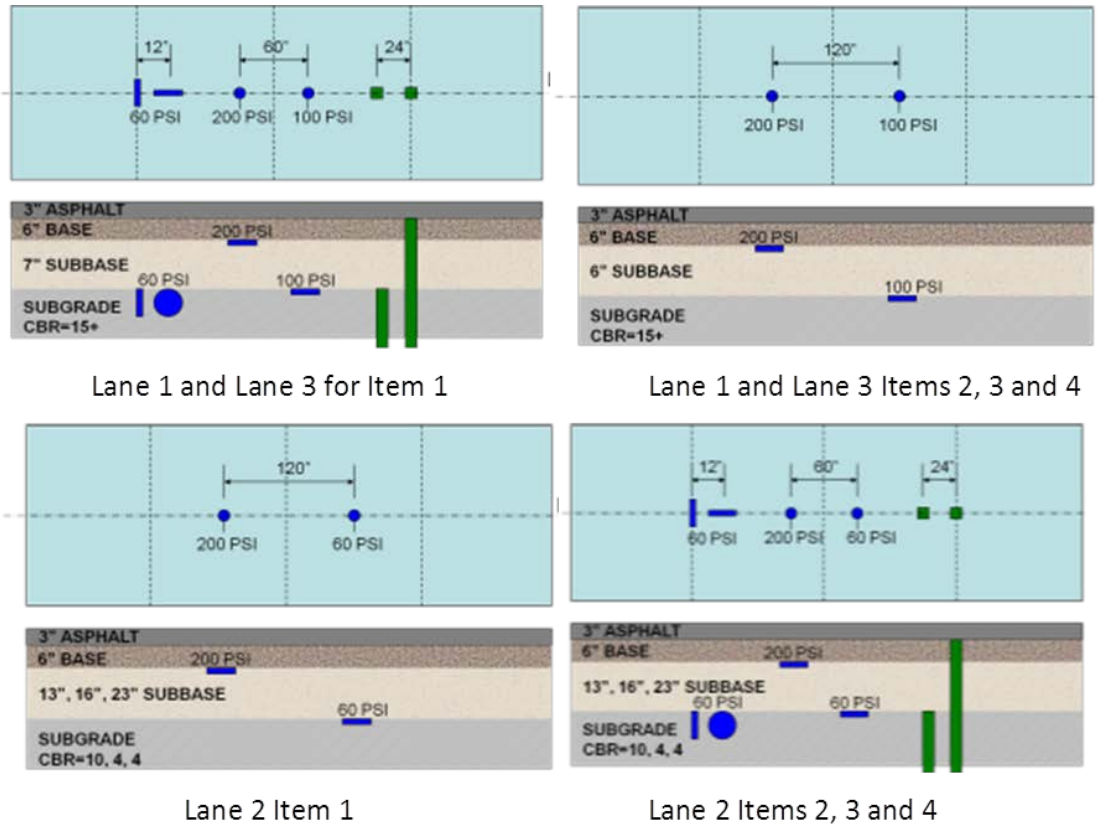

Figure 5.37 Instrumentation locations. Note: circles = ECP; rectangles = SDD (1 in.=25.4 mm, 1 psi=6.9 kPa)

Figure 5.38 SDD after installation

5.8.4 Surface Strain Gauges

To support the goals of another associated research project dealing with the measurement of strains in the asphalt and their relationship to minimum asphalt thicknesses, surface strain gauges were installed on Lanes 1. The data analyses, although considered valuable, were outside the scope of this research and described herein only for completeness. Eight surface strain gages were positioned on Lane 1, Item 4: four were parallel to traffic and four were transverse to traffic. Figure 5.39 shows the position of the gages on the pavement surface. The 2-inch (51-mm) long gauges were manufactured by Vishay, Precision Group, Wendell, NC. The surface strain gages were serviceable only during the rolling tests prior to trafficking the pavement. The impact of the high-pressure tire moving over the gauges limited gage functionality. The general procedure for installation of the gages was the following:

a. The asphalt surface was first cleaned and lightly sanded.
b. A thin film of a quick-setting epoxy was applied to the surface and allowed to completely cure.
c. The epoxy surface was then sanded such that only a very thin film of epoxy remained on the asphalt surface.
d. The foil strain gages were bonded to the epoxy surface.
e. Thin wire leads were attached to the gages.
f. The gages and connections were covered with a rubber-cement coating to provide water protection.
g. A shielded instrumentation cable was attached to the strain gage leads.
h. To provide additional protection from traffic, the gages and connections were covered with a thin rubber pad that was taped to the asphalt surface.

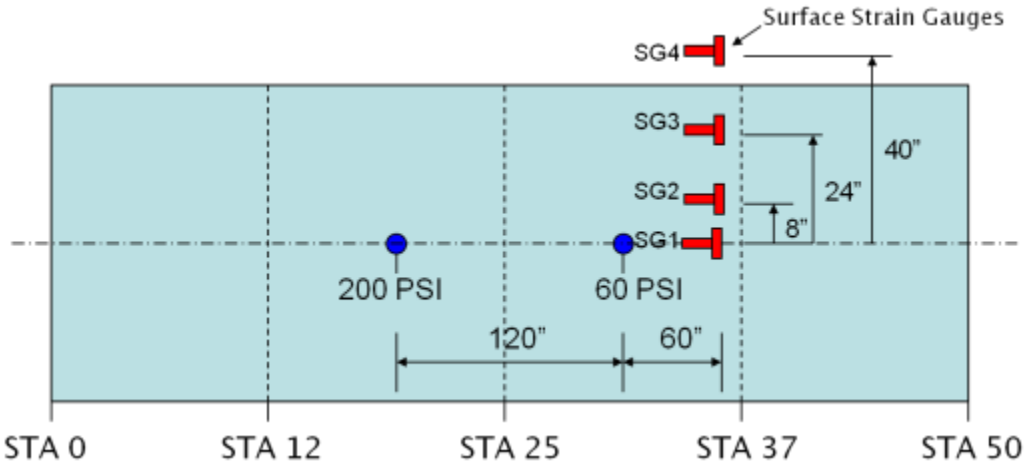

Figure 5.39 Strain gage locations on Lane 1 Item 4 (1 psi=6.9 kPa)

5.9 Loading Equipment Used for Traffic

All traffic was applied with a heavy vehicle simulator, HVS A Mark V, manufactured by Dynatest International. Each test item was trafficked individually by moving the HVS over the test item, applying bi-directional traffic until the item was deemed failed and then moving on to the next test item. Unlike typical highway pavements, airfield pavements are routinely subjected to traffic in both directions. Unidirectional trafficking of airfield pavements would likely result in more severe conditions (for example: more pavement rutting and shoving of the asphalt surface) than those anticipated in the field. Therefore, trafficking with the HVS was chosen to be applied in both directions to better simulate field conditions. Two types of gear were select to cover high and low pressure tires acting on single wheels. A third was select to apply traffic on a dual gear with low tire pressure. These types of gears were selected to account for the effects tire pressure, tire contact area and tire loading on the performance of each test item. A description of the loading used for testing is described in the following sections.

5.9.1 Heavy Vehicle Simulator

The HVS A, depicted in Figure 5.40, was employed to simulate each aircraft load. The HVS A is capable of applying traffic on a 40-foot (12.2 m) length of pavement. It has the capability of applying loads up to 100,000 lb (445 kN) with single-wheel or dual-wheel gear assemblies. The test gear assembly is mounted in a carriage that moves along a horizontal beam attached to the HVS-A frame. The gross weight of the HVS A acts as a reaction force when

applying the load to the test gear. The carriage is hinged at one end with a hydraulic ram applying the load at the other end. The movement of the carriage, both laterally and longitudinally and a hydraulic ram applies pressure on a pre-programmed fashion that is and controlled by a computer. The carriage is also capable of been shifted laterally a distance of 4 feet (1.22 m).

The maximum traffic lane width then becomes 4 feet (1.22 m) plus the distance from the centerline of the carriage to the outside tire of gear. The transverse movement of the carriage can be programmed to move laterally either by lifting the gear at the end of the test section and repositioning the gear at the next lateral interval position or by moving it laterally and diagonally along the lane during trafficking without picking it up. Lifting the gear is more time consuming than just shifting it as it travels, but results in wheel paths that are parallel with the HVS A frame and traffic lane and are more representative of actual field operations. During the traffic tests, both methods of moving the carriage transversely were tried. Traffic was applied in a distributed pattern over a lateral wander width of 4 feet (1.22 m) plus the width of the test gear and in bidirectional fashion in the longitudinal direction. The HVS A traveled at an approximate speed of 5 miles per hour (8 km per hour).

Figure 5.40 Heavy Vehicle Simulator (HVS A) used for traffic testing

5.9.2 Layout of Test Lanes and Traffic Patterns

While a test item is a portion of the entire test section, the traffic lane is an area of the pavement surface of a given width extending through the length of the test section. Thus, a traffic lane would extend across all four test items. The test section was divided into three traffic lanes to apply traffic with the F-15 single tire, the C-17 single tire and the C-17 dual-tire gear. The nominal widths for Lanes 1, 2 and 3 were 5 feet (1.52 m), 10 feet (3.05m) and 5 feet (1.52 m), respectively. The lanes had a 5-foot (1.52-m) of buffer strip between each lane and a 5-foot (1.52-m) clearance at each end of the test section. Figure 5.41 shows a schematic describing the lanes and items. Figure 5.42 shows pictures of the single and dual-tire assemblies used for the testing.

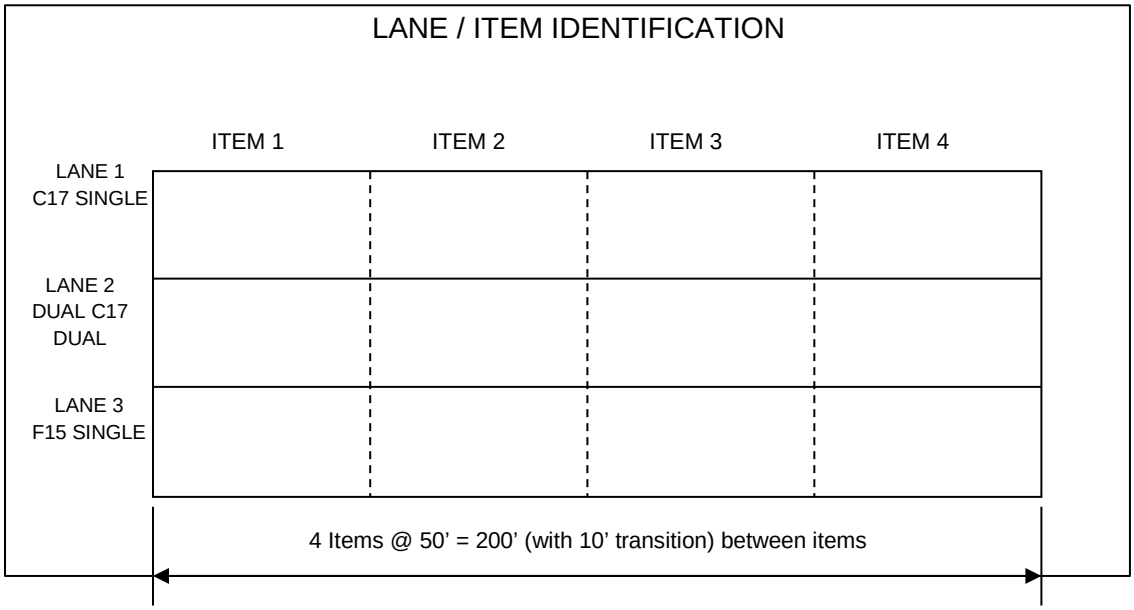

Figure 5.41 Test section layout with traffic lane details (1 ft=0.3048 m)

Figure 5.42 Single F-15 gear (left) and dual C-17 gear (right) tire assemblies

5.9.3 Traffic and Loading on Lane 3

Lane 3 was trafficked with the F15 tire. The tire was loaded to 35,235 lb (157 kN) with an internal tire pressure of 325 psi (2242 kPa). This loading and tire pressure yielded a computed contact area of 108 in^2 (697 cm^2). The measured contact area had a width of 8.8 inches (224 mm) and a length of 15 inches (381 mm). The computed area, based on the assumption of an elliptical shape, was 104 in^2 (671 cm^2). The contact area for this tire was slightly more squared than an ellipse, thus the computed elliptical area would be slightly lower than the actual contact area as shown in Figure 5.43. Nevertheless, it was concluded that the approach of using the tire load and tire pressure to compute an elliptic contact area was sufficiently accurate for design and evaluation.

Figure 5.43 F-15 tire imprint at 34,400 lb (153 kN) load, Contact Area = 107 in^2 (690 cm^2)

For each lane, the trafficking was applied in a predetermined laterally distributed pattern. A pattern is a completely repeatable set of tire or gear movements across a pavement. For Lane 3, the traffic pattern was over a lateral wander width of 4 feet (1.22 m) and bidirectional in the longitudinal direction. The 4-foot (1.22 m) wander width resulted in a 64.8 inch-width (1.65 m-width) of pavement being trafficked or covered. The traffic pattern began with the tire located at one corner of the traffic lane. Four longitudinal passes were made along the first tire path. After completion of the four passes, the carriage was lifted and moved laterally 8 inches (203 mm). The process was repeated until the carriage reached the opposite side of the traffic lane. The sweep created across the traffic lane resulted in seven wheel paths (28 tire passes), which in turn resulted in four coverages for 100% of the traffic lane. After reaching the opposite side of the traffic lane, the tire was lifted and moved laterally 4 inches (102 mm) (1/2 of a wheel path) back toward the beginning side to establish the beginning of the second sweep. The second sweep was one wheel path less than the previous sweep and included six wheel paths. This sweep resulted in an additional four coverages for the center 48.8 inches (1.24 m) of the traffic lane. The process of moving the tire laterally 4 inches (102 mm) toward the center area, narrowing the trafficked area at every sweep, was repeated to obtain sweeps of five and four wheel paths. The completion of the sweep for the four wheel paths completed the traffic pattern and resulted in a total of 88 passes and 16 coverages over the center 40.8 inches (1.04 m) of the traffic lane. Since the 88 passes resulted in 16 coverages, the pass-to-coverage ratio for the traffic pattern due to the F-15 single was 5.5. Figure 5.44 shows a graphical depiction of the traffic pattern used for the F-15 single tire.

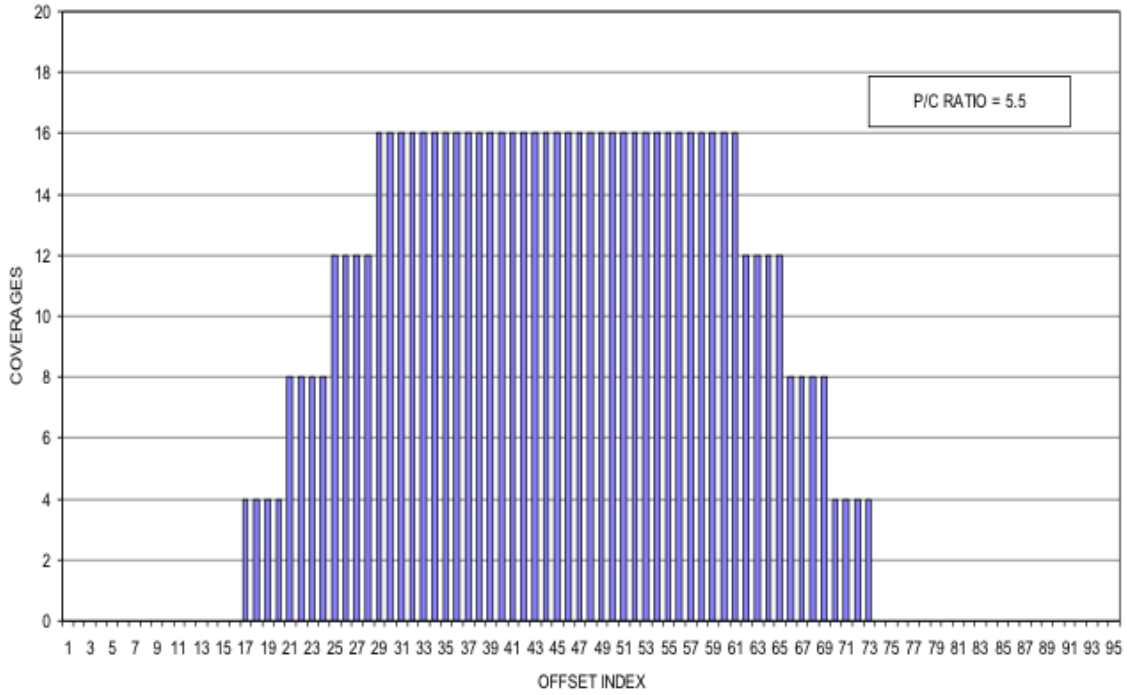

Figure 5.44 Approximate normally distributed traffic pattern for the F-15 single tire

5.9.4 Traffic and Loading on Lane 2

Lane 2 was trafficked with the dual-wheel assembly using two C-17 tires. The dual tires had a center-to-center spacing of 40.5 inches (1.03 m). Each tire was loaded to approximately 45,000 lb (200 kN) at a tire pressure of 142 psi (980 kPa). This loading and tire pressure resulted in a computed contact area of 305 in^2 (1968 cm^2). The tire print measured 17.2 inches (437 mm) wide and 22.0 inches (559 mm) long. With the assumption of an elliptical-shaped area, the computed area of the tire print was 297 in^2 (1916 cm^2). Similar to the F-15 tire, the C-17 tire also had a slightly square shape, thus the assumption of an elliptical-shaped contact area produced a slight underestimation of the effective tire contact area (Figure 5.45).

The carriage lateral movement of the dual-tire assembly was similar to that for the F-15 single tire. Because of the dual-tire arrangement, the C-17 dual assembly resulted in a much wider trafficked area. For traffic lane 2, the carriage was moved 16 inches (406 mm) for each lateral shift. The 16-inch (406-mm) shift produced two sets of four wheel paths, resulting in a pavement width of 105.7 inches (2.68 m) actually receiving traffic. With four wheel paths for

each tire, the first sweep of the carriage resulted in 16 passes, the second sweep (three wheel paths) resulted in 12 passes and the third and the fourth sweeps produced 8 and 4 passes, respectively, for a total 40 passes. This traffic pattern applied 16 coverages to the center 57.7 inches (1.47 m) of the traffic lane. This resulted in a pass-to-coverage ratio equal to 2.5. Figure 5.46 shows the traffic pattern for the C 17 dual gear.

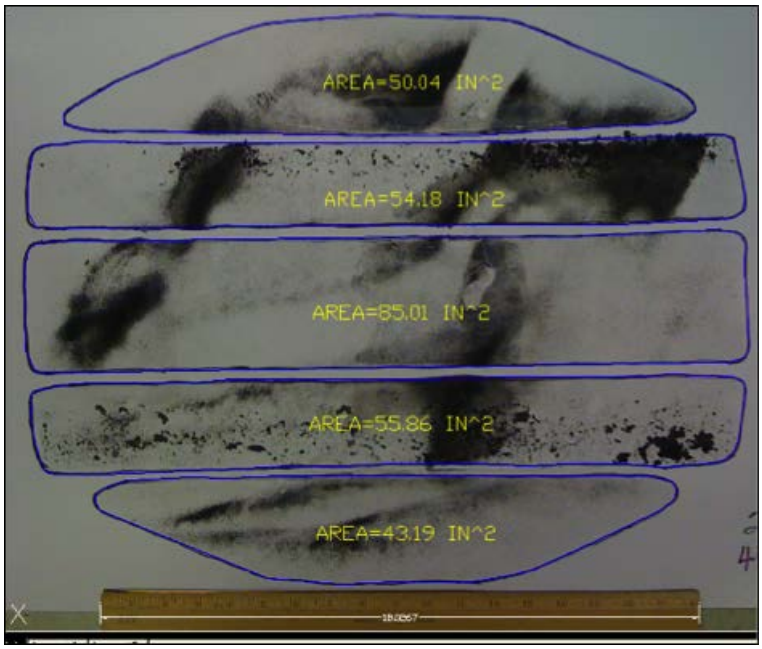

Figure 5.45 C-17 tire imprint at 45,000 lb (200 kN), Contact Area=288 in^2 (1858 cm^2)

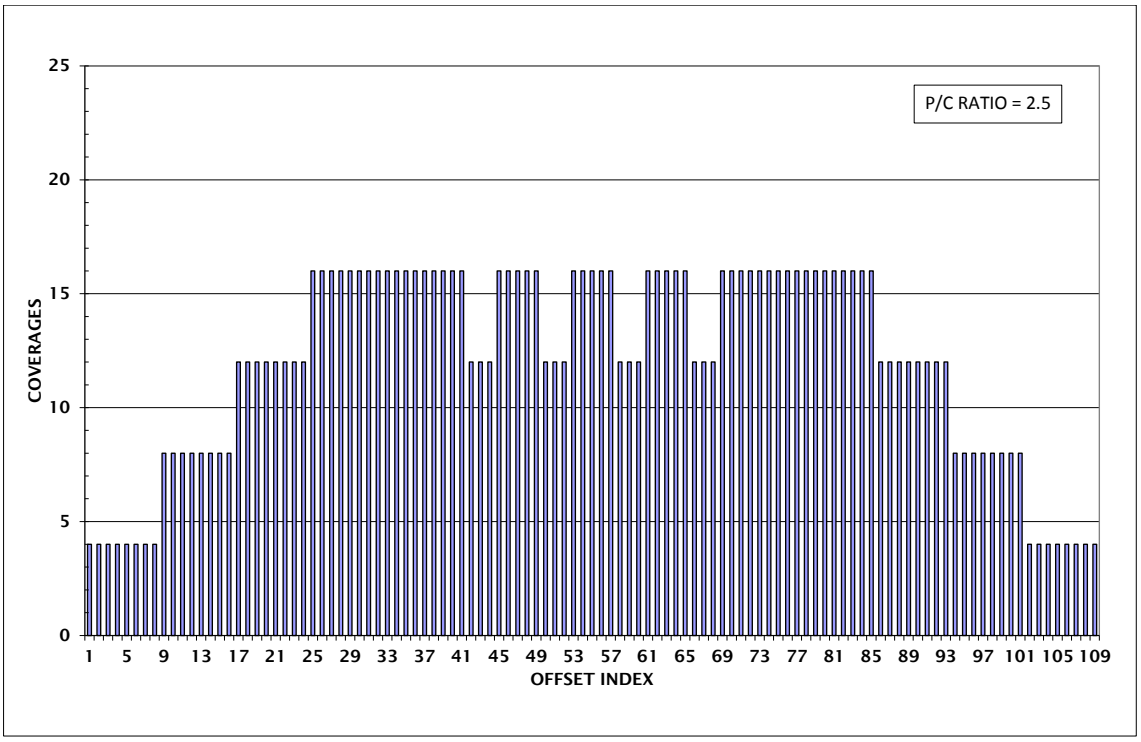

Figure 5.46 Traffic pattern for the C 17 dual-tire gear

5.9.5 Traffic and Loading on Lane 1

Lane 1 was trafficked with the C-17 single-wheel gear. The single C-17 tire had the same loading and tire pressure as the dual C-17 gear. The trafficked area was identical to one-half of the dual-wheel traffic area, with the exception that the trafficked area was shifted to the center of the traffic lane. The width of the trafficked area was 65.2 inches (1.66 m). The lateral shift of the carriage was 16 inches (406 mm), giving four wheel paths for the first sweep, three wheel paths for the second sweep, two wheel paths for the third sweep and one wheel path for the fourth sweep. This traffic pattern required 40 passes and resulted in 16 coverages for an effective pass-to-coverage ratio of 2.5 (Figure 5.47).

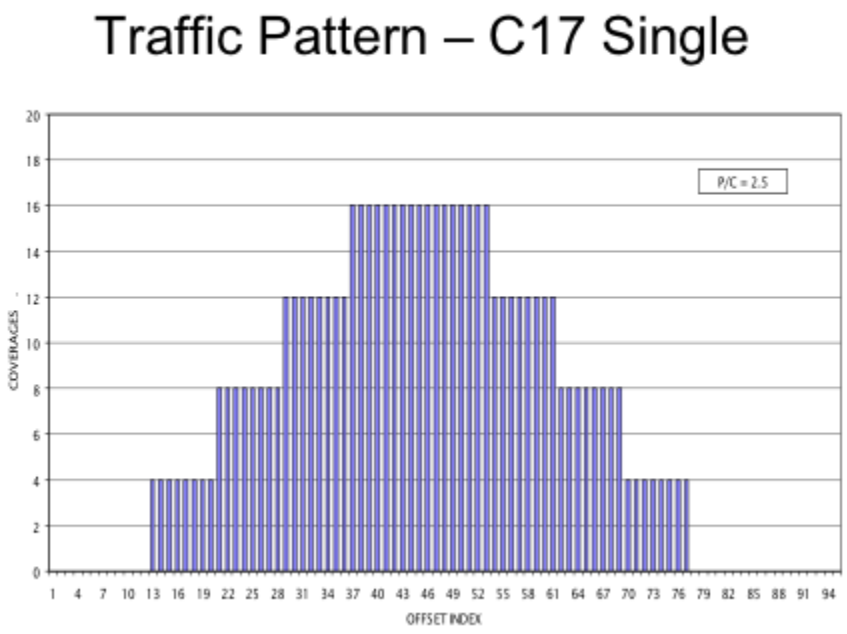

Figure 5.47 Approximate normally distributed traffic pattern for the C 17 single tire

5.9.6 Calibration of Heavy Vehicle Simulator Loading

The HVS A was calibrated prior to traffic to ensure the correct loading was applied. The HVS A applies the load through a hydraulic ram and lever arm system, as in Figure 5.48. The load applied to the tire was determined by measuring the oil pressure supplied to the hydraulic ram. Since there was no independent system to directly measure the load being applied to the test tire, a calibration of the ram and mechanical advantage of the carriage level arm was considered necessary. To perform this calibration, load cells were used to verify the HVS A loading, and strain gages were installed on the lever arm of the HVS A carriage and on the tire axle. Three load cells measured the load applied to a single tire, and four load cells were used with the C-17 dual tires. The load cells were placed between two steel plates in such a manner as to equalize the load between all load cells. Figure 5.49 shows the calibration setup, Figure 5.50 shows the strain gage arrangement and locations on the spindle, and Figure 5.51 shows the typical Wheatstone bridge gage arrangement for strain cross checking.

Figure 5.48 HVS-A carriage calibration setup

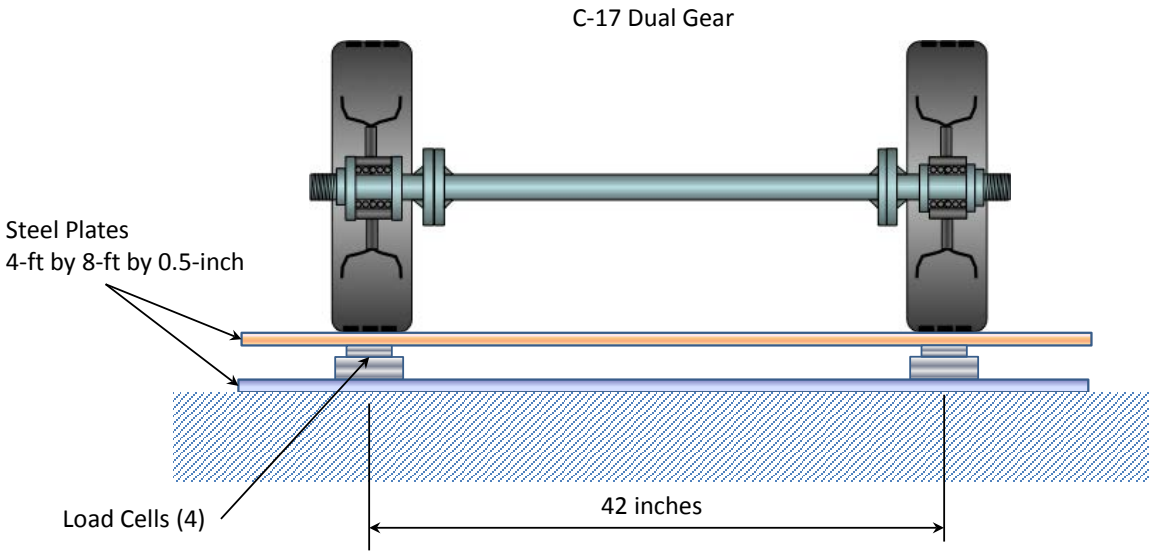

Figure 5.49 Dimensions of calibration setup (1 inch=25.4 mm, 1 ft=0.3048 m)

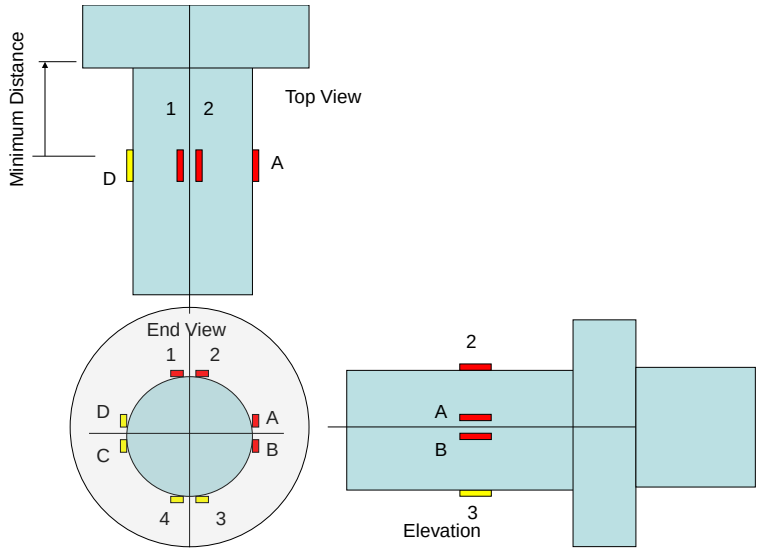

Figure 5.50 Schematic of strain gage arrangement on spindle

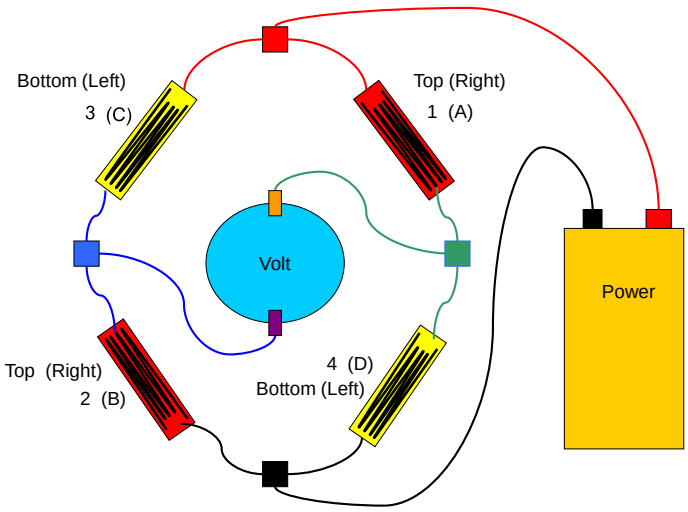

Figure 5.51 Gage Wheatstone bridge

For the C-17 dual gear, four load cells were arranged such that two cells measured the load on the left tire, and two cells measured the load on the right tire. This load cell arrangement allowed verification of the load distribution between the tires. Figure 5.52 shows the calibration results to verify that the load applied to the dual tires was evenly distributed between the two

tires. Figures 5.53 and 5.54 illustrate the data used for calibrating the strain gages attached to the carriage and to the axles. The loads, as defined by the HVS setting, where applied over the calibration scale and the actual load recorded. Loads were applied in a step-wise fashion and held for a minute or two before moving to the next load increment. Strain measurements collected from the carriage arm where correlated to the actual loads recorded from the calibration scale. Figure 5.55 shows the strain gage arrangement on the carriage. With this gage setting and calibration procedure, it was possible to measure the load applied to the pavement as the wheel traversed the test section. Figure 5.56 shows the HVS A final calibration correlated to the HVS A load setting. With this calibration in place, the HVS loading was set in terms of required HVS setting needed to achieve a desired load. This became important during pre-testing where the loading provided by the HVS was continuously recorded and related to pavement response in terms of pressures being transmitted to the pavement sub-layers.

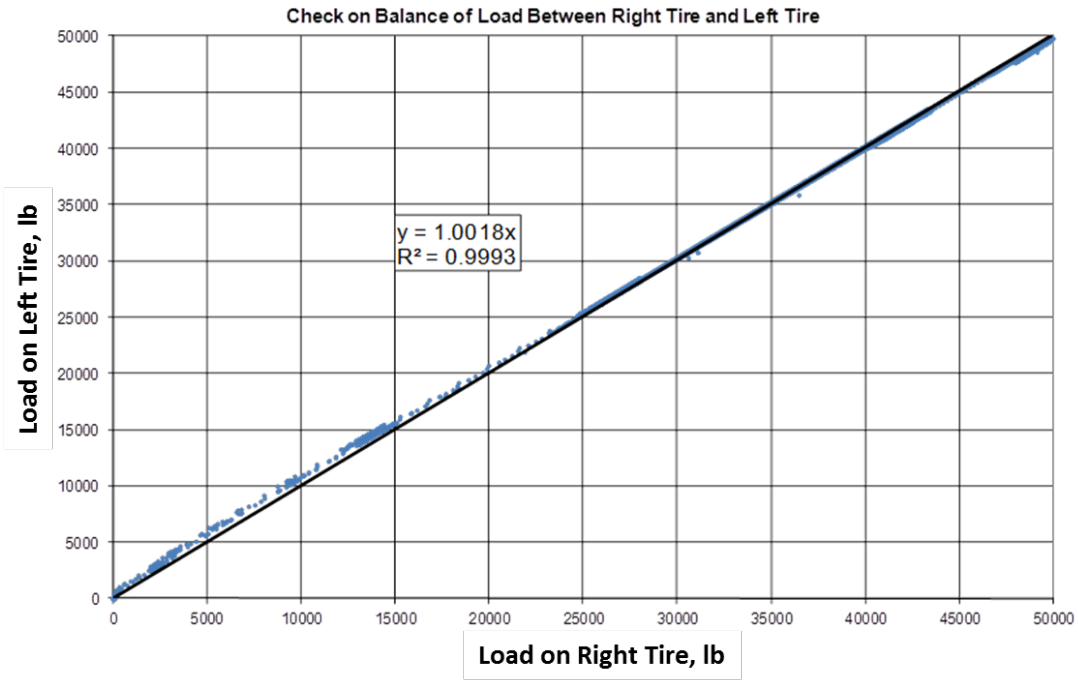

Figure 5.52 Load balance check between the C-17 dual tires (1 lb=4.45 N)

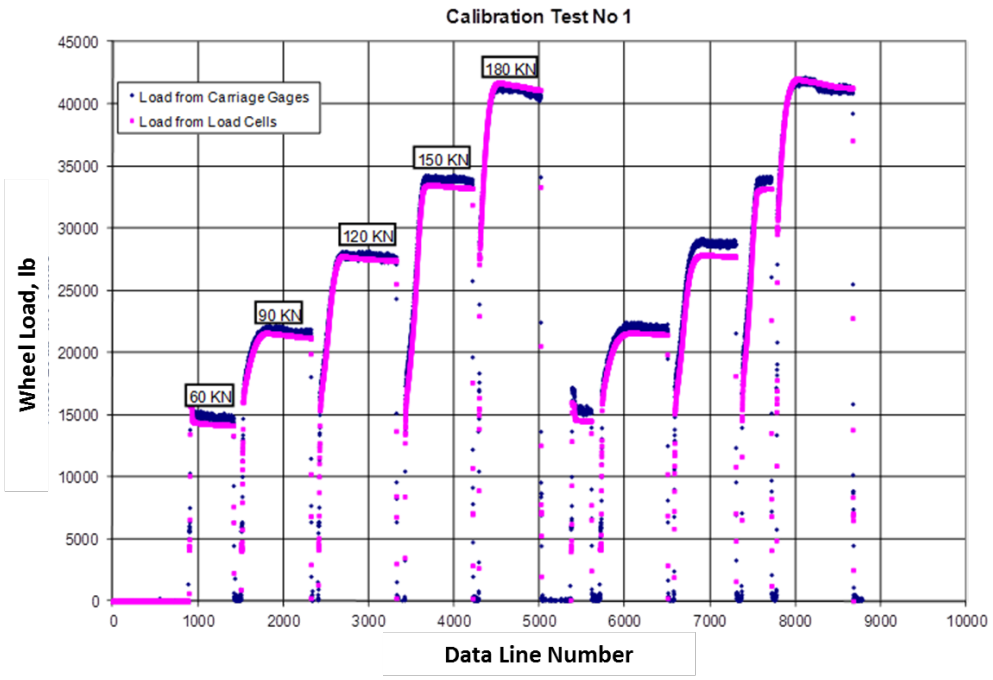

Figure 5.53 Load check for HVS A carriage and axle (1 lb=4.45 N)

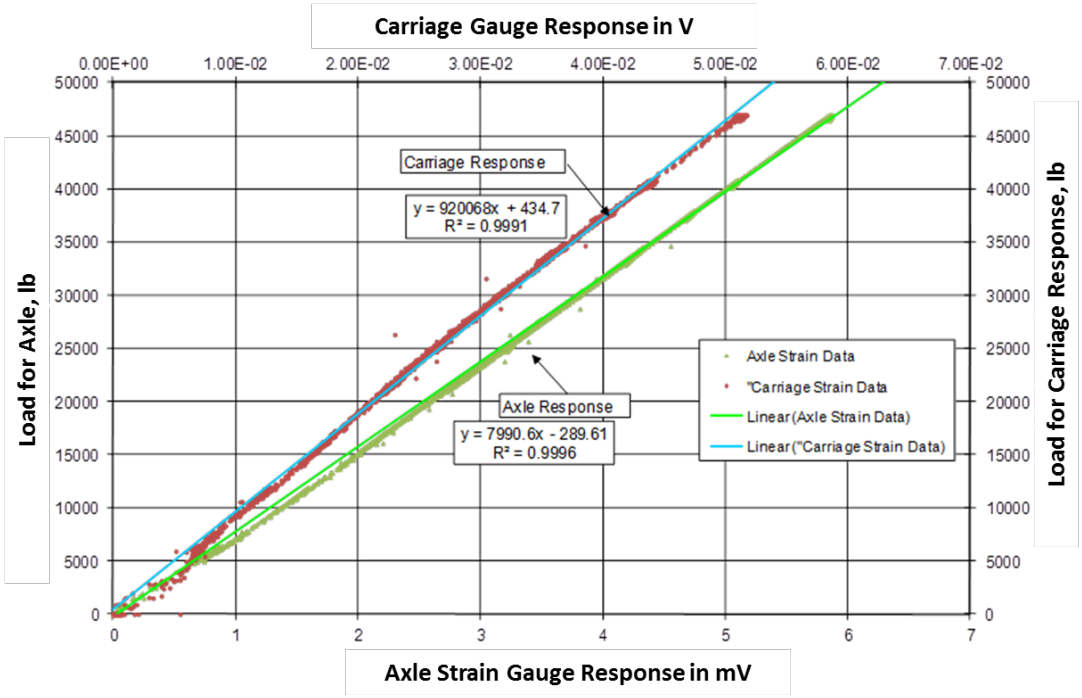

Figure 5.54 Carriage and axle load responses (1 lb=4.45 N)

Figure 5.55 Carriage strain gage arrangement

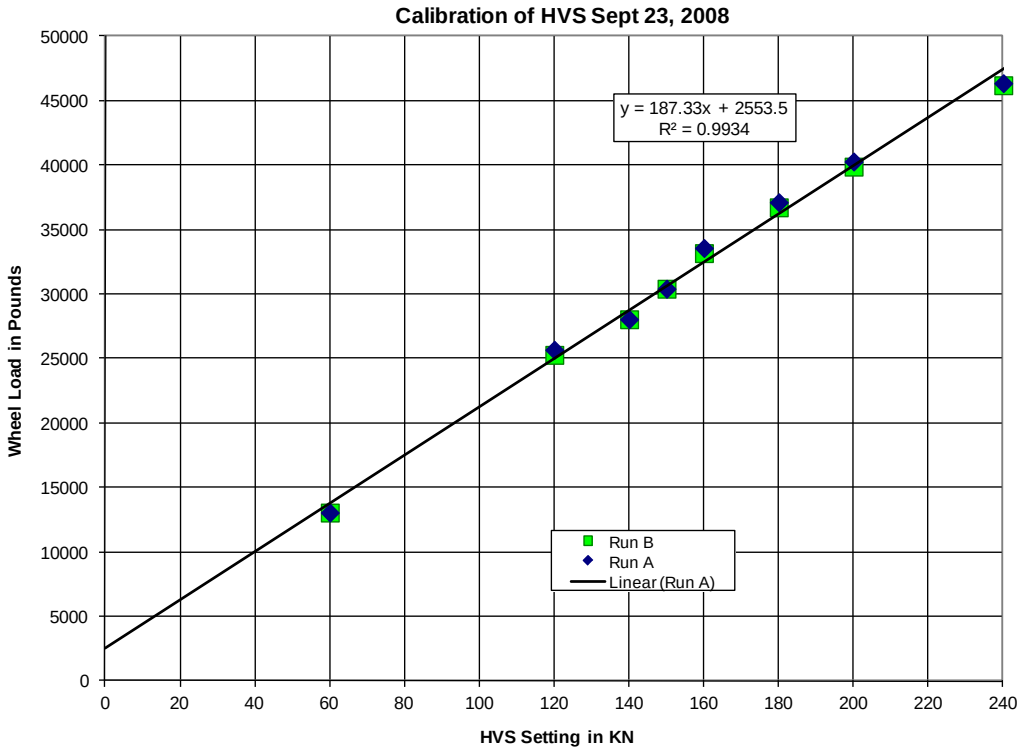

Figure 5.56 HVS A load calibration (1 lb=4.45 N)

5.10 Summary

A full-scale experimental pavement was constructed with the purpose of validating, not only the CBR-Beta performance criteria, but also the stress distribution patterns under full-size aircraft tires. A 200 foot-long by 40 foot-wide (61m by 12.2 m) flexible pavement was designed and constructed. Four different pavement structures, called test items, were laid out each having different total pavement thicknesses above the subgrade and different subgrade CBR values. Three traffic lanes were delineated to support the application of a single-wheel low-pressure aircraft tire (C-17 Single at 142 psi (980 kPa) tire pressure), a high-pressure single-wheel aircraft tire (F-15 Single at 325 psi (2242 kPa) tire pressure), and a dual-wheel low-pressure gear (C-17 Dual at 142 psi (980 kPa)). The layout of these pavement structures and traffic lanes resulted in twelve individual test items, which resulted twelve additional failure data points to be added to validate the CBR-Beta performance curve.

The flexible pavement section was constructed from standard airfield pavement materials. Each item was surfaced with a 3-inch (76 mm) asphalt concrete layer, a 6-inch (152 mm) crushed limestone layer, and varying thicknesses of a crushed-gravel subbase layer. The asphalt and base course layers were considered to be the minimum values for the loadings conditions planned for testing. The subgrades were built from high-plasticity clay and were placed at rated CBR values of 4, 10, and 15. The subgrade CBR values and total thicknesses above the subgrade were designed such that failure in the subgrade would occur after a reasonable amount of traffic. Laboratory and field testing, including field CBR tests, falling weight deflectometer tests, density tests, moisture tests, and Atterberg limits tests, was conducted to establish the basic mechanical properties of each layer within the pavement structure.

Each test item was instrumented with earth pressure cells and single-depth deflectometers placed on top of the subbase material and on top of the subgrade. Air and pavement temperatures were continually monitored throughout testing with temperature sensors installed within the asphalt pavement layer.

Traffic on the test section was applied with the WES Heavy Vehicle Simulator (HVS-A). Three aircraft gear axles were specifically designed and built for this testing. The rated loadings for the C-17 Single, F-15 Single, and C-17 Dual axles were: 45000-lb (200 kN), 35000-lb (156 kN) and 90000-lb (400 kN), respectively. The HVS-A was moved over each test item and predefined traffic pattern were applied over it. The predefined traffic patterns were chosen to

simulate aircraft ground operations on slow moving areas such as taxiways and runway ends. The pavement deterioration in terms of surface rutting and cracking was recorded at regular intervals of passes of the aircraft gear.

The data collected from this full-scale experiment was used to corroborate the stress distributions predicted by the Fröhlich stress model, the layered elastic model, and the axisymmetric finite element model. The performance of each test item was compared to the existing database of field data with the goal of validating the CBR-Beta criteria. The next chapter will present and discuss this analysis in detail in terms of predicted stresses by the different models and the performance of the test sections under traffic.

CHAPTER 6 - ANALYSIS OF TEST SECTION DATA

6.1 Introduction

This chapter presents the analysis of laboratory tests, test section field data, traffic tests and modelling effort conducted for this research. The results of stress measurements from earth pressure cells are presented along with the progression of surface rutting with passes. Prediction of stresses by the Fröhlich stress model, layered elastic model and the axi-symmetric finite element model are presented and assessed for quality of fitness. The performance of each pavement test item is individually analyzed before it is incorporated into the final form of the CBR-Beta criteria. Finally, the quality of the fitness of the CBR-Beta criteria to existing field and test section data were assessed with the purpose of establishing its validity.

6.2 Axisymmetric Finite Element Modelling

The first step to assess the validity and fidelity of measured stresses was to use tri-axial laboratory data conducted on the materials used to build the test pavements to establish the required parameters to fit the non-linear hyperbolic soil model. These parameters were later used to predict the laboratory tri-axial tests and the load-deflection curves resulting from field CBR tests conducted on the surface of the subbase and base layers constructed. The tri-axial tests conducted on the CH subgrade, the granular subbase material and the crushed limestone base are summarized in Appendix A. The parameters required to model the pavement layers using the hyperbolic soil model are summarized in Table 6.1. The triaxial tests conducted on the pavement materials were simulated by using the parameters from Table 6.1 and the non-linear finite element model, with the results shown in Figures 6.1 through 6.3.

Figure 6.1 shows the deviator stress versus axial strain for the CH clay subgrade material for CBR values equal to 4, 10 and 15. Samples for these tests were extracted from the as-constructed subgrade layer using the push cylinder method, preserved with paraffin to preserve its moisture condition and stored in a humid room until they were tested in the laboratory. The solid curves represent actual laboratory test results, while the dashed curves represent the predicted response from the hyperbolic soil model using the parameters from Table 6.1.

Table 6.1 Summary of hyperbolic parameters for non-linear finite element					
CH Clay Subgrade Material					
CBR	**Cohesion, psi**	**Angle Internal Friction, degrees**	**R_f**	**K**	**n**
4	9.2	0.0	0.86	3012	0
10	25.7	0.0	0.89	11765	0
15	30.4	0.0	0.88	11494	0
Crushed Gravel and Limestone Mix Subbase Material					
	8.0	48.0	0.77	3315	0.58
Crushed Limestone Base Material					
	7.0	50.0	0.67	10519	0.51
Note: 1 psi=6.9 kPa					

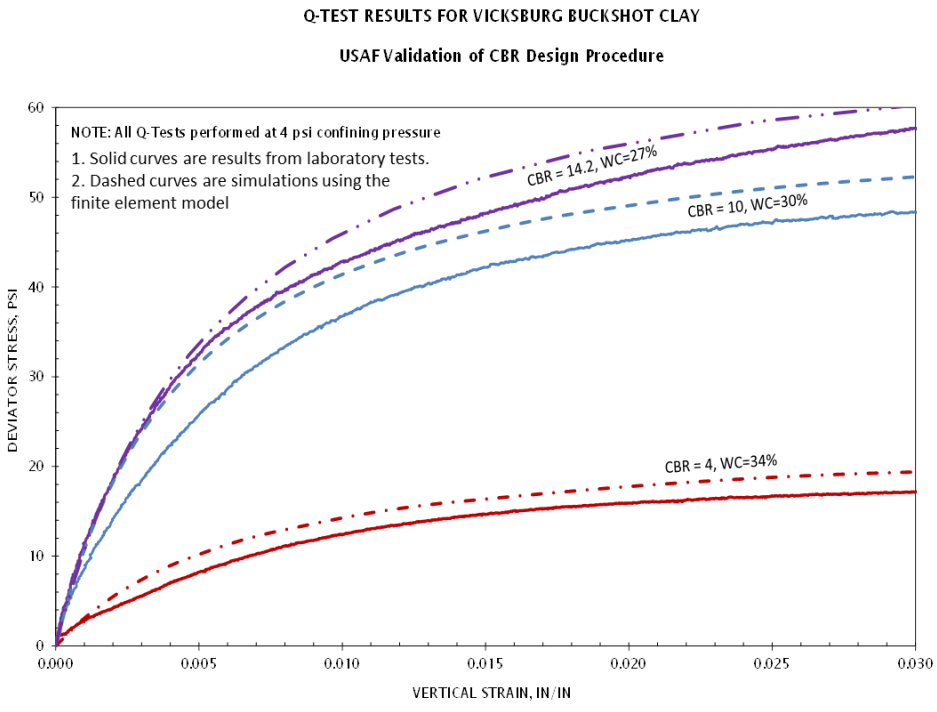

Figure 6.1 Finite element model simulation of triaxial tests conducted on CH clay used as subgrade material (1 psi=6.9 kPa)

It can be observed from Figure 6.1 that axial strain values below 0.005, the prediction are relatively close to the measured values. At larger values of axial strain, all simulated curves tend to predict slightly higher deviator stresses. This implies that the hyperbolic soil model using the results from Table 6.1 will simulate a slightly stiffer material as compared to the laboratory test results. However, for the purpose of this research, this difference was considered to be acceptable and the hyperbolic parameters determined and shown in Table 6.1 were deemed adequate to be used for stress predictions within the subgrade layer.

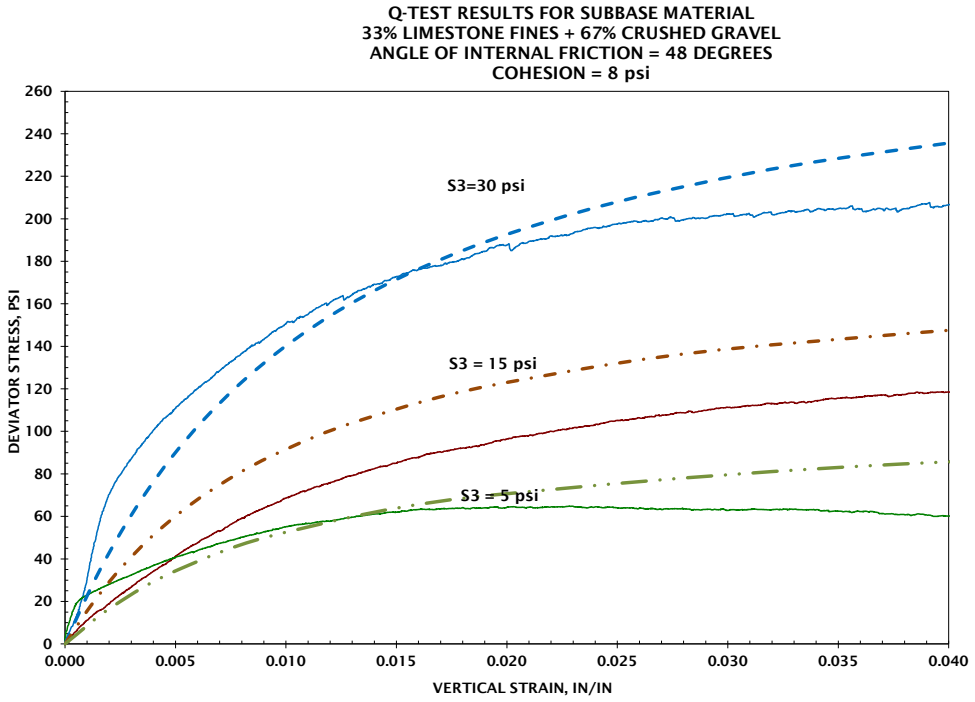

Figure 6.2 Finite element model simulation of triaxial tests conducted on crushed gravel and limestone mix used as subbase material (1 psi=6.9 kPa)

Figure 6.2 shows the simulated triaxial tests conducted on the crushed gravel and limestone mix as compared to the actual laboratory tests results. As was the case for the subgrade CH material, the hyperbolic soil model tends to predicted stiffer behavior. However, the predicted behavior depends on the confining pressure, approximating the curves for the 30-psi (207-kPa) and 5-psi (34.5 kPa) confining pressure curves a lot closer than that for the 15-psi (103.5 kPa) confining pressure. For the purpose of this research, the predicted behavior is also reasonable and considered acceptable for the stress predictions within the subbase material.

Figure 6.3 shows simulated triaxial test conducted on the crushed limestone base material. As was the case for the subbase, the base material behavior tends to be stiffer than measured in the laboratory and depend on confining pressure. Again, these differences are considered acceptable for stress predictions.

Additional checks of the finite element model were performed by simulating actual field CBR tests conducted on the surfaces of the subbase and base. Figure 6.4 shows a typical field CBR test setup on the surface on the subbase layer along with the idealized finite element model.

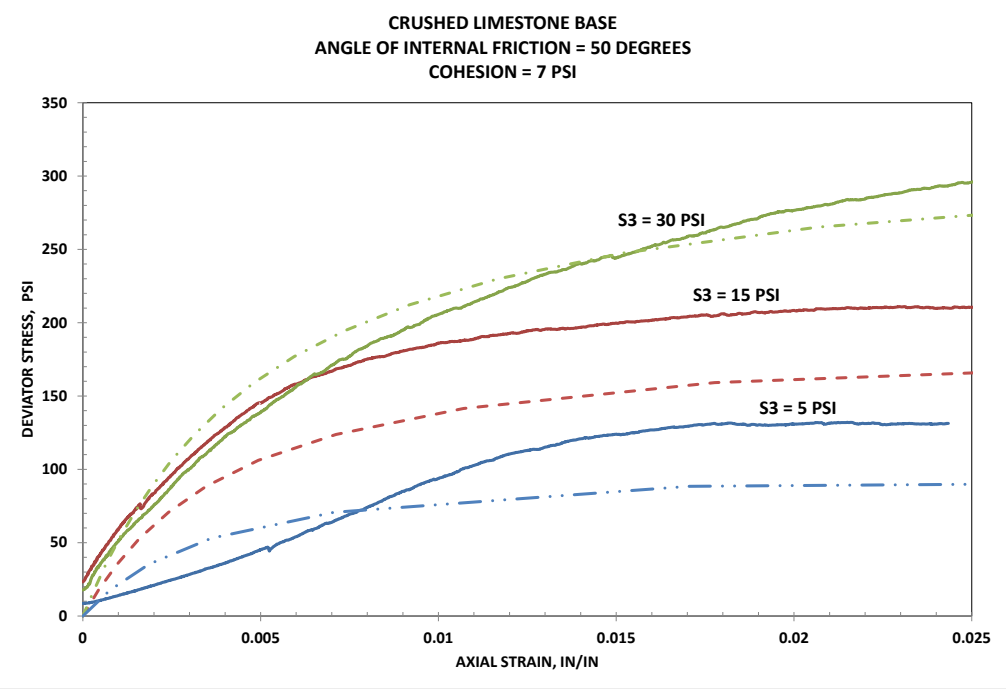

Figure 6.3 Finite element model simulation of crushed limestone used as base course material (1 psi=6.9 kPa)

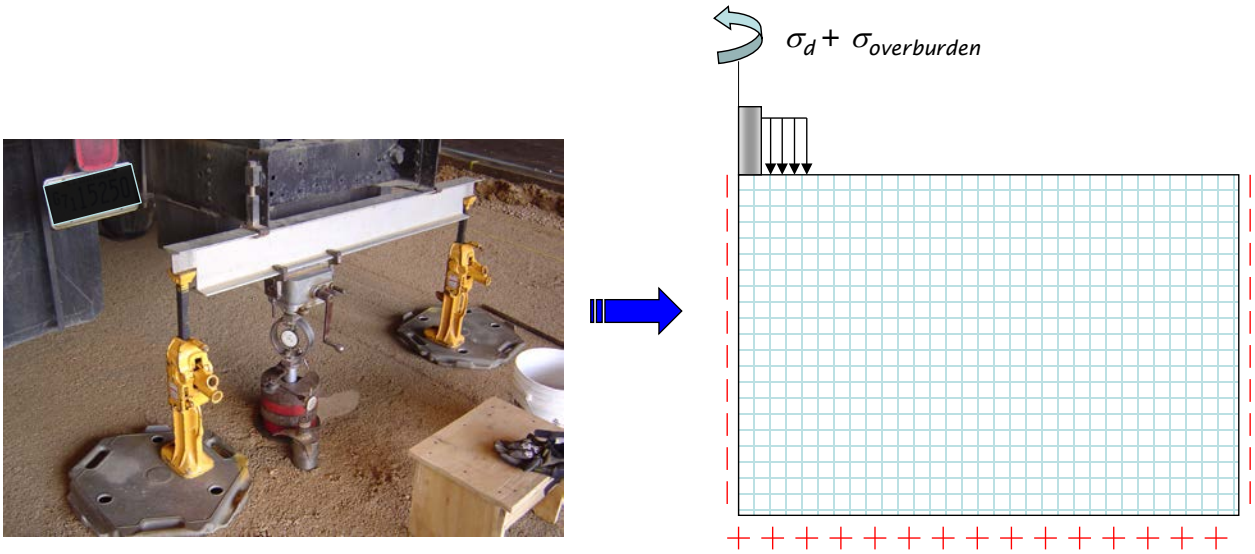

(a) Field CBR Setup **(b) Finite Element Method Idealization**

Figure 6.4 Validation of finite element model using field CBR test results

Although the field CBR test is a displacement-based test, where the loading plunger is pushed in the material at a constant rate and the resisting load measured, it was deemed more convenient to simulate the field CBR test by gradually incrementing the load and calculating the resulting deflection. The results of these simulations are presented in Figure 6.5 and Figure 6.6 for the subbase and base layers, respectively. The field CBR tests were modeled with and without surcharges applied by steel rings. As expected, better predictions of the load-deflections curves are obtained when the surcharges are simulated because it better represents the confining effects that happened during the tests. Simulations for all test items are included in Appendix A.

The results of these simulations with the finite element model utilizing the hyperbolic soil model were used in this research to make stress predictions under the actual aircraft loading applied though single and dual gear assemblies. These predictions were compared to measured stresses within the subbase and subgrade layers for each of the twelve test items tested. The finite element model predictions were also compared to those stresses predicted by the Fröhlich stresses model and the layered elastic theory.

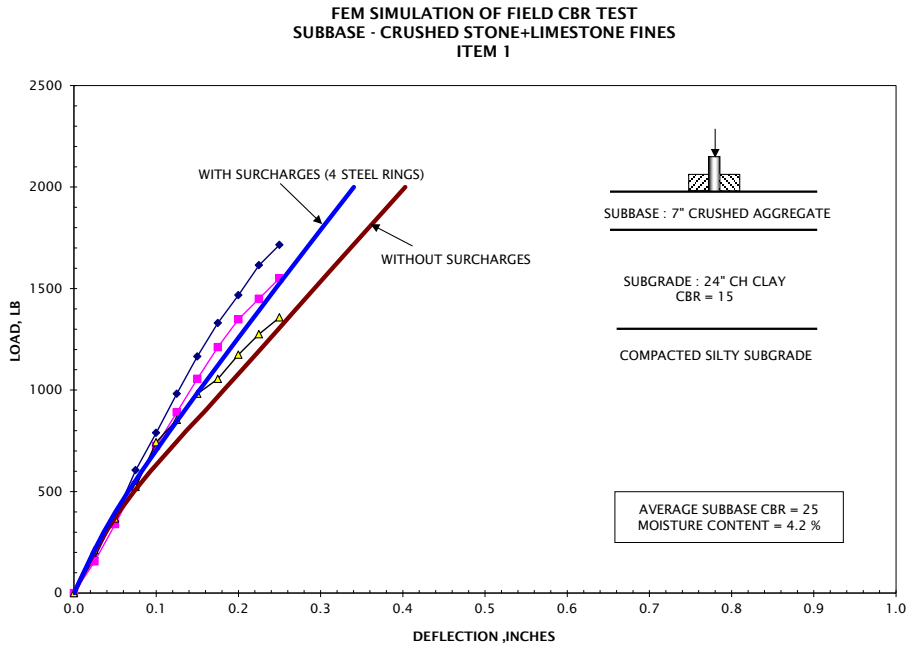

Figure 6.5 Finite element model simulations of field CBR tests performed on surface of subbase layer (1 in.=25.4 mm, 1 lb=4.45 N)

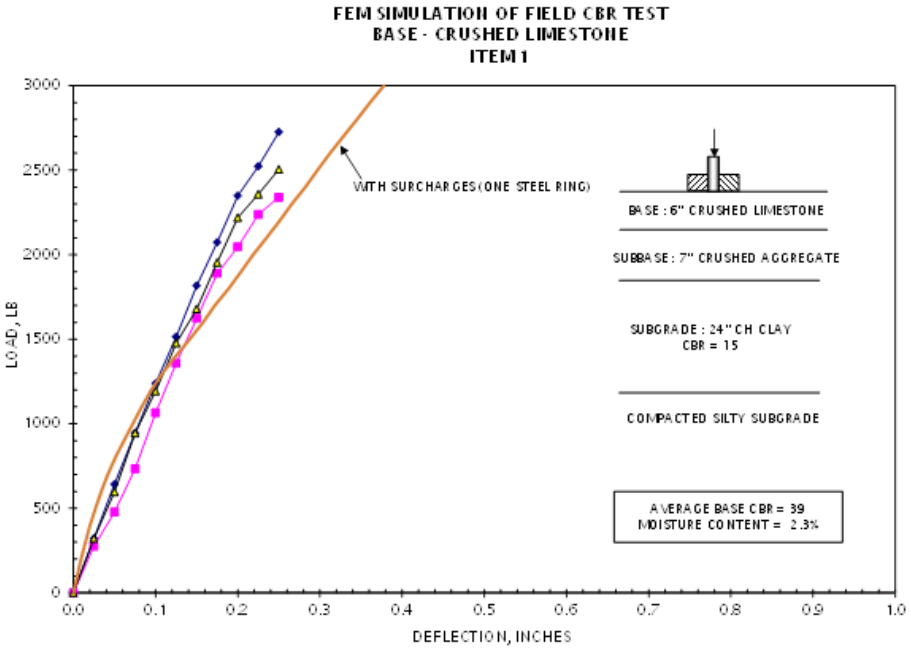

Figure 6.6 Finite element model simulations of field CBR tests performed on surface of base layer (1 in.=25.4 mm, 1 lb=4.45 N)

6.3 Measured Stresses vs Axisymmetric Finite Element Model Lanes 1 and 3

Figure 6.7 presents a comparison of the predicted vertical stresses using the finite element model and the measured vertical stresses for Lane 1 (C-17 Single Tire) and Lane 3 (F-15 Single Tire). These two lanes were selected because they were subjected to single loads, which is what the axi-symmetric finite element model is designed to do. The data points in Figure 6.7(a) and Figure 6.7(b) are for both the subbase and subgrade layers. The measured stresses with lower magnitudes are for the subgrade layer and those with higher values correspond to the subbase layer.

The data in Figure 6.7(a) indicates that the prediction of vertical stresses has less scatter for the subgrade layers than does the subbase layer. The predicted stresses on the lower end (subgrade stresses) are close to the measured stresses except for two points. Two points corresponding to predicted vertical stress values of 43 psi (297 kPa) and 46 psi (317 kPa), are for Items 1 of Lanes 1 and 3. It is believed the reliability of the measured vertical stresses by the earth pressure cells is in question. The corresponding CBR for Item 1 was 14.2, which in terms of a CH material, it is a relatively stiff layer and the compaction needed around the installed earth pressure cell might have an impact on the magnitude of the measured stress. The data on the upper right end of Figure 6.7(a) correspond to the subbase material. There exists more scatter in the data, but the points falls proportionally around the line of equality. The vertical stresses at the subbase layer are more influenced by the tire pressure applied at the surface.

In Figure 6.7(b), the predicted vertical stress values are plotted as ratios of the applied surface tire pressure. This approach normalizes the data and seems to collapse the data points closer to the line of equality. In general, the results of these predictions match well with the measured vertical stresses.

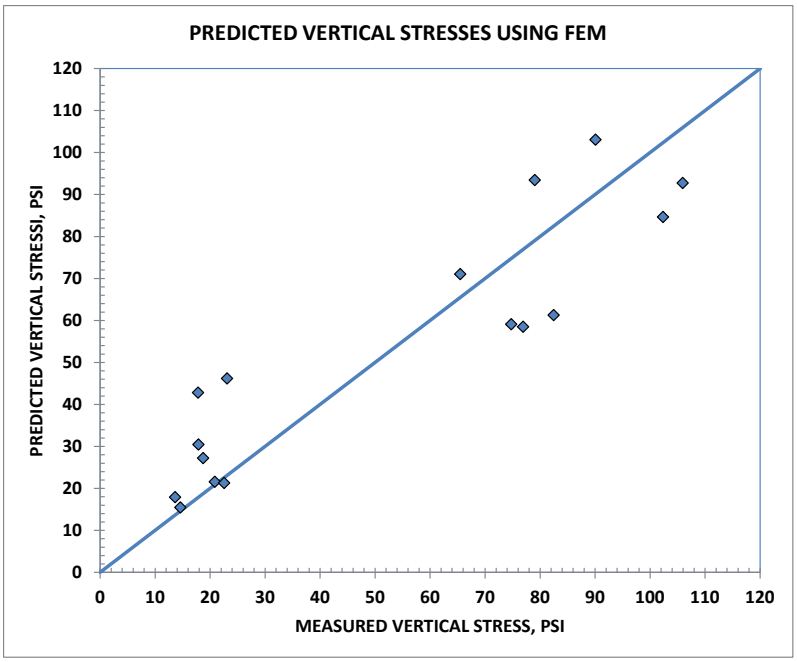

(a)

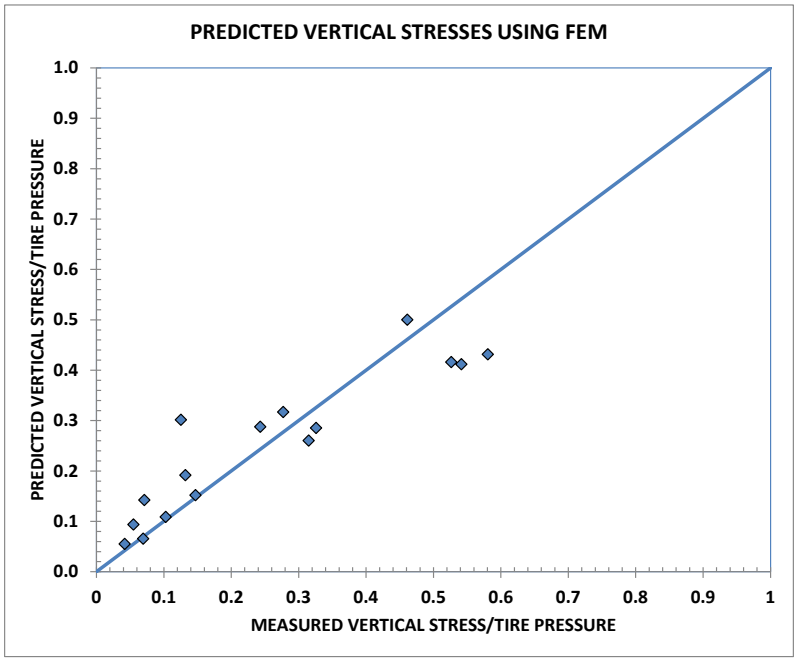

(b)

Figure 6.7 Comparison of measured versus predicted verticals stresses using FEM (1 psi=6.9 kPa)

6.4 Backcalculation of the n-factor from Measured Stresses

One of the objectives of this research was to investigate the distribution of stresses within a pavement structure subjected to aircraft loading. The proposed Fröhlich stress model uses a stress concentration factor (*n*-factor) that determines the decay and spread of the vertical stress with depth. For this reason, the measured vertical stresses in Lanes 1 and 3 (single-wheel traffic) were used to backcalculate a field *n*-factor using Fröhlich's equation for vertical stress directly under a circular loaded area. Table F.1 in Appendix F contains a complete analysis of the *n*-factors backcalculated from measured vertical stresses for Lanes 1 and 3 using Fröhlich stress model. Table 6.2 contains a summary of this backcalculation analysis. Stress concentration factors at the subbase level varied from 2.41 to 3.72 and at the subgrade level from 1.13 to 3.50. The average and standard deviation for n-factors at the subbase level was 3.12 and 0.52, respectively. The average and standard deviation for *n*-factors at the subgrade level was 2.47 and 0.82 respectively. The average backcalculated *n*-factor was 2.79 with a standard deviation of 0.79.

Table 6.2 Backcalculated Fröhlich stress concentration factor (*n*-factor)

Lane	Item	Subbase CBR	Subbase n-factor	Subgrade CBR	Subgrade n-factor
1	1	24	2.41	14.2	1.13
	2	24	3.72	9.8	2.37
	3	24	3.15	3.9	3.01
	4	24	3.28	3.9	3.23
3	1	24	2.56	14.2	1.59
	2	24	3.51	9.8	2.17
	3	24	3.67	3.9	3.50
	4	24	2.63	3.9	2.73
Average			3.12		2.47
Standard Deviation			0.52		0.82
Overall Average			2.79		
Overall Standard Deviation			0.79		

This indicates that the pavement layers above the subbase layer (asphalt and base courses) tend to have a higher *n*-factor, which translates into more stress concentration. The

combination of the asphalt layer, base and subbase layers on top of the subgrade tend to have a lower *n*-factor, which translates into a less stress concentration (or more stress dispersion).

The data in Table 6.2 was used to assess the proposed correlation between the stress concentration factor and the CBR of the layer underneath. Figure 6.8 presents the data from Table 6.2 in graphic form and compares it against the proposed correlation. It can be seen that in general, there is no a good correlation between the *n*-factor and an underlying layer CBR. This implies that the *n*-factor might not only be a function of the subgrade CBR, but it might also be a function of the layer thicknesses and material type above the subgrade. However, the proposed correlation falls below most the data points, which resulted from the earlier assumption that the stress distribution was dictated by an *n*-factor equal to 2. Two data points standout and correspond to Item 1 of Lanes 1and 3. As discussed, earlier in this chapter, the measured vertical stresses for this Item 1 of Lanes 1 and 3 were questionable. Also included in Figure 6.8 are the vertical stress predicted by the finite element method plotted against the CBR values. The predicted stresses track very well the measured values, except for the two data points just discussed.

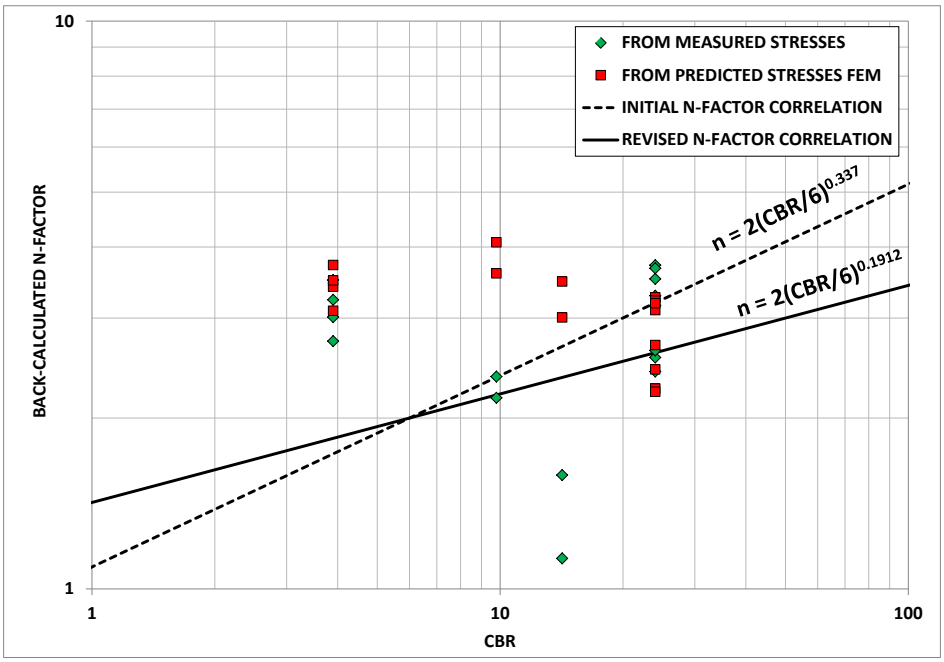

Figure 6.8 Assessment of Correlation between n-factor and CBR using Fröhlich Stress Model and Finite Element Method

The revised n-factor correlation was further checked by comparing the measured stresses in Lane 2 (due to the C-17 Dual gear) to the stresses predicted by the Fröhlich stress model. Figure 6.9 shows the results of this analysis where the vertical stress were computed at the center of the dual gear. The revised *n*-factor correlation seems to predict vertical stresses relatively well, with the exception of the two points corresponding to the subgrade of Item 1. Again, these two points are considered questionable and are considered outliers.

Even though the correlation between the n-factor and CBR is not proven by the data collected, it is believed by this author that there is not sufficient data to conclusively reject or accept the proposed correlation. Hence, this correlation needs further research and testing.

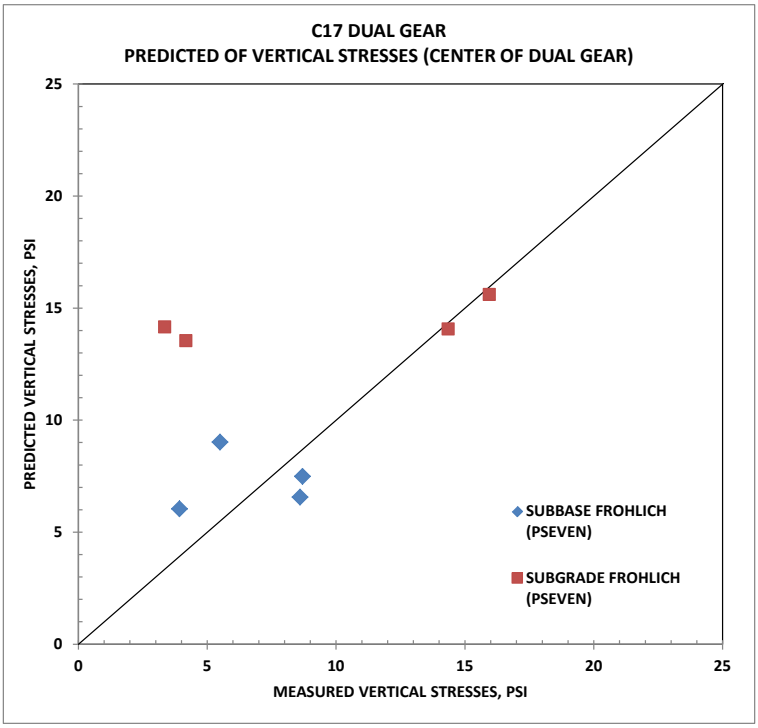

Figure 6.9 Comparison of Measured versus Predicted Verticals Stresses C-17 Dual Gear (1 psi=6.9 kPa)

6.5 Analysis of Layer Moduli from Falling Weight Deflectometer Data

A complete set of falling weight deflectometer (FWD) data was collected on each of the twelve items trafficked with the purpose of tracking any stiffness changes before, during and after traffic application. In addition, the Young's modulus of all pavement layers were

backcalculated to assess any changes in the moduli and used these data to make stress predictions for comparing against values predicted by Fröhlich's stress model and the layered elastic theory. The subset of the FWD database used for analyses within this research is included in Tables E.1, E.2 and E.3 of Appendix E.

6.5.1 Analysis of Impulse Modulus Stiffness

The load magnitude and deflection directly under the application of the FWD plate was used to compute an impulse stiffness modulus (ISM). The ISM is defined as the FWD load divided by the loading plate area and divided by the sensor deflection under the load. The ISM acts an indicator of the relative stiffness of the pavement structure. The result of these calculations are summarized in Figures 6.10, 6.11 and 6.12, where the average ISM change as a function of applied traffic has been normalized to the initial recorded ISM values. Figure 6.10 shows that for Lane 1, which was trafficked with the C-17 single-wheel, the ISM was reduced by approximately 25 percent on the average and remained relatively constant throughout the all traffic levels. Figure 6.11shows the ISM calculation results for Lane 2, which was trafficked by the C-17 dual-wheel gear. In this case, there was considerable change from the initial ISM values, dropping below one half of the initial ISM in Item 1 and Item 3. This change is probably due to the effects of: (1) doubling the magnitude of the total load (90,000-lb (400-kN) dual-wheel for Lane 2 and 45,000-lb (200-kN) single-wheel for Lane 1) acting on what are considered thick pavement structures for the subgrade CBR and (2) the effects of superposition of stresses under the C-17 dual-wheel gear. The ISM for Item 2 and Item 4 remained at about 8 percent of the initial ISM values. Figure 6.12 shows the ISM change for Lane 3, which was trafficked with the F-15 single-wheel gear. On the average the ISM was reduced to about 75 percent of the initial ISM values, which was consistent with Lane 1 (C-17 single-wheel). This analysis demonstrated that in general the ISM was reduced to about 75 percent of the initial ISM and remained relatively constant after 100 passes.

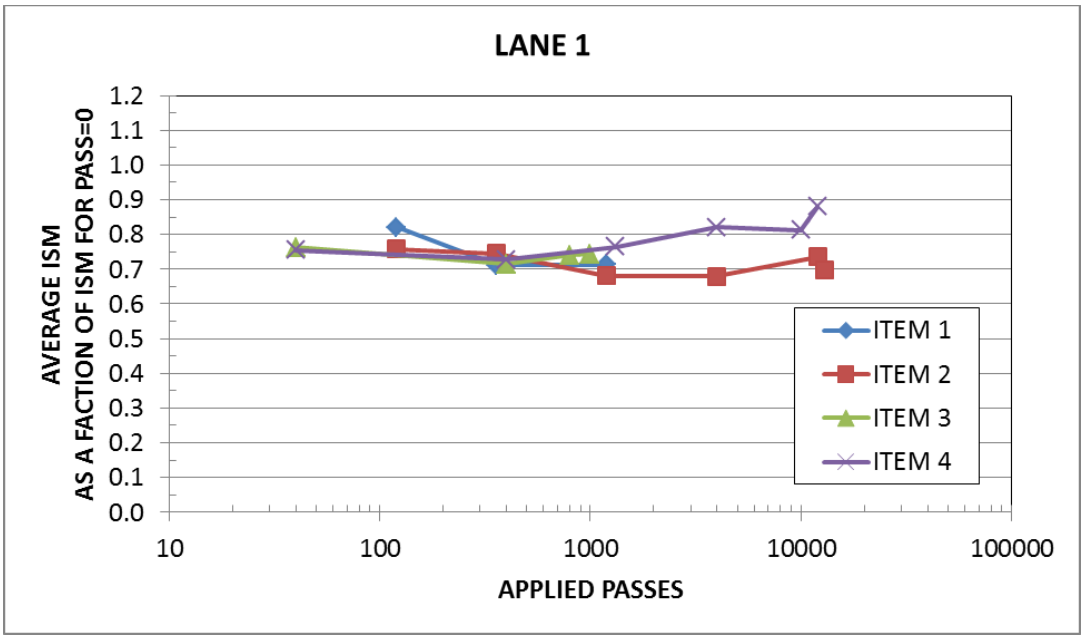

Figure 6.10 Average ISM as a fraction of ISM for pass=0 for Lane 1

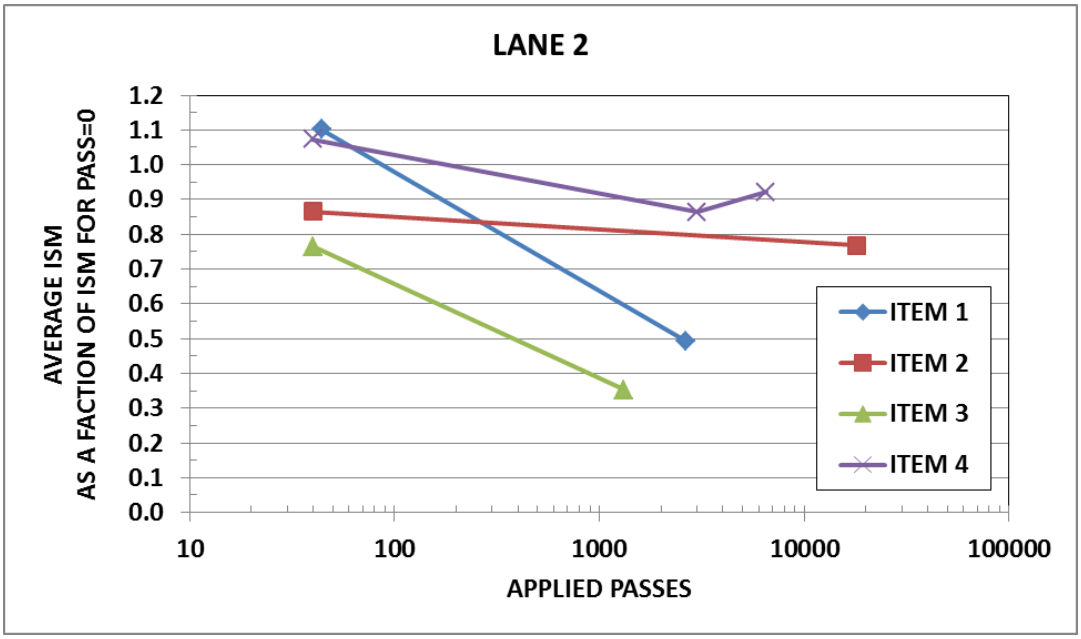

Figure 6.11 Average ISM as a fraction of ISM for pass=0 for Lane 2

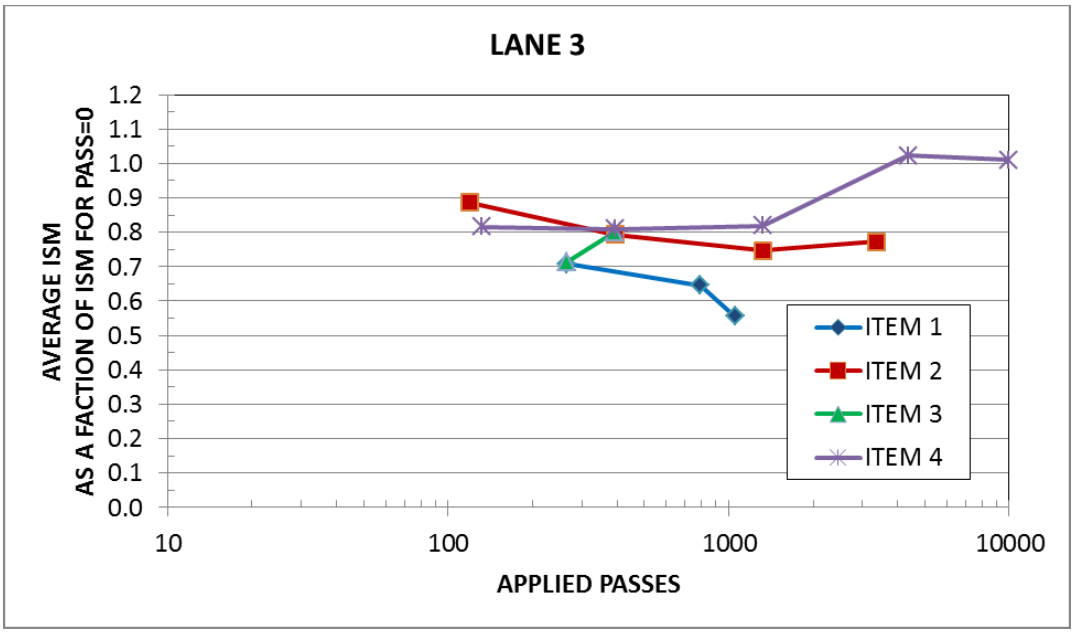

Figure 6.12 Average ISM as a fraction of ISM for pass=0 for Lane 3

6.5.2 Backcalculation of Pavement Layer Moduli

This research made use of procedures and algorithms based on the linear layered elastic theory that are included in the Pavement-Transportation Computer Assisted Structural Engineering (PCASE) package developed by the U.S Army Engineer Research and Development Center in Vicksburg, Mississippi. Tables 6.2 and 6.3 summarized the results of the backcalculation process. For these analyses, the author modified the backcalculation procedure included in the current PCASE software version 2.09 to control the iterative procedure with a root means square error (RMSE) parameter applied to the surface deflection basin and the calculated Young's modulus. This modification was incorporated into a software package called PSEVEN. Two screenshots from this computer program are shown in Figure 6.13 and Figure 6.14. The backcalculated layer moduli included in Tables 6.2 was performed by letting the software backcalculate the moduli for all layers within the pavement structure. Table 6.3 includes the results of backcalculation where the modulus values for the asphalt concrete layer were assigned based on temperature and not allowed to change during the iterative process. This procedure is commonly used in practice during the evaluation of relatively thin asphalt concrete layers.

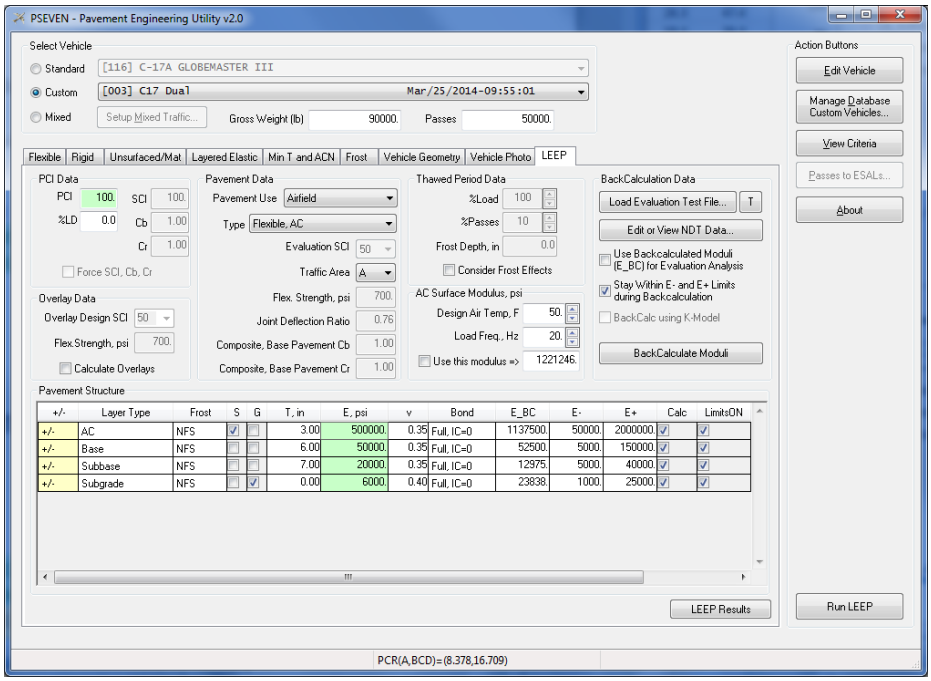

Figure 6.13 Main backcalculation screen of the PSEVEN utility

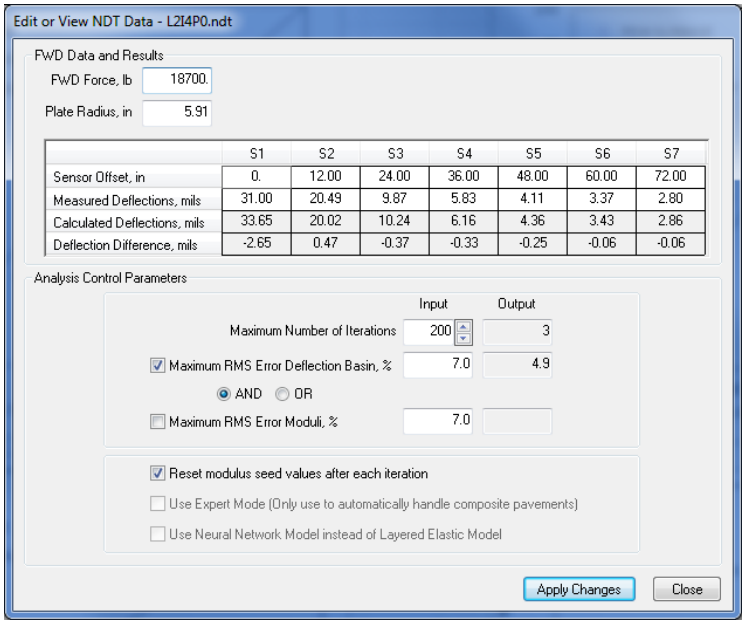

Figure 6.14 Control parameters for backcalculation included with the PSEVEN utility

Table 6.3 Backcalculated Young's modulus from falling weight deflectometer data

			Backcalculated Modulus, psi										
			Lane 1			Lane 2			Lane 3				
Item	Material	Thickness, inches	Initial	Final	% Change	Initial	Final	% Change	Initial	Final	% Change	v[1]	IC[1]
1	AC	3	56445	63333	12.2	1137500	56185	-95.1	771456	53810	-93.0	0.35	0
	Base	6	149992	149439	-0.4	52500	145323	176.8	140698	149614	6.3	0.35	0
	Subbase	7	10522	31659	200.9	12975	5271	-59.4	34319	24407	-28.9	0.35	0
	Subgrade		24906	18766	-24.7	23838	23293	-2.3	20770	18446	-11.2	0.40	0
2	AC	3	518232	803010	55.0	795313	1081250	36.0	1250000	1674488	34.0	0.35	0
	Base	6	45450	16251	-64.2	77980	10625	-86.4	27500	6901	-74.9	0.35	0
	Subbase	14	20209	13747	-32.0	18317	39154	113.8	30000	33586	12.0	0.35	0
	Subgrade		24833	19043	-23.3	24685	22770	-7.8	20238	19024	-6.0	0.40	0
3	AC	3	59093	54688	-7.5	698063	1764612	152.8	109297	1773465	1522.6	0.35	0
	Base	6	77500	54365	-29.9	104112	49367	-52.6	149929	149965	0.0	0.35	0
	Subbase	16	5025	5373	6.9	5780	13257	129.4	6247	5009	-19.8	0.35	0
	Subgrade		12001	13438	12.0	15081	19980	32.5	12402	13024	5.0	0.40	0
4	AC	3	1625000	1936457	19.2	551562	1282813	132.6	1625000	1625000	0.0	0.35	0
	Base	6	65989	43302	-34.4	91532	6230	-93.2	41681	31546	-24.3	0.35	0
	Subbase	23	8584	9671	12.7	14913	11171	-25.1	8996	10052	11.7	0.35	0
	Subgrade		15666	14513	-7.4	19639	12566	-36.0	15273	14711	-3.7	0.40	0

1 v = Poisson's ratio, IC = interface condition between layers. Fully Bonded Condition = 0, Un-bonded Condition=100000
Note: 1 in.=25.4 mm, 1 psi= 6.9 kPa

The backcalculation procedure is a process that in many cases is user and equipment dependent. The experience of the analyst becomes a primary factor in the backcalculation process and the resulting moduli. A single measured basin can yield multiple answers in terms of layer moduli depending on the selection initial seed values, moduli tolerance, moduli limit constrains and number of layers chosen to backcalculate. It is not the intention of this research to

quantify the accuracy or quality of the backcalculation procedure, but rather use an existing procedure to produced moduli which could be later used to predict stresses within the pavement structure. In general, typical seed values, limiting values of moduli and RMSE error tolerance were used. An answer was considered acceptable as long as the combined RMSE of the surface basin was less or equal to 7%. The results in Tables 6.2 and 6.3 indicate that generally the backcalculated procedure captured a decreased of layer moduli, with the greater changes occurring in the base and subbase layers. This same behavior was found to occur even when the asphalt concrete was assigned based on pavement temperature as shown in Table 6.4. However, these analyses did not show a consistent pattern and it is believed to require a more rigorous analytical process. It important to note that, in some instances, the backcalculated moduli of the subgrade were less than the field achieved subgrade modulus. This might not represent an actual field condition and it is believed to be a limitation of the layered elastic theory dealing with improper modeling of the actual pavement behavior. Nevertheless, the backcalculated layer moduli were considered for further analyses and stress predictions were generated due to the loads applied during traffic.

Table 6.4 Backcalculated Young's modulus from falling weight deflectometer data assigning asphalt modulus from pavement temperature

			Backcalculated Modulus, psi										
			Lane 1			Lane 2			Lane 3				
Item	Material	Thickness inches	Initial	Final	% Change	Initial	Final	% Change	Initial	Final	% Change	v[1]	IC[1]
1	AC	3	225885	225885	0.0	451300	451300	0.0	225885	225885	0.0	0.35	0
	Base	6	75000	75161	0.2	93465	42099	-55.0	57213	140645	145.8	0.35	0
	Subbase	7	12500	37287	198.3	10225	6159	-39.8	25093	9052	-63.9	0.35	0
	Subgrade		27570	17966	-34.8	24640	20601	-16.4	20489	19095	-6.8	0.40	0
2	AC	3	323528	323528	0.0	811488	811488	0.0	240264	240264	0.0	0.35	0
	Base	6	98813	9348	-90.5	105049	12006	-88.6	66342	15320	-76.9	0.35	0
	Subbase	14	12914	20761	60.8	20163	28608	41.9	30004	19632	-34.6	0.35	0
	Subgrade		25778	19441	-24.6	24746	23240	-6.1	21705	19894	-8.3	0.40	0

Table 6.4 Backcalculated Young's modulus from falling weight deflectometer data assigning asphalt modulus from pavement temperature

			Backcalculated Modulus, psi										
			Lane 1			Lane 2			Lane 3				
Item	**Material**	**Thickness inches**	**Initial**	**Final**	**% Change**	**Initial**	**Final**	**% Change**	**Initial**	**Final**	**% Change**	**v[1]**	**IC[1]**
3	AC	3	287858	287858	0.0	1004594	1004600	0.0	212210	212210	0.0	0.35	0
	Base	6	99629	65788	-34.0	82523	5035	-93.9	41250	25495	-38.2	0.35	0
	Subbase	16	5547	8550	54.1	5496	39999	627.8	5084	5579	9.7	0.35	0
	Subgrade		12060	25349	110.2	14717	12321	-16.3	12430	12304	-1.0	0.40	0
4	AC	3	225885	225885	0.0	1221246	1221250	0.0	287858	287858	0.0	0.35	0
	Base	6	125000	101271	-19.0	58853	5012	-91.5	100000	125000	25.0	0.35	0
	Subbase	23	10600	9980	-5.8	11793	16395	39.0	8816	10638	20.7	0.35	0
	Subgrade		15521	14377	-7.4	14916	12513	-16.1	15094	14943	-1.0	0.40	0

1 v = Poisson's ratio, IC = interface condition between layers. Fully Bonded Condition = 0, Un-bonded Condition=100000
Note: 1 inch=25.4 mm, 1 psi=6.9 kPa

6.5.3 Analysis of Pavement Stresses using Backcalculated Moduli

The backcalculated layer moduli reported in Table 6.3 and Table 6.4 were used to compare vertical stresses predicted by the linear layered elastic theory and those vertical stress values measured during traffic testing. Figure 6.15(a) and Figure 6.15(b) present a comparison of the measured versus the predicted vertical stresses for Lane 1 (C-17 single-wheel) and Lane 3 (F-15 single-wheel). The cluster of data points on the lower left corner of Figure 6.15(a) correspond to the subgrade stresses and the rest of data points correspond to the subbase layer. These predictions show the layered elastic theory is better at making predictions of vertical stresses at the subgrade level than at the subbase level. The subgrade vertical stresses predicted by layered elastic are very close to the line of equality, while those for the subbase are as much as one half of those measured. This pattern was consistent even when the stresses were normalized as shown in Figure 6.15(b). The same stress predictions were performed when the moduli of asphalt concrete layer was assigned based on pavement temperature. The resulting

predictions followed the same pattern as those used when all layers were backcalculated. These comparisons are included in Figure 6.16. Therefore, there was no significant improvement in the predictions of vertical stresses by using assigned asphalt concrete moduli, primarily in the predictions of stresses within the subbase material.

a)

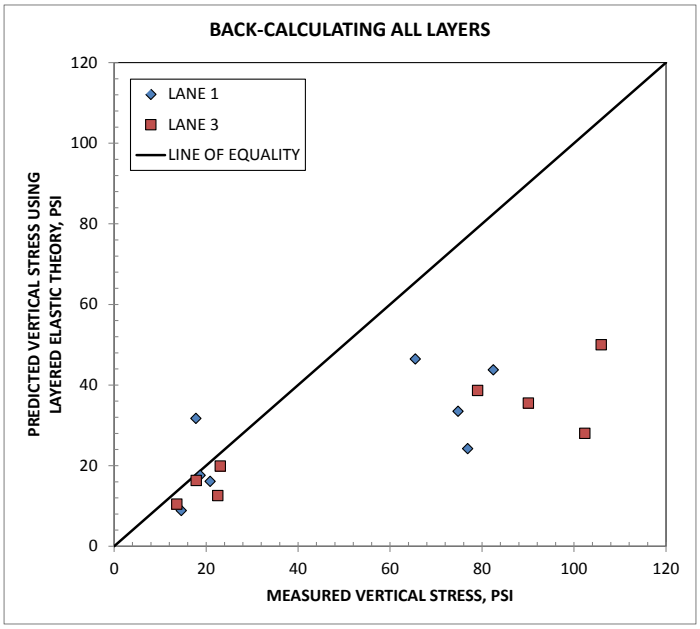

b)

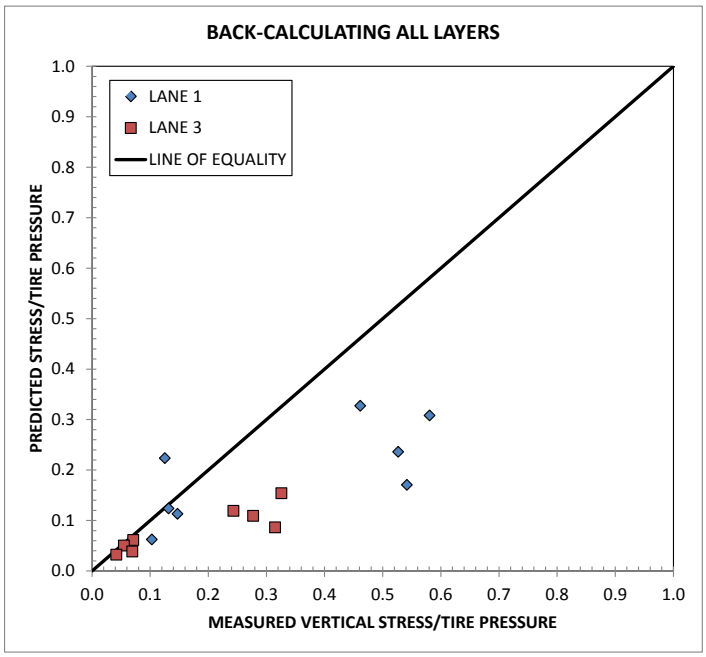

Figure 6.15 Measured versus predicted vertical stresses using layered elastic theory where all layers were backcalculated (1 psi=6.9 kPa)

(a)

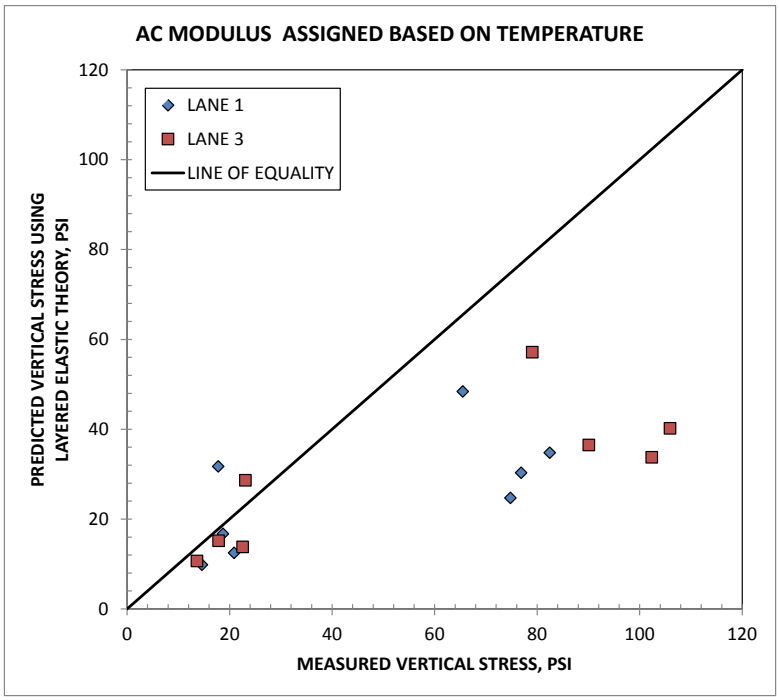

(b)

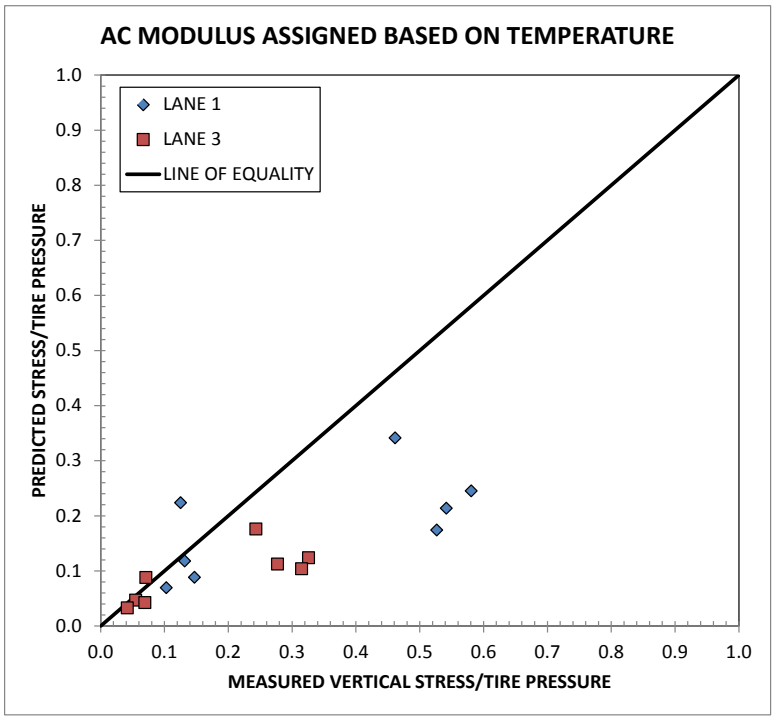

Figure 6.16 Measured versus predicted verticals stresses using backcalculated moduli where asphalt concrete moduli was assigned based on pavement temperature (1 psi=6.9 kPa)

6.5.4 Vertical Stresses Predicted by Layered Elastic Theory and Fröhlich Stress Model

The backcalculated layer moduli were used to compare the predicted vertical stresses by layer elastic theory and by the Fröhlich stress model. These comparisons were made for stress concentration factor (*n*-factor) as a function of CBR, for *n*-factor = 2 and for *n*-factor = 3. Figures 6.17, 6.18, 6.19 and 6.20 show the results for the assumed stress concentration factors. It is evident from these figures that the vertical stresses at the subgrade level predicted by the layered elastic theory matched very well those values predicted by Fröhlich's stress model. However, that was not the case for the stresses at the subbase layer, where the layered elastic predicted stresses that were almost half of those predicted by Fröhlich's stress model. The best predictions for the subgrade level occurred for an *n*-factor=2. For an *n*-factor = 3, the layer elastic under-predicted all vertical stresses as compared to Fröhlich's stress model. From this analysis it can be concluded that the layered elastic model may perform adequately when predicting subgrade stresses. However, it does not give good predictions of vertical stresses for materials that are stress dependent such as the granular base and subbase layers.

(a)

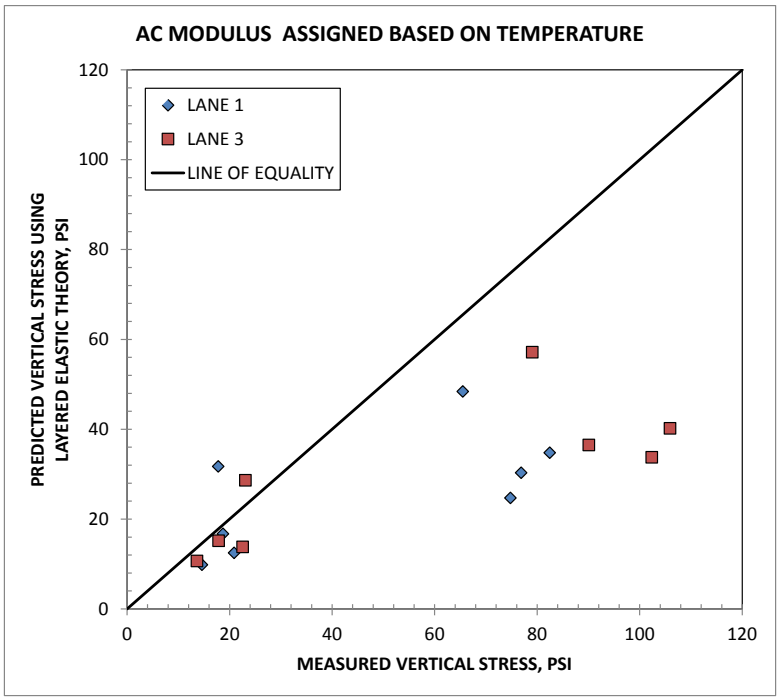

(b)

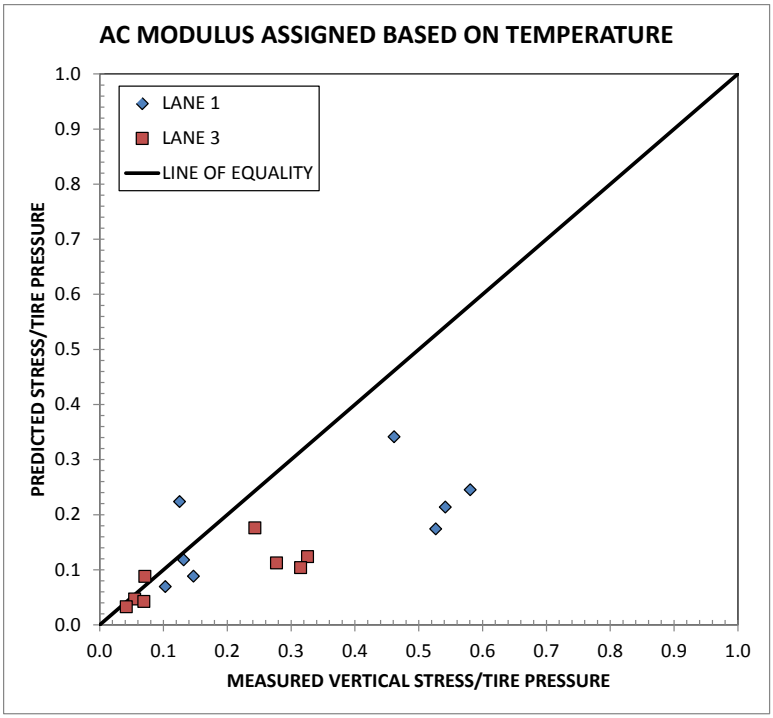

Figure 6.17 Measured versus predicted verticals stresses using backcalculated moduli where asphalt concrete moduli was assigned based on pavement temperature (1 psi=6.9 kPa)

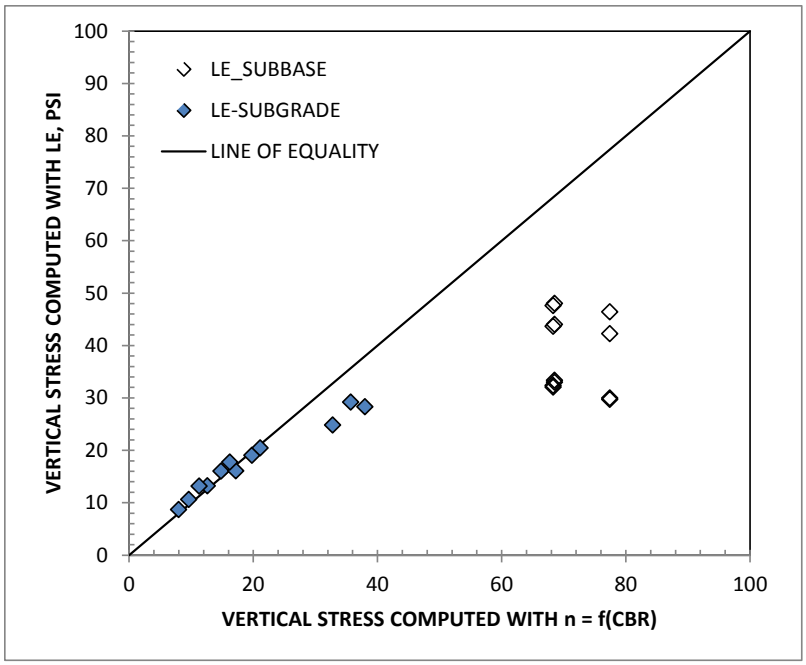

Figure 6.18 Comparison of vertical stresses predicted by Fröhlich, *n* = *f*(CBR) and layered elastic theory (1 psi=6.9 kPa)

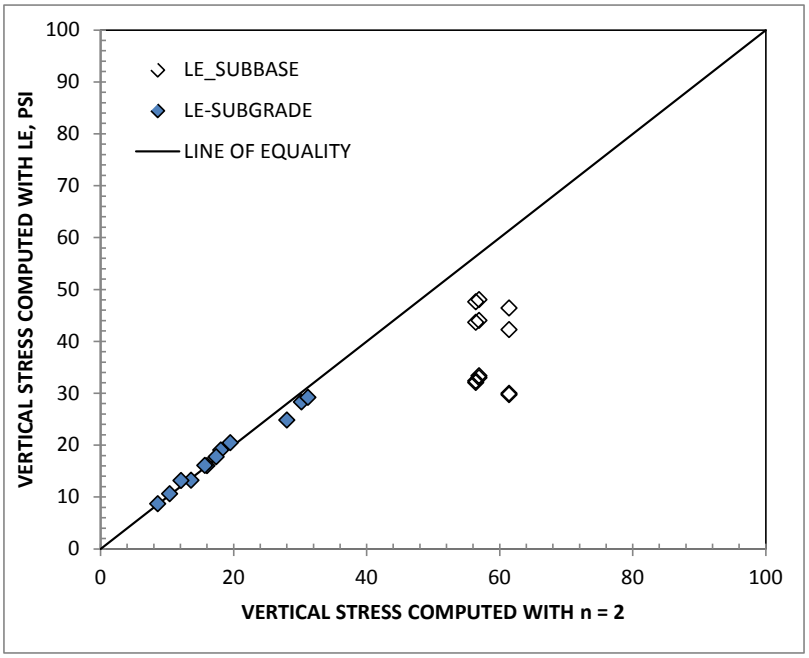

Figure 6.19 Comparison of vertical stresses predicted by Fröhlich (*n* = 2) and layered elastic theory (1 psi=6.9 kPa)

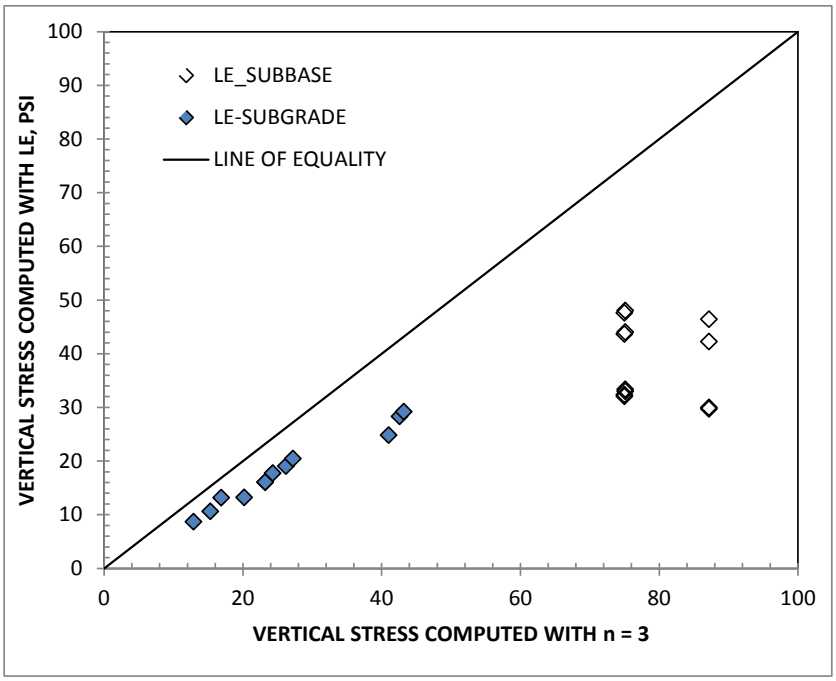

Figure 6.20 Comparison of vertical stresses predicted by Fröhlich (*n* = 3) and layered elastic theory (1 psi=6.9 kPa)

6.5.5 Vertical Stresses Predicted by Finite Element Model and Fröhlich Stress Model

Further analyses were performed to compare the predicted vertical stresses by the finite element model described earlier in this chapter to those stresses predicted by Fröhlich's stress model. Figures 6.21, 6.22 and 6.23 present the results of these predictions. For the comparisons at an *n*-factor as a function of CBR and an *n*-factor = 2, the finite element model tends to slightly over predict the vertical stresses as compared to Fröhlich's model (Figures 6.21 and 6.22). However, both subgrade and subbase vertical stress predictions fall close to or around the line of equality. Better comparisons at the subgrade levels are obtained for an *n* = 3 and a better match is obtained at the subbase level for an n-factor as a function of CBR (Figure 6.21). In general, unlike the case for layered elastic theory, the finite element model compares very favorable to the Fröhlich' stress model at both the subbase and subgrade layers.

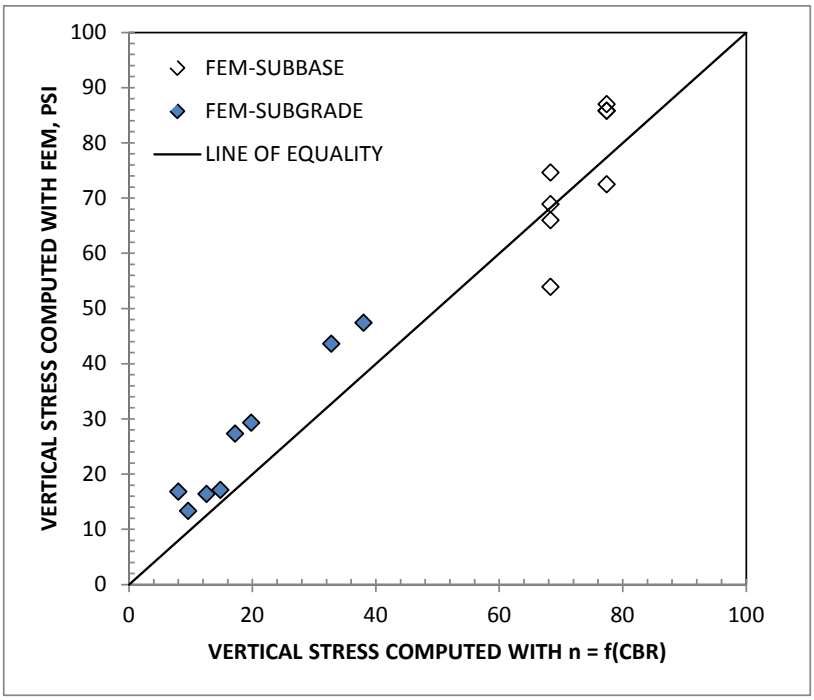

Figure 6.21 Comparison of vertical stresses predicted by Fröhlich, *n* = *f*(CBR) and FEM (1 psi=6.9 kPa)

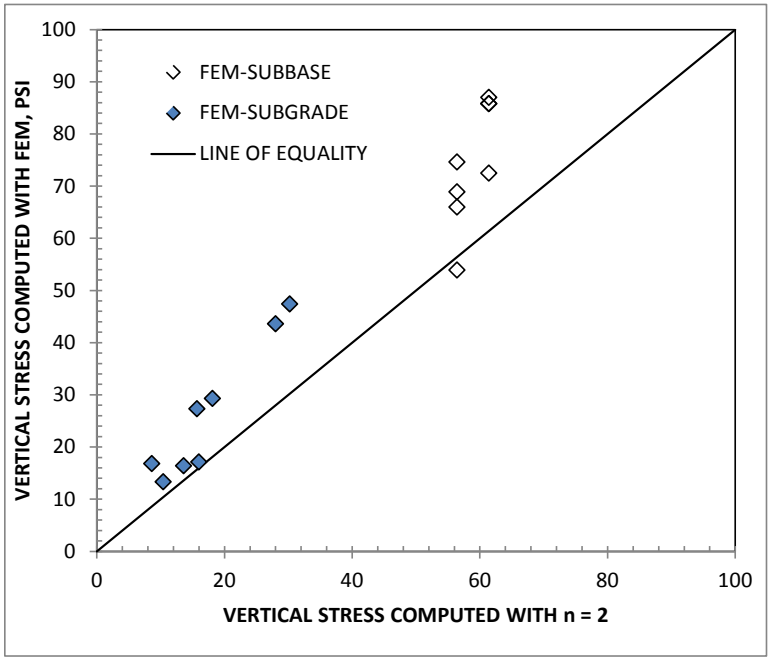

Figure 6.22 Comparison of vertical stresses predicted by Fröhlich(n = 2) and FEM (1psi=6.9 kPa)

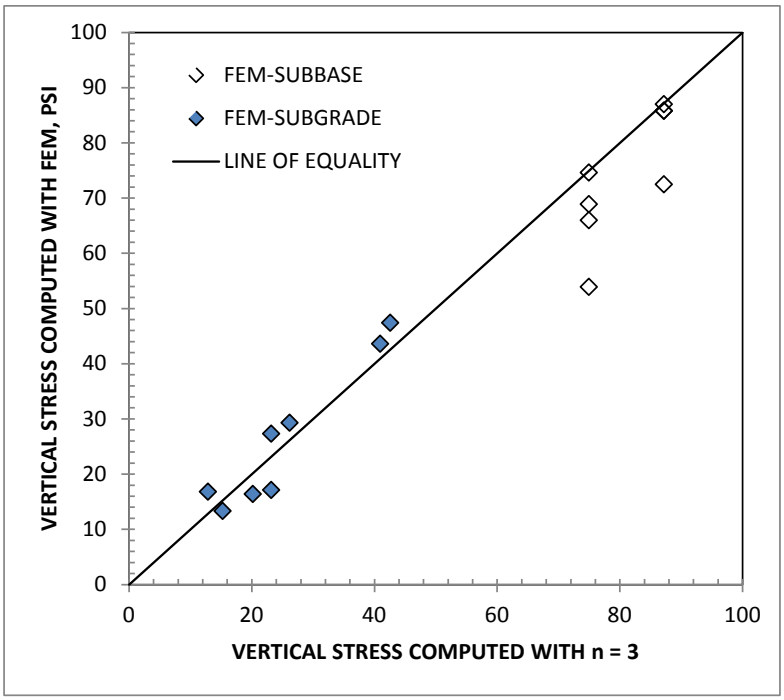

Figure 6.23 Comparison of vertical stresses predicted by Fröhlich(*n* = 3) and FEM (1 psi=6.9 kPa)

6.6 Analysis of Traffic Results

The behavior of the full-scale test items under traffic was monitored through instrumentation responses and visual inspections as the progression of distresses occurred. Rutting depths and surface profile measurements of each lane and item were obtained after a pre-set number of passes of the gear assemblies. Prior to the start of the traffic testing, additional slow rolling tests were conducted on each item where the gear was moved over the installed gauges to assess the pavement response.

6.6.1 Pavement Failure Criteria

Historically, failure of a flexible pavement in a test section was defined by either cracking or rutting of the asphalt surface. Ahlvin (1991) recognized in his publication on the origins of the development of structural pavement design, that the determination of failure had not been historically very specific. On the other hand, it was generally accepted that the effects of internal shearing within a pavement structure were reflected on the surface by patterns of alligator cracking and surface rutting rapidly progressing with the application of traffic loading.

In this study, one of the main objectives was to verify the thickness criteria with regards to rutting. Failure with regards to rutting is generally based on a 1-in. (25.4 mm) rut depth. When considering the thickness criteria to protect the subgrade, this definition of rutting failure may not provide a complete assessment of the section condition; in fact, base and subbase densification instead of subgrade shear may cause surface rutting. For this reason, in order to determine a better indication of when rutting occurred in the subgrade due to shear, the rut depth was plotted as a function of the logarithm of the number of passes of the test load.

Failure was then defined as the point at which the slope of the rut depth curve showed a significant increase. For almost all of the test items, the slope of the curve increased rapidly at rut depths between 1 inch (25.4 mm) and 1.5 inches (38.1 mm). This threshold point was also anticipated by cracking of the asphalt surface. However, generally the rutting failure occurred before the appearance of cracking in the asphalt concrete. The average rut depth was measured for each item at three locations as is shown in a Figures 6.24 and Figure 6.25. Figure 6.24 exemplifies a typical longitudinal profile collected at several traffic pass levels. Cross sections at Stations 13, 25 and 37 within each individual test item were select for rut depth measurements. The procedure to collect the rut depths is depicted in Figure 6.25. A 10-foot (3.05 m) straightedge was placed on the surface of the pavement at each station, and the distance from the bottom of the straight edge to the deepest point of the deflection basin was recorded. The average rut depth of the readings from stations 13, 25 and 37 was recorded as the rut depth value for a specific traffic pass level.

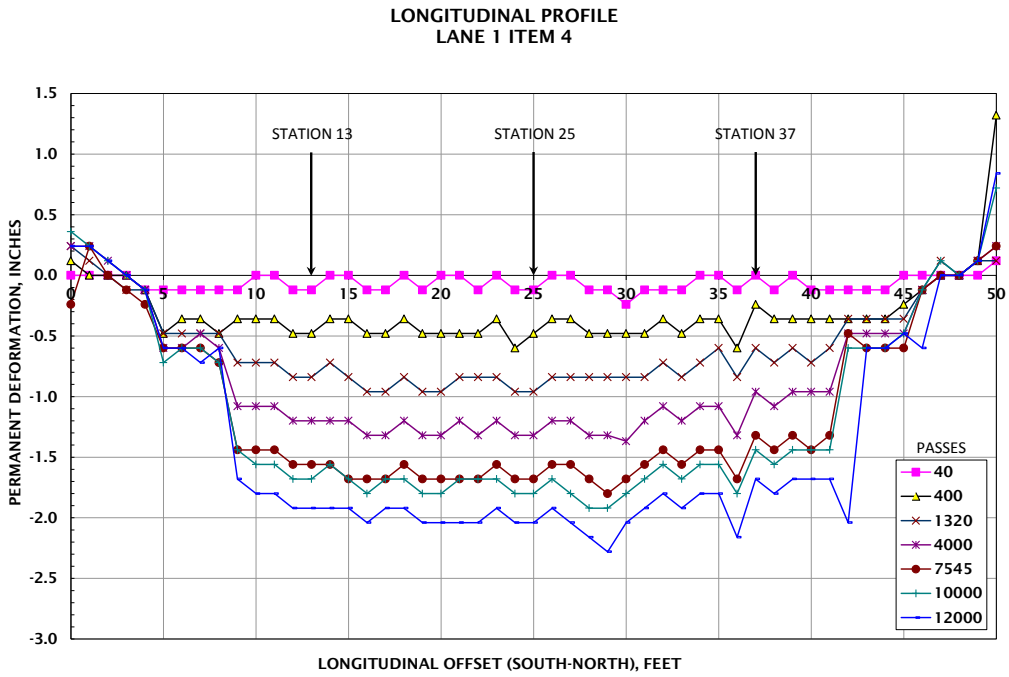

Figure 6.24 Typical rutting longitudinal profiles as a function of passes and rut depth station location (1 inch=25.4 mm, 1 ft=0.3048 m)

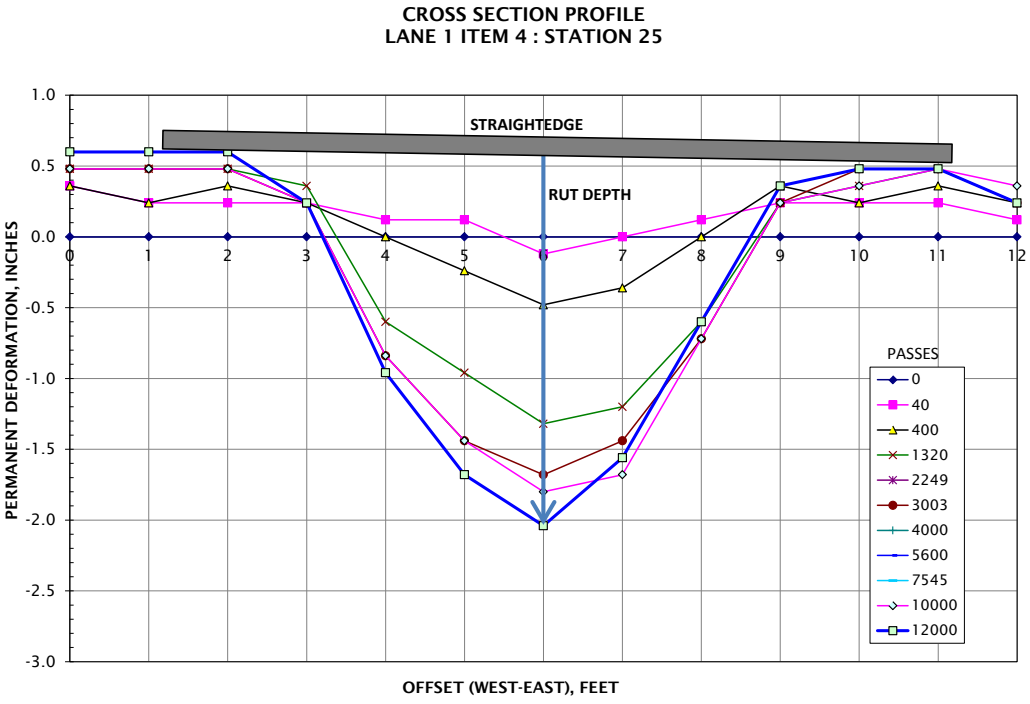

Figure 6.25 Typical rutting profiles as a function of passes for Station 25 (1 in=25.4 mm, 1 ft=0.3048 m)

6.6.2 Analysis of Rutting Performance

Rutting depths measurements were taken at a predetermined number of traffic passes to monitor the deterioration rate of each item tested. Appendix D contains a detailed account of the progression of deterioration with applied passes. Even though failure was usually defined at a rut depth of at least one inch (25 mm), cracking of the asphalt concrete layer and the lack of a waterproofing surface also contributed to what was considered a failed pavement structure. Table 6.5 summarizes the rutting performance of all three lanes and items tested, which resulted in an additional twelve new data points to be added to the historical flexible pavement performance criteria. The failure points from Table 6.5 were plotted by traffic lane in the rutting performance curves included in Figures 6.26 through 6.28 and by item in Figures 6.29 through 6.32. Analyzing the rutting performance by lane of traffic allows for the evaluation of the effects of pavement structure on rutting performance. Likewise, analyzing by item permits the assessment of the effects of loading magnitude and type of gear (single versus dual gear). The shaded band on all these figures indicates the range of rut depths at which failure usually occurs. Each failure data point from Table 6.5 is identified on each figure by a star symbol on top of each curve.

Table 6.5 Summary of the number of passes to failure and rut depth

Lane	Item	Passes at Failure	Pass-to-Coverage Ratio	Coverages to Failure	Average Rut Depth (in.)	Surface Cracking Observations
1	1	840	2.5	336	1.45	Initiated after 1,200 passes near center of traffic lane
	2	5000	2.5	2000	1.15	Inittaited after 8,354 passes on edge of traffic lane and near center after 12,000 passes
	3	400	2.5	160	1.10	Initiated after 1,500 passes near center of traffic lane
	4	2000	2.5	800	1.05	Initiated after 1,320 passes near center of traffic lane

Table 6.5 Summary of the number of passes to failure and rut depth						
Lane	**Item**	**Passes at Failure**	**Pass-to-Coverage Ratio**	**Coverages to Failure**	**Average Rut Depth (in.)**	**Surface Cracking Observations**
2	1	2000	2.5	800	0.90	Initiated after 800 passes near center of traffic lane
	2	16000	2.5	6400	1.10	Initiated after 10,000 passes in wheel path
	3	1100	2.5	440	1.20	Initiated after 120 passes in wheel path. Considerable cracking observed after 1,320 passes in whole test item
	4	3000	2.5	1200	1.00	Initiated after 2740 passes in wheel path
3	1	380	5.5	69	1.05	Initiated after 264 passes in wheel path
	2	1050	5.5	191	1.00	Initiated after 1,320 passes outside of wheel path
	3	105	5.5	19	0.73	Initiated after 264 passes in wheel path
	4	2200	5.5	400	1.20	No surface racking
Note: 1 in.=25.4 mm						

6.6.3 Comparing Rutting Performance by Lane – Effects of Pavement Structure

Figure 6.26 summarizes the rutting performance of Lane 1 where Items 1, 2, 3 and 4 were trafficked with a C-17 single tire. The failure data points for this lane fell within the rut depth range of 1.0 to 1.5 inches (25.4 mm to 38.1 mm). A best fit curve was passed through each of the item's data points to make easier to track and visualize the rutting performance with applied traffic. For the C-17 single tire, Item 2 was the best performer, while Item 3 was the least performer in terms of passes to failure. The rutting performance of Items 1 and Item 3 were very similar in terms of rut depth, but the failure points were called at different pass levels because the progression of traffic in Item 3 occurred at an earlier pass level. In terms of rutting performance,

Items 1 and Item 3 are equivalent pavement structures. The same phenomenon occurs between Items 2 and 4, but to a lesser extent. Item 2 was a thinner pavement section constructed on a CBR=10, while Item 4 was a thick pavement section constructed on a CBR=4.

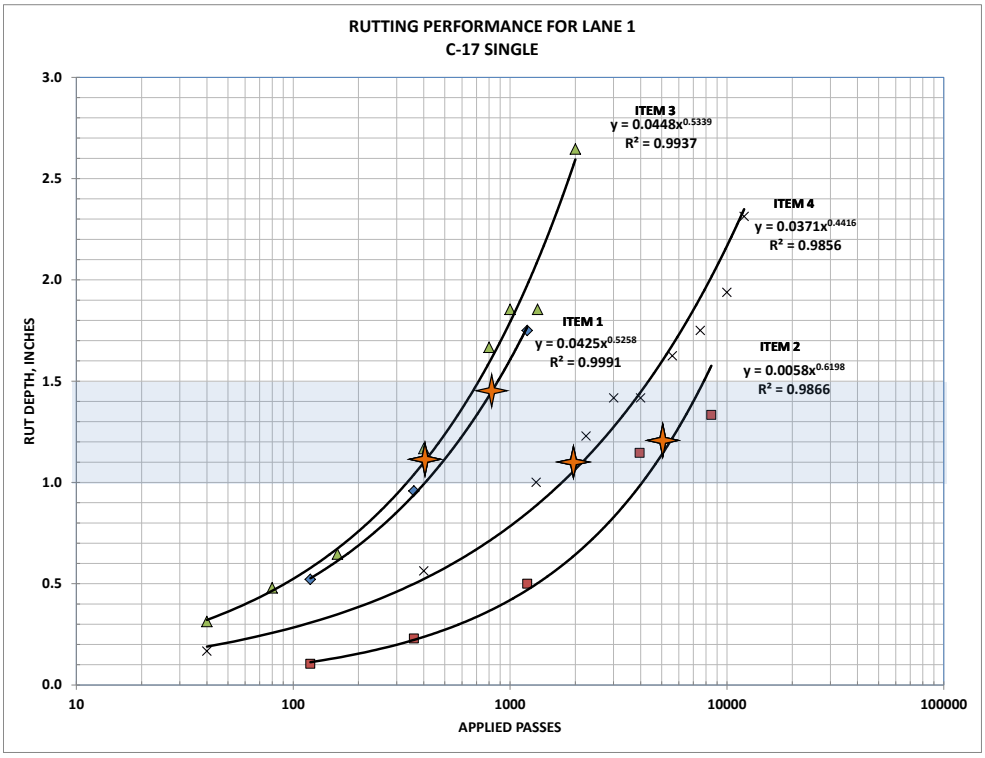

Figure 6.26 Rutting performance of Items 1, 2, 3 and 4 for Lane 1 – C-17 Single (1 inch=25.4 mm)

Figure 6.27 shows the rutting performance of all items on Lane 2 subjected to the C-17 dual-tire gear. As was the case for Lane 1, Item 2 outperformed all other items and Item 3 was the least performer of the group. Even though the load per tire on the C-17 dual on Lane 2 (45,000 lb (200 kN) per tire) was the same as the C-17 single tire on Lane 1, the number of passes to failure of the C-17 dual gear was about three times as large as that of the C-17 single tire. This is believed to be caused by the kneading and healing characteristics of the C-17 dual gear as is moves laterally during traffic. This was a known phenomenon during the development of the original CBR equation and the MWHGL tests conducted in the early 1970's (Cooksey and Ladd, 1971). Thickness adjustments factors were applied to compensate for this performance improvement by the applying of a load reduction factor (known here as the alpha factor).

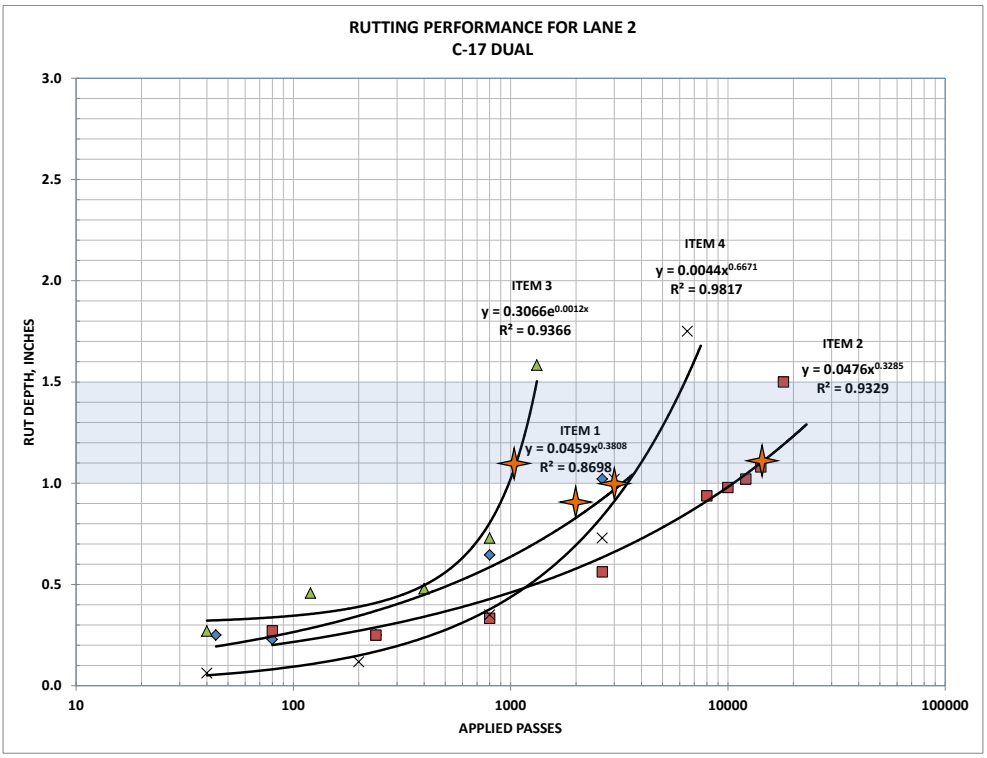

Figure 6.27 Rutting performance of Items 1, 2, 3 and 4 for Lane 2 – C-17 Dual (1 inch=25.4 mm)

Figure 6.28 shows the rutting performance of Lane 3 subjected to the F-15 single gear. For this type of loading, Item 2 and Item 4 had nearly equal rutting performance while Items 3 and Item 1 did not performed very well having failure data points at pass levels below 500 passes. The rate at which rutting occurred also increased as shown by the steepness of the curves. In all cases, failure points were attained for pass levels ranging from a low of 105 passes to a high of 16,000 passes, which was one of the objectives of this research.

Another way to examine the rutting performance is to plot the failure data points by test item as shown in Figures 6.29 through 6.32. For each item in these figures, the pavement cross section is identical. In this manner, the effects of loading and gear type on rutting performance can be visualized.

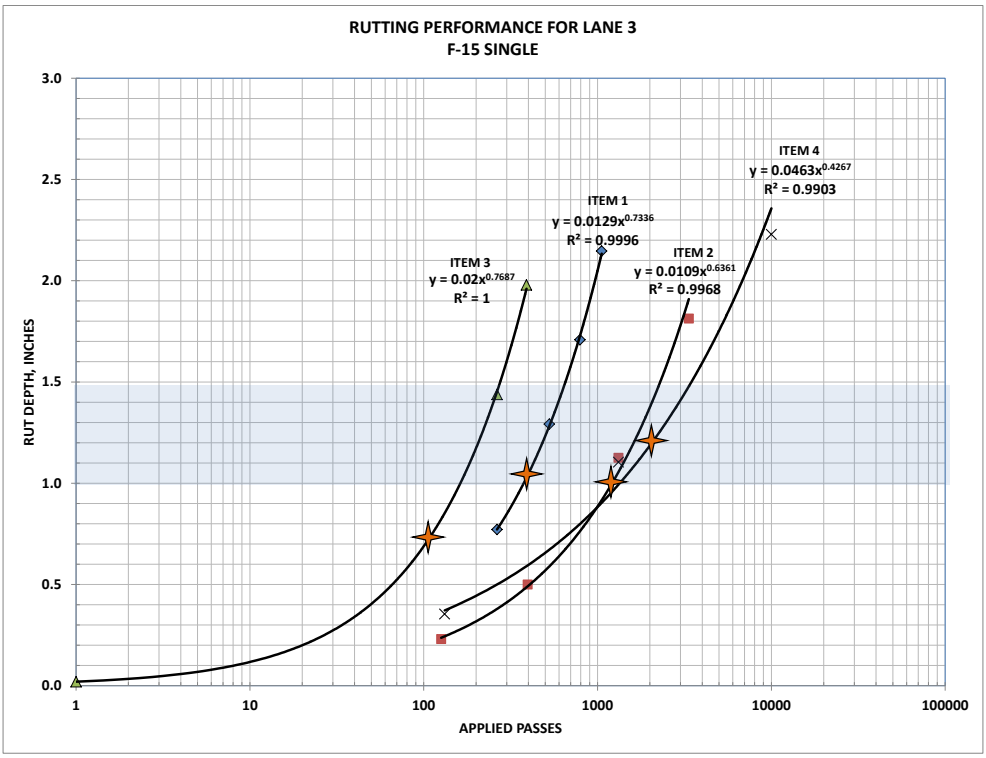

Figure 6.28 Rutting performance of Items 1, 2, 3 and 4 for Lane 3 – F-15 Single (1 inch=25.4 mm)

6.6.4 Comparing Rutting Performance by Item – Effects of Loading and Gear Type

Figure 6.29 shows the results of traffic for Item1, which consisted of 3 inches (76 mm) of asphalt concrete, 6 inches (152 mm) of base and 7 inches (178 mm) of subbase over a subgrade CBR of 14.2. Figure 6.29 clearly illustrates that the C-17 Dual gear (Lane 2) outperformed Lanes 1 and 3 by a factor of 3 or 4. Lanes 1, which was trafficked with the C-17 single tire at 45,000 lb (200 kN), did not performed as well as the C-17 dual gear loaded at 45,000 lb (200 kN) per tire. The effects of the kneading action on the pavement as the dual gear traverses back and forth and it is shifted laterally creates a healing effect in terms of the rutting potential. Another important observation is that the rate of rutting for the C-17 dual gear (Lane 2) is relatively flat until a considerable amount of traffic is applied. On the other hand, Lane 1 outperformed Lane 3. This is believed to be attributed to the effects of the F-15 high contact pressure (325 psi (2242 kPa) for the F-15 versus 142 psi (980 kN) for the C-17 tire). However, the rate of rutting is more pronounced for the F-15 single tire than for the C-17 single.

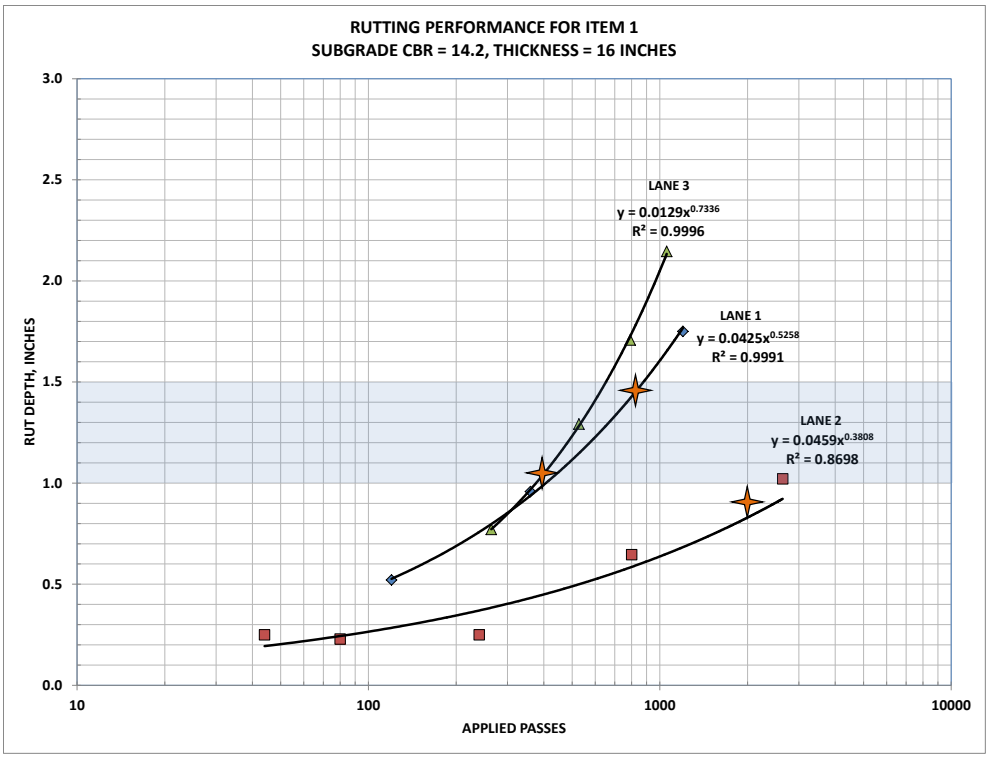

Figure 6.29 Rutting performance of Item 1 for Lanes 1, 2 and 3 (1 inch=25.4 mm)

Figure 6.30 shows the results for Item 2, which consisted of 3 inches (76 mm) of asphalt concrete, 6 inches (152 mm) of base and 14 inches (356 mm) of subbase over a subgrade CBR of 9.8. Just as was the case for Item 1, the C-17 dual gear outperformed the other two traffic lanes. However, even though the CBR for Item 2 is equal to 9.8, the pavement section has a considerably thicker subbase layer (7 inches (178 mm) for Item1 versus 14 inches (356 mm) for Item 2), which help distribute the stresses to the subgrade and resulted in a rutting performance closer to the C-17 dual. However, the rutting performance for the F-15 single in Lane 3 was not improved by this same fact, so the high tire pressure may be overstressing the upper layers enough to offset any gain in stress distribution to the subgrade. Very similar results can be observed from the rutting performance of Item 3 in Figure 6.31, with the exception that the rutting increased at a faster rate as compared to Items 1and 2.

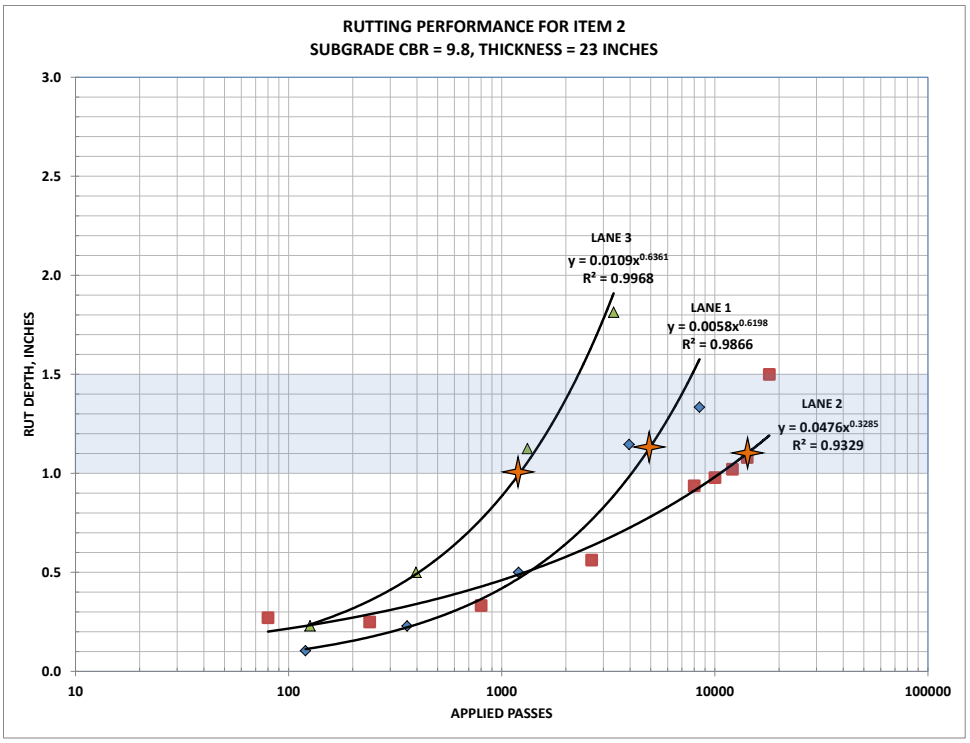

Figure 6.30 Rutting performance of Item 2 for Lanes 1, 2 and 3 (1 inch=25.4 mm)

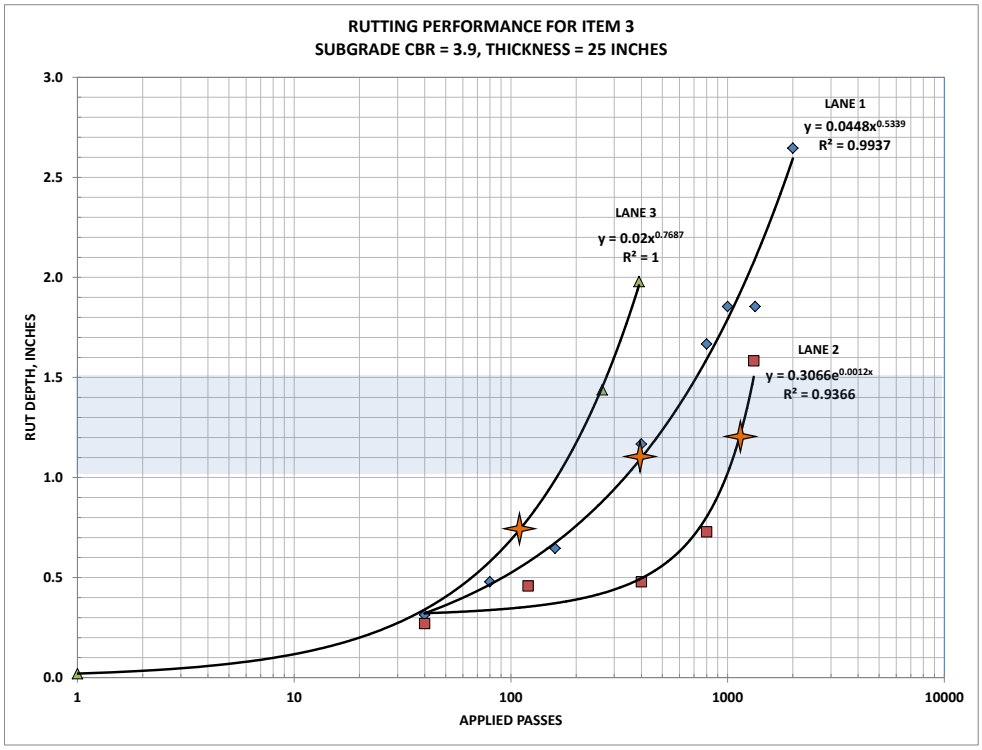

Figure 6.31 Rutting performance of Item 3 for Lanes 1, 2 and 3 (1 inch=25.4 mm)

Figure 6.32 shows the results for Item 4. This item had the thickest cross section with a 32-inches (813 mm) subbase above the subgrade, which had a CBR of 3.9. Again, Lane 2 outperformed Lanes 1 and 3, but not as distinctly as the other three items. However, all three lanes gain in terms of rutting performance with failure points occurring beyond 2,000 passes.

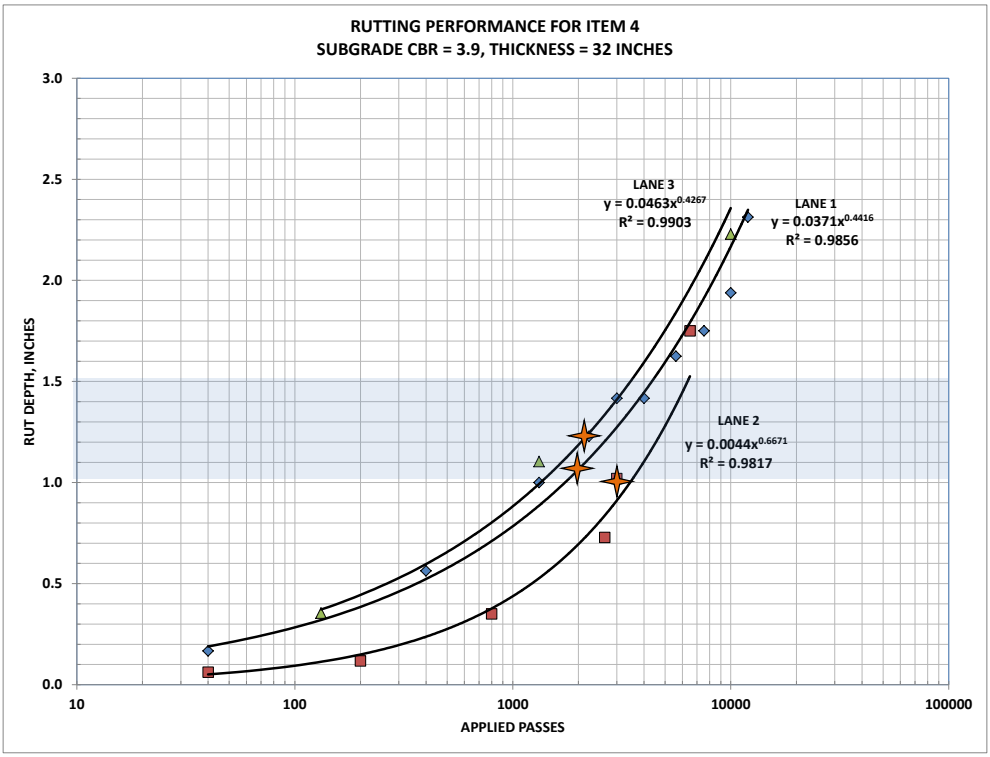

Figure 6.32 Rutting performance of Item 4 for Lanes 1, 2 and 3 (1 inch=25.4 mm)

6.7 Validation of Stress-Based CBR-Beta Criteria

The performance data collected in this research relating coverages to failure, thicknesses and material strengths in terms of CBR and corresponding Beta parameter are summarized in Table 6.6. The coverages to failure and the Beta parameter are plotted in Figure 6.33 to compare it against the proposed CBR-Beta stress-based criteria. The additional points resulting from this research are identified in Figure 6.33 with the diamond-shaped symbols. The diamond-shaped points correspond to Lane 1 trafficked with a C-17 single tire, Lane 2 trafficked with a C-17 dual tire assembly and Lane 3 trafficked with an F-15 single tire.

Table 6.6 Summary of test section performance data

Point No.	Source	Coverages to Failure	Thickness, inches	CBR	Beta, psi
1	FAA-Six-wheel Gear (CC3)	57	35.50	3.72	14.50
2		1009	45.10	4.38	9.72
3		12720	57.10	4.38	9.54
4		8273	30.70	7.45	7.14
5	FAA-Four-wheel Gear (CC3)	55.9	35.50	4.32	12.58
6		1258	45.10	4.32	9.80
7		16968	57.10	4.32	9.64
8		5825	30.70	7.34	7.39
9		9225	28.20	7.43	8.16
10	MWHGL 747	40	33.00	3.80	17.01
11		40	33.00	4.00	16.16
12		280	41.00	4.00	12.51
13	MWHGL C5A	8	15.00	3.70	26.26
14		104	24.00	4.40	12.35
15		1500	33.00	3.80	9.53
16		1500	33.00	4.00	9.06
17		3850	41.00	4.00	7.25
18	Single Wheel Data	150	39.00	6.00	16.68
19		1700	44.00	9.00	9.21
20		10	18.00	16.00	15.59
21		60	20.50	18.00	12.37
22		360	23.50	15.50	12.53
23		1500	30.00	17.50	8.29
24		1300	49.00	8.00	8.68
25		3760	10.00	8.00	10.44
26		3760	10.00	9.00	9.28
27		6	15.00	3.70	42.80
28		200	24.00	4.40	17.04
29		120	15.00	3.70	25.68
30		216	12.00	14.00	11.18
31		178	12.00	7.00	22.35
32		203	12.00	6.00	26.08
33		40	5.00	6.00	30.88
34	Validation CBR	336	15	14.2	12.78
35		2000	23	9.8	8.93
36		160	25	3.9	14.68

Table 6.6 Summary of test section performance data					
Point No.	Source	Coverages to Failure	Thickness, inches	CBR	Beta, psi
37		800	32	3.9	9.47
38		800	15	14.2	11.80
39		6400	23	9.8	8.40
40		440	25	3.9	14.26
41		1200	32	3.9	12.94
42		69	15	14.2	12.72
43		191	23	9.8	7.46
44		19	25	3.9	11.72
45		400	32	3.9	7.35
Note: 1 inch=25.4 mm, 1 psi=6.9 kPa					

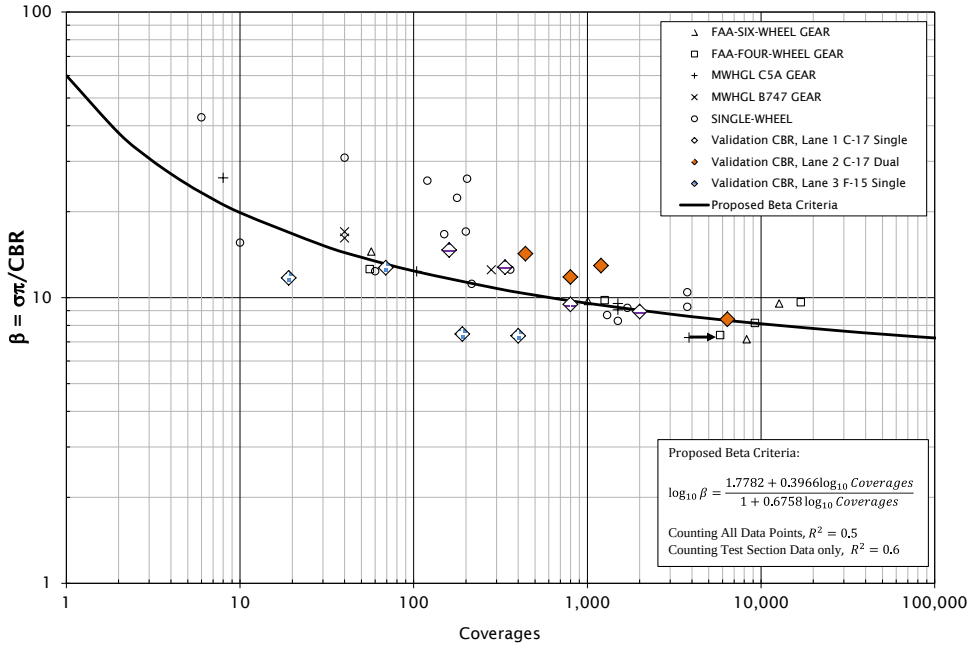

Figure 6.33 Performance data collected from the field testing

It is seen in Figure 6.33 that the new data points plot above, on top of and below the proposed CBR-Beta criteria curve. Four out of the twelve data points collected fall right on top on this curve, while the remaining eight points are distributed almost equally above and below the proposed criteria curve. It deserves to be noted, that four of the new data points collected fall

below the curve. These data points correspond to Lane 3 which was trafficked with the F-15 single tire. This indicates that the combination of the F-15's high load of 35,000 lb (156 kN) and high tire pressure of 325 psi (2242 kPa) produced early pavement failures. Since the upper layers were composed of a relatively thin asphalt layer of 3 inches (76 mm) and a 6-inch (152-mm) base, it can be deduced that for high-load and high-tire pressure gear assemblies, the upper layers would have to be constructed from thicker layers to sustain this type of loading.

Lanes 1 and 2, which were trafficked with C-17 assemblies with tire pressure of 142 psi (980 kPa), outperformed the values predicted by the proposed CBR-Beta criteria, with most of the data points falling above and to the right of the performance curve. The results of traffic with the C-17 single and dual tire assembly achieved coverage levels comparable to those of the FAA and MWHGL tests. This fact adds credibility to the newly collected data points and therefore supports the validity of the proposed CBR-Beta criteria.

The goodness of fit, represented here by the R^2, did not changed significantly from the data collected from historical test sections. If all historical data and new performance data collected in this research is counted, the $R^2 = 0.5$, while, if only the data collected in this research is used the R^2 increases slightly to a value of $R^2 = 0.6$. The form of the equation used to described the CBR-Beta performance criteria as is shown in Figure 6.33, was retained because is a well-behaved equation and predicts reasonable values even at large numbers of coverages. If the numerator and denominator of the right side of Equation 6.1 is divided by the log_{10} *Coverages*,

$$\log_{10}\beta = \frac{1.7782+0.3966\log_{10} Coverages}{1+0.6758\log_{10} Coverages} \quad (6.1)$$

Then, Equation 5.1 can be expressed as follows.

$$\log_{10}\beta = \frac{\frac{1.7782}{\log_{10} Coverages}+0.3966}{\frac{1}{\log_{10} Coverages}+0.6758} \quad (6.2)$$

As the number of coverages in Equation 6.2 becomes large, as would be the case of very thick pavements structures or perpetual pavements, $log_{10}\beta$ will approach a limiting value of $log_{10}\beta$ = 0.3966/0.6758 = 0.587, which equates to an asymptotic value of β=3.86. If a coverage level reaches a minimum value of one coverage, then Equation 6.1indicates that $log_{10}\beta$=1.7782,

or β =60. For any values of β inside this range, Equation 6.1 will predict reasonable coverage levels.

From this analysis, the performance curve describing the proposed CBR-Beta criteria is considered to be reasonable and able to predict either, β limiting values for a predetermined level of coverages, or allowable numbers of coverages for limiting values of β.

6.8 Summary

Detailed analyses of the relevant laboratory tests, test section field data, traffic tests and modelling effort conducted for this research was presented. Emphasis was put on the results obtained from earth pressure cells, since these data directly relates to the analysis and validation of the proposed stress-based CBR-Beta design procedure for military airfield pavements.

Laboratory data was collected to determine the fundamental mechanical properties of the materials forming the pavement structures tested. These properties were used to calibrate the axisymmetric finite element model employed for this research study. Measured stresses obtained from earth pressure cells were compared to those values predicted by the Fröhlich stress model, layered elastic theory and the axisymmetric finite element method model. The validity of the correlation between Fröhlich stress concentration factor (n-factor) and CBR was assessed by backcalculating *n-factors* for the four pavement sections tested. Falling weight deflectometer data was used to backcalculated layer moduli, predict stresses in the subbase and subgrade and make comparisons to stresses calculated using Fröhlich's stress model and the axisymmetric finite element method model.

The performance of the test sections constructed was analyzed in terms of the amount of traffic cycles they took before failure was reached. The resulting number of traffic cycles to failure was related to the proposed CBR-Beta criteria to evaluate the goodness of the fit of the CBR-Beta curve around the data points collected in this research and those derived from historical test sections. Finally, the last sections of this chapter laid out the mathematical foundation used to implement the stress-based CBR-Beta procedure into a complete pavement design system.

The results of these analyses were used to validate and complete the final form of the CBR-Beta criteria. In its final formulation, the CBR-Beta was found to fit the collection of existing test section data, and therefore it was deemed to be acceptable for design purposes. This successful validation now leads to the next logical step of incorporating the CBR-Beta criteria into a complete system for the design of standard flexible pavements. The following chapter describes in detail the process and implementation steps required to accomplish this task.

CHAPTER 7 - IMPLEMENTATION OF STRESS-BASED CBR-BETA PROCEDURE

7.1 Introduction

One the benefits of expressing the performance criteria in terms of Equation 6.1 is that it lends itself to the implementation of a more direct mechanistic-empirical design procedure for the design of flexible pavements. It is believed that the results obtained in this research from field and test section data substantiates extending the use of the CBR-Beta procedure from what was believed to be a totally empirical CBR equation to a more modern design system that uses cumulative damage concepts. The need to use equivalent single wheel loads (ESWL) to model multi-wheel landing gears and thickness reduction factors (alpha factors) to compensate for gear type and traffic is completely eliminated. The multi-wheel landing gears are directly modeled by the use of Fröhlich's stress model and the traffic accounted for by the CBR-Beta criteria described in Chapter 6. Before the implementation procedure is discussed in detail, it is important to point out that the results of the analyses and recommendations were derived from standard flexible airfield pavements. Pavements constructed with stabilized layers were not considered here and may require further research.

This chapter presents an additional refinement performed on the proposed CBR-Beta criteria from an in-service flexible pavement failure that occurred at very low pass levels. The details of the implementation of the CBR-Beta into a completed pavement design system are introduced in terms of cumulative damage concepts. Later, the framework designed to combine the CBR-Beta criteria, Fröhlich's stress response model, multi-wheel loading considerations, and cumulative damage concepts are discussed in detail. Finally, with the implementation complete, several thickness comparisons are made between the CBR-Alpha and the CBR-Beta procedure for both airfield and road loadings.

7.2 Refinement of the CBR-Beta Criteria

Analysis of Fröhlich's and Boussinesq's theories and a review of full-scale test data allowed the first formulation of the revised CBR criteria and provided Equation7.1. This

equation essentially links the vertical stress to strength ratio of a pavement subgrade to the number of coverages of the design traffic.

$$\log \beta = \frac{1.7782 + 0.3966 \log Coverages}{1 + 0.6758 \log Coverages} \quad (7.1)$$

An additional review and validation of the design criteria summarized in Equation 7.1 was performed from field data collected after the completion of the full-scale testing was completed. This re-analysis was performed with new field data from actual in-service pavement failures and will be described in the next section.

A visual and structural pavement evaluation performed after a pavement failure at Las Cruces International Airport, NM, (AFCESA 2004 included in Appendices B and C), allowed the refinement of the CBR-Beta procedure when applied to very low traffic volumes (less than 10 coverages). In addition, data from the Multiple-Wheel Heavy Gear Load (MWHGL) full-scale testing (WES, 1971) were also included to improve and support the criteria when addressing low-traffic scenarios.

The MWHGL database included three data points which were specific for low-volume traffic. The data points were Test Lane 2A, 50,000 lb (222 kN) single-wheel assembly on Items 1 and 2, and Test Lane 3B, 240,000 lb (1068 kN) twin-tandem assembly on Item 3. On Item 1, the traffic at failure for the 50,000 lb (222 kN) single-wheel load was at 6 coverages, but test records reported that cracking developed during the first pass, whereas at 6 coverages the rut depth was greater than 1 inch (25.4 mm). Therefore, it was concluded that failure occurred earlier than 6 coverages.

The Las Cruces pavement evaluation reported that the ruts at the end of the runway were made by one pass (two coverages) of the C-17 aircraft. Previous assumptions on the Las Cruces pavement failure included a traffic volume of four coverages composed of at least one pass of the C-17 aircraft and one pass of the B-757 aircraft which, because of overlapping of gears, produced a total of 4 coverages. In the absence of gear overlapping, the possible traffic scenario was of only 2 coverages. A detailed analysis of the Las Cruces pavement failure is included in Appendix B.

The data points from the MWHGL study and the data from Las Cruces pavement failure were combined to address the low-volume traffic portion of the CBR-Beta criteria. The analysis of the low-volume traffic scenarios with the selected data points produced two criteria which were both acceptable in terms of approximation of the pavement performance. Equation 7.2 represents the less conservative curve, whereas Equation 7.3 is the more conservative design curve. Due to the limited amount data for the very low traffic level, the more conservative option was chosen. Figure 7.1 shows the two curves and the position of the field data point.

$$\log \beta = \frac{1.8451 + 0.2144 \log Coverages}{1 + 0.4667 \log Coverages} \tag{7.2}$$

$$\log \beta = \frac{1.5441 + 0.0730 \log Coverages}{1 + 0.2354 \log Coverages} \tag{7.3}$$

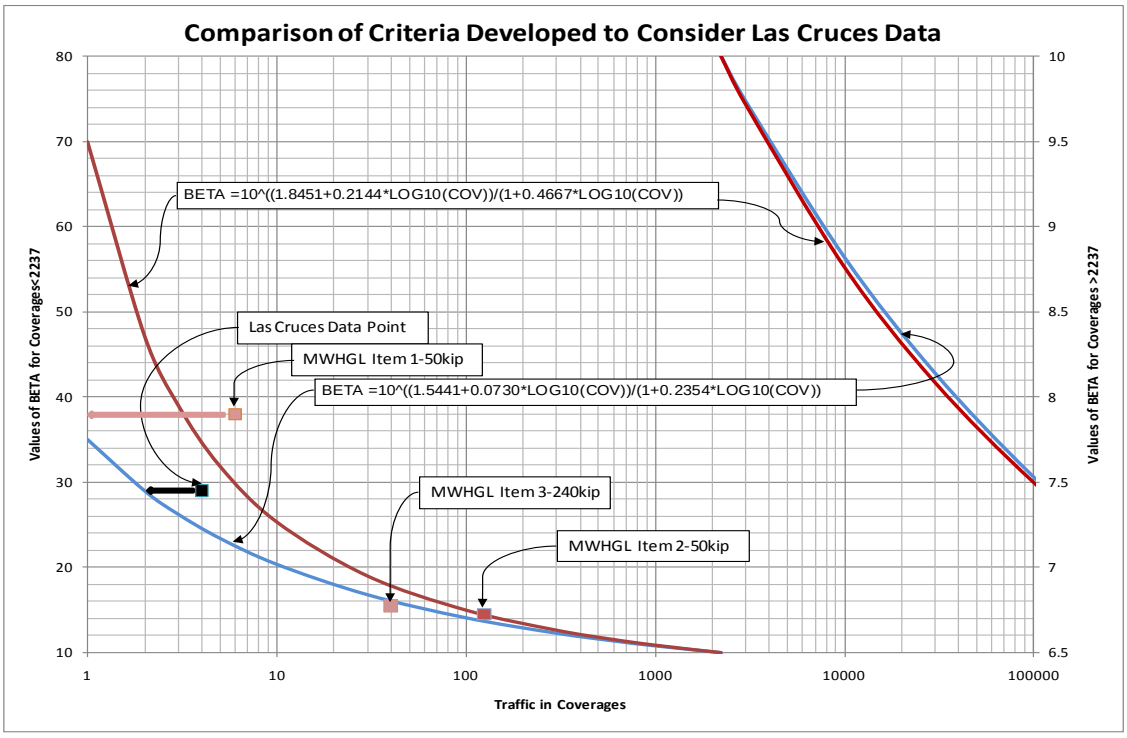

Figure 7.1 Comparison of the criteria from Equations 7.1 and 7.2 for low volume traffic

From Figure 7.1, the difference between the curves between 1 and 300 coverages may be considered significant, but for traffic volumes above 300 coverages, the two curves almost coincide. In fact, at coverage levels above 2,237 and 300,000 coverages, the equations for two criteria curves dictate that the criteria are identical. Table 7.1 compares the two criteria in terms

of required pavement thickness for operations of the C-17 aircraft. As a result of this analysis and the desire to be conservative at low pass traffic levels, the CBR-Beta criteria curve described by Equation 7.3, was chosen and is recommended to be implemented in the design of flexible pavements.

Table 7.1 Criteria comparison for C-17 operations

CBR	Passes	Coverages	Thickness (in.)			$(T_2-T_1)/T_2$ %
			T_1 (Eq. 7.2)	T_2 (Eq. 7.3)	T_2-T_1	
3	1	2	13.6	19.9	6.3	31.7
	5	4	16.8	22.1	5.3	24.0
	10	7	20.4	24.7	4.3	17.4
	100	72	31.6	33.7	2.1	6.2
	1,000	725	42.4	42.9	0.5	1.2
	5,000	3,623	49.2	49.1	-0.1	-0.2
	50,000	36,232	57.7	57.4	-0.3	-0.5
	100,000	72,464	59.9	59.7	-0.2	-0.3
6	1	2	7.3	12.4	5.1	41.1
	5	4	10.0	14.0	4.0	28.6
	10	7	12.8	15.8	3.0	19.0
	100	72	20.0	21.1	1.1	5.2
	1,000	725	25.8	26.1	0.3	1.1
	5,000	3,623	29.4	29.3	-0.1	-0.3
	50,000	36,232	34.0	33.8	-0.2	-0.6
	100,000	72,464	35.3	35.1	-0.2	-0.6
10	1	2	0.1	7.6	7.5	98.7
	5	4	5.0	9.1	4.1	45.1
	10	7	7.9	10.7	2.8	26.2
	100	72	14.2	15.1	0.9	6.0
	1,000	725	18.6	18.8	0.2	1.1
	5,000	3,623	21.1	21.0	-0.1	-0.5
	50,000	36,232	24.1	24.0	-0.1	-0.4
	100,000	72,464	24.9	24.8	-0.1	-0.4

Note: 1 in.=25.4 mm

7.3 Implementation of Fröhlich Stress Model

The simplest implementation of Fröhlich's stress model is that of a point load applied on the surface of semi-infinite elastic solid as is illustrated in Figure 7.2. In reality, loads on

pavements are always applied through distributed areas and are usually shaped as elliptical areas. Equation 7.2 is used to calculate the vertical stress according to Fröhlich stress model for a point load at any arbitrary depth ***z*** and offset radius ***r***.

$$\sigma_z = \frac{nP}{2\pi z^2} cos^{n+2}\theta \tag{7.4}$$

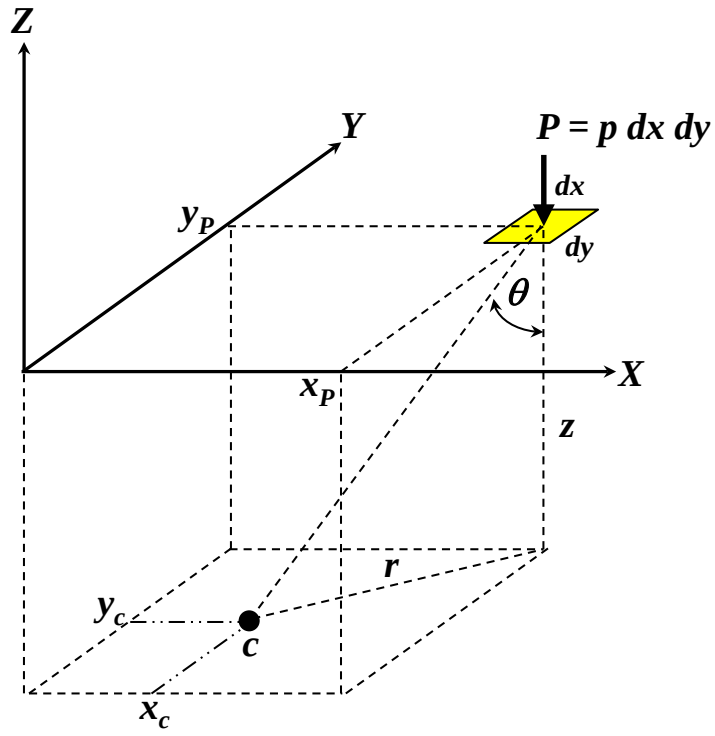

Figure 7.2 Point load Fröhlich stress model

To compute the stress due to loaded contact areas, Equation 7.4 was extended by subdividing a tire imprint into small rectangular contact areas as is shown in Figure 7.3. These small contact areas are then integrated to cover the entire tire imprint and the vertical stress is determined by superposition of the stresses of each individual rectangle. The final vertical stress is then corrected by multiplying the resulting stress by the ratio of applied tire load to the sum of the individual infinitesimal point loads acting on each rectangular area. This process is then extended to multiple tires or contact areas and the stress at any location and depth is computed as described by Equation 7.5.

$$\sigma_z = \sum_{i=1}^{N_T} \sum_{j=1}^{N_P} \frac{nP_{ij}}{2\pi z^2} cos^{n+2} \theta_{ij} \quad (7.5)$$

In Equation 7.5,

n = stress concentration factor

z = depth from surface of pavement to calculation point

r = radial distance from point load to calculation point

θ_{ij} = angle formed from vertical line under point load to calculation point

P_{ij} = elemental point load

N_T = number of tires

N_P = number of elemental point loads

Since the pavement response used to relate an applied stress to the CBR-Beta criteria is the maximum stress due to a gear assembly, a search grid, as illustrated in Figure 7.4, is required to determine the location and magnitude of the maximum vertical stress. Calculations are performed at each individual grid point and the contribution of each infinitesimal point load for each tire is accounted for. The maximum resulting vertical stress is then selected as the value to be used in the CBR-Beta criteria.

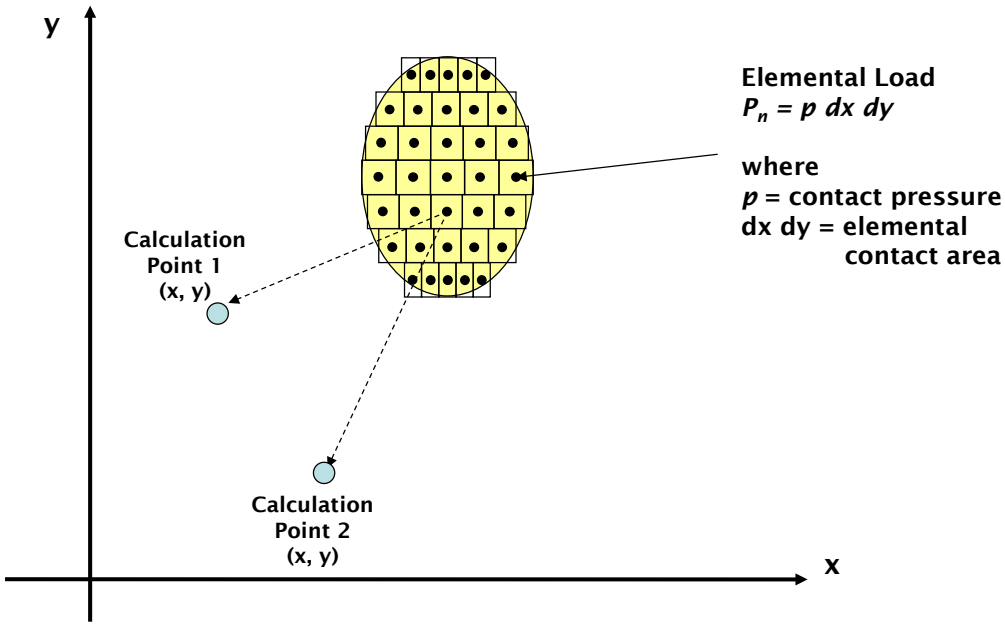

Figure 7.3 Tire contact area integration

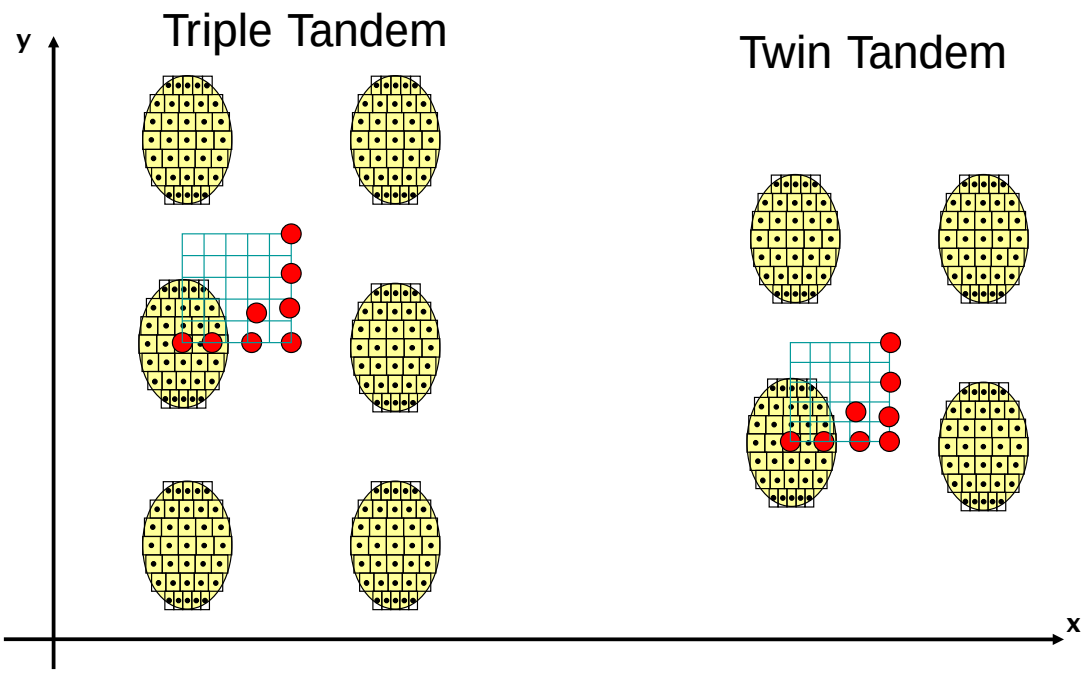

Figure 7.4 Extension of tire contact area integration to multiple tires imprints

7.4 Cumulative Damage Concept

One of the advantages resulting from implementing the proposed CBR-Beta criteria is that it can be expanded to account for the concept of damage imparted to the pavement by wheel loading. The cumulative damage concept, proposed by A. M. Miner in 1945 to account for the fatigue of material due to cycles of loading, is applied here to pavement structures. As shown conceptually in Figure 7.5, as cycles of loading are applied, the material strength or stiffness is reduced, resulting in a reduction of life in terms of the number of cycles at which the material fails. The concept postulated by Miner as the ratio $d = n/N$ represents the ratio of applied number of stress cycles over the allowable number of stress cycles to failure. In Miner's hypothesis, if the ratio n/N is equal to 1.0, then the applied number of stresses equals the allowable number of stresses in the material and is considered failed. When the ratio n/N is less than 1.0, the material has some life left and when the ratio n/N is greater than 1.0 the material has gone pass what the material is capable of supporting. This damage ratio can also be calculated at various offset distances from a reference lateral line of traffic on the pavement surface.

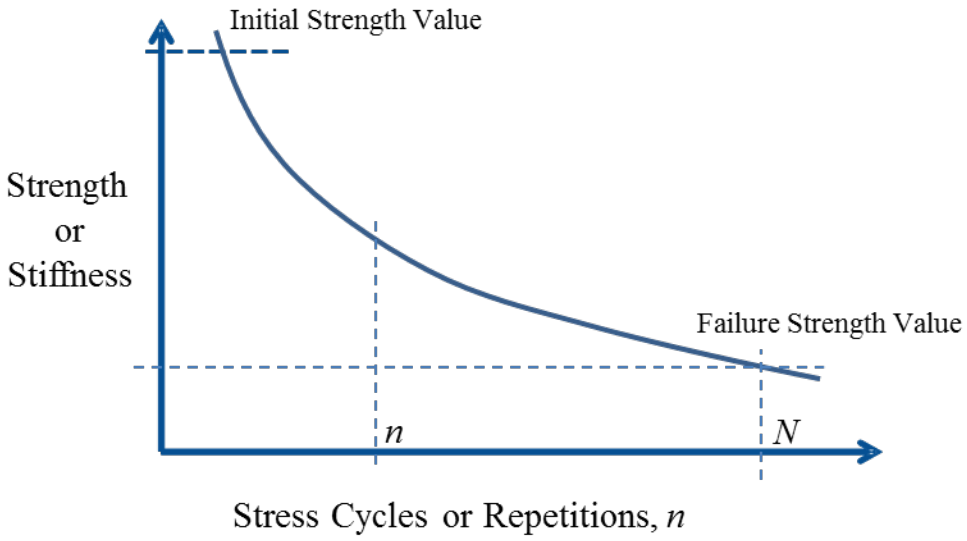

Figure 7.5 Cumulative damage concept applied to pavement materials

By applying this concept, the handling of multiple tires in a gear and multiple aircraft and vehicles can be combined into a single analytical procedure where lateral damage can be computed for each individual aircraft or vehicle. In addition, since the allowable stress cycles, *N*, are dependent on the material strength at a particular time period or condition, the damage concept can even be expanded to account for changes in moisture content, and both frost and thawed conditions. This concept is mathematically expressed by Equation 7.6, where the damage ratios are summed for a number of aircraft or vehicles and for different material strength conditions.

$$CDF_k = \sum_{i=1}^{NAC} \sum_{j=1}^{NS} \frac{n_{ij}}{N_{ij}} \tag{7.6}$$

where

k = pavement lateral offset from a reference line

CDF = cumulative damage factor

i = aircraft or vehicle

j = time period or season

NAC = total number of aircraft or vehicles

NS = total number of time periods of seasons for analysis.

When the CDF is greater than 1.0, a pavement structure is said to be under-designed for the intended traffic over the design life. When the CDF is less than 1.0, a pavement structure is considered over-designed and when CDF is equal to 1.0, the pavement structure is optimally designed to carry the traffic over the design life. The CBR-Beta procedure has implemented this damage concept by calculating the allowable number of stress application, counted by the number of coverages to failure, using the proposed CBR-Beta criteria Equation 7.6. Any aircraft or vehicle in a traffic mix is now directly evaluated for the damage it causes as a function of offset, as is illustrated in Figure 7.6. The maximum cumulative damage factor (CDF) resulting from the addition of damage due to each individual aircraft or vehicle is then used as the target value for design.

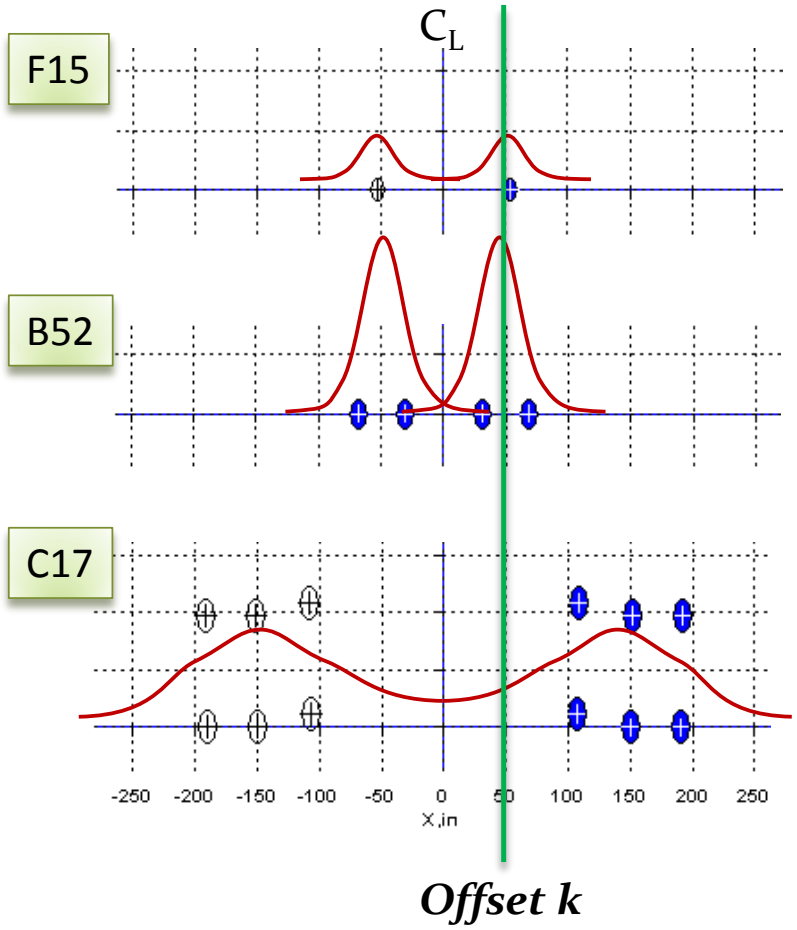

Figure 7.6 Example of cumulative damage concept applied to multiple aircraft or vehicles

7.5 CBR-Beta Implementation Framework

The inclusion of the cumulative damage concept as a way of comparing applied stress to the allowable number of stress applications sets the framework for the implementation of a cohesive flexible pavement design procedure where the CBR-Beta criteria and Fröhlich's stress model can readily be incorporated. Figure 7.7 illustrates a flowchart designed for the generic implementation of a pavement design procedure where the cumulative damage concept is used.

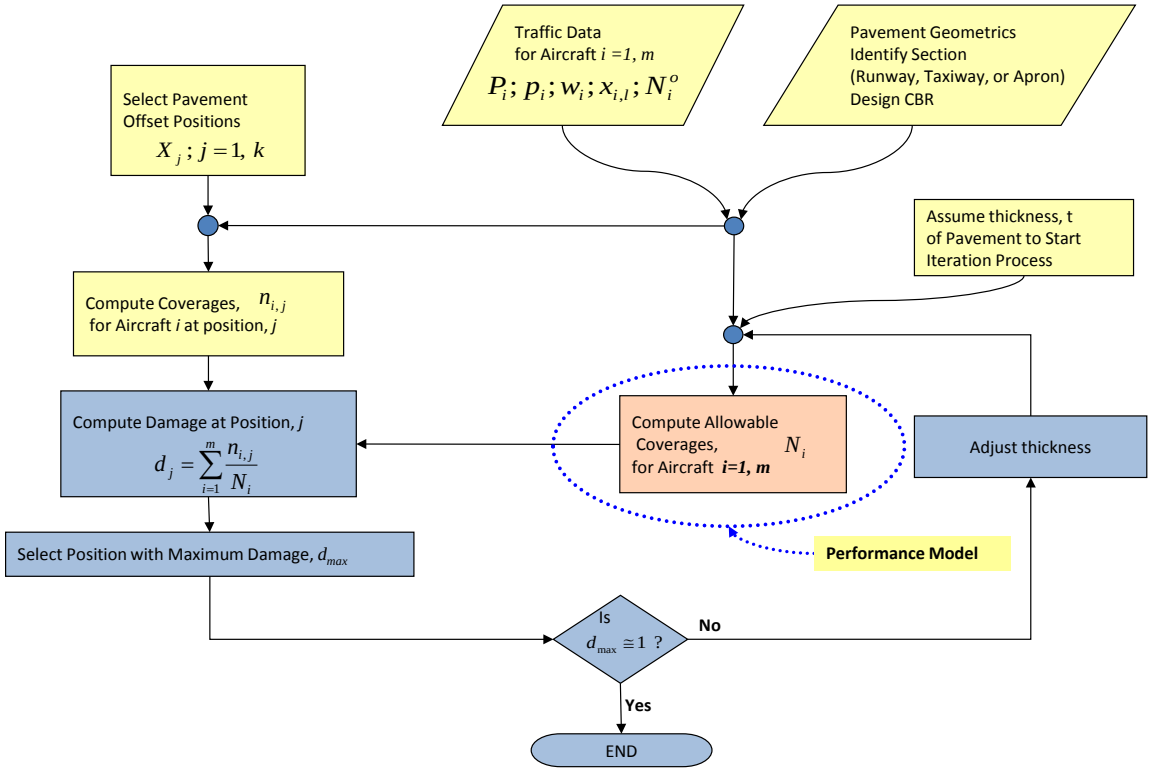

Figure 7.7 Diagram showing the proposed framework for the implementation of the stress-based CBR-Beta design procedure of flexible pavements

As is shown in Figure 7.7, this procedure is of an iterative nature. Major inputs to the design procedure include aircraft traffic and loading, pavement traffic areas and strength in terms of CBR and lateral offset for damage calculations. At the core of this framework is the pavement performance model, which will supply the allowable number of stress applications. The performance model to be used can be any model that supplies an allowable number of stress applications and the framework was designed with this feature in mind.

In general, a pavement thickness is assumed, traffic is applied and established at different offsets and the damage ratios calculated at the different offsets. Lateral damage is accumulated and compared to the optimal value of 1.0, and adjusted accordingly until a value of CDF is equal to 1.0 within a prescribed tolerance.

In this study, the performance model in Figure 7.7 is supplied by the stress-based CBR-Beta model founded on the Fröhlich' stress model and the developed CBR-Beta criteria. Figure 7.8 contains a flowchart showing details of the performance model based on Fröhlich stress equation extended to loads applied through surface contact areas and multiple tires in a gear. In this performance model, the allowable number of stress applications, *N*, is counted as the allowable number of surface coverages according to the proposed criteria described by Equation 7.5.

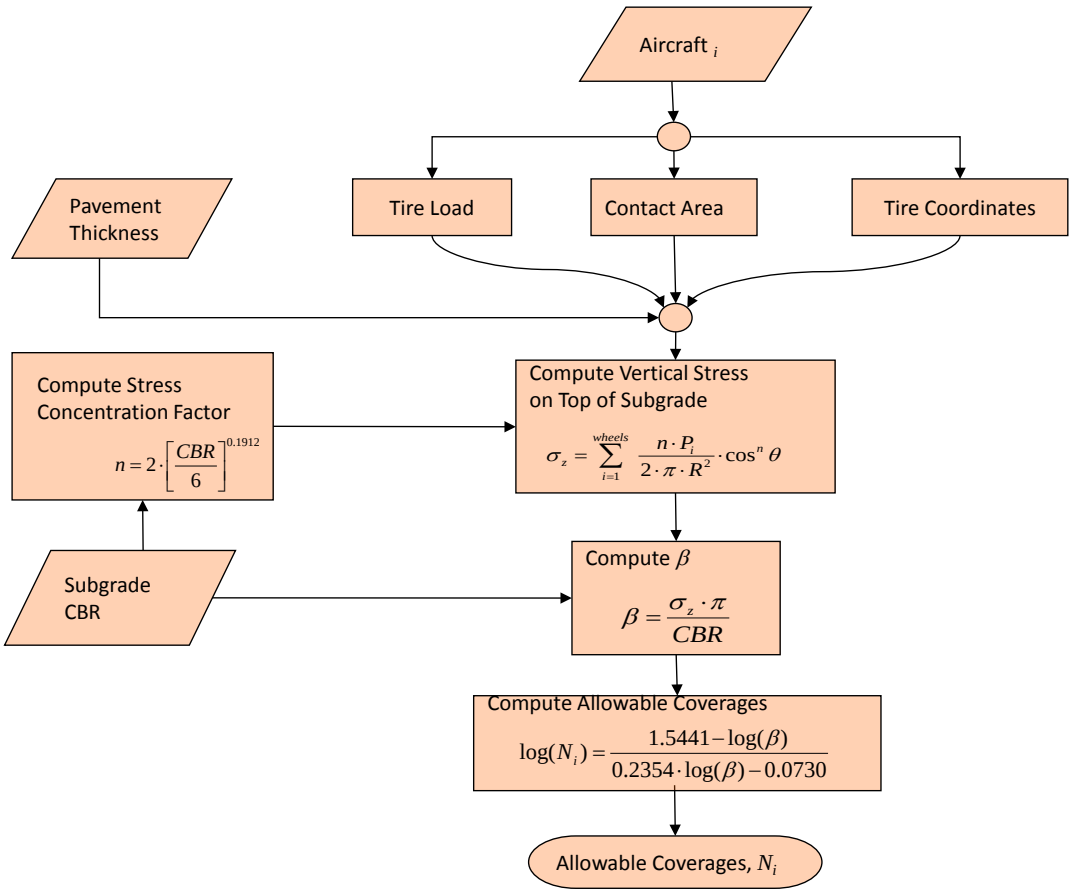

Figure 7.8 Diagram showing the stress-based CBR-Beta performance model

7.6 Software Development

The stress-based CBR-Beta framework described by Figures 7.7 and 7.8 was implemented into the pavement design and evaluation software package (PCASE) utilized by the United States Department of Defense for their design and evaluation of pavements structures. A subset derived from this software package was written for the analysis of the test pavement sections constructed for this research study. A sample screenshot of this utility is shown in Figure 7.9. This computer program, which was used extensively throughout this research to compute stresses and make predictions of damage and thicknesses, will form the basis for the next implementation of PCASE version 7.0. It implements the CBR-Beta criteria as described by Equation 7.5, as well as the cumulative damage factor and Fröhlich's stress model. Gear configurations of any number of tires and gear geometries can be accommodated.

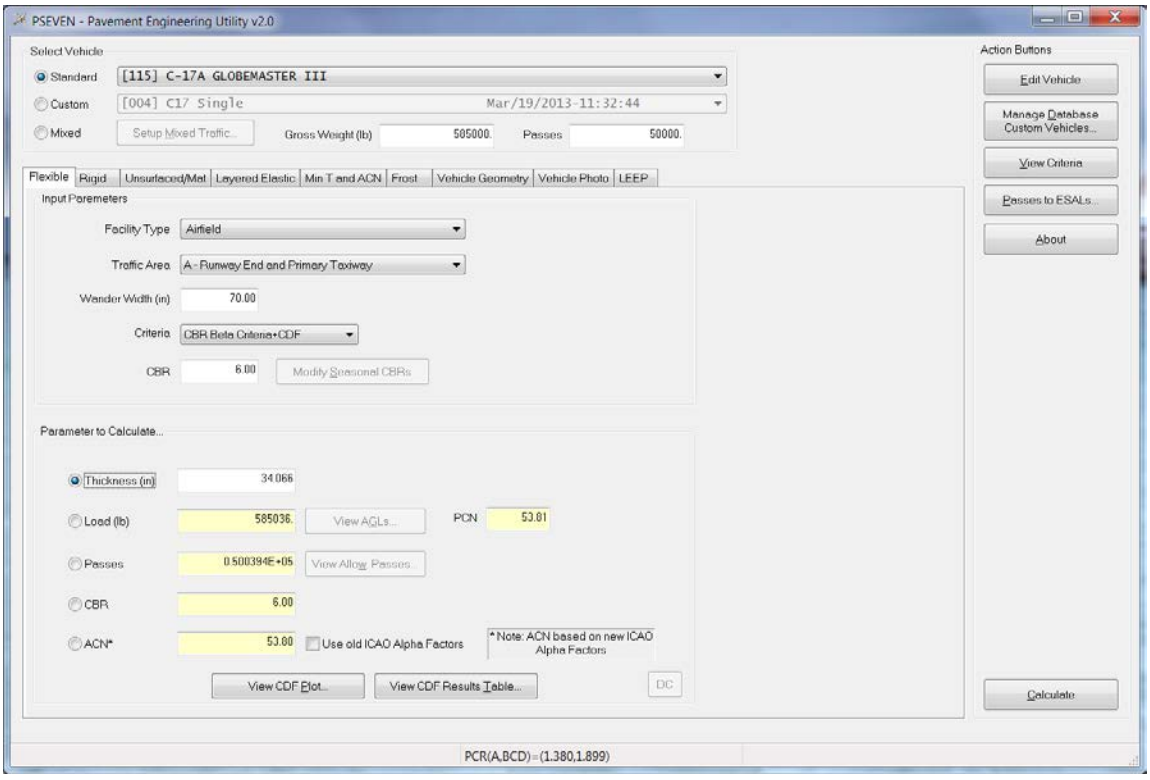

Figure 7.9 Implementation of CBR-Beta Procedure into PCASE 7 Module

7.7 Thickness Design Comparisons between CBR-Alpha Criteria and CBR-Beta Criteria

The results of this research and the implementation of the final recommended CBR-Beta criteria as implemented by the PSEVEN computer program were used to determine thickness designs for the F-15E single-wheel gear, the B-737-200 two-wheel gear, the C-17 six-wheel gear and the B-777-300 six-wheel gear. These thickness designs were compared to the existing CBR-Alpha criteria as implemented in its current form. The thickness calculations were performed for 50,000 passes of each individual aircraft and a range of subgrade CBR values of 3, 6, 10 and 15. The results of these designs are presented in Figures 7.10 through 7.13.

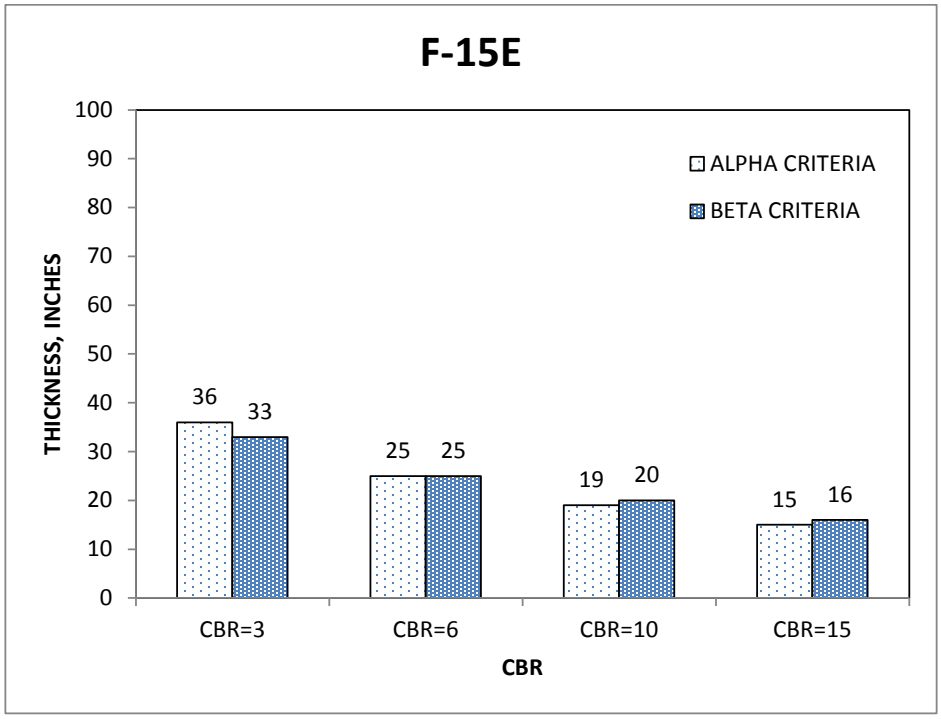

Figure 7.10 Thickness comparisons for F-15E single-wheel gear (1 inch=25.4 mm)

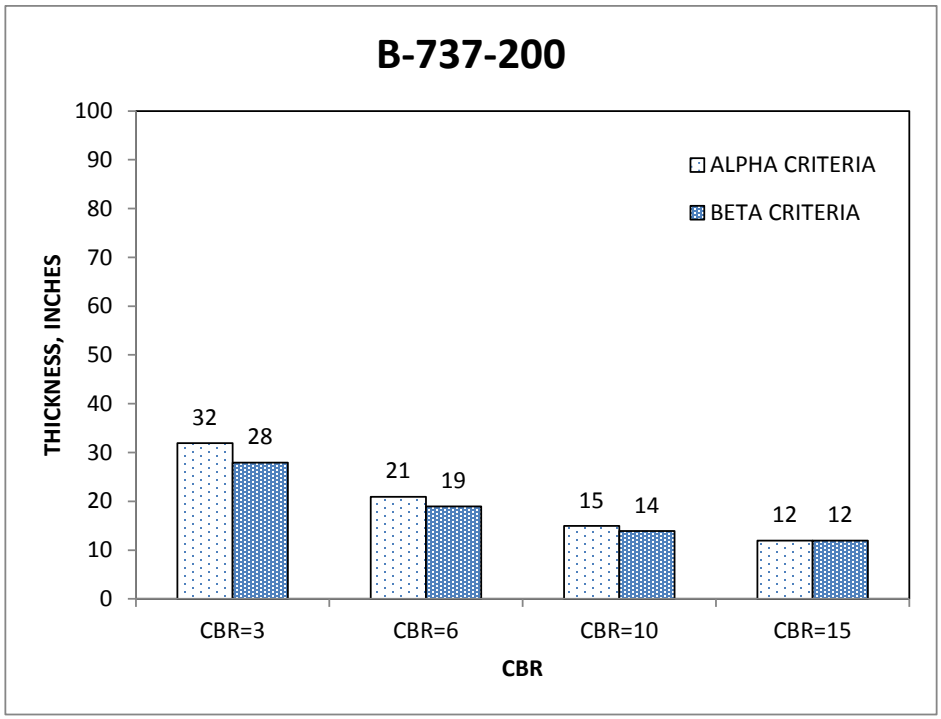

Figure 7.11 Thickness comparisons for B-737-200 two-wheel gear (1 inch=25.4 mm)

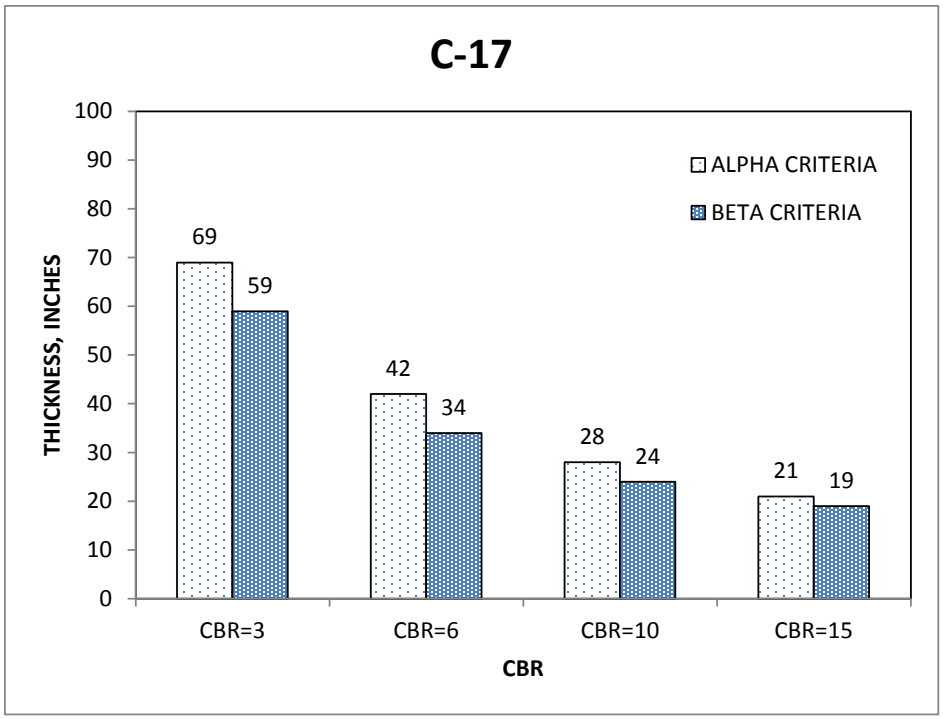

Figure 7.12 Thickness comparisons for C-17 six-wheel gear (1 inch=25.4 mm)

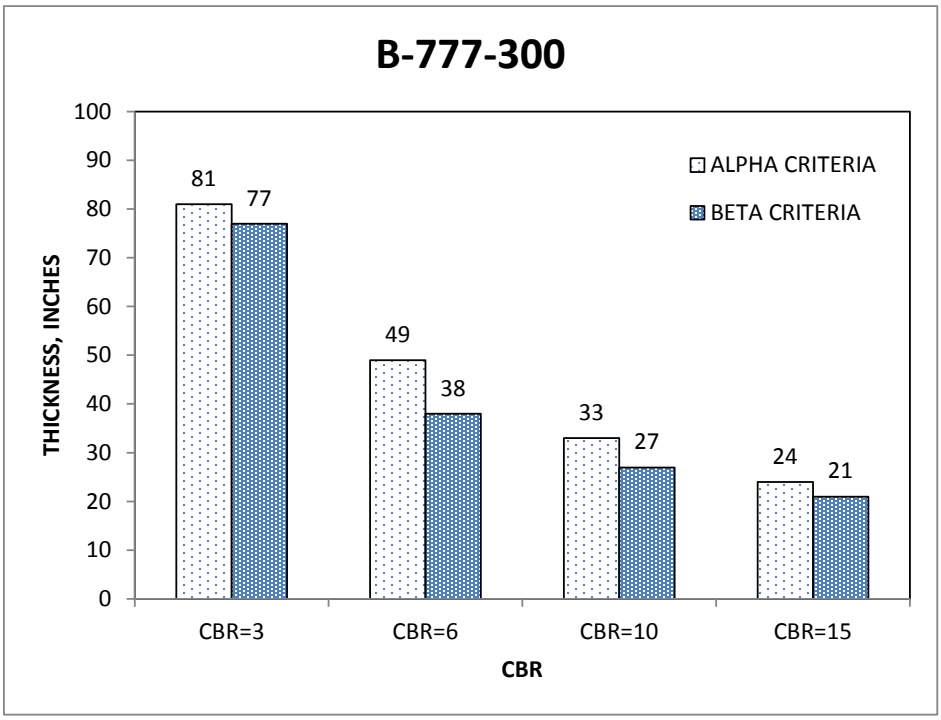

Figure 7.13 Thickness comparisons for B-777-300 six-wheel gear (1 inch=25.4 mm)

Additionally, thickness designs were also performed on two ground vehicles: the M1A1 tank with 14 road wheels and the standard 18-kip (80-kN) single axle load. The same airfield CBR-Beta criteria were developed from airfield pavements was used to determine the required thickness for the ground vehicles. The results of these analyses are shown in Figures 7.14 and 7.15.

In general, the trend is for the CBR-Beta criteria to give slightly thinner pavement thickness requirements than the CBR-Alpha criteria (Figures 7.10 through 7.13). The only exception is for the F-15E single-wheel gear, where the required thickness is only slightly lower at the CBR equal to 3, and either equal or greater for larger values of CBR. For all other aircraft analyzed, there was a thickness reduction using CBR-Beta as compared to the CBR-Alpha. When the CBR-Beta is applied to the ground vehicles, the difference between the two criteria is more significant as illustrated by Figures 7.14 and 7.15. It is worth noting that the impact on thickness is more pronounced for the very low CBR value of 3.

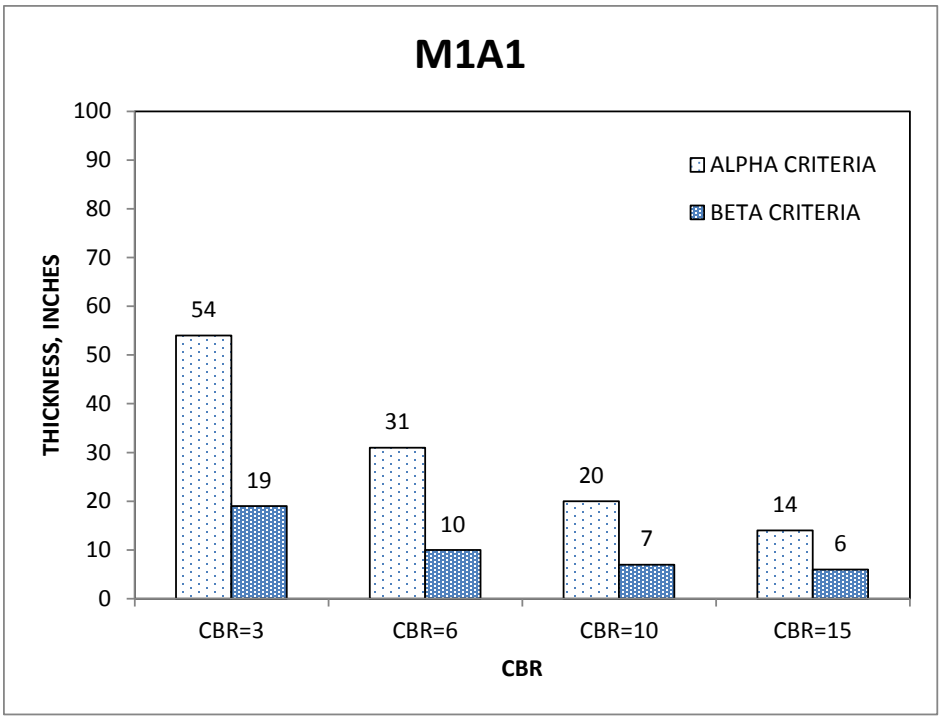

Figure 7.14 Thickness comparisons for M1A1 tank 14 road-wheel gear (1 inch=25.4 mm)

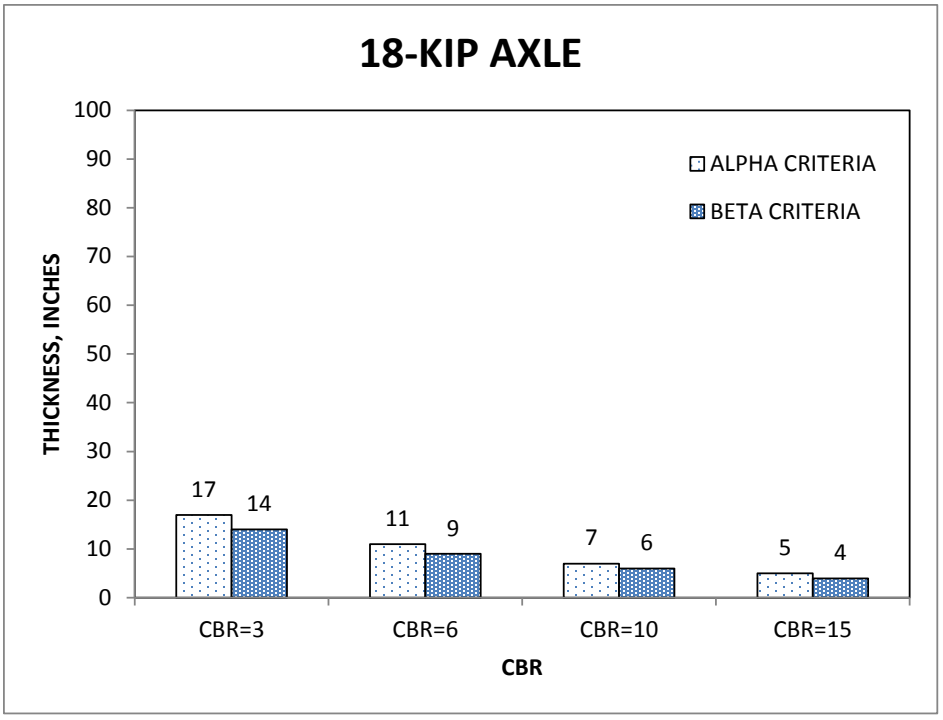

Figure 7.15 Thickness comparisons for standard 18-kip axle (1 inch=25.4 mm)

The thickness differences, expressed as a percent of the CBR-Alpha thicknesses, are shown in Figure 7.16. For the aircraft and ground vehicles analyzed, the thickness reduction by using the CBR-Beta criteria is generally in the order of 10 to 20 percent, but increasing as more tires exist within the gear. This is due to the conservative corrections that are applied to the equivalent single-wheel load (ESWL) calculations by the CBR-Alpha criteria and the use of the load repetition reduction factor. As more tires are used to calculate the ESWL, the more the error increases and the more conservative the CBR-Alpha procedure becomes. This is even more evident when comparing thickness designs for the M1A1 tank (Figure 7.16), where the vehicle is comprised of 14 road wheels and tracks that further spread the wheel loads.

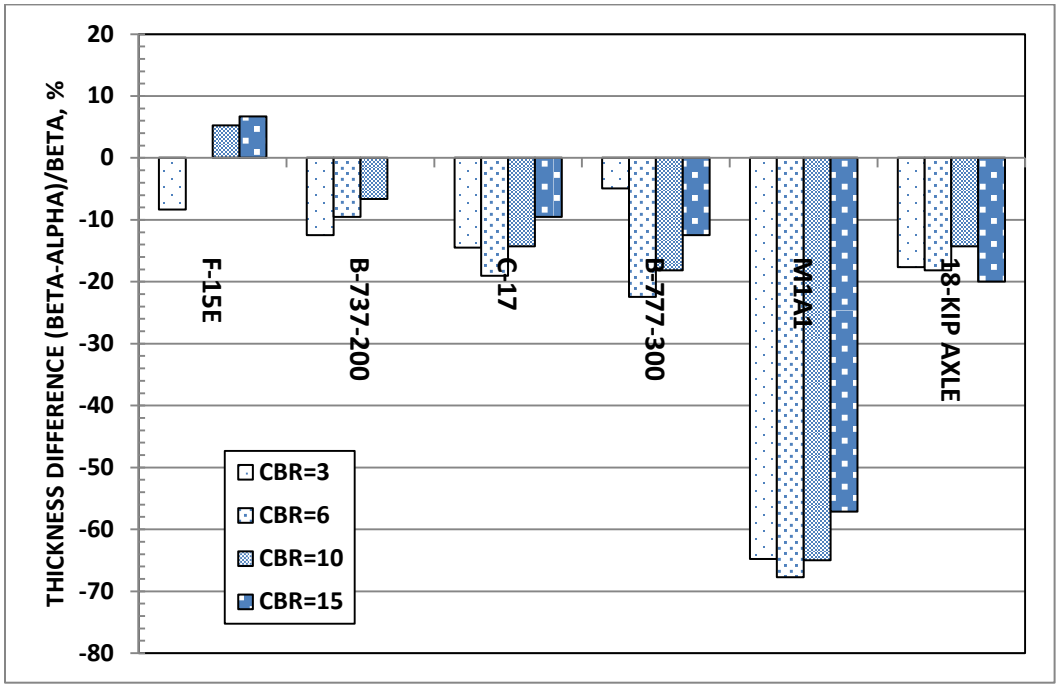

Figure 7.16 Thickness differences between the Alpha criteria and the CBR-Beta criteria

7.8 Summary

The implementation of CBR-Beta criteria and the design framework described in this chapter produces thinner sections in the order of 10 to 20 percent as compared to the CBR-Alpha criteria. However, the results will depend on the number of tires within a gear. The CBR-Alpha criteria are believed to produce thicknesses that are too conservative when used with multiple-wheel gears, particularly with gears with more than four wheels per gear. Overall, the CBR-Beta

criteria predict thickness designs that are in line with those produced by the CBR-Alpha criteria, while maintaining a more direct and consistent methodology without resorting to thickness reduction factors of equivalent wheel loads.

The implementation of the CBR-Beta facilitates the handling of not only multiple tires within a gear, but also multiple aircraft. This is accomplished by the addition of cumulative damage concepts, which enables the CBR-Beta procedure to account for lateral aircraft or vehicular lateral traffic distribution. Additionally, multiple seasons associated with changes in subgrade CBR due to moisture variability or weather conditions can now be accommodated directly. The CBR-Beta procedure can now be used as an alternative design system for those circumstances where only a subgrade CBR can be obtained. Although considered a simplistic procedure, the fact that the CBR-Beta procedure still uses the CBR test to establish pavement layer strength is considered a positive attribute since it inherits the extensive field validation associated with the classical CBR-Alpha design procedure.

CHAPTER 8 - CONCLUSIONS AND RECOMMENDATIONS

8.1 Introduction

This research study was undertaken to investigate the mechanistic nature of the California Bearing Ratio (CBR) design procedure of flexible pavements, improve upon it, and propose and validate a new stress-based CBR design procedure. This study sought to prove the validity of implementing a stress-based approach while maintaining an accurate and simplified design procedure based on subgrade CBR.

The current CBR design procedure of flexible pavements has been used by many government and military agencies since its inception in the 1940's. This procedure, which was originally developed from empirically derived highway pavement design curves, has been evolving throughout the years as new aircraft, landing gears and traffic conditions have changed. Even though early developments of the procedure included the application of theoretical approaches based on Boussinesq stress theory, the mechanistic nature of the original CBR equation was not clearly established.

The CBR procedure, mainly implemented by the CBR equation, has several technical limitations in terms of the handling of multi-wheel gear geometries, and proper handling of load repetitions. The limitations of the CBR equation have been accounted for by introducing correction factors to adjust the resulting design pavement thickness for load repetitions (alpha factor correction) and for multi-wheel gears (equivalent single-wheel load correction).

A literature review of the origins of the CBR equation revealed that the CBR equation inherently had a mechanistic based vertical stress approach (Ullidtz, 1998). This latter finding prompted this researcher to study this topic further. The CBR equation was indeed found to have a mechanistic nature and set the stage to propose modifications for improvement based on the stress-based approach.

This research study built upon these early findings to propose a set of objectives, including: (1) the reformulation of the original CBR equation in terms of stresses, (2) develop

and validate a CBR stress-based design criteria, and (3) and incorporate the newly proposed CBR stress-based criteria into a complete system for designing flexible pavements. To accomplish these objectives, traffic tests accompanied by a suite of laboratory tests were conducted on a full-scale experimental pavement. The experimental pavement was designed and instrumented with pressure sensors to validate the stress distributions within the pavement layers. The number of gear passes applied during traffic, were monitored to establish the failure points of each pavement test item.

8.2 Summary of Findings

On the basis of detailed analyses of the results from the full-scale experimental pavement, along with theoretical predictions and comparisons to real pavement responses, the fulfillment of the objectives set out in this research is summarized in the following overall findings:

1. Reformulating the CBR equation in terms of stress concentration factors permitted the development of design criteria based on the β parameter, which represents an allowable vertical stress. The new CBR equation, for which the stress distribution can be defined by any stress concentration factor, allows selecting the stress distribution which best models measured data.
2. The analysis of the CBR equation revealed an apparent correlation with a Fröhlich-defined stress concentration factor of 2. Realizing that the CBR equation represented a stress distribution was the catalyst of the study, which led to the identification of the mechanistic nature of the CBR design procedure.
3. The identification of the stress distribution represented by the CBR equation provided the explanation about the unconservative values of vertical stress obtained in the development of the ESWL. In fact, the ESWL was computed using the Boussinesq equations, whereas the CBR equation was found to be based on a stress distribution with a Fröhlich's stress concentration factor equal to 2.
4. An analysis of measured data along with theoretical considerations led to the conclusion that the stress distribution is a function of the subgrade CBR. The data indicated that the stress concentration factor, and therefore the stress distribution, varied from a value of about 1.0 for low strength subgrades to a value of about 6.0 for very strong subgrades. In

this study, the stress distributions were obtained based on a layered-elastic analysis using the U.S. Army Corps of Engineers' method for characterizing pavement materials. The analysis indicated that the stress distributions from the layered-elastic procedures can be approximated by concentration factors of 1.15 for a subgrade with CBR equal to 3.0, 1.4 for a subgrade CBR equal to 6, and 1.9 for a subgrade CBR equal to 15. Comparing measured vertical stresses to layered-elastic computed stresses indicated that the layered elastic model -predicts less than measured vertical stress.

Although it needs further development, the relationship between the stress concentration factor and subgrade CBR predicts realistic stress distributions, and therefore the new CBR equation formulation along with this relationship can be adopted as the design model for flexible pavements. The mechanistic-empirical nature of the proposed CBR-Beta methodology provides a reasonable justification for selecting the Beta criteria as a replacement for the current Alpha criteria.

8.3 Conclusions

Based on the research conducted in this study, the following conclusions were developed:

1. The classic CBR equation represents a distribution of vertical stresses defined by Fröhlich's stress concentration factor of 2.0.
2. A formulation of the CBR equation has been developed to represent any arbitrary stress concentration factor.
3. The distribution of vertical stresses within a pavement structure can be approximated by a function of the subgrade strength in terms of CBR.
4. Flexible pavement design criteria were developed based on the ratio of vertical stress to subgrade CBR, which would be independent of the aircraft landing gear, thus eliminating the need for thickness adjustment factors (α-factors) and load equivalencies through the use of equivalent single wheel loads.
5. The CBR-Beta design procedure represents a mechanistic-empirical design procedure, in which the critical response is computed using the stress distribution described by the revised CBR equation and an appropriate stress concentration factor. The critical pavement response is then associated to pavement performance using an empirically-

derived stress-based performance model based on existing pavement performance data and validated from full-scale test section data.

6. Layered elastic models tend to under-predict the vertical stress, specifically vertical stresses in upper pavement layers.
7. The proposed stress-based CBR design procedure is considered to be an important improvement over the existing CBR equation in the sense that it eliminates most of the shortcomings of the current CBR equation and improves on the handling of multi-wheel gears, proposes a more direct method of handling traffic pass levels, and utilizes more modern damage concepts. Specifically, the new CBR design procedure for flexible pavements completely eliminates the need for equivalent single-wheel load conversions and adjustments to design thickness through the use of load repetition factors. While the implementation of this new CBR design procedure brings the CBR methodology to the realm of more mechanistic designs, it still retains the simplicity of its predecessor and inherits the vast knowledge base and field performance data accumulated throughout the years.

8.4 Recommendations for Future Research

The recommendation is made to replace the current CBR-Alpha criteria for design of flexible pavements with the proposed CBR-Beta criteria. Based on the performances of the flexible pavement test sections constructed for this study, traffic testing with different loadings, and the analyses and evaluation of the theoretical models, it is recommended that:

1. Additional studies should be conducted to evaluate if the CBR-Beta procedure can also be implemented for road designs characterized by lighter load ranges and the high number of passes expected on typical highway flexible pavements.
2. Pavement structures with thicker asphalt layers should also be investigated and correlated to the results obtained from these tests.
3. Pavement structures containing stabilized layers should also be investigated and correlated to the CBR-Beta procedure.
4. The influence of granular layers of different thicknesses on the resulting pressure distribution for the subgrade should be further investigated.

5. Additional data collected from the falling weight deflectometer, surface strain gages, and single-depth deflectometer should be analyzed with the objective of developing advanced finite element models and analysis procedures.

The fulfillment of the proposed research ideas stated above, will definitely improve on the new CBR stress-based design procedure, particularly in those cases where non-standard flexible pavements are to be designed. Even more, pursuing the research ideas presented here will not only benefit the CBR-Beta methodology, but will also benefit other flexible pavement design methodologies as well.

REFERENCES

Aerodrome Operations and ICAO Services Working Group (2006), Discussion Paper No.21.

Ahlvin, Richard G. (1991) "Origin of developments for structural design of pavements", Technical Report GL-91-26. Vicksburg, MS: U.S. Army Corps of Engineers, Waterways Experiment Station.

Air Force Civil Engineer Support Agency (AFCESA) (2004), "Pavement Evaluation, Las Cruces International Airport New Mexico", Tyndall Air Force Base, FL.

Airport Technology Research and Development Branch (2004), "Alpha factor determination from NAPTF data", Letter Report Submitted to Associate Administrator for Airports, AAR-410 2004. Revised March 21, 2005.

American Society of Civil Engineers (1950), "Development of CBR flexible pavement design method for airfields a Symposium", Paper No. 2406 Reprinted from Transactions 115:453.

American Society for Testing and Materials (ASTM), D6938-10 "Standard Test Method for In Place Density and Water Content of Soil and Soil-Aggregate by Nuclear Methods (Shallow Depth)"

ASTM, D1557-12 "Standard Test Methods for Laboratory Compaction Characteristics of Soil Using Modified Effort (56,000 ft-lbf/ft^3 (2,700 kN-m/m^3))"

ASTM, D1883-07e2 "Standard Test Method for CBR (California Bearing Ratio) of Laboratory-Compacted Soils"

ASTM C568 / C568M - 10 "Standard Specification for Limestone Dimension Stone"

Barker, Walter R. (1994) "ACN presentation. FAX to Orv Preston July 8, 1994" (unpublished, attachment 2).

Barker, Walter R. (1994) "Technical summary, review of alpha factors", FAX to Ed Gervais September 9, 1994 (unpublished, attachment 3).

Barker, W.R., and Gonzalez, C.R. (2006) "Independent Evaluation of 6-Wheel Alpha Factor Report", Letter Report to the Federal Aviation Administration, U.S. Army Engineer Research and Development Center, Vicksburg, Mississippi.

Barker, W.R., and Gonzalez, C.R. (2006) "Renovation of the CBR Design Procedure", Paper 02-005, Second International Airports Conference. Sao Paulo, Brazil.

Barker, Walter R., and William Brabston (1975) "Development of a structural design procedure for flexible airport pavements", U. S. Department of Transportation, Federal Aviation Administration Report No. FAA-RD-74-199. Vicksburg, MS: U.S. Army Corps of Engineers, Waterways Experiment Station.

Barker, Walter R., and Carlos R. Gonzalez (1994) "Super-heavy aircraft study", Technical Report GL-94-12. Vicksburg, MS: Waterways Experiment Station, U.S. Army Corps of Engineers.

Boyd, W.K. and C.R. Foster (1950) "Design Curves for Very Heavy Multiple Wheel Assemblies. In Development of CBR Flexible Pavement Design Method for Airfields: A Symposium", Transactions, ASCE, Vol. 115, Paper 2406, pp.534-546.

Brown, D.N. and O.O. Thompson (1973) "Lateral distribution of aircraft traffic", Miscellaneous paper S-73-56. Vicksburg, MS: Waterways Experiment Station, U.S. Army Corps of Engineers

Cooksey, D. L., and D. M. Ladd (1971) "Pavement design for various levels of traffic volume" Air Force Weapons Laboratory, Air Force Systems Command, Technical Report No. AFWL-TR-70-133 (attachment 1). Vicksburg, MS: Waterways Experiment Station.

Department of the Army, Corps of Engineers, Sacramento District (1948) "Accelerated traffic test at Stockton Airfield", Stockton, California.

Duncan, J. M. and Chang, C. Y. (1970) "Nonlinear Analysis of Stress and Strain in Soils", Journal of the Soil Mechanics and Foundations Division, Proceedings of the American Society of Civil Engineers.

Fine, L. and J. Remington (1972) "The Corps of Engineers : construction in the United States", Washington, Office of the Chief of Military History, U.S. Army.

Gonzalez, C. R., W. R. Barker, and A. Bianchini (2012) "Reformulation of the CBR procedure", ERDC/GSL TR-12-16, Vol 1. Vicksburg, MS: U.S. Army Engineer Research and Development Center.

Hayhoe, G. F. (2004) "Traffic testing results from the FAA's National Airport Pavement Testing Facility", Proceeding of the 2nd International Conference on Accelerated Pavement Testing, University of Minnesota, Minneapolis, MN

Hinton, E and Owen, D.R.J. (1989) "Finite Element Programming", Academic Press Inc, San Diego CA 92101

Headquarters, Department of the Army (HQDA). (1952) "Design of Flexible Airfield Pavements for Multiple-Wheel Land Gear Assemblies, Report No. I Test Section with Lean-Clay Subgrade", Technical Manual TM 3-349, Washington, DC.

International Civil Aviation Organization (ICAO) (1983) "Aerodrome design manual", Doc 9157-AN/901. Montreal: International Civil Aviation Organization.

Information and Technology Platform for Transport, Infrastructure and Public Space (CROW) (2004) "The PCN Runway Strength Rating and Load Control System", Report D04-09. Amsterdam, the Netherlands.

Kondner, K. L. (1963) "Hyperbolic stress-strain response: Cohesive soils", J. of the Soil Mechanics and Foundation, ASCE 89(SM 1):115-143.Kulhawy, F. H. Duncan, J. M. and Bolton,

S. H. Bolton (1969) "Finite element analyses of stresses and movements in embankments during construction", University of California, Berkeley, Vicksburg, MS: U.S. Army Engineer

Waterways Experiment Station.Ledbetter, R. H., J. L. Rice, H. H. Ulery, F. W. Kearney, J. B. Gambill, and J. W. Hall (1971) "Multiple-wheel heavy gear load pavement tests", Technical Report S-71-17. Vicksburg, MS: U.S. Army Engineer Waterways Experiment Station.

Jumikis, A. R. (1964) "Mechanics of soils". Princeton, NJ: D. Van Nostrand Company, Inc.

Jumikis, A. R. (1969) "Stress distribution tables for soil under concentrated loads", College of Engineering, Rutgers University, Engineering Research Publication No. 48.

Love, A.E.H. (1929) "The Stress Produced in a Semi-Infinite Solid by Pressure on Part of the Boundary", Phil. Trans. R. Soc. 228 (659-669) 377-420, London, England.

Middlebrooks, T.A. and G.E. Bertram (1950) "Adaptation to the Design of Airfield Pavements" Transactions, ASCE, pp.468-470.

Porter, O. J. & Co. (1949) "Accelerated Traffic Test at Stockton Airfield Stockton, California (Stockton Test No. 2)", Corps of Engineers Sacramento District, Department of the Army

Ullidtz, P. (1998) "Modeling flexible pavement response and performance", Polyteknish Forlag.
Unified Facilities Guide Specifications (UFGS) 32 12 15.13 "Hot-Mix Asphalt Airfield Paving", U.S. Army Corps of Engineers

Vedros, P. J. (1960) "Study of lateral distribution of aircraft traffic on runways" Miscellaneous Paper No. 4-369. Vicksburg, MS: U.S. Army Engineer Waterways Experiment Station.

Waterways Experiment Station (1951) "Collection of letter reports on flexible pavement design curves", Miscellaneous Paper No. 4-61. Vicksburg, MS: U.S. Army Corps of Engineers.

Waterways Experiment Station (1951) "Investigations of pressures and deflections for flexible pavements", Technical Memorandum No. 3-323. 1951. Vicksburg, MS: U.S. Army Corps of Engineers.

Waterways Experiment Station (1956) "Mathematical expression of the CBR relations", Technical Report No. 3-441. Vicksburg, MS: U. S. Army Corps of Engineers.

Waterways Experiment Station (1956) "Instructions for use of Field In-place California Bearing Ratio Apparatus", Instruction Report No. 1. Vicksburg, MS: U. S. Army Corps of Engineers.

Waterways Experiment Station (1955) "Design of flexible airfield pavements for multiple-wheel landing gear assemblies, Report No. 2, Analysis of Existing Data", Technical Memorandum No. 3-349, June 1955. Vicksburg, MS: U.S. Army Corps of Engineers.

Waterways Experiment Station (1945) "Certain Requirements for Flexible Pavement Design for B 29 Planes", Vicksburg, MS: U.S. Army Corps of Engineers.

Waterways Experiment Station (1949) " Minutes of conference on stress distribution investigation 21-22 December 1949", Conference on Stress Distribution Investigation. Vicksburg, MS: U.S. Army Corps of Engineers.

Waterways Experiment Station (1959) "Developing a set of CBR design curves. Instruction Report No. 4", Vicksburg, MS: U.S. Army Corps of Engineers.

Waterways Experiment Station (1971) "Multiple-wheel heavy gear load pavement tests" Technical Report S-71-17. Vicksburg, MS: U.S. Army Corps of Engineers.

APPENDIX A - HYPERBOLIC TRANSFORMATION OF LABORATORY DATA USED FOR NON-LINEAR FINITE ELEMENT MODELING

A.1 Introduction

This appendix contains a summary of the laboratory testing sequence designed to obtain the hyperbolic model parameters required for non-linear modeling using an axi-symmetric finite element method. Figures A.1 and A.2 shows pictures of the test chambers for the CH clay material before and after failure occurred. Figures A.3 and A.4 show pictures of the test chamber used for the crushed gravel subbase and crushed limestone base. Tables A.1 and A.2 and Figure A5 illustrate the testing sequence follow during triaxial laboratory test for the base, subbase and subgrade materials. Figures A.6 through A.7 show the deviator stress curves and the transformed hyperbolic deviator stress curves resulting from laboratory samples.

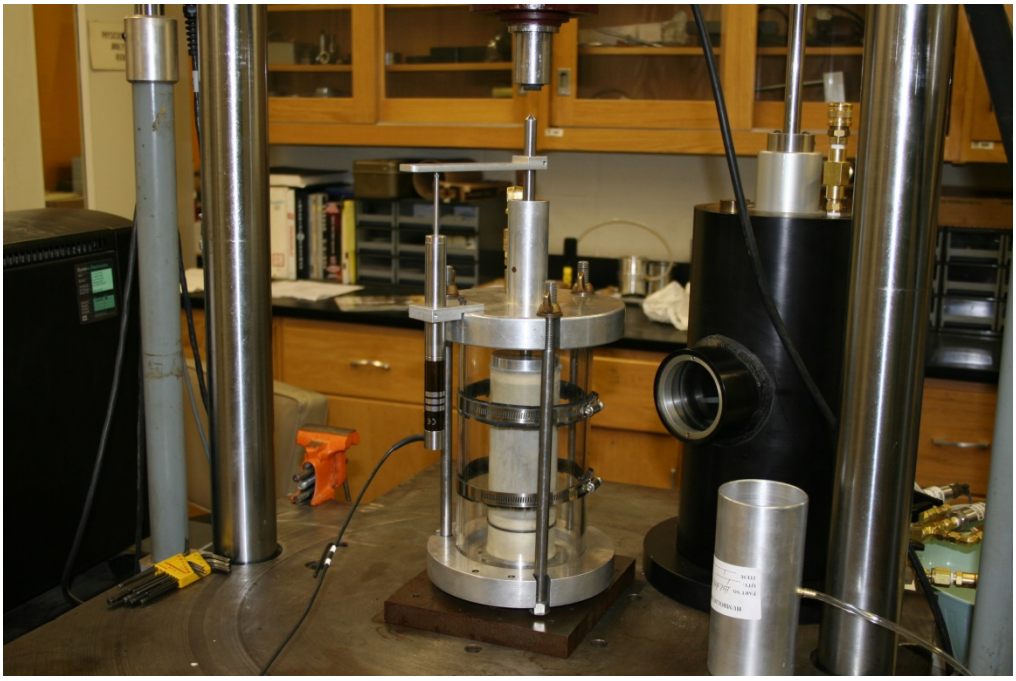

Figure A.1 Triaxial Chamber used for Subgrade CH Clay Material

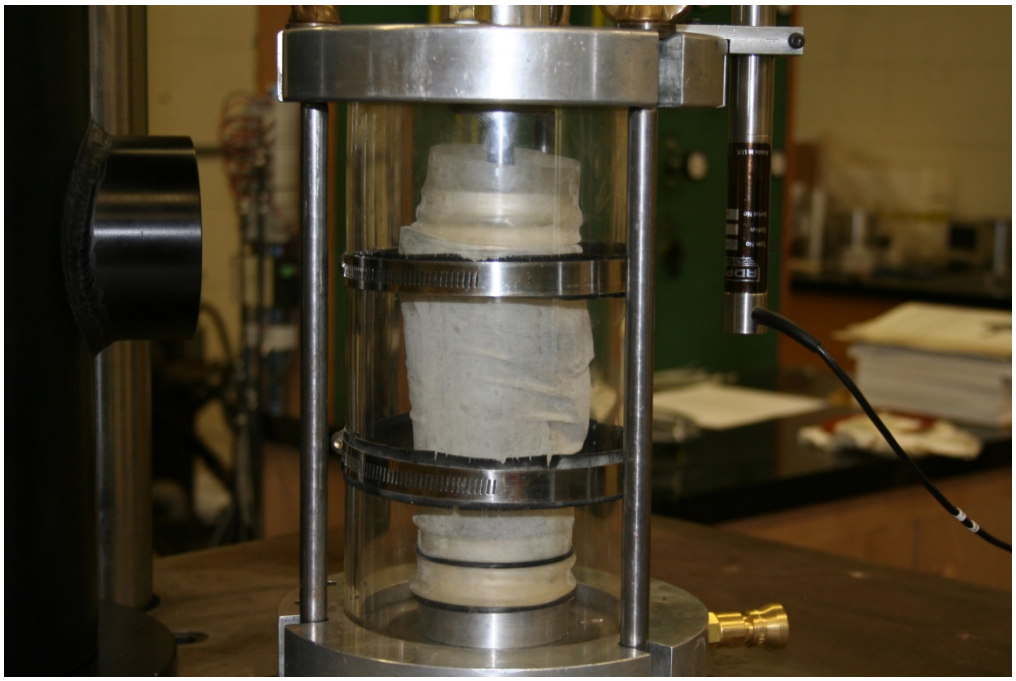

Figure A.2 Subgrade CH Clay Material after Failure

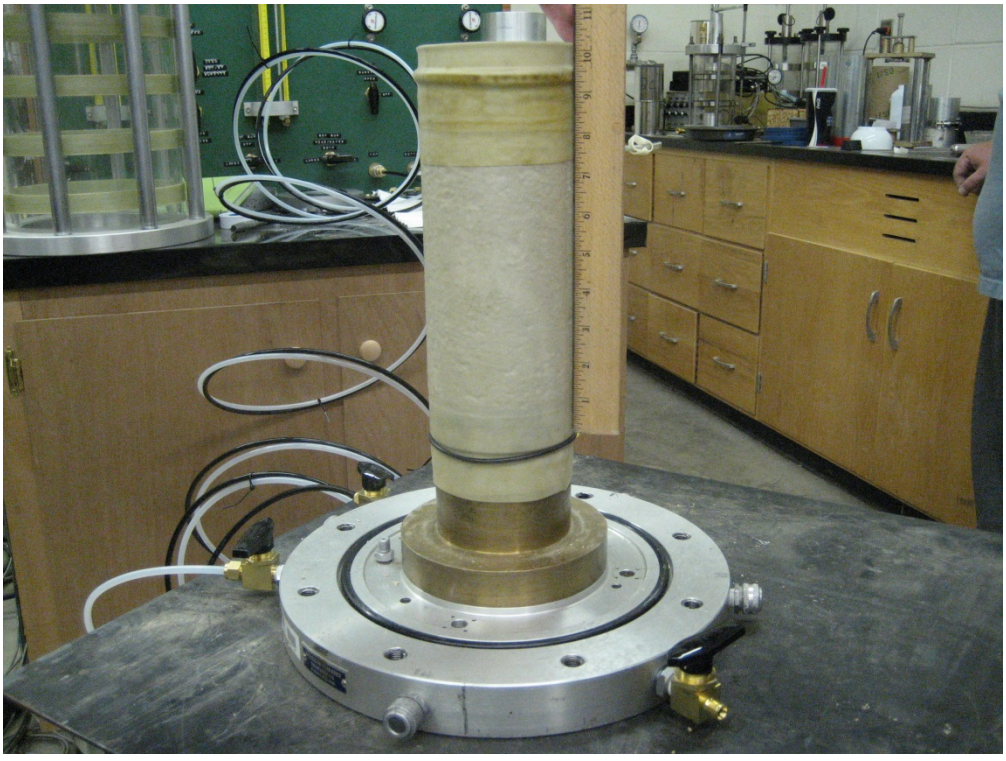

Figure A.3 Triaxial Chamber used for Subbase and Base Materials

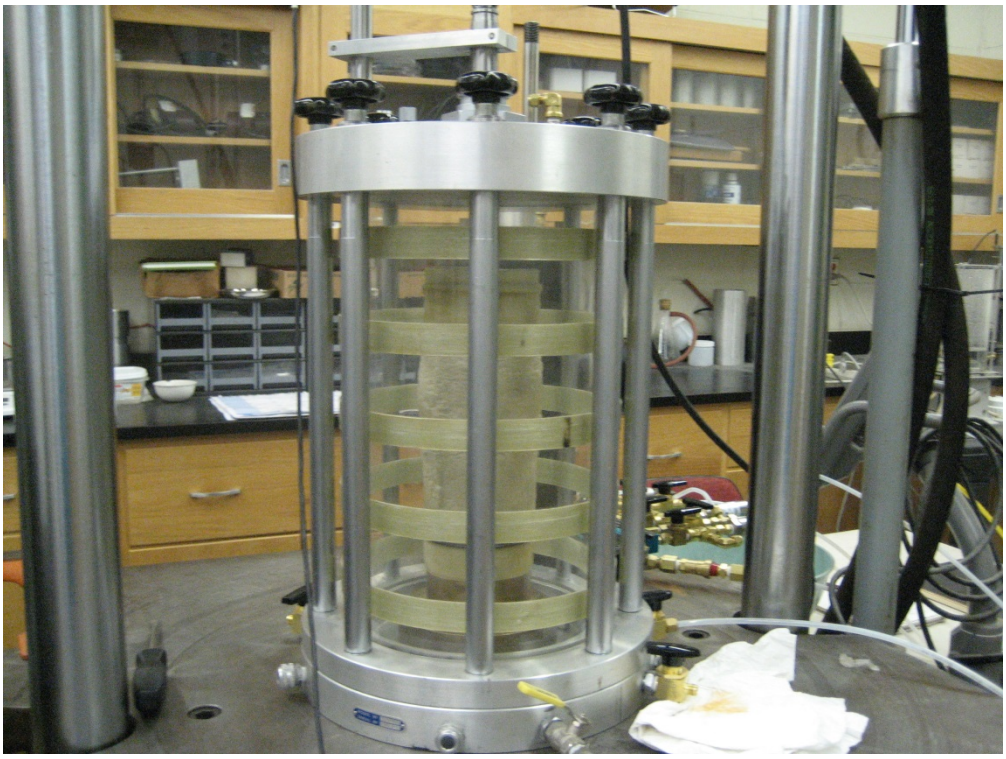

Figure A.4 Example of Subbase Material after Failure

Table A.1 Testing Sequences for Base/Subbase Materials (AASHTO DESIGNATION T 307-99)											
	Confining	Max. Axial	Cyclic	Constant	No. of Load	Required Load for Max Axial Load, lb			Required Load for Min Axial Load, lb		
Sequence	Pressure, S3	Stress, Smax	Stress	Stress	Applications	Sample Size Diameter			Sample Size Diameter		
No.	psi	psi	psi	psi		2.8-in x 5.6-in	4-in x 6-in	6-in x 12-in	2.8-in x 5.6-in	4-in x 6-in	6-in x 12-in
0	15	15	13.5	1.5	500-1000	92.4	188.5	424.1	9.2	18.8	42.4
1	3	3	2.7	0.3	100	18.5	37.7	84.8	1.8	3.8	8.5
2	3	6	5.4	0.6	100	36.9	75.4	169.6	3.7	7.5	17.0
3	3	9	8.1	0.9	100	55.4	113.1	254.5	5.5	11.3	25.4
4	5	5	4.5	0.5	100	30.8	62.8	141.4	3.1	6.3	14.1
5	5	10	9.0	1.0	100	61.6	125.7	282.7	6.2	12.6	28.3
6	5	15	13.5	1.5	100	92.4	188.5	424.1	9.2	18.8	42.4
7	10	10	9.0	1.0	100	61.6	125.7	282.7	6.2	12.6	28.3
8	10	20	18.0	2.0	100	123.2	251.3	565.5	12.3	25.1	56.5
9	10	30	27.0	3.0	100	184.7	377.0	848.2	18.5	37.7	84.8
10	15	10	9.0	1.0	100	61.6	125.7	282.7	6.2	12.6	28.3
11	15	15	13.5	1.5	100	92.4	188.5	424.1	9.2	18.8	42.4
12	15	30	27.0	3.0	100	184.7	377.0	848.2	18.5	37.7	84.8
13	20	15	13.5	1.5	100	92.4	188.5	424.1	9.2	18.8	42.4
14	20	20	18.0	2.0	100	123.2	251.3	565.5	12.3	25.1	56.5
15	20	40	36.0	4.0	100	246.3	502.7	1131.0	24.6	50.3	113.1
Qtest*	5	---	---	---	---	---	---	---	---	---	---
* Strain Rate = 1% /minute											
Note: 1 inch=25.4 mm, 1 psi= 6.9 kPa, 1 lb=4.45 kN											

Table A.2 Testing Sequences for Subgrade Soil (AASHTO DESIGNATION T 307-99)

Sequence No.	Confining Pressure, S3 psi	Max. Axial Stress, Smax psi	Cyclic Stress psi	Constant Stress psi	No. of Load Applications	Required Load for Max Axial Stress, psi Sample Size Diameter			
						2.8-in x 5.6-in	4-in x 6-in	6-in x 12-in	3.4-in x 6.8-in
0	6.0	4.0	3.6	0.4	500-1000	24.6	50.3	113.1	36.3
1	6.0	2.0	1.8	0.2	100	12.3	25.1	56.5	18.2
2	6.0	4.0	3.6	0.4	100	24.6	50.3	113.1	36.3
3	6.0	6.0	5.4	0.6	100	36.9	75.4	169.6	54.5
4	6.0	8.0	7.2	0.8	100	49.3	100.5	226.2	72.6
5	6.0	10.0	9.0	1.0	100	61.6	125.7	282.7	90.8
6	4.0	2.0	1.8	0.2	100	12.3	25.1	56.5	18.2
7	4.0	4.0	3.6	0.4	100	24.6	50.3	113.1	36.3
8	4.0	6.0	5.4	0.6	100	36.9	75.4	169.6	54.5
9	4.0	8.0	7.2	0.8	100	49.3	100.5	226.2	72.6
10	4.0	10.0	9.0	1.0	100	61.6	125.7	282.7	90.8
11	2.0	2.0	1.8	0.2	100	12.3	25.1	56.5	18.2
12	2.0	4.0	3.6	0.4	100	24.6	50.3	113.1	36.3
13	2.0	6.0	5.4	0.6	100	36.9	75.4	169.6	54.5
14	2.0	8.0	7.2	0.8	100	49.3	100.5	226.2	72.6
15	2.0	10.0	9.0	1.0	100	61.6	125.7	282.7	90.8
Qtest*	4.0	---	---	---	---	---	---	---	---

* Strain Rate=1% /minute

Note: 1 inch=25.4 mm, 1 psi= 6.9 kPa

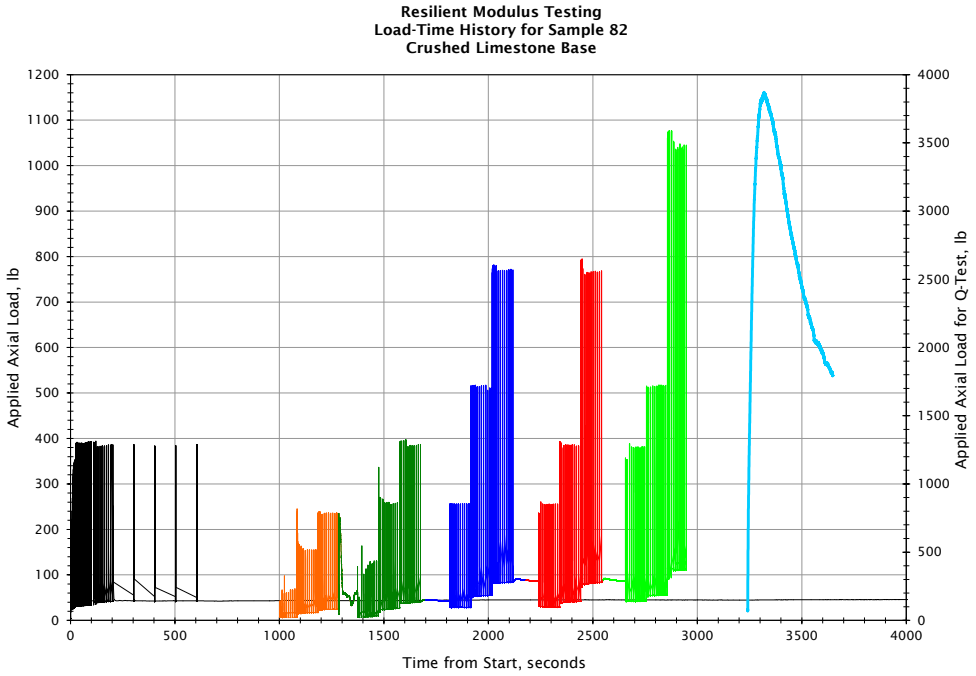

Figure A.5 Plot Showing Example of Triaxial Testing Sequence for the Crushed Limestone Base (1 lb=4.45 kN)

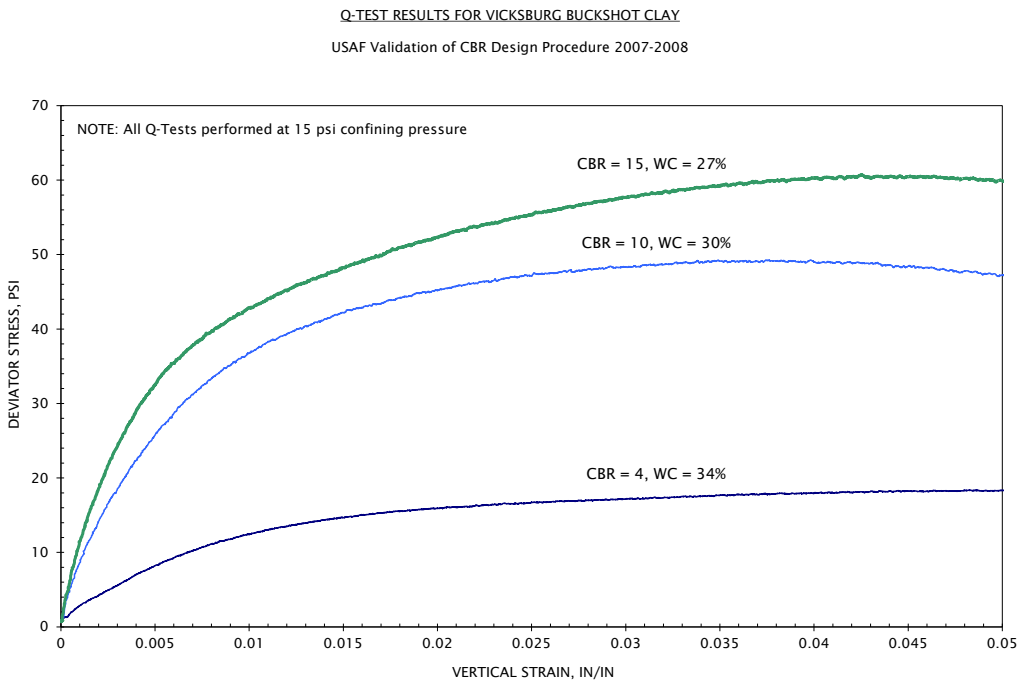

Figure A.6 Triaxial Test Results for Vicksburg Buckshot Clay (CH) Used as Subgrade Layer (1 psi=6.9 kPa)

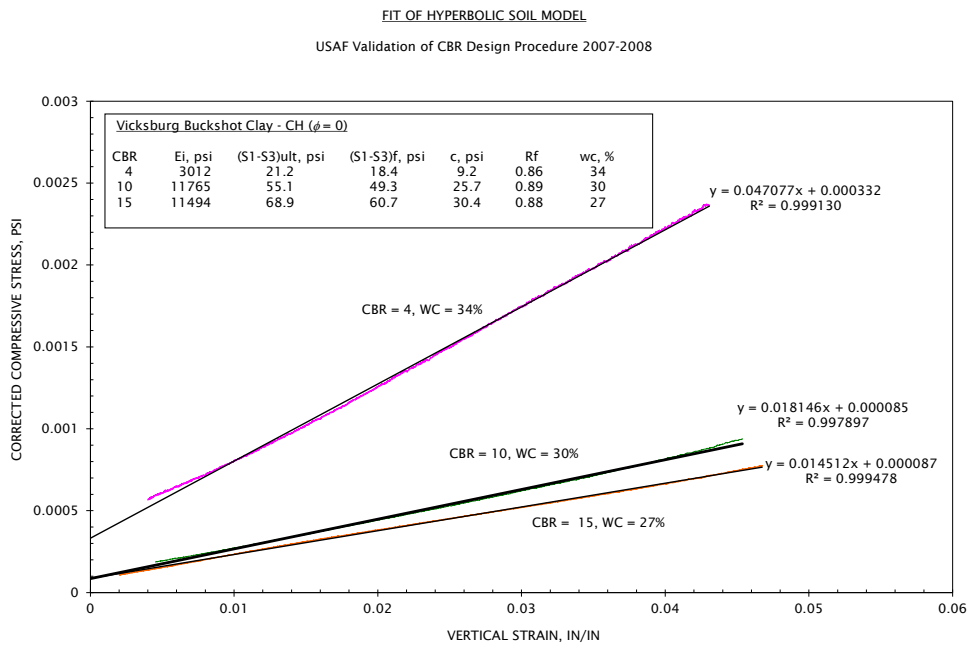

Figure A.7 Hyperbolic Transformation and data fit of Triaxial Test Results for Vicksburg Buckshot Clay (CH) Used as Subgrade Layer (1 psi=6.9 kPa)

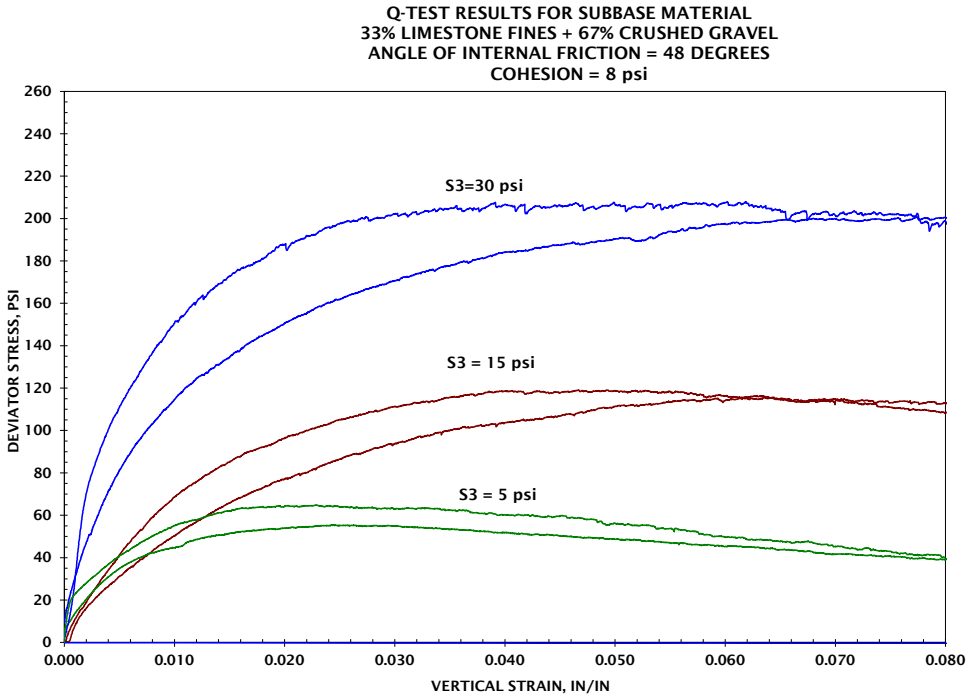

Figure A.8 Triaxial Test Results for Crushed Gravel Mix Used as Subbase Layer (1 psi=6.9 kPa)

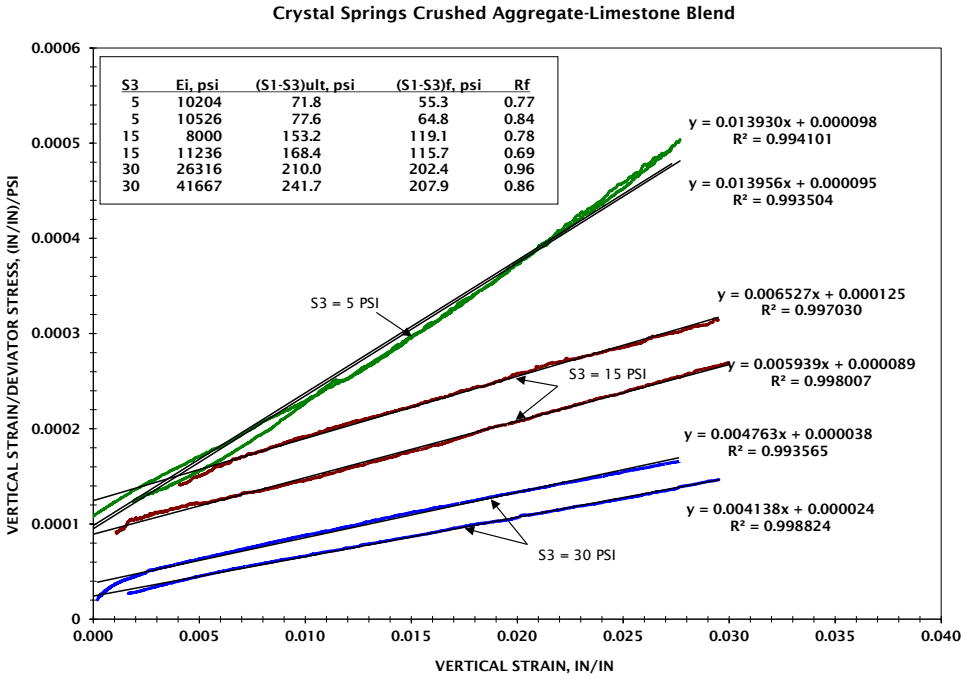

Figure A.9 Hyperbolic Transformation of Triaxial Test Results for Crushed Gravel Mix Used as Subbase Layer (1 psi=6.9 kPa)

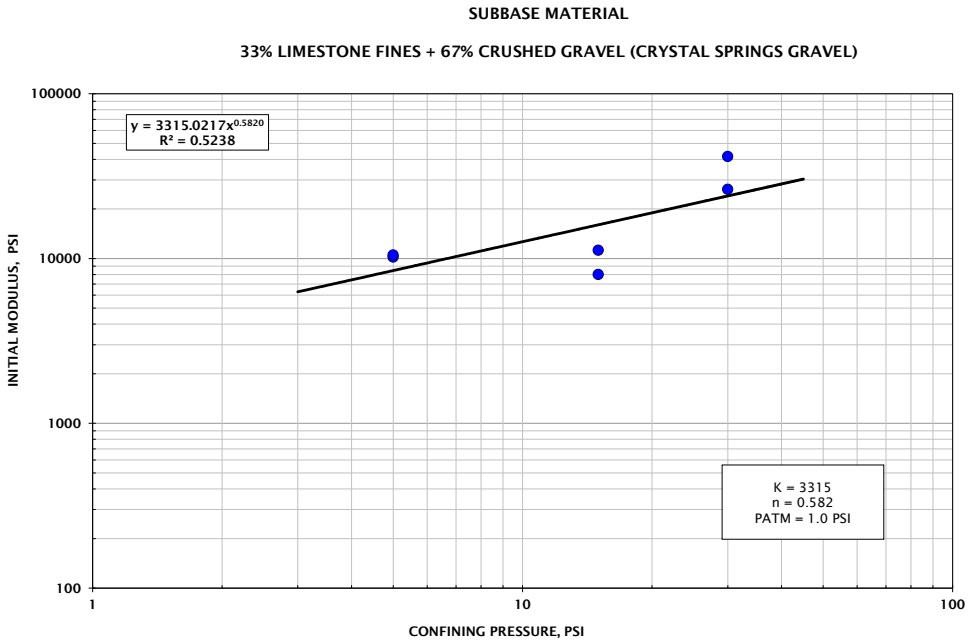

Figure A.10 Relationship Between Confining Pressure and Initial Modulus for Crushed Gravel Mix Used as Subbase Layer (1 psi=6.9 kPa)

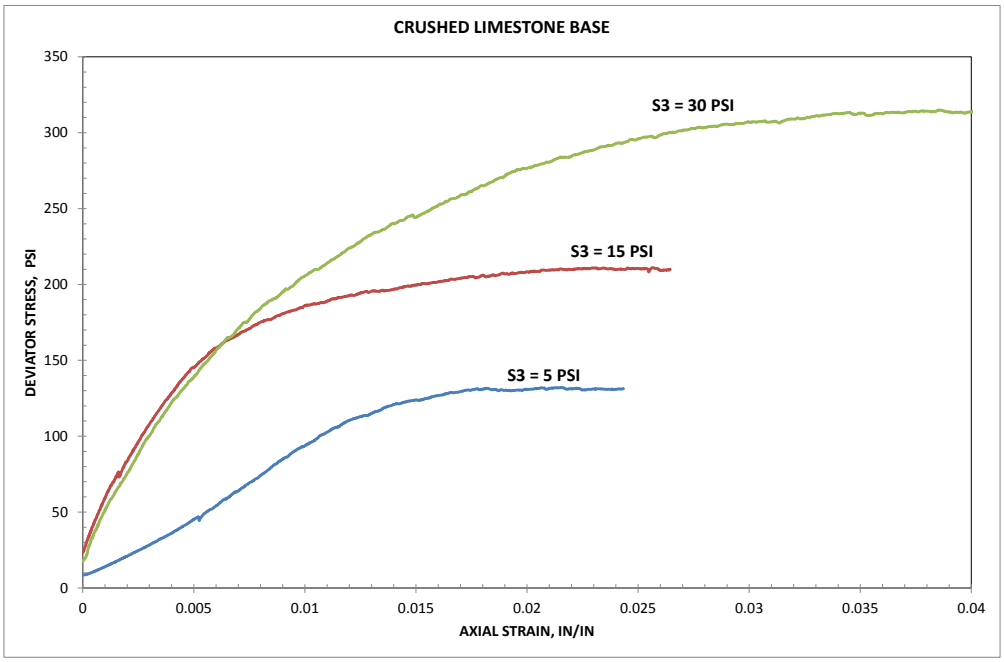

Figure A.11 Triaxial Test Results for Crushed Stone Mix Used as Base Layer (1 psi=6.9 kPa)

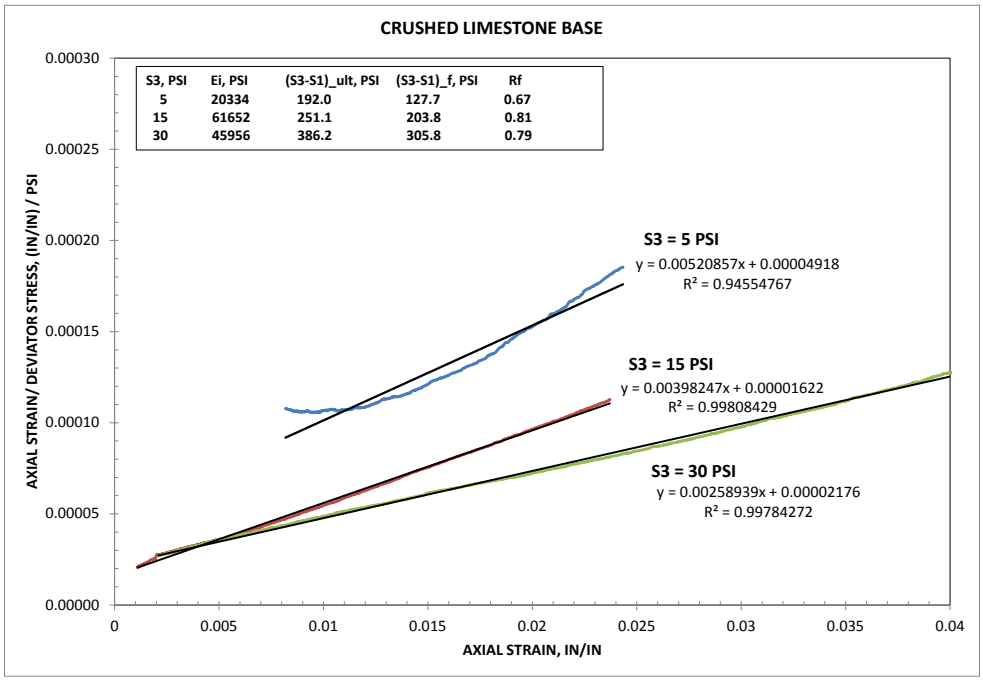

Figure A.12 Hyperbolic Transformation of Triaxial Test Results for Crushed Stone Mix Used as Base Layer (1 psi=6.9 kPa)

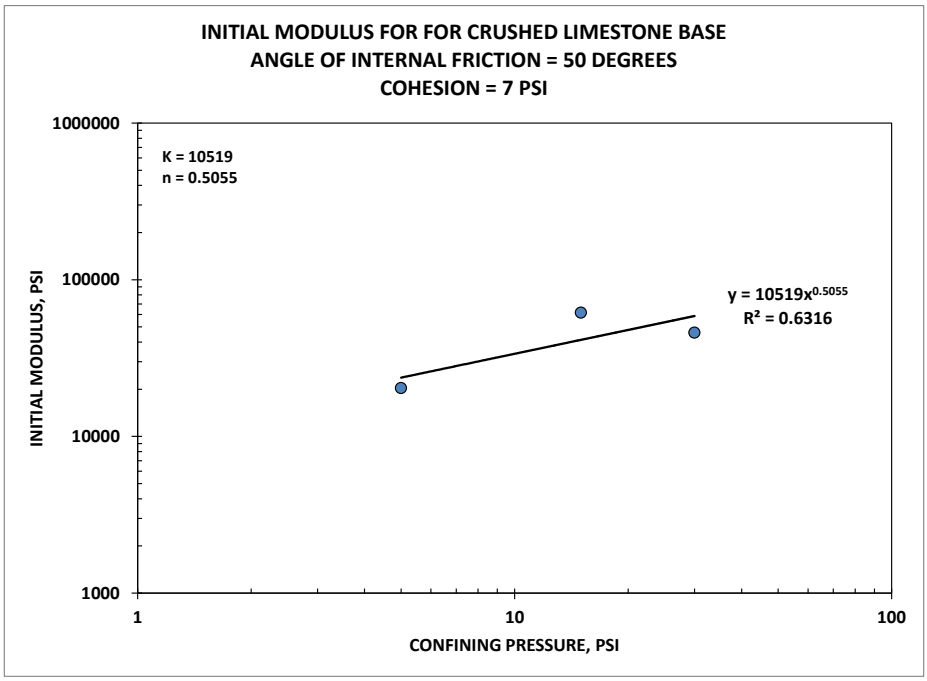

Figure A.13 Relationship between confining pressure and initial modulus for crushed gravel mix used as base layer (1 psi=6.9 kPa)

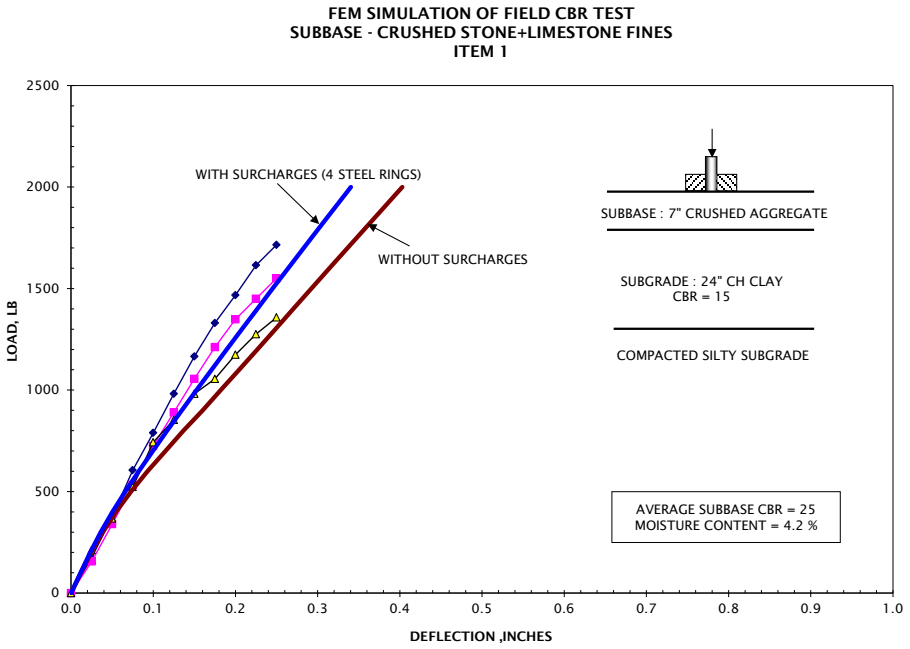

Figure A.14 Finite element simulation of field CBR test on surface of subbase layer Item 1 (1 inch=25.4 mm, 1 lb=4.45 kN)

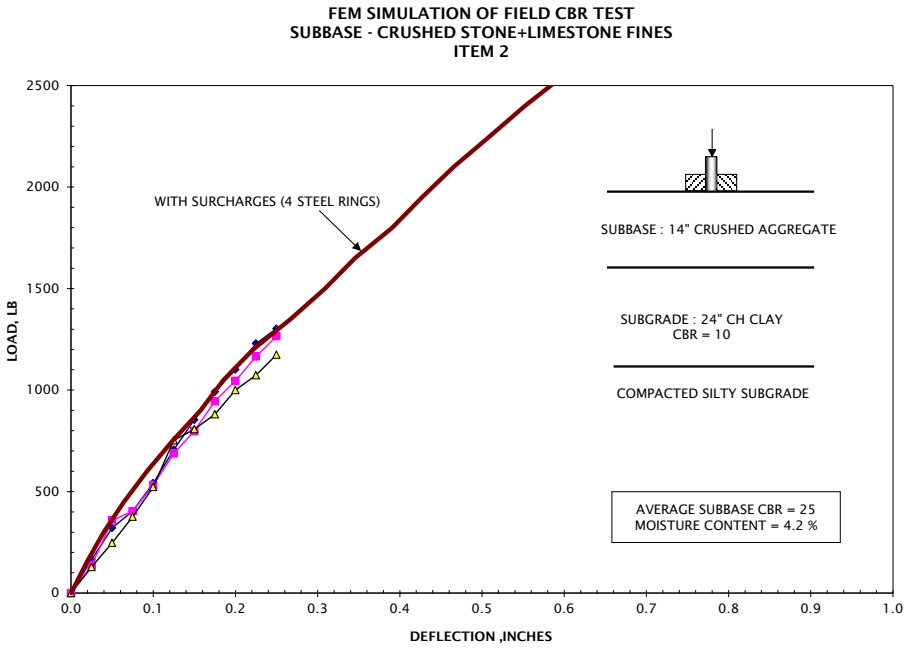

Figure A.15 Finite element simulation of field CBR test on surface of subbase layer Item 2 (1 inch=25.4 mm, 1 lb=4.45 kN)

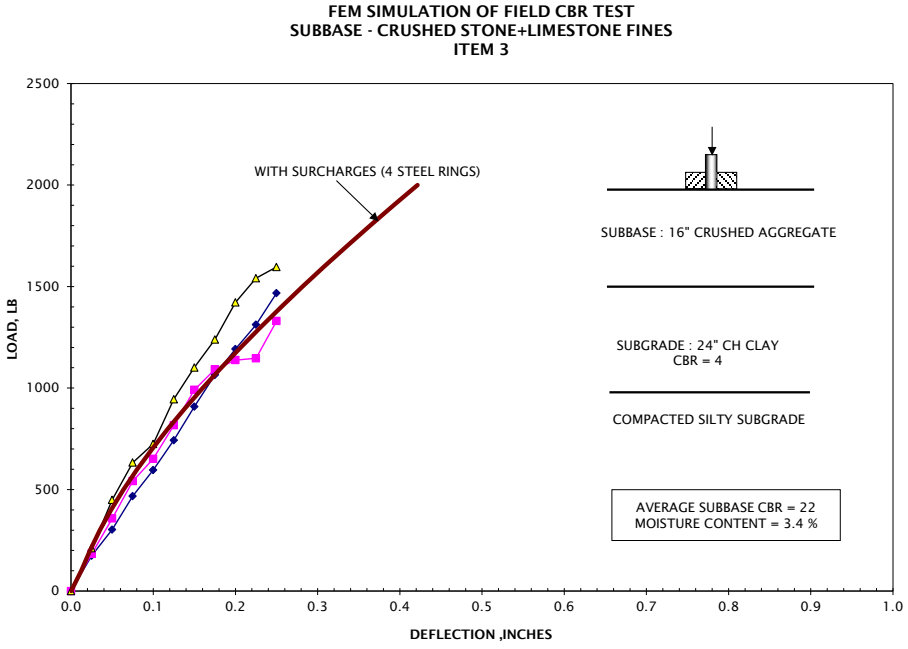

Figure A.16 Finite element simulation of field CBR test on surface of subbase layer Item 3 (1 inch=25.4 mm, 1 lb=4.45 kN)

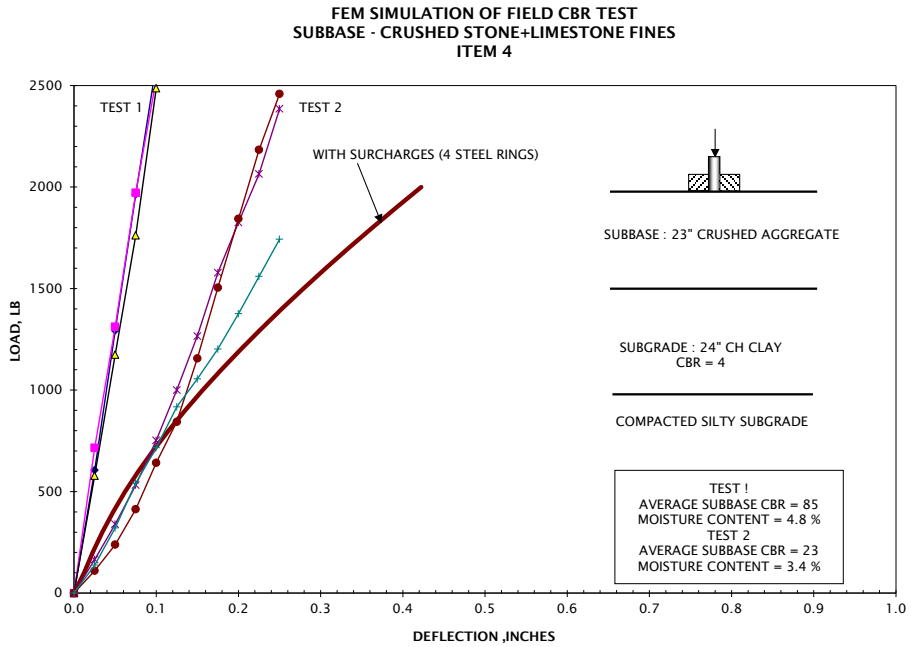

Figure A.17 Finite element simulation of field CBR test on surface of subbase layer Item 4 (1 inch=25.4 mm, 1 lb=4.45 kN)

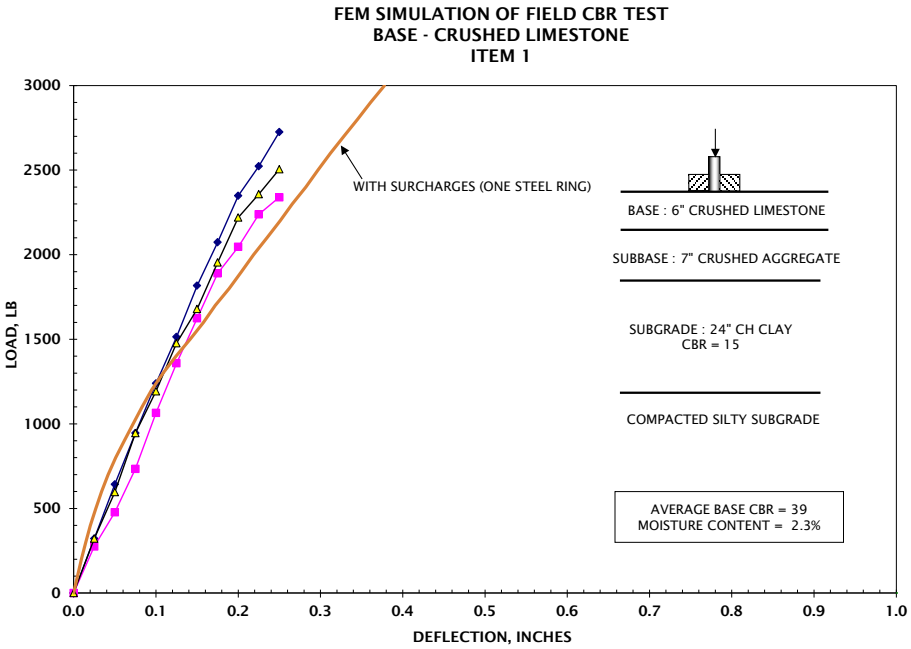

Figure A.18 Finite element simulation of field CBR test on surface of base layer Item 1 (1 inch=25.4 mm, 1 lb=4.45 kN)

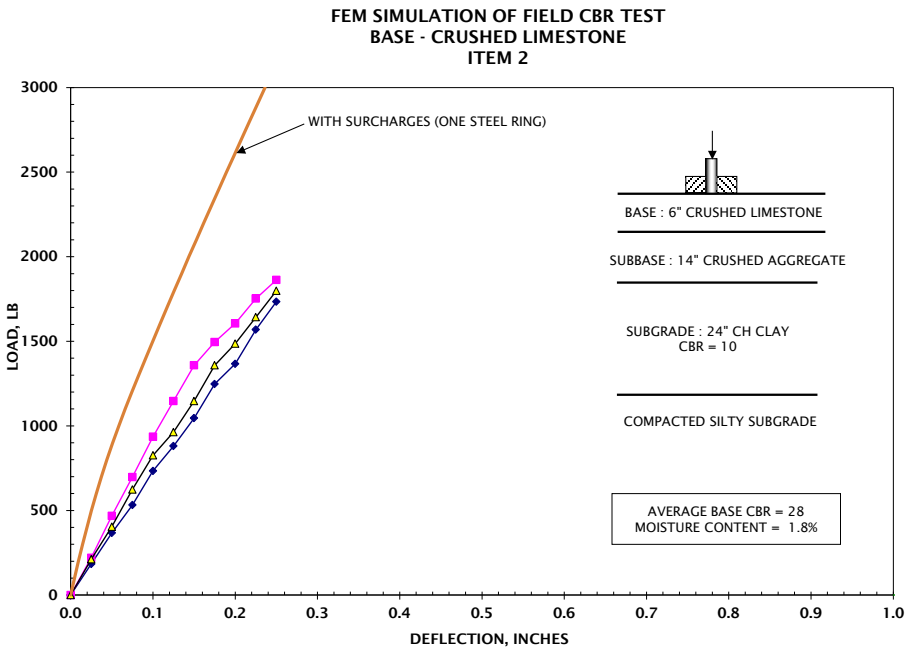

Figure A.19 Finite element simulation of field CBR test on surface of subbase layer Item 2

(1 inch=25.4 mm, 1 lb=4.45 kN)

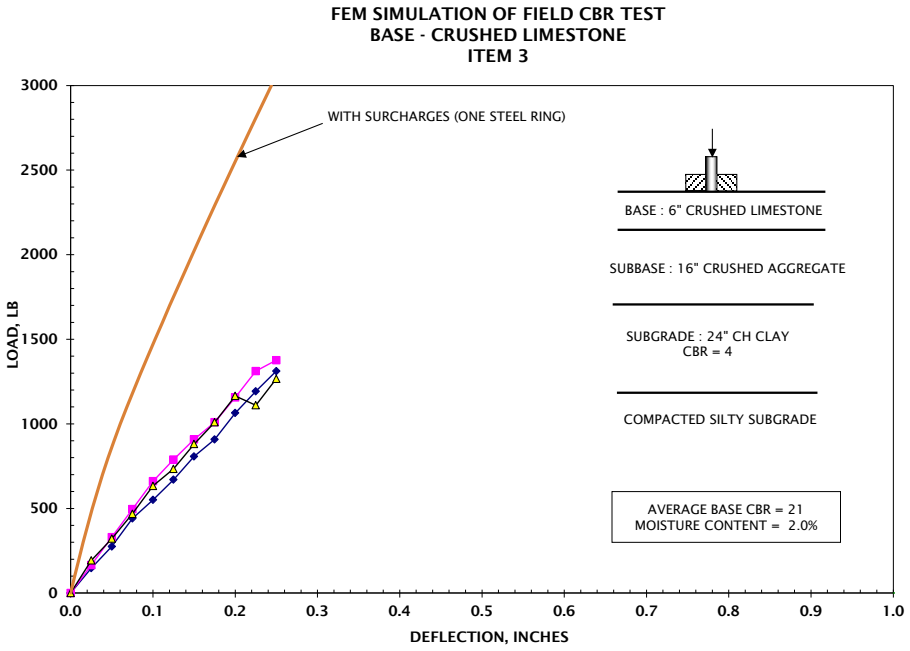

Figure A.20 Finite element simulation of field CBR test on surface of subbase layer Item 3

(1 inch=25.4 mm, 1 lb=4.45 kN)

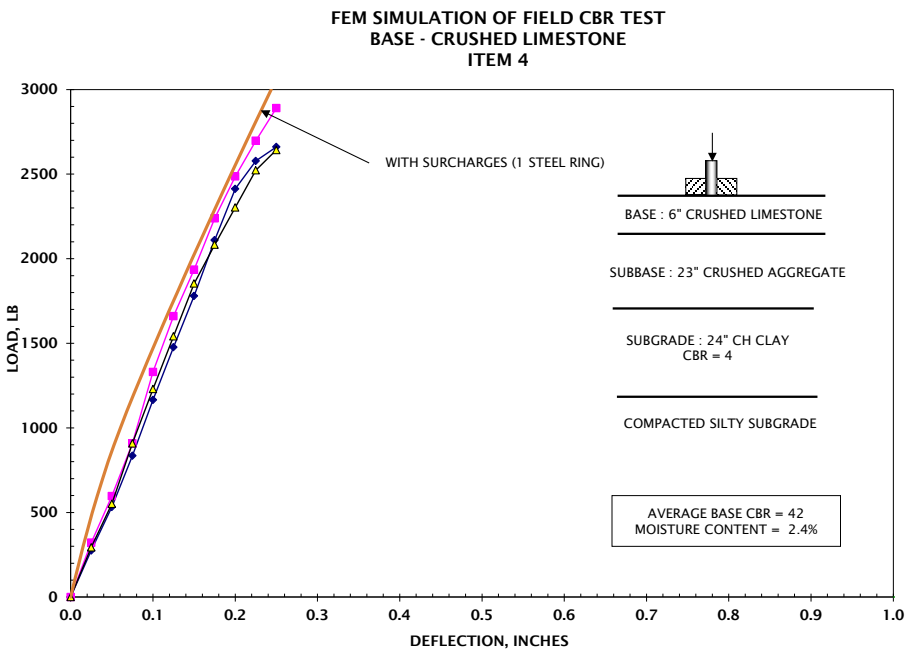

Figure A.21 Finite element simulation of field CBR test on surface of subbase layer Item 4 (1 inch=25.4 mm, 1 lb=4.45 kN)

APPENDIX B - VERIFICATION OF BETA CRITERIA USING DATA FROM LAS CRUCES EVALUATION REPORT

B.1 Introduction

On 30 November and 1 December 2010, external consultants reviewed the proposed CBR-Beta procedure for design of flexible pavements. The recommendation of the consultants was to proceed with the implementation of the proposed pavement design procedure. Following the review of the proposed design procedure, an evaluation report of the Las Cruces airport was received from Dr. Craig Rutland, U.S. Air Force Civil Engineer Support Agency (AFCESA). Excerpts from this report are included in Appendix C. It was understood that Dr. Rutland would like to use the data contained in the report as additional verification for the CBR-Beta design procedure. Portions of the evaluation report are attached for convenient reference.

B.2 Discussion

The Las Cruces evaluation report, dated October 2004, is a report of a pavement investigation conducted as a result of damage to the main runway at Las Cruces, NM, caused by operations of Air Force B-757, C-17 and C-130 aircraft. The damage is described in the following paragraphs taken from the report.

"Pavement Surface Condition:

The runway was divided into two features with Runway 12/30 being the dividing line.

The Runway 22 end feature (R01A-1) has a cursory PCI rating of Failed due to ruts within 25 feet (7.62 m) of centerline on both sides. The ruts are as deep as 2" (51 mm) on the Runway 22 end and decrease in severity to the Runway 12/30 intersection where they are less than ½" (12.7 mm) in depth.

The Runway 04 end feature (R01A-2) has a cursory PCI rating of Very Poor due to ruts 25 feet (7.62 m) of centerline on both sides. The ruts are ¼" (6.4 mm) or less on the Runway 04 end with the exception of two small areas that have ruts as deep as ¾" (19 mm) identified in drawings in Appendix A. The runway asphalt exhibits medium and low severity alligator cracking in areas

with heavy rutting, medium and low severity block cracking, depressions, raveling, longitudinal/transverse cracking, and low severity slippage."

As can be seen in the report, the ruts were as deep as 2" (51 mm) on the Runway 22 end with decreasing rut depth toward the center of the runway. Less severe ruts were present on the Runway 04 end with two small areas of more severe ruts a short distance from the end. The location of photo C.1 is identified as being in the touchdown area of Runway 22. The tire imprints would seem to indicate that the ruts in this area were made by the C-17 aircraft. The location of photo C.2 is not identified but it is assumed that the photograph shows the more severe ruts at the end of Runway 22. Again the pattern of the ruts would indicate the ruts were made by the C-17.

The report states the rutting extended 25' (7.62 m) on both sides of the centerline. The outside tires for the B-757 are about 13.5' (4.12 m) from the centerline of the aircraft and outside tires for the C-17 tires are about 16' (4.9 m) from the centerline of the aircraft. With these spacing it is quite likely there is some overlapping of tire paths for the two aircraft. Since the reports states that the operations of the Air Force aircraft had been recent, it is assumed the Runway 22 would have been the primary runway for takeoffs and landings, thus the runway end with the greatest damage would have been subjected to takeoff traffic.

Traffic volume and the aircraft weights are not given for any of the aircraft. The base, subbase and subgrade strengths were measured using the DCP with correlations made to CBR. No field CBR tests were conducted to measure CBR directly. Without traffic volume, aircraft weights and reliable measurements of material strengths, the reliability of the data as a data point would be very low and may even give misleading information. Even though the data are considered to have low fidelity, with a number of assumptions the data can be used to provide a rough verification of the criteria primarily at failures at low pass levels.

B.3 Analysis

To make the analysis, a number of assumptions are necessary. The first assumptions are in regard to the applied aircraft traffic. Since no aircraft weights are given, it was assumed that on takeoffs, the aircraft would be at the design weights. The C-130 is a much lighter aircraft, and the rutting was at a location wider than the C-130 gear; therefore, the C-130 was not used in the analysis. For traffic volume there had to be at least one takeoff for the C-17 and one for the B-757, and if it is assumed the tires overlapped, there would have been a minimum of four coverages of the aircraft tires.

The strength of base was given as 20 CBR and the strength of subbase was given as 6 CBR. The thickness of asphalt above the base was given as 3.5 in. (89 mm) and the thickness above the subbase was given as 12.5 in. (318 mm). It was assumed that the strength and thickness data are averages and that there would be some variability in the data. The airfield is in a high plains area in which the soil conditions could be unusually uniform. The report states that the runway had recently received a slurry seal treatment; therefore, it was assumed that the asphalt surface contained some type of cracking. The fact that more severe rutting was at the end of the runway than at some distance from the end could indicate that the pavement was either weaker toward the end of the runway or that the decreasing rut depth was due to decreasing load as the aircraft gained speed during takeoff. To show the effect of possible variation in base strengths different base strengths were assumed. For the subbase only, the 6 CBR strength was used (this being considered as the lowest strength existing).

B.4 CBR-Beta Criteria

The data that were developed using the CBR-Beta criteria are given in Tables C-2, C-3, C-4 and C-5. For making a comparison of Beta criteria with the Las Cruces pavement performance, the traffic volume to failure was assumed to be four coverages, the strength of the base was assumed to be 20 CBR and the strength of subbase was assumed to be 6 CBR. The comparison developed is shown in Figure C.1. The comparison shows the predicted performance to be better than the observed performance. In the tables it is seen that when considering the 20 CBR base, the CBR-Beta criteria predicts failure at 11 coverages and 22 coverages for the B-757 and C-17, respectively. When considering the subbase as a 6 CBR layer, the predicted coverages

to failure are 15 coverages and 7 coverages for the B-757 and C-17, respectively. In analyzing the comparison shown in Figure C.1 between the Beta criteria and observed performance, it should be remembered that the four coverages to failure were considered to be a minimum level of traffic applied to the pavement and that the 20 CBR was the average base strength. If the base CBR had been as low as 12 or the traffic volume had been greater than four coverages, the predicted pavement performance would have been in-line with the observed pavement performance. When considering the possibility that the failure could be caused by shear in the subbase, the seven coverages predicted to failure for the C-17 is not too far from the assumed coverages to failure. From these comparisons, it is seen that the proposed design criteria predicts performance that compares well with the observed performance. Again, it is reiterated that the predicted performance is based on gross assumptions of aircraft loads, traffic volume and material strengths.

B.5 Conclusions

The conclusions are presented in the absence of reliable data on material strengths, aircraft weights and traffic volume, and should be viewed as having a low degree of reliability. The conclusions are as follows:

- The failures observed were likely to have been caused by the C-17 overloading the subbase material.
- The agreement between the predicted traffic level of 7 coverages, as predicted by the CBR-Beta, and the estimated minimum traffic that may have been applied to the pavement is considered to be at an acceptable level.
- Given the material strengths, thicknesses and aircraft at the design loads, both the CBR-Beta criteria and the minimum thickness criteria would have predicted early failure of the pavement.

APPENDIX C - PAVEMENT EVALUATION LAS CRUCES INTERNATIONAL AIRPORT

C.1 Excerpt from Las Cruces Evaluation Report, New Mexico, ICAO:KLRU, October 2004 APE-668

"Pavement Surface Condition

The runway was divided into two features with Runway 12/30 being the dividing line.

The Runway 22 end feature (R01A-1) has a cursory PCI rating of Failed due to ruts within 25 feet (7.62 m) of centerline on both sides. The ruts are as deep as 2" (51 mm) on the Runway 22 end and decrease in severity to the Runway 12/30 intersection where they are less than ½" (13 mm) in depth.

The Runway 04 end feature (R01A-2) has a cursory PCI rating of Very Poor due to ruts 25 feet (7.62 m) of centerline on both sides. The ruts are ¼" (6 mm) or less on the Runway 04 end with the exception of two small areas that have ruts as deep as ¾" (19 mm) identified in drawings in Appendix A. The runway asphalt exhibits medium and low severity alligator cracking in areas with heavy rutting, medium and low severity block cracking, depressions, raveling, longitudinal/transverse cracking, and low severity slippage."

C.2 Photographs from Las Cruces Evaluation Report

Figure C.1 Rutting in asphalt with tire imprints – Runway 22 touchdown area.

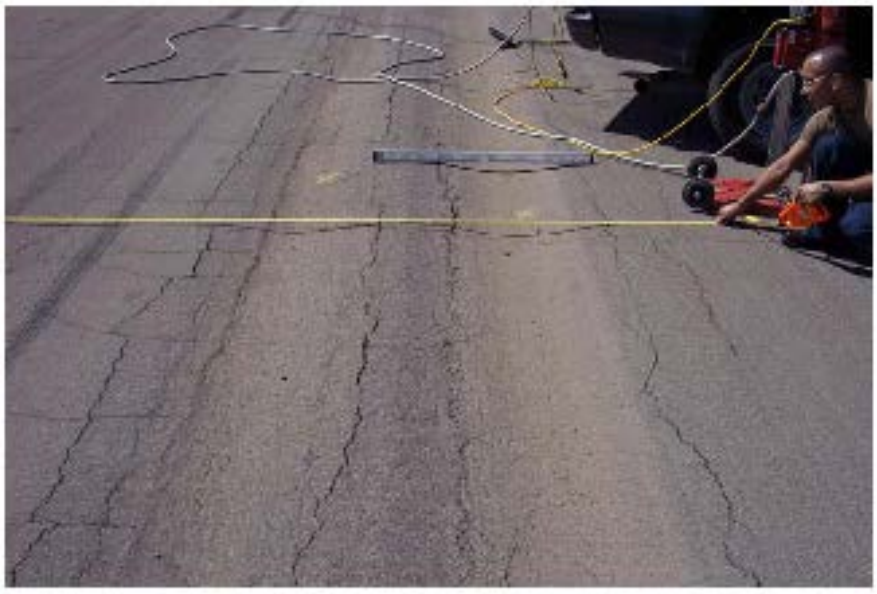

Figure C.2 Runway asphalt distresses include cracking and rutting.

C.3 Tables from Las Cruces Evaluation Report

Table C.1 Physical Property Data, Las Cruces IAP, New Mexico

				Pavement			Base			Subbase			Subgrade	
Feat.	ID	Area	Cond.	Thick.	Desc.	Flex.	Thick.	Desc	K/CBR	Thick.	Desc.	K/CBR	Desc	K/CBR
		ft^2		in		psi	in			in				
R0A-1	RUNWAY 04-22 (22 END)	316,400	Failed	3.5	AC	---	9.0	Silty Sand with Gravel	20	20.0	Sandy Silt	6	Sandy Gravel	40
R01A-2	RUNWAY 04-22 (04 END)	425,000	Very Poor	3.5	AC	---	9.0	Silty Sand with Gravel	20	20.0	Sandy Silt	6	Sandy Gravel	40

Note: 1 in.=25.4 mm, 1 ft=0.3048 m, 1 psi=6.9 kPa

Table C.2 Based on 3.5 Asphalt Surface over Base Data for B757 at 234655 pounds gross weight

Base CBR	Thickness of Asphalt Surface, in.	Beta	Predicted Coverage
20	3.5	25	11
18	3.5	28	8
15	3.5	33	5
12	3.5	40	3

Note: 1 in.=25.4 mm

Table C.3 Based on 3.5 Asphalt Surface over Base Data for C17 at 585000 pounds gross weight

Base CBR	Thickness of Asphalt Surface, in	Beta	Predicted Coverage
20	3.5	20	22
18	3.5	23	15
15	3.5	27	9
12	3.5	32	4

Note: 1 in.=25.4 mm

Table C.4 Predicted Life based on minimum thickness criteria for asphalt surface

Aircraft	Base CBR	Thickness of Asphalt Surface, in.	Predicted Coverage
B757	20	3.5	2
C17	20	3.5	3

Note: 1 in.=25.4 mm

Table C.5 Analysis Based on 12.5" of Surface and Base over Subbase Data for B757 at 234655 pounds gross weight

Subbase CBR	Thickness of Surface & Base, in.	Beta	Predicted Coverage
6	12.5	23	15

Note: 1 in.=25.4 mm

Table C.6 Analysis Based on 12.5" of Surface and Base over Subbase Data for C17 at 585000 pounds gross weight

Subbase CBR	Thickness of Asphalt Surface, in.	Beta	Predicted Coverage
6	12.5	29	7

Note: 1 in.=25.4 mm

Table C.7 Predicted Life based on min thickness criteria for asphalt surface and base			
Aircraft	**Subbase CBR**	**T of Asphalt & Base, in.**	**Predicted Coverage**
B757	6	12.5	3
C17	6	12.5	1<
Note: 1 in.=25.4 mm			

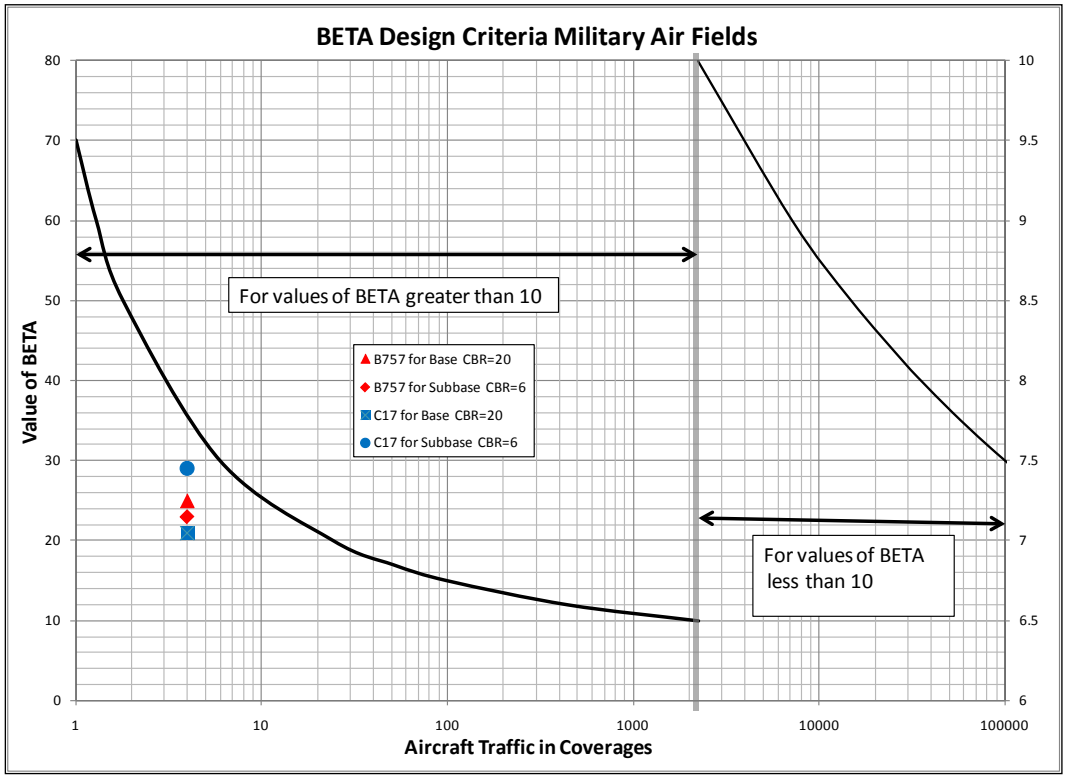

Figure C.3 Beta design criteria military air fields.

APPENDIX D - SUMMARY OF TEST SECTION PERFORMANCE UNDER TRAFFIC

D.1 Introduction

This appendix presents a general description of the performance of each individual item tested during the application of traffic loading. Tables indicating the date of testing, number of applied passes and average rut depth determined for each item are presented. A chart showing the development of rutting as a function of traffic is shown for each item tested. The results of traffic testing are presented in the order the traffic was applied.

Lane 1 Item 4: Lane 1 Item 4 was trafficked with a C-17 single tire with a tire pressure of 142 psi (980 kPa) and loaded to 45,000 lb (200 kN). The traffic pattern was shown in Figure 44 and included 40 passes. Traffic testing on this item started on June 3, 2008. After application of one traffic pattern, a full set of data was obtained. The data included transverse and longitudinal profiles; rut depths at station 10, 20, and 30; static load tests at the EPC and strain gage locations; and surface deflections. The average rut depth after 40 passes was approximately 0.167 in (4 mm). Additional traffic patterns were applied until June 12, 2008, recording data at specified intervals. Table D.1 summarizes the traffic data and pavement performance of the Lane 1 Item 4.

Table D.1 Lane 1 Item 4 cumulative passes and rut depth

Month/Day (2008)	Cumulative Number of Passes	Average Rut Depth (in.)
06/03	40	0.167
06/04	400	0.563
06/04	1,320	1.000
06/05	2,240	1.229
06/09	3,003	1.417
06/10	4,000	1.417
06/11	5,600	1.625
06/12	7,545	1.750
06/12	10,000	1.938

Note: 1 in.=25.4 mm

The first crack on the asphalt surface appeared after a total of 1720 passes; the crack was less than 1/16 in. (1.6mm) wide. After 4143 passes, the crack had not propagated any further and had not gotten any wider. After 6456 passes, new cracks had appeared on the surface, and the very first crack had propagated. On June 13, due to an HVS A malfunction in lifting the tire for repositioning, a zigzag traffic pattern was applied in order to complete traffic testing on the lane item and to limit testing delays. The P/C ratio for this pattern was 2.412. Since the applied passes were already in the order of the thousands, the change in the traffic pattern did not seem to have any influence on the permanent deformation (rutting) of the pavement section. Figure D.1 summarizes the rutting development as a function of the number of total passes applied to Lane 1 Item 4.

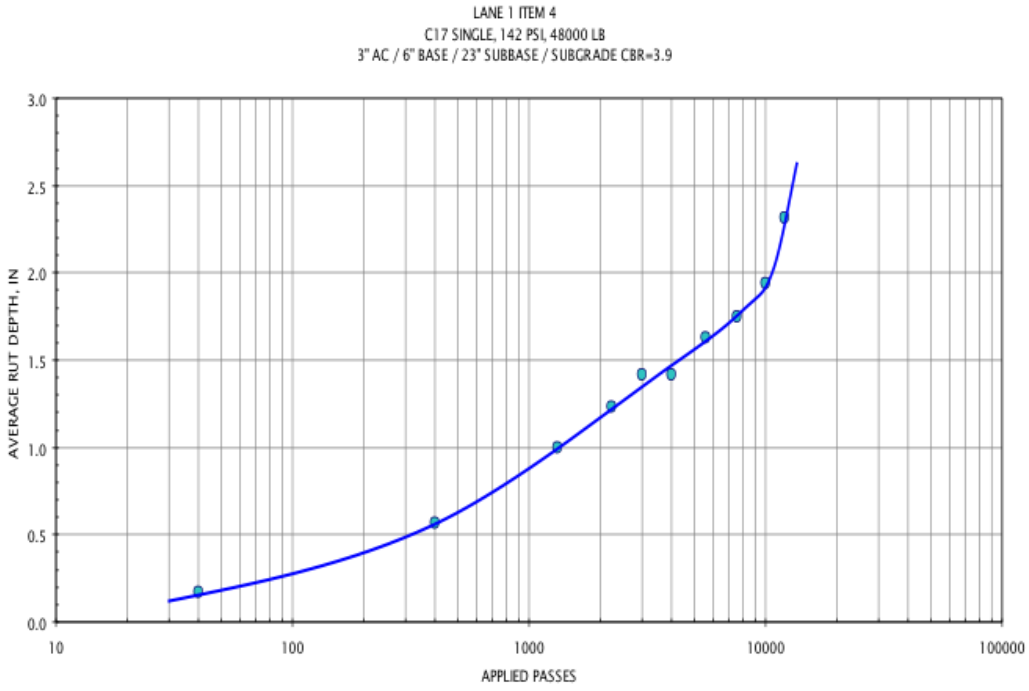

Figure D.1 Rutting development on Lane 1 Item 4 (1 inch=25.4 mm)

Lane 1 Item 3: Testing of Lane 1 Item 3 started on June 20, 2008. The C-17 single tire with pressure of 142 psi (980 kPa) and loaded to 45,000 lb (200 kN) was applied to the pavement. After the initial 40 passes, there was already some rutting. The maximum rutting depth was 0.375 in. (9.5 mm). After an additional 80 passes, the maximum rut depth increased to

0.563 in. (14 mm); and after 160 passes, a maximum rut depth of 0.813 in. (21 mm) was reached. After a total of 2,000 passes, the maximum rutting was 3 in. (76 mm), although the section showed an average rut depth of 2.646 in. (67 mm). Table D.2 summarizes the traffic data and pavement performance of Lane 1 Item 3. Cracking appeared on the pavement surface after 1,500 to 2,000 total passes during the last day of testing. Figure D.2 includes the rutting development as a function of the number of passes.

Table D.2 Lane 1 Item 3 cumulative passes and rut depth

Month/Day (2008)	Cumulative Number of Passes	Average Rut Depth (in.)
06/20	40	0.313
06/20	80	0.479
06/20	160	0.646
06/21	400	1.167
06/23	800	1.667
06/24	1,000	1.854
06/24	1,339	1.854
06/25	2,000	2.646
Note: 1 in.=25.4 mm		

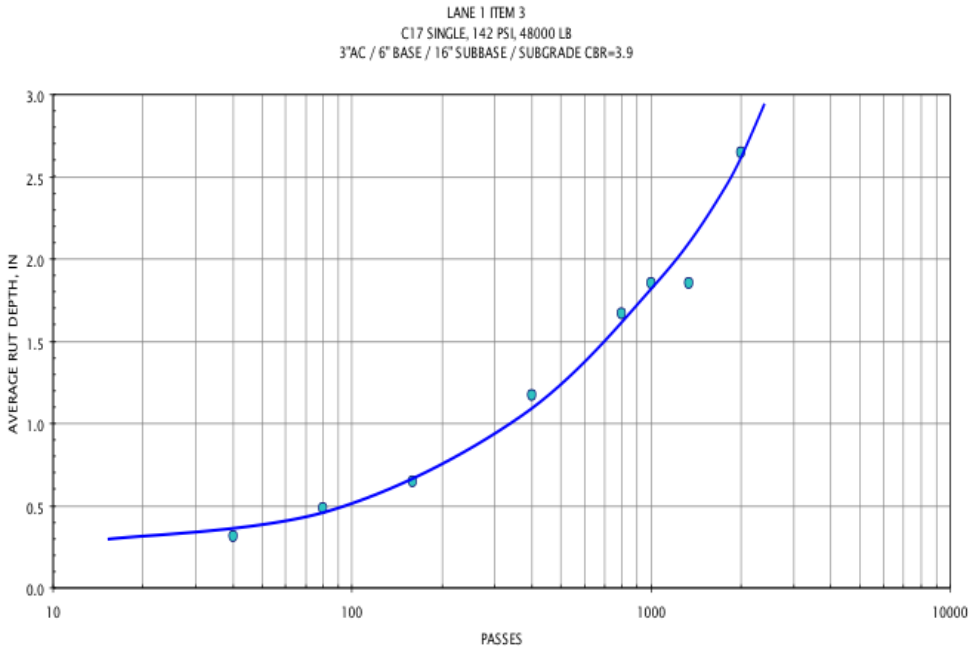

Figure D.2 Rutting development on Lane 1 Item 3 (1 inch=25.4 mm)

Lane 1 Item 2: Testing of Lane 1 Item 2 started on July 1, 2008. The C-17 single tire with a tire pressure of 142 psi (980 kPa) and loaded to 45,000 lb (200 kN) was applied to the pavement. After the completion of 3,960 passes, the rut depth at the center of the traffic area was 1.25 in. (32 mm). There was no visible cracking. After 8,354 passes, a crack had formed along the southeast edge of the traffic lane outside the wheel path. Additional hairline cracks had appeared after 12,000 passes. Table D.3 and Figure D.3 show the rutting data as a function of the number of passes up to 8,473 passes.

Table D.3 Lane 1 Item 2 cumulative passes and rut depth

Month/Day (2008)	Cumulative Number of Passes	Average Rut Depth (in.)
06/20	40	0.313
06/20	80	0.479
06/20	160	0.646
06/21	400	1.167
06/23	800	1.667
06/24	1,000	1.854
06/24	1,339	1.854
06/25	2,000	2.646
Note: 1 inch=25.4 mm		

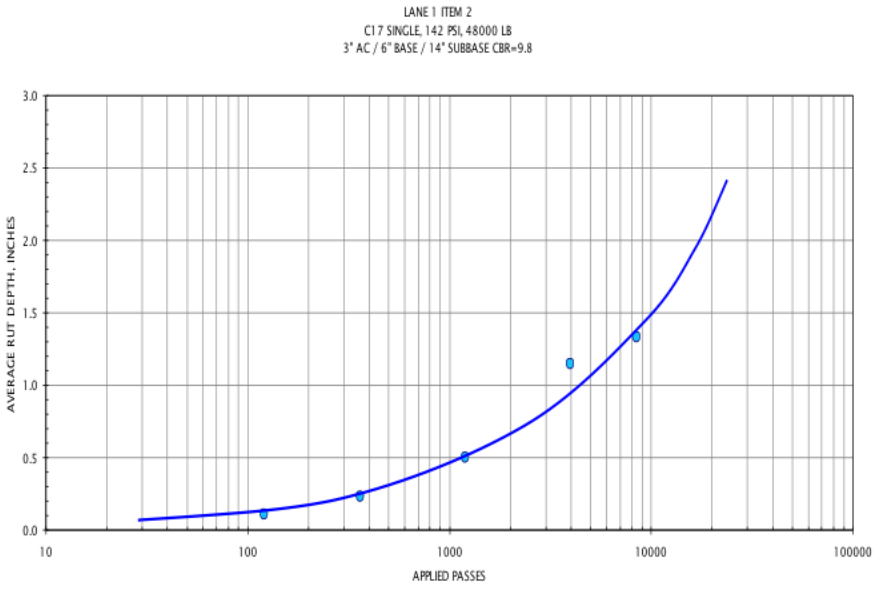

Figure D.3 Rutting development on Lane 1 Item 2(1 inch=25.4 mm)

Lane 1 Item 1: Testing of Lane 1 Item 1 started on July 11, 2008. The C-17 single tire with tire pressure set at 142 psi (980 kPa) and loaded to 45,000 lb (200 kN) was applied to the pavement. After the completion of 1,200 passes, the rut depth at the center of the area was 1.75 in. (44 mm). There were no visible cracks. Table D.4 and Figure D.4 show the rutting data as a function of the number of passes.

Table D.4 Lane 1 Item 1 cumulative passes and rut depth

Month/Day (2008)	Cumulative Number of Passes	Average Rut Depth (in.)
07/01	120	0.104
07/01	360	0.229
07/01	1,200	0.500
07/01	3,960	1.146
07/03	8,473	1.333
(1 inch=25.4 mm)		

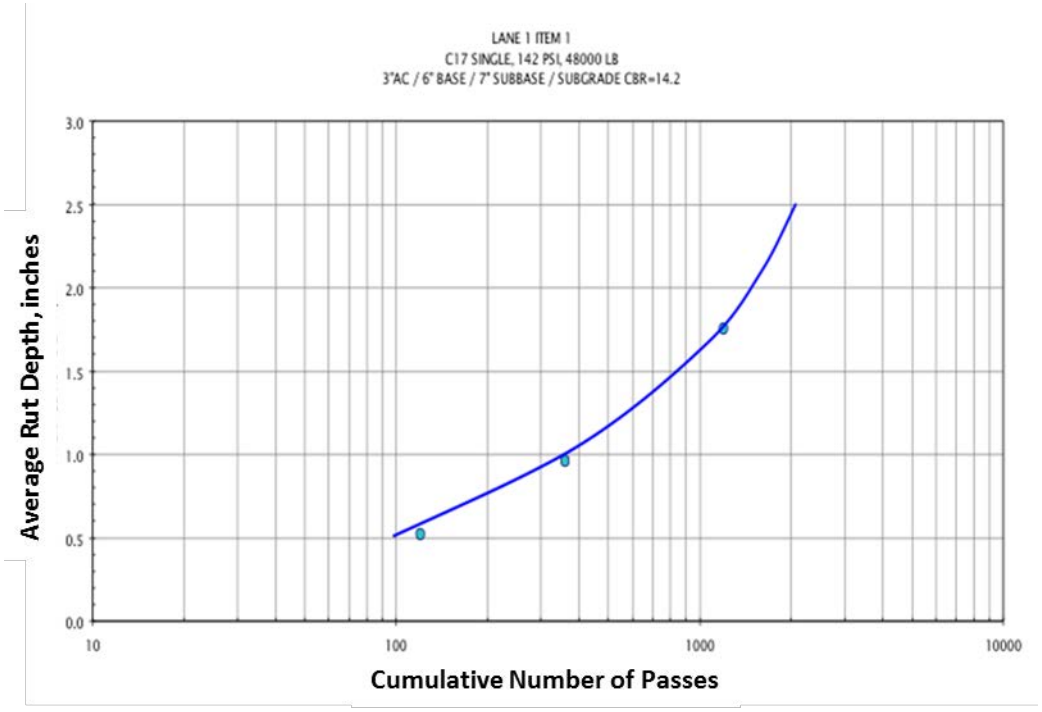

Figure D.4 Rutting development on Lane 1 Item 1(1 inch=25.4 mm)

Lane 3 Item 1: Testing of Lane 3 Item 1 started on July 15, 2008. The F-15 single tire with a tire pressure set at 325 psi (2242 kPa) and loaded to 35,000 lb (156 kN) was applied to the pavement. After the completion of 264 passes, the rut depth at the center of the trafficked area was 1.0 in. (25.4 mm). There was visible cracking in the center of the test item. With the addition of 264 more passes for a total of 528 passes, multiple longitudinal cracks had developed throughout the test item. The average rut depth was 1.5 in. (38 mm) and increased to 1.7 in. (43 mm) after 792 passes. Traffic was concluded after 1,056 passes with the pavement having an average rut depth of 2.146 in. (55 mm). Table D.5 and Figure D.5 show the rutting data as a function of the number of passes.

Table D.5 Lane 3 Item 1 cumulative passes and rut depth

Month/Day (2008)	Cumulative Number of Passes	Average Rut Depth (in.)
07/16	5	0.000
07/16	264	0.771
07/16	528	1.292
07/16	792	1.708
07/16	1,056	2.146

(1 inch=25.4 mm)

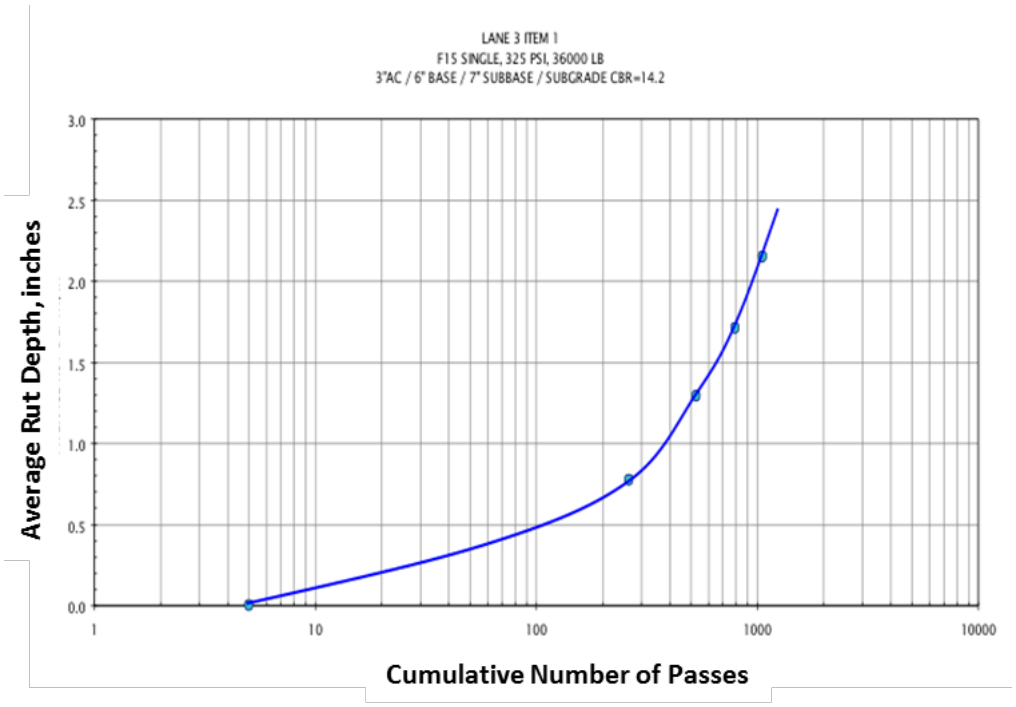

Figure D.5 Rutting development on Lane 3 Item 1 (1 inch=25.4 mm)

Lane 3 Item 3: Testing of Lane 3 Item 3 started on July 22, 2008. The F-15 single tire with a tire pressure set at 325 psi (2242 kPa) and loaded to 35,000 lb (156 kN) was applied to the pavement. After 264 passes, multiple cracks appeared in the asphalt surface. The total number of passes applied to this item was 390. Table D.6 and FigureD.6 show rutting depth in relation to the number of passes.

Table D.6 Lane 3 Item 3 cumulative passes and rut depth

Month/Day (2008)	Cumulative Number of Passes	Average Rut Depth (in.)
07/16	5	0.000
07/16	264	0.771
07/16	528	1.292
07/16	792	1.708
07/16	1,056	2.146
(1 inch=25.4 mm)		

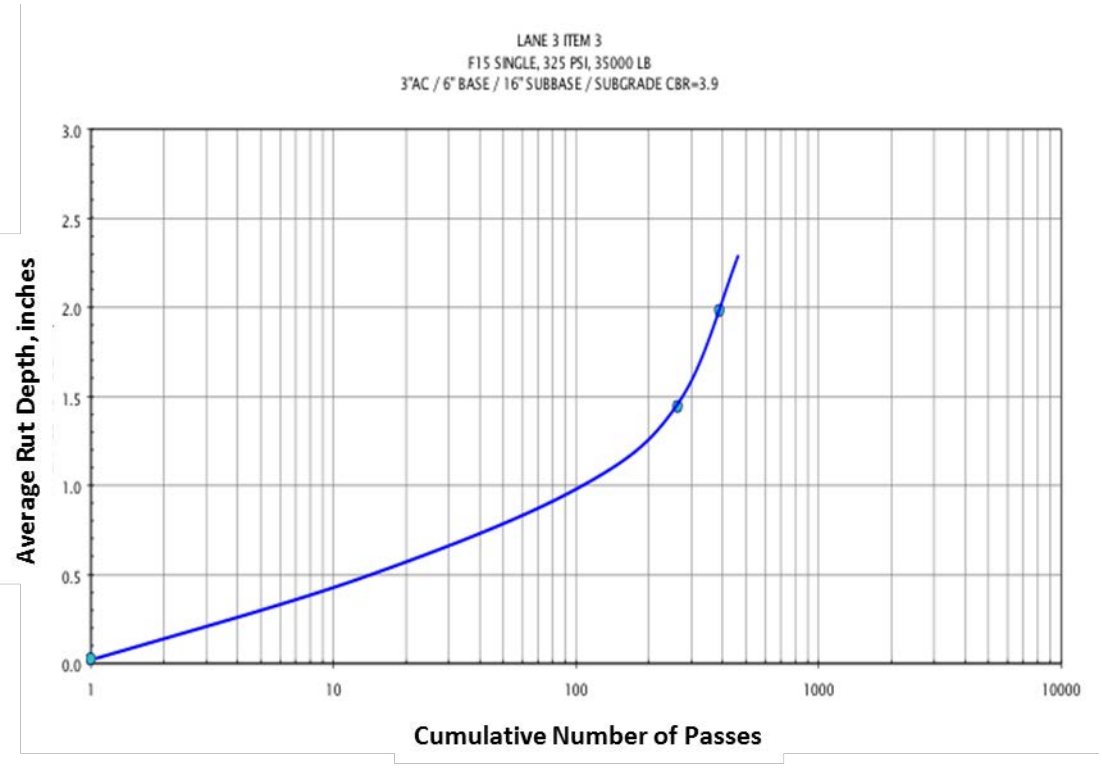

Figure D.6 Rutting development on Lane 3 Item 3 (1 inch=25.4 mm)

Lane 3 Item 2: Testing of Lane 3 Item 2 started on July 25, 2008. The F 15 single tire with a tire pressure set at 325 psi (2242 kPa) was applied to the pavement. The load was reduced from 35,235 lb to 33,800 lb (157 kN to 150 kN) with the intention of increasing the expected traffic level. In addition, the initial traffic pattern was changed from 12 passes per wheel location to 6 passes per wheel location in order to better capture the initial deterioration curve. After 1,320 passes, the rut depth was 1.13 in. (29 mm), and few cracks had appeared on the asphalt surface. The total number of passes applied to this item was 3,350, causing an average rut depth of 1.813 in.(46 mm). Table D.7 and Figure D.7 show rutting depth in relation to the number of passes.

Table D.7 Lane 3 Item 2 cumulative passes and rut depth

Month/Day (2008)	Cumulative Number of Passes	Average Rut Depth (in.)
07/24	5	0.000
07/24	126	0.230

Table D.7 Lane 3 Item 2 cumulative passes and rut depth		
07/25	396	0.500
07/26	1,320	1.125
07/29	3,350	1.813
(1 inch=25.4 mm)		

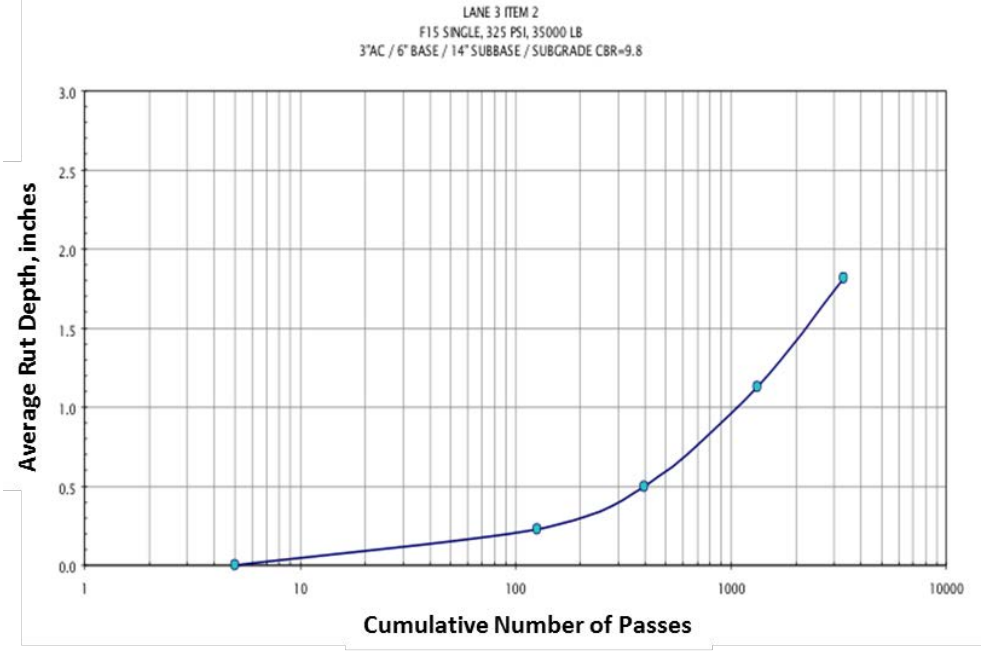

Figure D.7 Rutting development on Lane 3 Item 2 (1 inch=25.4 mm)

Lane 3 Item 4: Testing of Lane 3 Item 4 started on August 13, 2008. The F 15 single tire with a tire pressure set at 325 psi (2242 kPa) and loaded to 35,235 lb (157 kN) was applied to this section item. After 132 passes, the rut depth was 0.354 in. (9 mm). The total number of passes applied to this item was 10,000, causing an average rut depth of 2.229 in. (57 mm). Table D.8 and Figure D.8 show rutting depth in relation to the number of passes.

Table D.8 Lane 3 Item 4 cumulative passes and rut depth		
Month/Day (2008)	**Cumulative Number of Passes**	**Average Rut Depth (in.)**
08/13	132	0.354
08/13	1,320	1.104
08/14	10,000	2.229
(1 inch=25.4 mm)		

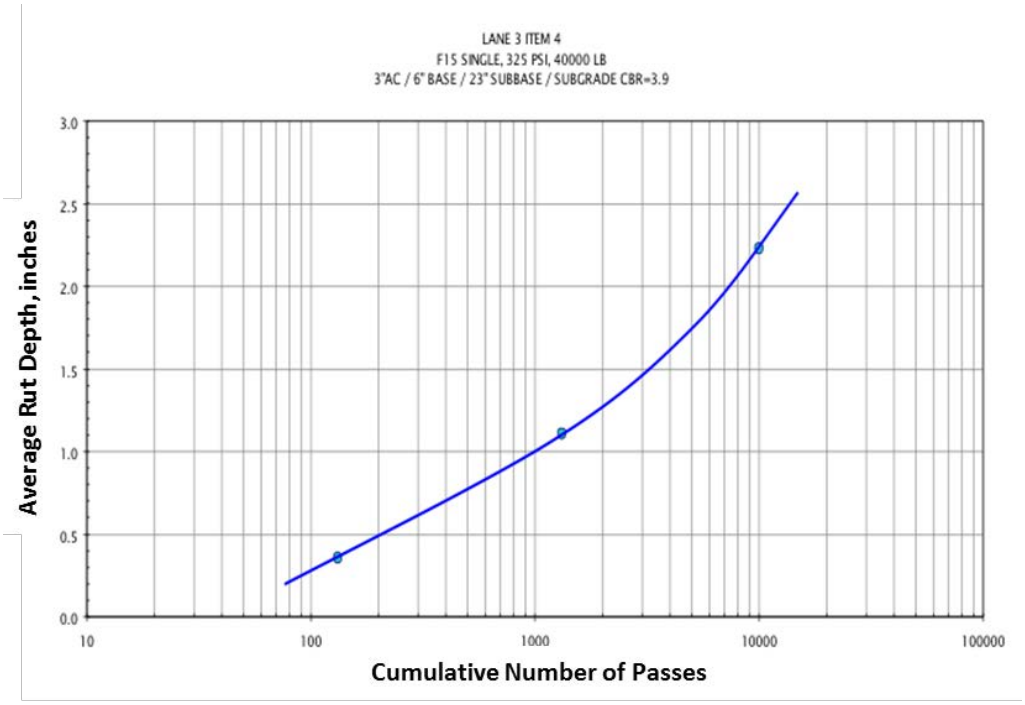

Figure D.8 Rutting development on Lane 3 Item 4(1 inch=25.4 mm)

Lane 2 Item 1: Testing of Lane 2 Item 1 started on October 7, 2008. The C-17 dual tires with a tire pressure of 142 psi (980 kPa) and loaded to 45,000 lb (200 kN) per tire was applied to this section item. The rut depth after 2,640 passes was 1.021 in. (26 mm). On the other hand, cracking had appeared on the pavement surface after 800 passes; after 2,500 passes, cracks had progressed considerably, existing cracks had widened, and new cracks had appeared on the pavement surface. Table D.9 and FigureD.9 show rutting depth in relation to the number of passes.

Table D.9 Lane 2 Item 1 cumulative passes and rut depth

Month/Day (2008)	Cumulative Number of Passes	Average Rut Depth (in.)
10/07	44	0.250
10/09	80	0.229
10/10	240	0.250
10/10	800	0.646
10/14	2,640	1.021

(1 inch=25.4 mm)

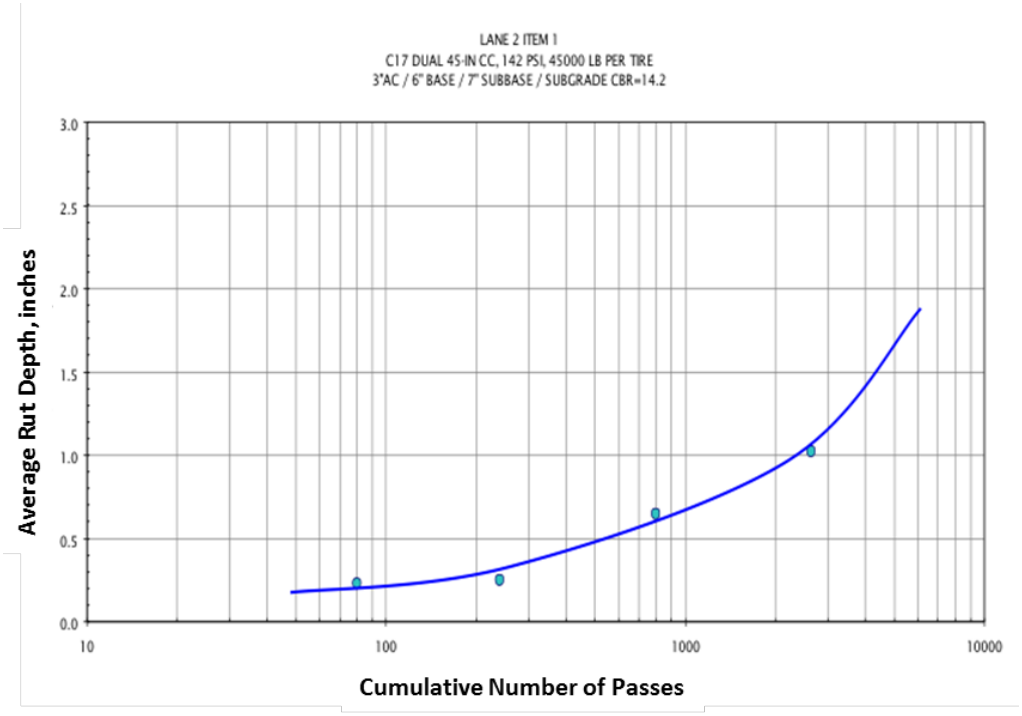

Figure D.9 Rutting development on Lane 2 Item 1 (1 inch=25.4 mm)

Lane 2 Item 2: Testing of Lane 2 Item 2 started on October 21, 2008. The C-17 dual tires with a tire pressure of 142 psi (980 kPa) and loaded to 45,000 lb (200 kN) per tire was applied to this section item. Only 40 passes were applied the first testing day. On October 23, 2008, 240 passes were completed, and the rut depth was 0.25 in. (6 mm). No cracks were detected. After the completion of 10,000 passes, the maximum rut depth was 1 in. (25 mm), and fine cracks had appeared on the pavement surface. Additional passes were applied; and, at 14,600 passes, rut depth was 1.125 in. (29 mm) and more cracks affected the test item. Table D.10 and Figure D.10 show rutting depth in relation to the number of passes.

Table D.10 Lane 2 Item 2 cumulative passes and rut depth.

Month/Day (2008)	Cumulative Number of Passes	Average Rut Depth (in.)
10/21	80	0.271
10/23	240	0.250

11/04	800	0.333
11/04	2,640	0.563
11/05	8,000	0.938
11/06	10,000	0.979
11/06	12,080	1.021
11/06	14,160	1.080
11/07	18,000	1.500
(1 inch=25.4 mm)		

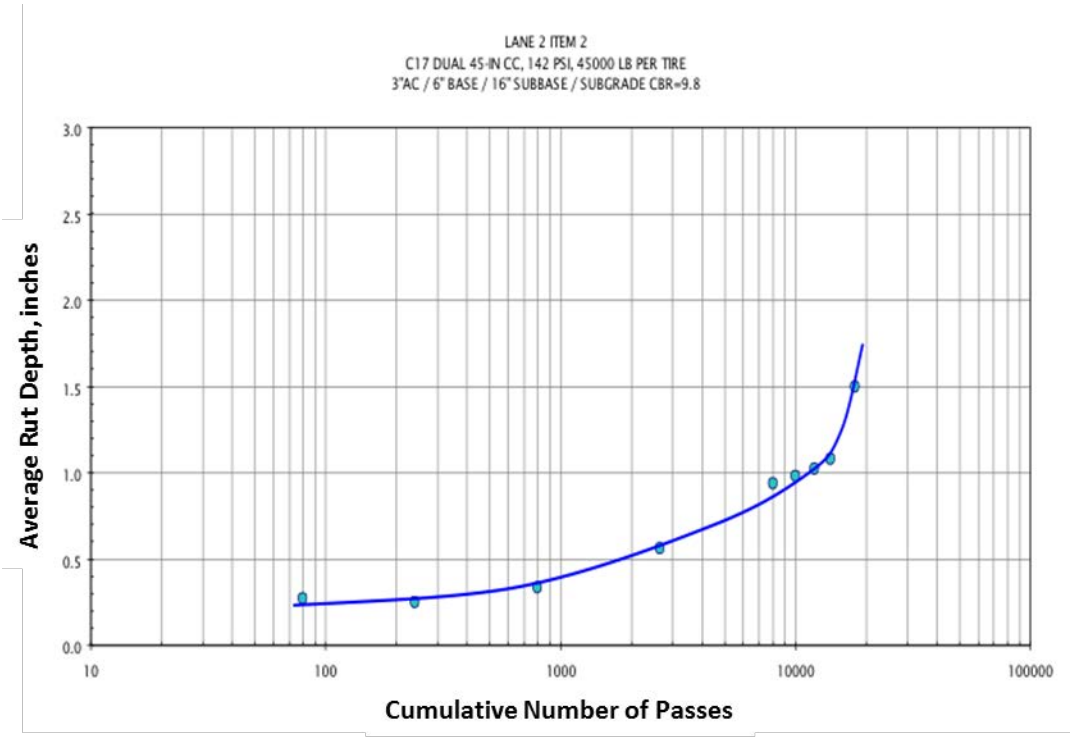

Figure D.10 Rutting development on Lane 2 Item 2(1 inch=25.4 mm)

Lane 2 Item 3: Testing of Lane 2 Item 3 started on November 19, 2008. The C-17 dual tires with a tire pressure of 142 psi (980 kPa) and loaded to 45,000 lb (200 kN) per tire were applied to this section item. The first 40 passes caused rutting of 0.063 in. (1.6 mm). After 400 passes, rutting was 0.25 in. (6 mm), and multiple fine cracks had appeared on the pavement surface. At 1,320 passes, the section was considerably cracked; the cracks extended for the full length of the test item. The maximum rut depth was 2 in. Table D.11 and Figure D.11 show rutting depth in relation to the number of passes.

Table D.11 Lane 2 Item 3 cumulative passes and rut depth		
Month/Day (2008)	**Cumulative Number of Passes**	**Average Rut Depth (in.)**
11/17	40	0.270
11/17	120	0.458
11/17	400	0.479
11/19	800	0.729
11/20	1,320	1.583
(1 inch=25.4 mm)		

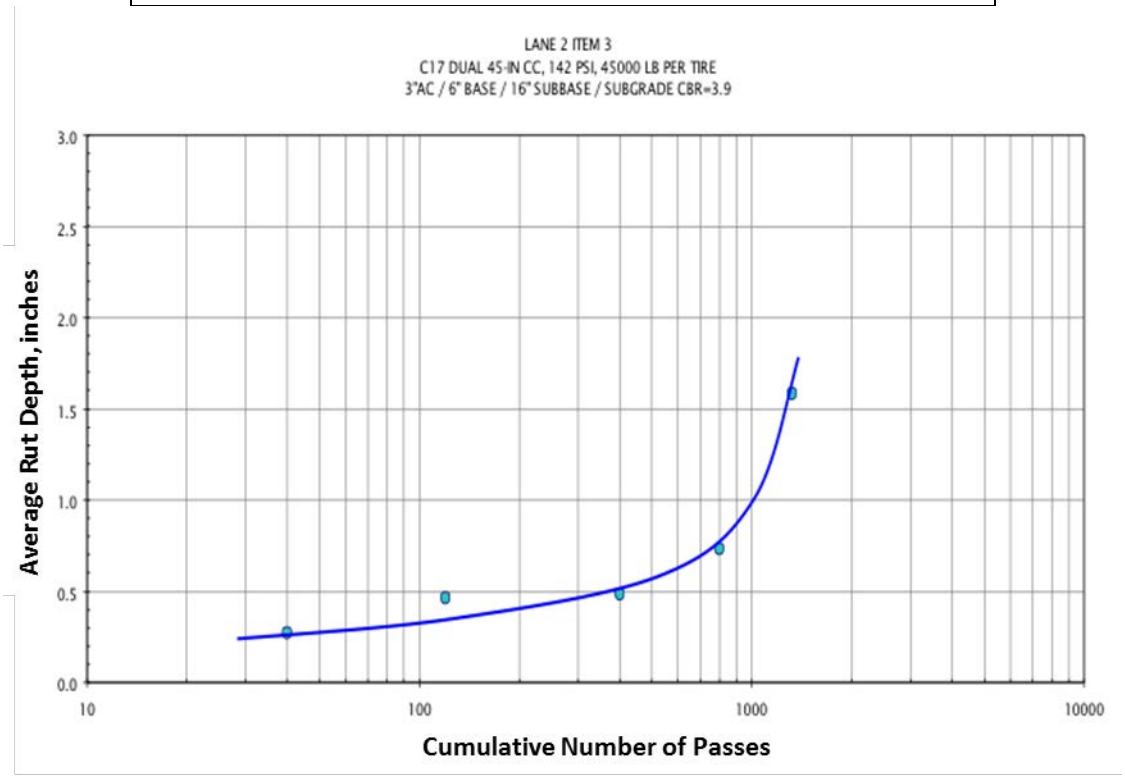

Figure D.11 Rutting development on Lane 2 Item 3 (1 inch=25.4 mm)

Lane 2 Item 4: Testing of Lane 2 Item 4 started on December 1, 2008. The C-17 dual tires with a tire pressure of 142 psi (980 kPa) and loaded to 45,000 lb (200 kN) per tire were applied to this section item. The first 40 passes caused rutting of 0.063 in. (1.63 mm). At 2,640 passes, the section was considerably cracked with a crack extending the full length of the test item; the maximum rut depth was 0.729 in. (19 mm). Traffic was stopped after 6,500 passes with

an average rut depth of 1.25 in. (32 mm). Table D.12 and FigureD.127 show rutting depth in relation to the number of passes.

Table D.12 Lane 2 Item 4 cumulative passes and rut depth		
Month/Day (2008)	**Cumulative Number of Passes**	**Average Rut Depth (in.)**
12/01	40	0.063
12/01	200	0.118
12/03	800	0.350
12/04	2,640	0.729
12/04	3,000	1.020
12/05	6,500	1.750
(1 inch=25.4 mm)		

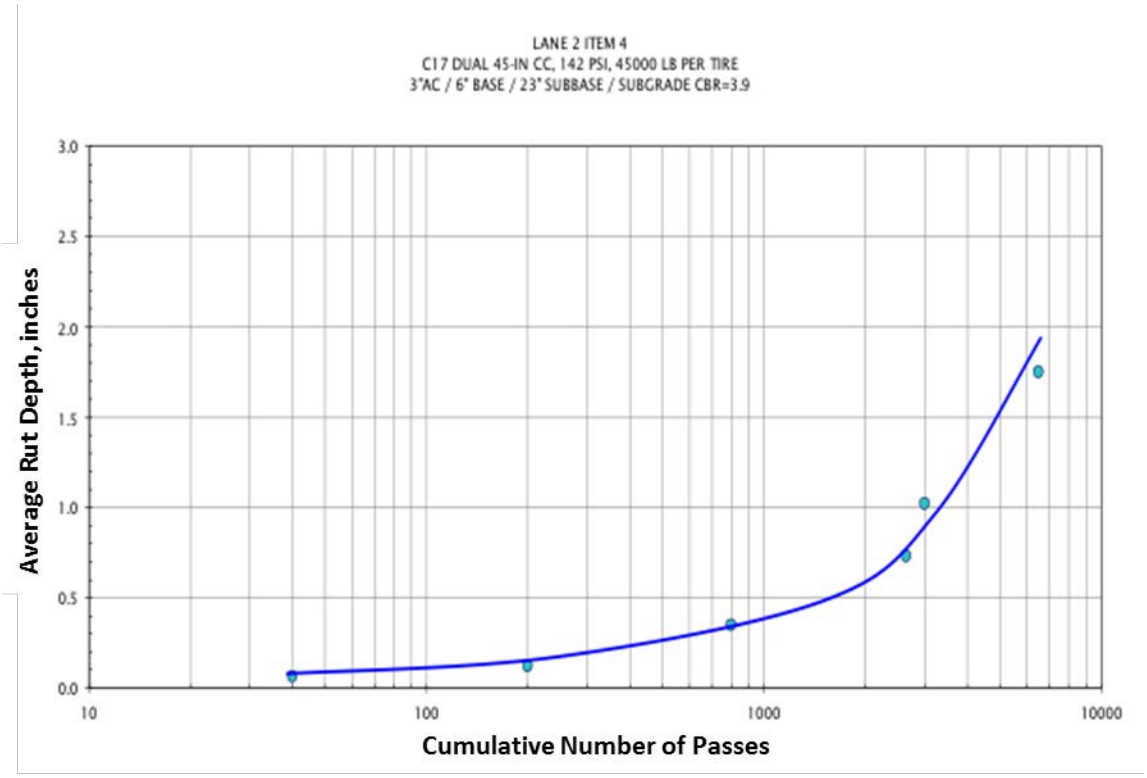

Figure D.12 Rutting development on Lane 2 Item 4 (1 inch=25.4 mm)

APPENDIX E - FALLING WEIGHT DEFLECTOMETER DATA WITH TRAFFIC

E.1 Introduction

The tables presented in the appendix summarize the falling weight deflectometer (FWD) data collected as a function of the applied traffic passes. They are divided into Lanes 1, 2 and 3 and Items 1 through 4. The stress indicated in the tables is the applied stress under the FWD plate, which had a radius of 5.91 inches (150 mm). FWD data was collected at three station indicated by STATION 1, STATION 2, and STATION 3 and they were located at 13 feet (3.96 m), 25 feet (7.62 m) and 35 feet (10.7 m) from the south end of each test item. Each test item was 40 feet (12.2 m) in length. The sensors were identified as D1 trough D7 and they were spaced at 12 inches (305 mm) from each other. The loading plate was located at sensor D1.

Table E-1. Lane 1, C-17 Single-Wheel Traffic (1 inch=25.4 mm, 1 lb=4.45 N, 1 psi=6.9 kPa)												
			Stress	**Load**	**ISM**	**D1**	**D2**	**D3**	**D4**	**D5**	**D6**	**D7**
	Station	**Passes**	**psi**	**lb**	**lb/in**	**0 in**	**12 in**	**24 in**	**36 in**	**48 in**	**60 in**	**72 in**
Item 1	1	0	155	16952	456	37.14	20.56	8.74	4.91	3.72	3.22	2.54
	1	120	161.4	17650	401	43.98	25.85	10.84	5.39	4.24	3.92	3.15
	1	360	162.3	17753	367	48.32	28.35	11.27	5.39	4.62	4.55	3.7
	1	1200	160.9	17594	370	47.58	28.32	10.93	5.5	4.53	4.71	3.48
	2	0	155.7	17031	485	35.09	21.14	9.17	4.96	3.68	2.91	2.36
	2	120	154.9	16944	354	47.83	27.3	11.76	5.8	4.24	3.67	3.06
	2	360	155.3	16987	283	60.08	29.89	12.15	5.71	4.5	4.06	3.38
	2	1200	155.5	17007	286	59.51	30.35	11.68	5.59	4.4	3.96	3.49
	3	0	156.2	17087	454	37.65	21.17	9.09	4.89	3.62	2.96	2.42
	3	120	159.5	17443	386	45.22	29.04	12.19	5.76	4.27	3.71	3.15
	3	360	158.8	17367	339	51.2	31.81	12.06	5.46	4.49	4.12	3.51
	3	1200	158.9	17375	335	51.83	31.62	12.26	5.49	4.34	3.98	3.15
Item 2	1	0	156.7	17134	520	32.93	19.2	8.82	5.15	3.84	3.18	2.63
	1	120	156	17058	417	40.93	24.19	10.8	5.92	4.46	3.79	3.18
	1	360	156.2	17087	411	41.56	25.21	11.53	6.2	4.7	4.12	3.5
	1	1200	155.5	17002	363	46.86	27.34	11.81	6.22	4.88	4.35	3.7
	1	3960	162.2	17737	390	45.46	28.99	12.97	6.78	5.27	4.66	3.96
	1	12000	162.7	17788	400	44.51	25.77	11.73	6.4	4.93	4.26	3.58
	1	13000	160.8	17586	381	46.17	27.69	11.94	6.31	4.98	4.41	3.76
	2	0	159.2	17407	546	31.89	19.72	9.31	5.3	3.8	3.09	2.43
	2	120	158.7	17351	433	40.06	24.67	11.2	5.94	4.33	3.77	2.98
	2	360	155.5	17010	413	41.16	25.88	12.12	6.36	4.54	4.09	3.2
	2	1200	154.2	16864	380	44.38	27.03	12.04	6.33	4.69	4.06	3.4
	2	3960	155.8	17039	377	45.21	28.29	12.87	6.66	4.93	4.43	3.54
	2	12000	159.3	17420	407	42.78	26.67	12.11	6.32	4.8	4.13	3.4
	2	13000	157.3	17198	382	45.04	27.87	12.28	6.39	4.72	4.19	3.42
	3	0	154	16841	609	27.67	17.93	8.49	5.04	3.75	3.04	2.49
	3	120	151.5	16571	414	40.05	22.25	10.22	5.67	4.2	3.53	2.98
	3	360	156.3	17094	418	40.87	24.48	11.36	6.07	4.45	3.87	3.28
	3	1200	154.9	16936	394	42.99	25.41	11.23	5.97	4.55	3.96	3.37
	3	3960	154.1	16857	363	46.42	26.59	12.04	6.3	4.73	4.16	3.57
	3	12000	161	17610	423	41.66	25.4	11.46	6.08	4.68	4.06	3.37
	3	13000	159	17383	404	43.01	26.65	11.65	6.05	4.63	4.1	3.44
Item 3	1	0	154.4	16884	256	66.02	45.35	23.51	12.81	8.32	6.08	5.13
	1	40	156.8	17145	245	69.98	49.34	26.07	13.88	8.48	6.39	5.57

Table E-1. Lane 1, C-17 Single-Wheel Traffic (1 inch=25.4 mm, 1 lb=4.45 N, 1 psi=6.9 kPa)												
	1	400	162.9	17811	246	72.39	50.28	26.56	13.8	8.25	6.22	5.41
	1	800	164.5	17994	264	68.22	50.17	26.35	13.94	8.4	6.2	5.64
	1	1000	85.4	9334	279	33.46	22.48	11.49	6.24	4.01	3.01	2.54
	1	2000	96.6	10568	271	38.99	24.43	11.98	6.31	4.04	3.1	2.66
	2	0	156.2	17079	234	73.05	48.79	24.86	13	8.19	6.1	5.01
	2	40	159	17383	224	77.54	51.97	26.64	13.44	8.17	6.14	5.28
	2	400	155.8	17039	200	85.04	52.78	27.31	13.91	7.75	6.04	5.24
	2	800	161.1	17621	217	81.32	51.38	26.47	13.69	7.91	5.82	4.65
	2	1000	81.1	8874	217	40.82	25.09	12.07	6.3	3.8	3	2.56
	2	2000	83.1	9088	211	43.13	25.87	11.04	5.62	3.59	2.78	2.41
	3	0	154.6	16904	263	64.18	48.9	21.8	11.35	7.13	5.43	4.43
	3	40	158.9	17380	227	76.67	49.77	25.68	13.39	7.98	6.18	5.35
	3	400	156.1	17071	214	79.77	54.58	25.28	12.26	7.33	5.58	4.93
	3	800	157	17169	207	83.04	53.93	24.76	11.86	6.92	5.5	4.82
	3	1000	79.7	8712	201	43.41	25.55	11.02	5.62	3.66	2.84	2.43
	1	0	215.4	23553	372	63.25	41.04	22.75	13.83	9.19	6.87	5.53
	1	40	214.9	23502	299	78.54	53.73	28.91	16.82	10.79	8.14	6.58
	1	400	153.5	16788	284	59.09	40.23	21.69	12.69	8.19	6.09	4.91
	1	1320	160.2	17523	296	59.14	40.82	21.86	12.73	8.21	6.15	5.02
	1	4000	159.4	17431	312	55.87	38.42	20.6	12.12	7.87	5.91	4.77
	1	10000	161.2	17634	323	54.59	35.67	18.83	11.57	7.73	5.72	4.5
	1	12000	161.5	17661	350	50.52	32.51	17.17	10.49	7.06	5.33	4.27
	2	0	216	23616	401	58.87	39.64	21.8	13.39	9.15	7.06	5.42
	2	40	216.6	23692	318	74.5	50.77	28.04	16.68	10.7	8.44	6.6
	2	400	155.6	17015	321	52.94	37.07	20.34	11.93	7.96	6.25	4.92
Item 4	2	1320	159.7	17459	325	53.67	37.89	20.79	12.17	8.04	6.15	4.95
	2	4000	163.9	17919	357	50.22	35.33	19.4	11.58	7.8	6	4.86
	2	10000	162.4	17756	346	51.36	34.6	18.29	11.18	7.74	5.93	4.7
	2	12000	160.3	17534	373	46.95	31.57	16.97	10.3	7.11	5.46	4.41
	3	0	222.5	24335	494	49.26	36.39	20.29	13.3	8.93	6.76	6.15
	3	40	216.6	23692	329	72.07	48.54	26.82	16.17	10.85	8.29	9.39
	3	400	161.2	17634	305	57.83	36.34	19.99	11.87	8.09	6.34	7.07
	3	1320	162.3	17753	339	52.33	35.17	19.52	11.69	7.98	6.17	5.35
	3	4000	165.2	18070	362	49.98	33	18.67	11.43	7.42	6.18	5.34
	3	10000	164.9	18033	349	51.63	33.51	17.87	11.02	7.96	8.62	6.46
	3	12000	158.3	17317	380	45.61	30.07	16.36	10.09	7.23	5.65	4.58

Table E-2. Lane 2, C-17 Dual-Wheel Traffic (1 inch=25.4 mm, 1 lb=4.45 N, 1 psi=6.9 kPa)												
			Stress	**Load**	**ISM**	**D1**	**D2**	**D3**	**D4**	**D5**	**D6**	**D7**
	Station	**Passes**	**psi**	**lb**	**lb/in**	**0 in**	**12 in**	**24 in**	**36 in**	**48 in**	**60 in**	**72 in**
Item 1	1	0	173	18914	610	31	21.26	9.98	5.33	3.86	3.22	2.71
	1	44	170.2	18617	525	35.46	23.18	11.04	5.73	4.07	3.48	2.98
	1	2640	168.7	18451	389	47.43	29.17	12.54	6.37	4.83	4.43	3.71
	2	0	171	18700	604	30.95	20.49	9.87	5.83	4.11	3.37	2.8
	2	44	169.9	18585	541	34.37	22.15	10.69	6.15	4.3	3.54	2.93
	2	2640	166.5	18205	356	51.2	30.5	12.69	6.77	4.65	3.97	3.19
	3	0	164.7	18010	1270	14.18	20.79	9.59	5.33	4.16	3.43	2.87
	3	44	162.3	17745	1967	9.02	22.86	10.07	5.3	4.3	3.56	3.01
	3	2640	164.8	18025	323	55.78	27.69	10.92	6.23	5.19	4.65	3.91
Item 2	1	0	175.1	19148	640	29.9	20.71	10.5	6.02	4.31	3.54	2.96
	1	40	170.5	18649	550	33.91	21.87	10.73	6.04	4.35	3.59	2.98
	1	18000	95.9	10489	487	21.56	12.56	6	3.33	2.51	2.18	1.84
	2	0	175.5	19191	667	28.76	19.38	9.89	5.91	4.33	3.5	2.9
	2	40	169.7	18562	579	32.07	20.73	10.25	6.1	4.38	3.53	2.95
	2	18000	95.6	10460	477	21.95	12.57	5.9	3.22	2.49	2.06	1.66
	3	0	174.1	19041	668	28.52	18.54	9.67	5.93	4.37	3.65	3.01
	3	40	167.3	18295	581	31.49	19.98	10.19	6.15	4.4	3.57	3.02
	3	18000	94.1	10290	554	18.58	12.04	5.81	3.37	2.41	2.3	1.73
Item 3	1	0	171.1	18715	407	46.02	33.39	18.34	10.52	6.79	5.35	4.52
	1	40	170.8	18676	349	53.51	38.06	20.75	11.84	7.62	6.02	5.13
	1	1320	162.7	17796	138	128.76	66.69	20.7	10.63	8.2	6.84	5.77
	2	0	172.4	18858	376	50.12	36.06	20.5	11.75	7.39	5.5	4.83
	2	40	171.9	18803	325	57.78	39.89	22.52	12.92	8.07	6.09	5.25
	2	1320	171.2	18720	148	126.3	72.61	24.76	10.74	8.06	7.15	5.97
	3	0	171.2	18723	395	47.35	34.3	19.59	11.43	7.28	5.42	4.44
	3	40	171.8	18792	351	53.61	38.28	22.07	12.9	8.24	6.26	5.2
	3	1320	164.7	18010	178	101.13	70.72	23.09	12.15	8.64	6.96	5.51
Item 4	1	0	125.1	13684	382	35.83	24.02	13.71	8.17	5.37	4.29	3.51
	1	40	169	18485	408	45.34	29.98	16.74	9.91	6.63	5.2	4.3
	1	3000	168.4	18411	344	53.52	36.68	19.35	10.77	7.23	6.05	5.01
	1	6500	167.7	18343	244	75.07	48.15	18.18	11.36	8.3	6.64	5.58
	2	0	123.7	13526	436	31.02	21.74	12.56	7.76	5.23	4.11	3.3
	2	40	171.6	18771	470	39.93	28.1	16	9.74	6.6	5.22	4.26
	2	3000	169.3	18514	360	51.43	35.72	18.65	11.15	7.59	5.91	4.73
	2	6500	165	18046	257	70.35	45.41	19.37	10.91	7.9	6.47	5.28

Table E-2. Lane 2, C-17 Dual-Wheel Traffic (1 inch=25.4 mm, 1 lb=4.45 N, 1 psi=6.9 kPa)												
	3	0	123.3	13486	177	76.11	22.36	12.93	7.81	5.26	4.04	3.33
	3	40	167.5	18316	715	25.62	28.18	16.18	9.76	6.5	5.14	4.22
	3	3000	163.3	17864	2727	6.55	36.26	19.57	10.78	7.26	5.74	4.66
	3	6500	162.7	17792	272	65.44	46.04	21.85	10.66	7.89	6.18	5.16

Table E-3 Lane 3, F-15 Single-Wheel Traffic (1 inch=25.4 mm, 1 lb=4.45 N, 1 psi=6.9 kPa)												
			Stress	Load	ISM	D1	D2	D3	D4	D5	D6	D7
	Station	Passes	psi	lb	lb/in	0 in	12 in	24 in	36 in	48 in	60 in	72 in
Item 1	1	0	164	17938	524	34.25	20.15	9.24	6.05	4.84	3.94	3.3
	1	264	159.8	17470	324	53.96	30.2	11.98	7.22	6.28	5.5	4.56
	1	792	155.9	17050	289	58.96	31.4	10.94	6.85	6.4	5.36	4.43
	1	1056	158.2	17304	287	60.32	31.98	11.47	7.06	6.53	5.72	4.69
	2	0	158.8	17367	476	36.51	20.16	8.94	5.86	4.78	3.91	3.26
	2	264	160.6	17558	344	50.97	29.25	11.23	6.44	5.79	5.12	4.14
	2	792	158.9	17380	351	49.53	31.3	10.45	6.24	5.84	5.18	4.34
	2	1056	157.8	17256	303	56.87	30.89	11.16	6.82	6.44	5.63	4.46
	3	0	161	17610	456	38.62	21.75	9.01	5.59	4.7	3.95	3.35
	3	264	161.1	17621	356	49.52	31.63	12	6.51	5.86	5.28	4.32
	3	792	157.4	17217	296	58.23	32.11	10.76	6.28	5.97	5.27	4.35
	3	1056	157.6	17237	220	78.48	31.31	11.39	6.54	5.7	5.44	4.32
Item 2	1	0	167	18268	569	32.08	18.84	9.25	6.19	4.82	3.96	3.3
	1	120	170.5	18644	498	37.41	22.34	10.71	6.63	5.18	4.31	3.69
	1	396	162.6	17784	427	41.63	24.3	11.29	7.11	5.7	4.75	3.87
	1	1320	166.7	18232	408	44.68	25.27	11.76	7.24	5.84	4.93	3.76
	1	3350	165.5	18094	416	43.52	27.71	12.96	7.96	6.31	5.44	4.46
	2	0	164.1	17946	547	32.8	18.84	9.28	6.05	4.69	3.81	3.17
	2	120	164.5	17991	490	36.72	22.16	10.86	6.76	5.2	4.28	3.44
	2	396	163	17824	432	41.24	23.75	11.12	7.01	5.51	4.54	3.83
	2	1320	162.5	17769	418	42.47	25.17	11.65	7.33	5.86	4.86	4.01
	2	3350	163.7	17903	444	40.33	26.29	12.38	7.62	5.94	5.05	4.23
	3	0	165.9	18144	533	34.05	20.07	9.9	6.02	4.67	4.11	3.44
	3	120	168.2	18395	474	38.84	23.49	10.93	6.51	5.11	4.33	3.55
	3	396	165.3	18078	447	40.41	25.23	10.89	6.57	5.43	4.66	3.87
	3	1320	165.4	18089	405	44.67	26.2	11.59	6.87	5.63	4.93	4.12
	3	3350	165.2	18070	413	43.74	26.69	12.21	7.19	5.79	4.94	4.21
Item 3	1	0	94	10282	294	35.02	23.3	11.62	6.48	4.5	3.62	2.86
	1	264	91.1	9960	231	43.13	27.29	12.23	6.48	4.48	3.63	2.89
	1	390	94.5	10330	235	44.04	28.31	12.92	5.95	2.91	3.17	3.52
	2	0	89.5	9791	231	42.41	26.23	12.56	7.03	4.63	3.45	2.8
	2	264	88.4	9672	188	51.42	26.1	11.93	6.69	4.87	3.62	2.6
	2	390	93.6	10235	224	45.62	27.09	12.61	6.85	4.65	3.74	2.98
	3	0	92.6	10124	237	42.7	25.31	11.57	6.48	4.6	3.56	2.77
	3	264	90.9	9945	218	45.66	26.07	11.44	6.45	4.53	3.68	3.09
	3	390	93.1	10182	241	42.29	25.76	11.53	6.24	4.44	3.62	3.12
	1	0	165.5	18094	376	48.15	33.44	17.67	10.51	7.1	5.44	4.42
	1	132	157.1	17182	310	55.47	37.01	18.96	10.83	7.3	5.54	4.47

Table E-3 Lane 3, F-15 Single-Wheel Traffic (1 inch=25.4 mm, 1 lb=4.45 N, 1 psi=6.9 kPa)												
Item 4	1	396	154.9	16944	319	53.16	36.93	18.69	10.67	7.31	5.6	5.01
	1	1320	157.9	17264	311	55.55	36.21	18.18	10.41	6.96	5.36	4.4
	1	4356	167.3	18295	401	45.58	31.65	17.07	10.34	7.06	5.44	4.39
	1	10000	164.2	17954	403	44.55	33.02	17.27	10.58	7.24	5.46	4.4
	2	0	163.4	17867	402	44.49	29.94	17.02	10.48	6.97	5.24	4.15
	2	132	155.8	17039	346	49.2	34.35	19.04	11.21	7.34	5.5	4.43
	2	396	153.7	16812	321	52.41	34.33	18.69	10.95	7.18	5.38	4.29
	2	1320	156.7	17134	341	50.26	33.88	18.26	10.73	7.12	5.38	4.36
	2	4356	166.4	18192	425	42.84	30.48	17.33	10.63	7.16	5.39	4.32
	2	10000	167.2	18287	434	42.18	30.33	17.32	10.82	7.33	5.56	4.43
	3	0	168.4	18414	450	40.92	30.48	17.01	10.44	7.15	5.48	4.34
	3	132	154.7	16920	342	49.41	34.75	18.68	11.02	7.37	5.59	4.41
	3	396	160.7	17573	351	50.07	34.33	18.33	10.73	7.13	5.43	4.34
	3	1320	161.8	17697	351	50.49	33.69	17.65	10.53	7.18	5.6	4.53
	3	4356	170.9	18688	424	44.03	30.11	16.78	10.35	7.11	5.5	4.43
	3	10000	169.3	18514	395	46.92	30.5	17.04	10.64	7.26	5.58	4.5

APPENDIX F - SUMMARY OF EARTH PRESSURE CELL DATA

F.1 Introduction

This appendix presents the reduced pavement stress data collected from earth pressure cells (EPC) installed at the various depths within the pavement structures. The figures are organized by Lane and Item numbers. Curves identified by EPC-SB are those EPC cells installed in the subbase layer and have the larger values. Curves identified by EPC-SG are those EPC cells installed in the subgrade layer and have the lower values. The vertical load is also indicated in the figures on the top portion of each chart. The record number is the index of the time series collected at a rate of 250 Hz. Numbers atop each curve represent the maximum response stress value and the numbers at the bottom represent the initial stress value. The difference of these numbers is the resulting stress due to the applied loading.

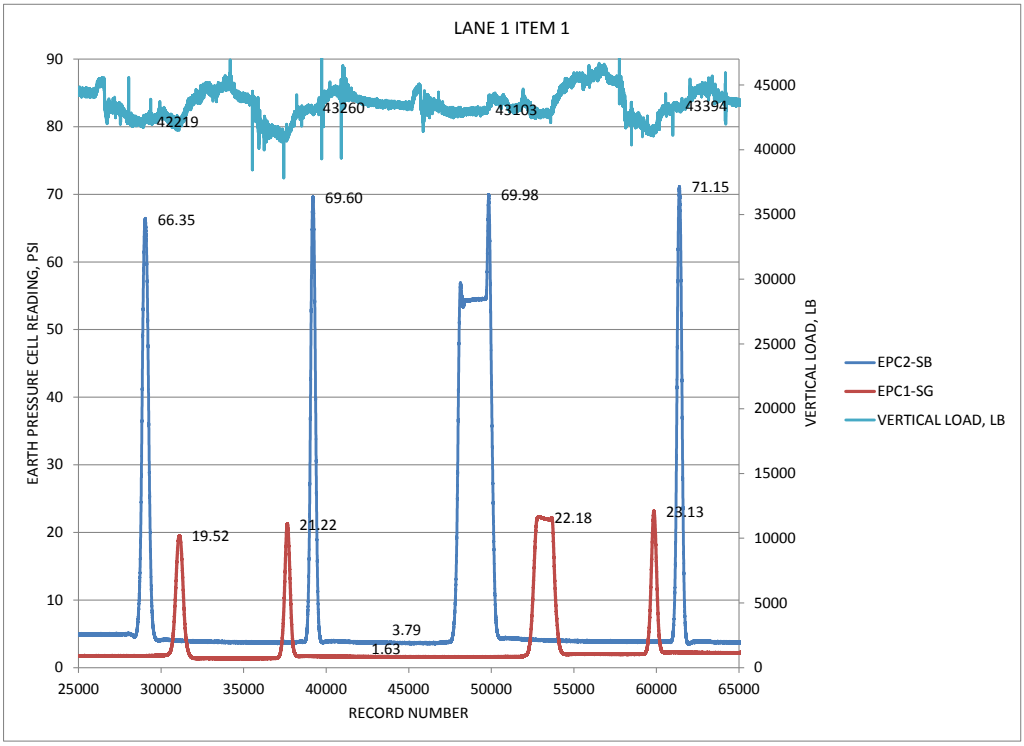

Figure F.1 Lane 1 Item 1 (1 lb=4.45 N, 1 psi=6.9 kPa)

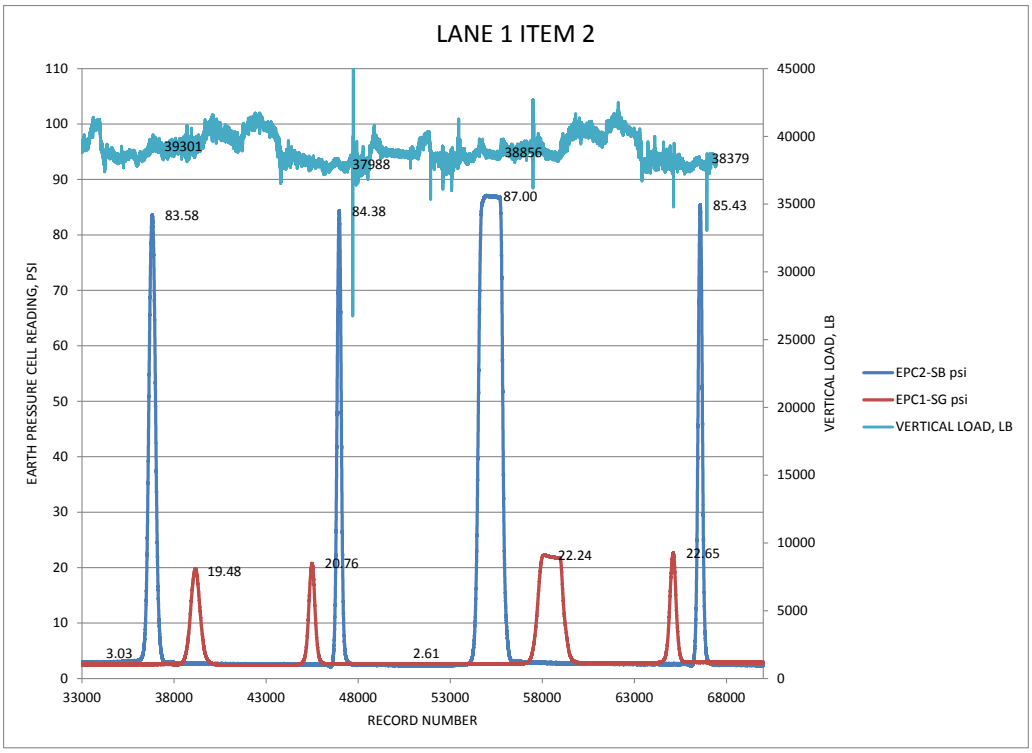

Figure F.2 Lane 1 Item 2 (1 lb=4.45 N, 1 psi=6.9 kPa)

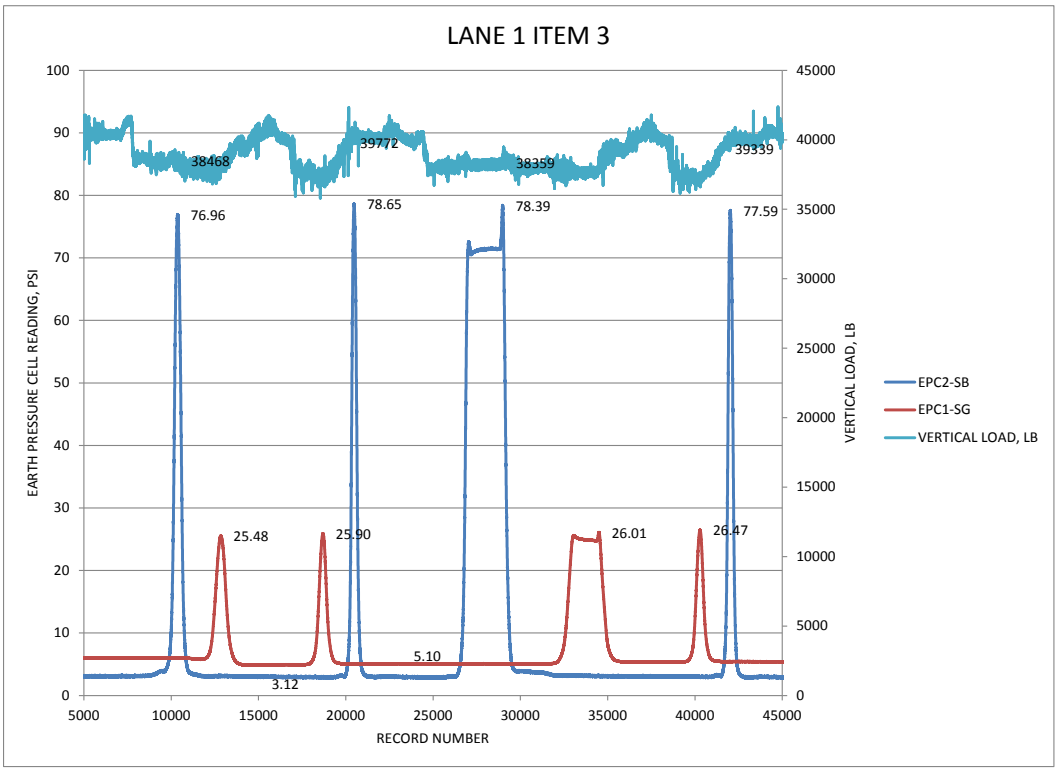

Figure F.3 Lane 1 Item 3 (1 lb=4.45 N, 1 psi=6.9 kPa)

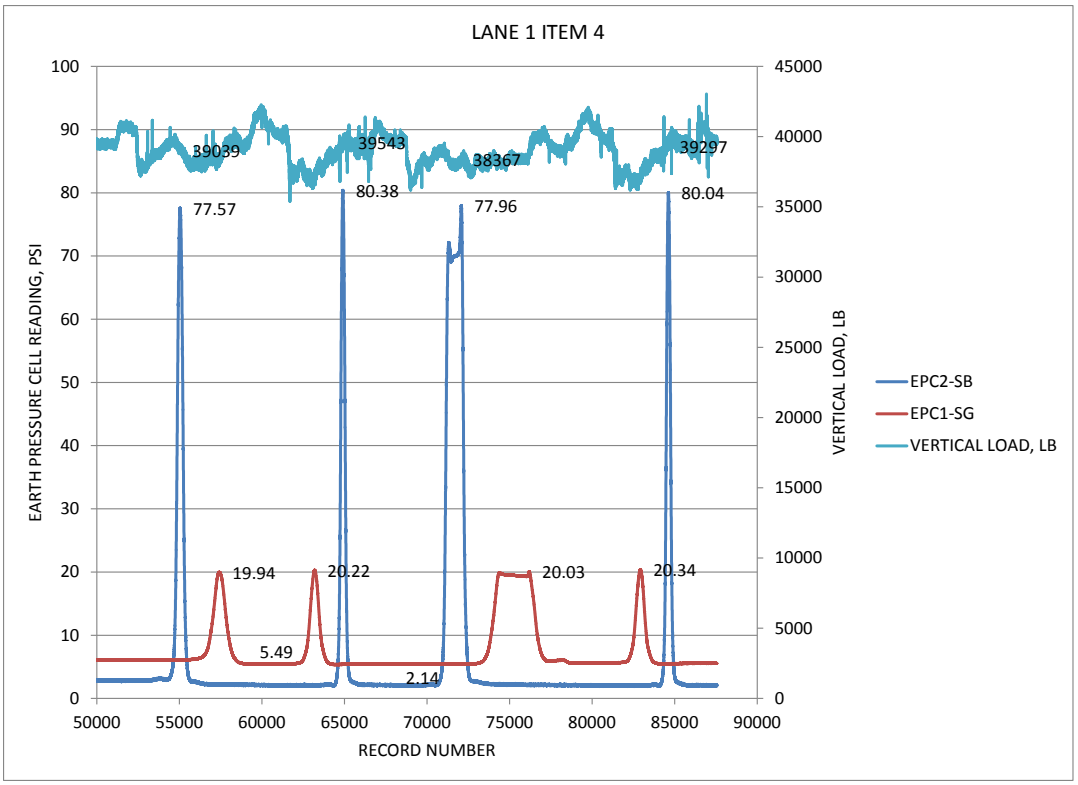

Figure F.4 Lane 1 Item 4 (1 lb=4.45 N, 1 psi=6.9 kPa)

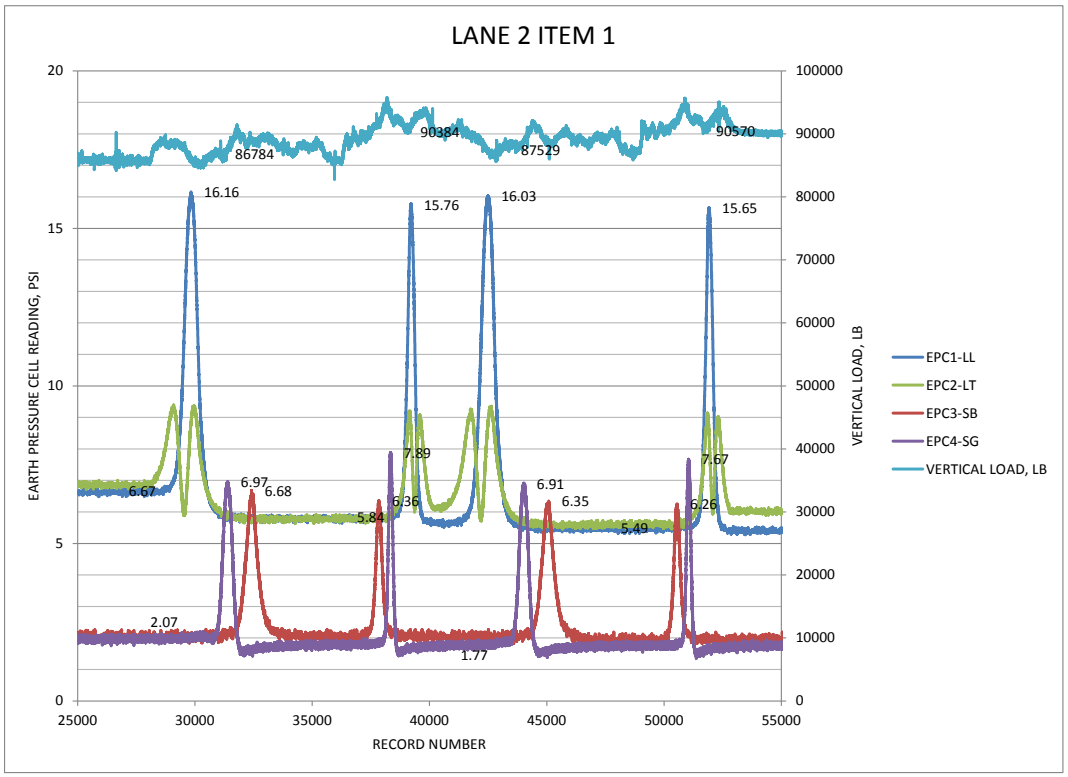

Figure F.5 Lane 2 Item 1 (1 lb=4.45 N, 1 psi=6.9 kPa)

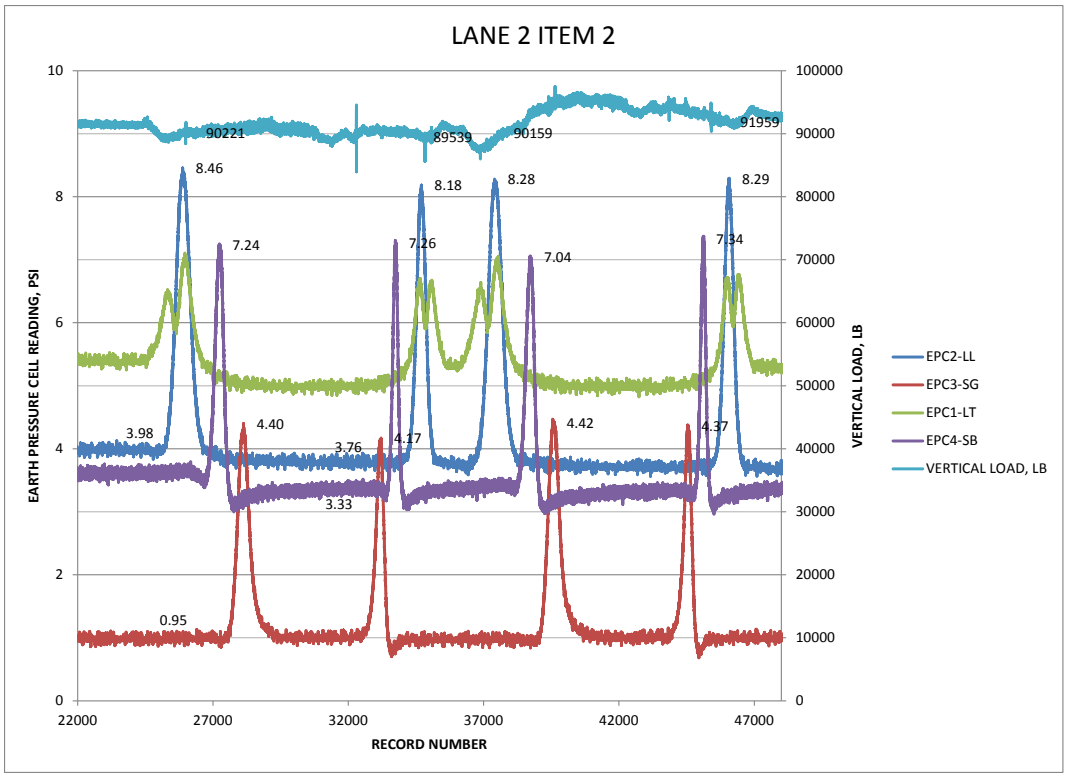

Figure F.6 Lane 2 Item 2 (1 lb=4.45 N, 1 psi=6.9 kPa)

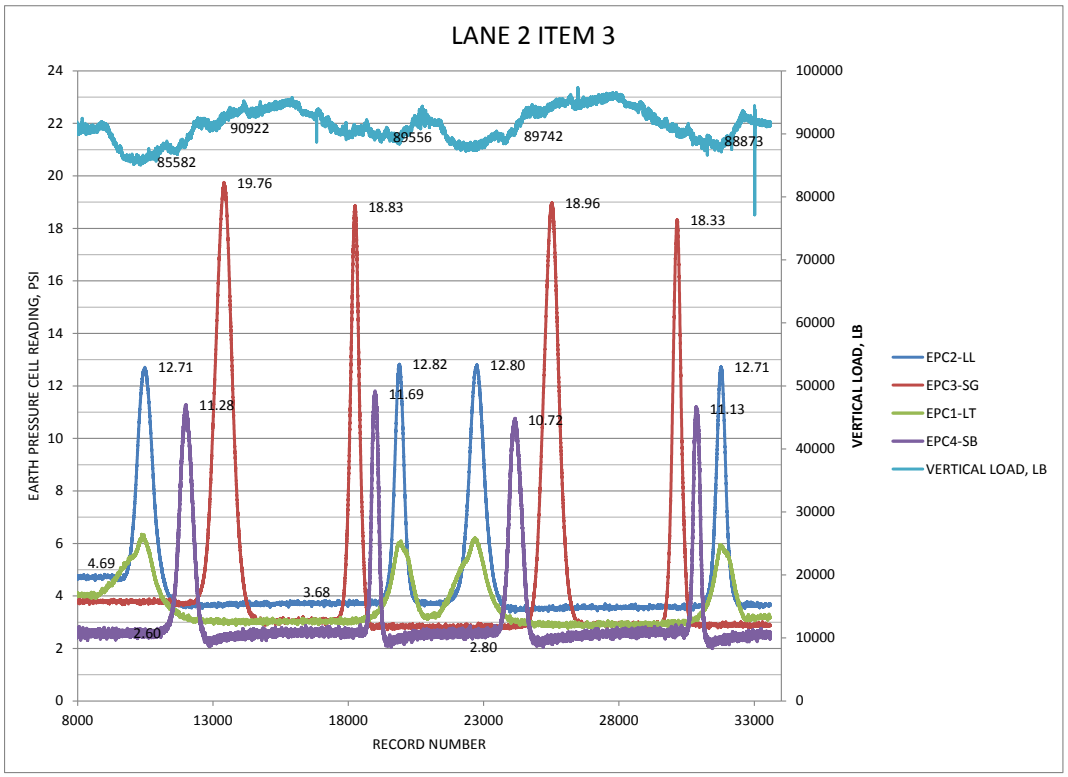

Figure F.7 Lane 2 Item 3 (1 lb=4.45 N, 1 psi=6.9 kPa)

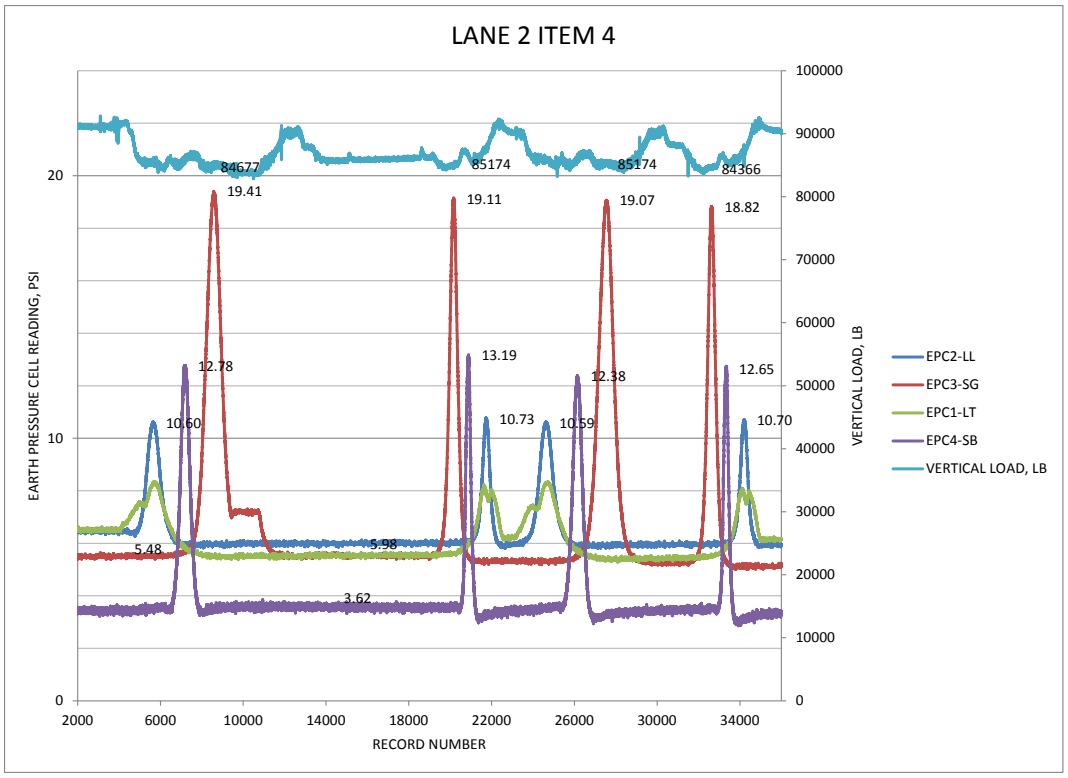

Figure F.8 Lane 2 Item 4 (1 lb=4.45 N, 1 psi=6.9 kPa)

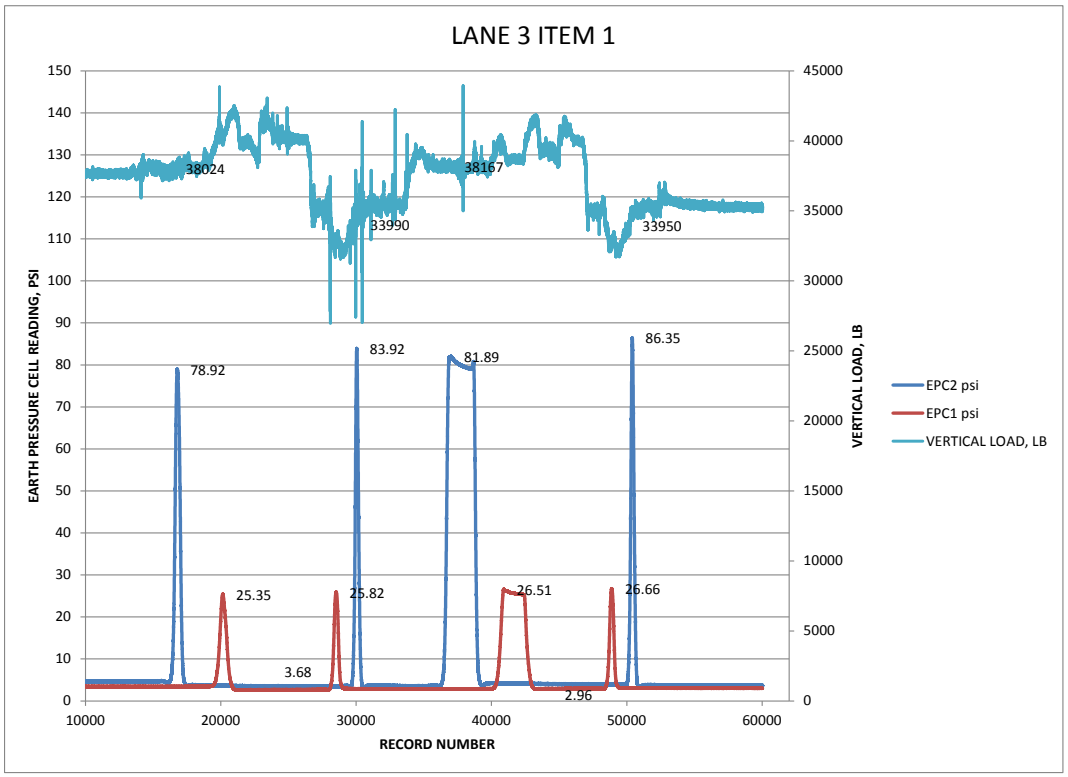

Figure F.9 Lane 3 Item 1 (1 lb=4.45 N, 1 psi=6.9 kPa)

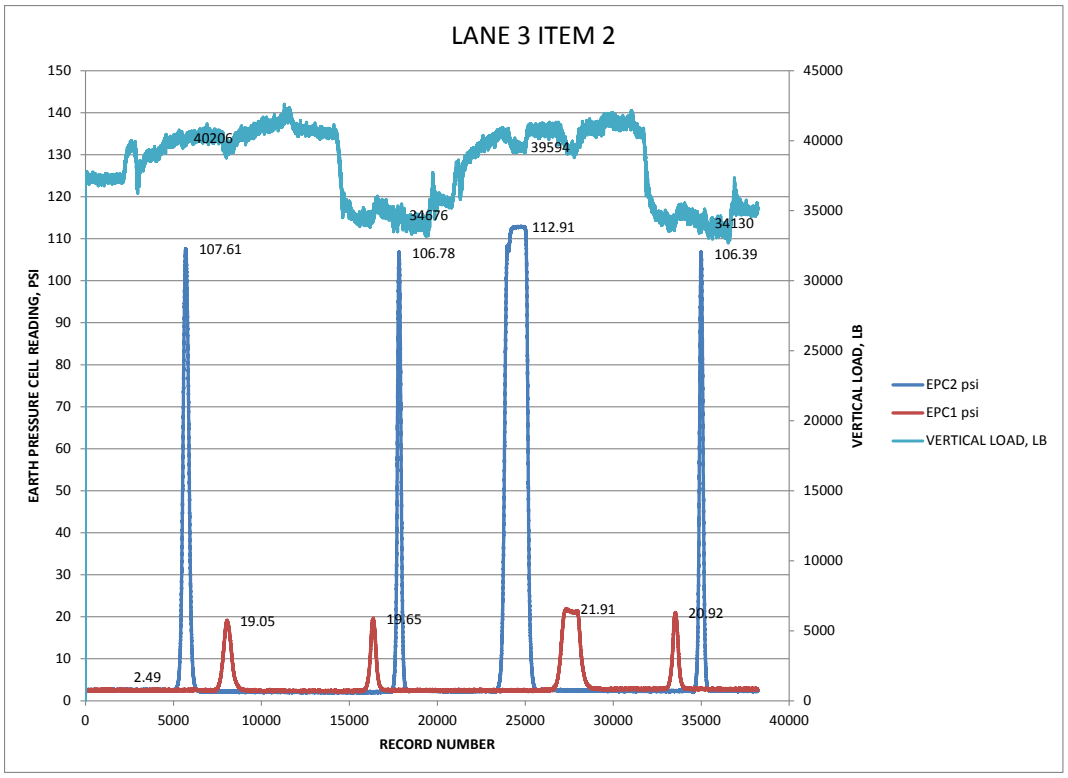

Figure F.10 Lane 3 Item 2 (1 lb=4.45 N, 1 psi=6.9 kPa)

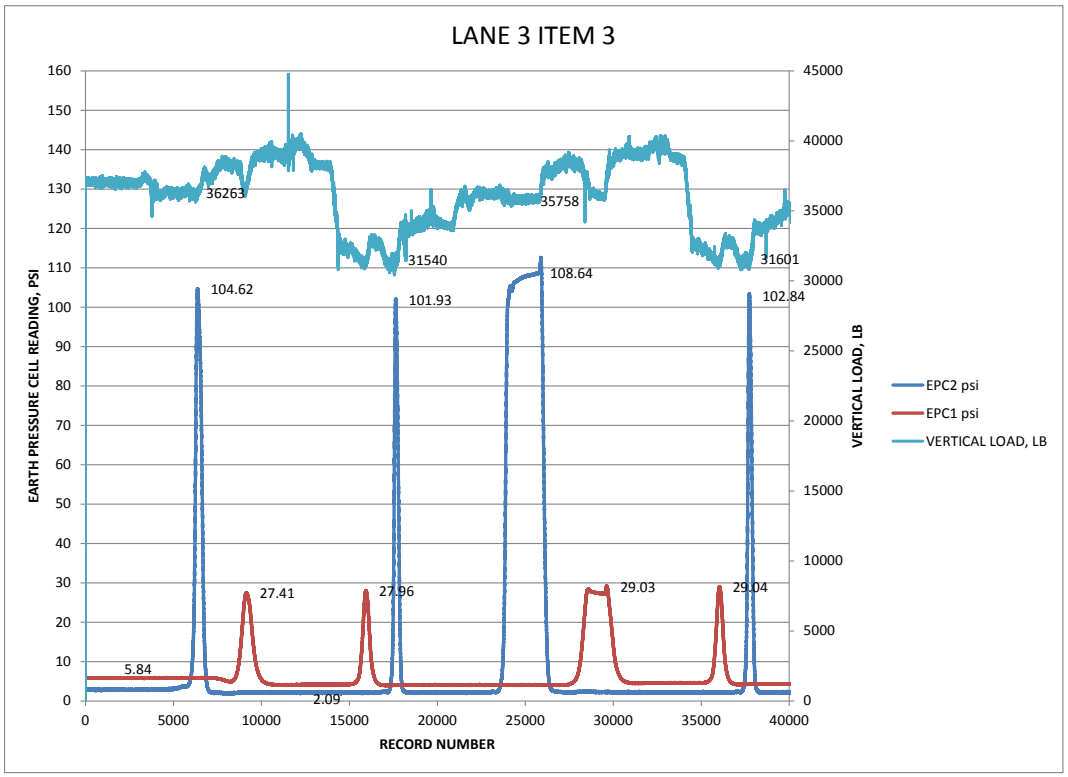

Figure F.11 Lane 3 Item 3 (1 lb=4.45 N, 1 psi=6.9 kPa)

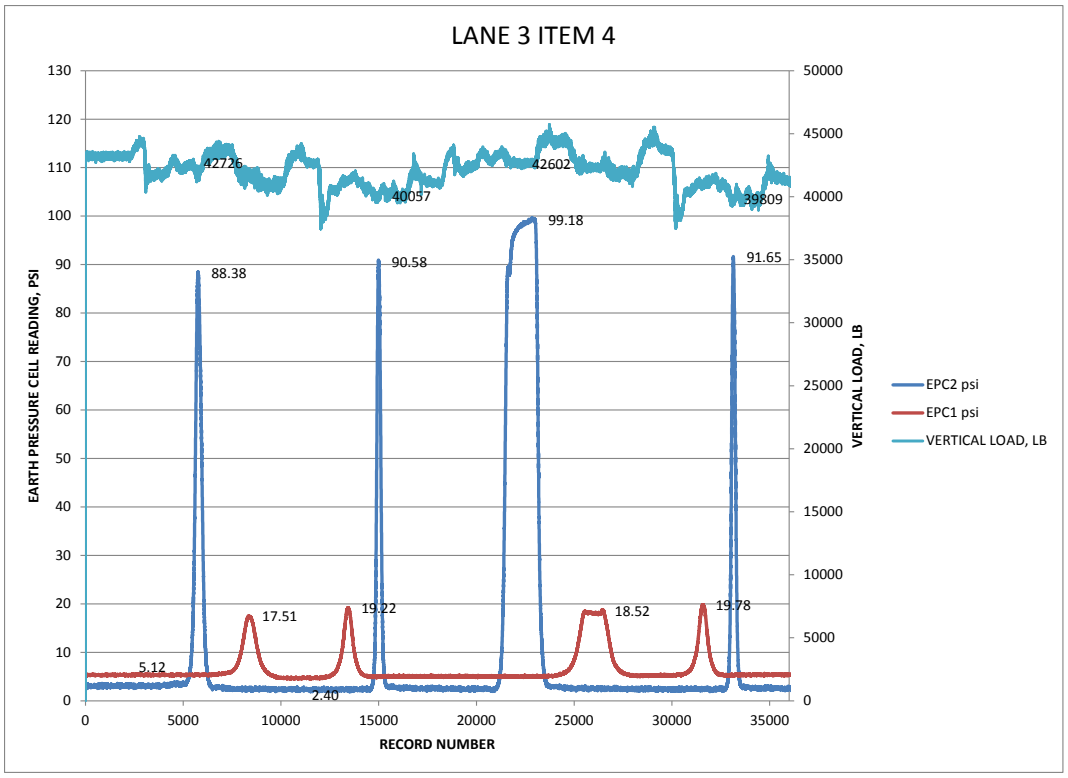

Figure F.12 Lane 3 Item 4 (1 lb=4.45 N, 1 psi=6.9 kPa)

Table F.1 Backcalculated Fröhlich stress concentration factor (n-factor)
(1 inch=25.4 mm, 1 lb=4.45 N, 1 psi=6.9 kPa)

Lane	Item	Load	Location	CBR	Peak No.	Gear Load, lb	Pressure, psi	Radius, in	Depth, in	Vertical Stress, psi	Average Vertical Stress, psi	n-factor	Average n-factor
1	1	C17 Single	Top Subbase	24	1	42200	142	9.73	12	62.30		2.29	
					2	43300	142	9.85	12	65.90		2.42	
					3	43100	142	9.83	12	66.30		2.45	
					4	43400	142	9.86	12	67.50	65.50	2.50	2.41
			Top Subgrade	14.2	1	42200	142	9.73	19	15.80		1.01	
					2	43300	142	9.85	19	17.50		1.10	
					3	43100	142	9.83	19	18.50		1.18	
					4	43400	142	9.86	19	19.40	17.80	1.23	1.13
1	2	C17 Single	Top Subbase	24	1	39050	142	9.36	12	80.90		3.55	
					2	37860	142	9.21	12	81.80		3.70	
					3	38550	142	9.30	12	84.40		3.84	
					4	37890	142	9.22	12	82.80	82.48	3.77	3.72
			Top Subgrade	9.8	1	39050	142	9.36	26	17.20		2.12	

Table F.1 Backcalculated Fröhlich stress concentration factor (n-factor)

(1 inch=25.4 mm, 1 lb=4.45 N, 1 psi=6.9 kPa)

Lane	Item	Load	Location	CBR	Peak No.	Gear Load, lb	Pressure, psi	Radius, in	Depth, in	Vertical Stress, psi	Average Vertical Stress, psi	n-factor	Average n-factor
					2	37860	142	9.21	26	18.10		2.31	
					3	38550	142	9.30	26	19.60		2.47	
					4	37890	142	9.22	26	20.00	18.73	2.57	2.37
1	3	C17 Single	Top Subbase	24	1	38470	142	9.29	12	73.90		3.13	
					2	39770	142	9.44	12	75.50		3.15	
					3	38360	142	9.27	12	75.30		3.23	
					4	39340	142	9.39	12	74.40	74.78	3.11	3.15
			Top Subgrade	3.9	1	38470	142	9.29	28	20.40		2.97	
					2	39770	142	9.44	28	20.80		2.94	
					3	38360	142	9.27	28	20.90		3.06	
					4	39340	142	9.39	28	21.40	20.88	3.06	3.01
1	4	C17 Single	Top Subbase	24	1	39040	142	9.35	12	75.50		3.20	
					2	39543	142	9.41	12	78.30		3.34	
					3	38370	142	9.27	12	75.90		3.27	
					4	39300	142	9.39	12	77.90	76.90	3.33	3.28
			Top Subgrade	3.9	1	39040	142	9.35	35.5	14.40		3.19	
					2	39543	142	9.41	35.5	14.70		3.22	
					3	38370	142	9.27	35.5	14.50		3.26	
					4	39300	142	9.39	35.5	14.80	14.60	3.26	3.23
3	1	F15 Single	Top Subbase	24	1	38020	325	6.10	12	75.20		2.29	
					2	33990	325	5.77	12	80.20		2.73	
					3	38170	325	6.11	12	78.20		2.39	
					4	33950	325	5.77	12	82.60	79.05	2.82	2.56
			Top Subgrade	14.2	1	38020	325	6.10	19	22.40		1.45	
					2	33990	325	5.77	19	22.80		1.65	
					3	38170	325	6.11	19	23.50		1.52	
					4	33950	325	5.77	19	23.70	23.10	1.72	1.59
3	2	F15 Single	Top Subbase	24	1	40200	325	6.27	12	105.10		3.23	
					2	34680	325	5.83	12	104.30		3.65	
					3	39600	325	6.23	12	110.40		3.48	
					4	34130	325	5.78	12	103.90	105.93	3.69	3.51
			Top Subgrade	9.8	1	40200	325	6.27	26	16.50		1.84	
					2	34680	325	5.83	26	17.20		2.22	
					3	39600	325	6.23	26	19.40		2.21	

Table F.1 Backcalculated Fröhlich stress concentration factor (n-factor)

(1 inch=25.4 mm, 1 lb=4.45 N, 1 psi=6.9 kPa)

Lane	Item	Load	Location	CBR	Peak No.	Gear Load, lb	Pressure, psi	Radius, in	Depth, in	Vertical Stress, psi	Average Vertical Stress, psi	n-factor	Average n-factor
					4	34130	325	5.78	26	18.40	17.88	2.42	2.17
3	3	F15 Single	Top Subbase	24	1	36260	325	5.96	12	102.50		3.44	
					2	31540	325	5.56	12	99.80		3.78	
					3	35700	325	5.91	12	106.50		3.65	
					4	31600	325	5.56	12	100.70	102.38	3.81	3.67
			Top Subgrade	3.9	1	36260	325	5.96	28	21.60		3.10	
					2	31540	325	5.56	28	22.20		3.66	
					3	35700	325	5.91	28	23.20		3.39	
					4	31600	325	5.56	28	23.23	22.56	3.83	3.50
3	4	F15 Single	Top Subbase	24	1	42730	325	6.47	12	86.00		2.41	
					2	40060	325	6.26	12	88.20		2.63	
					3	42200	325	6.43	12	96.80		2.80	
					4	39800	325	6.24	12	89.30	90.08	2.68	2.63
			Top Subgrade	3.9	1	42730	325	6.47	35.5	12.40		2.38	
					2	40060	325	6.26	35.5	14.10		2.89	
					3	42200	325	6.43	35.5	13.40		2.61	
					4	39800	325	6.24	35.5	14.70	13.65	3.04	2.73